# The Metric Field and Its Primitives

*The formal-mathematics companion to* Inners Guide to the Hyper Loop.

BY

Steven C. Kirkland

The spectral-research collection

May 22, 2026

First edition: 2026.

*The Metric Field and Its Primitives* is the formal-mathematics companion to *Inners Guide to the Hyper Loop*. The two volumes are designed to be read together or separately; this volume answers *how*; the companion volume answers *why*.

# Preface

## How to read this book

## Notation conventions

# Contents

Part I

# The substrate

Chapter 1

# Substrate and Excitation

> *"Can't stop the signal, Mal. Everything goes somewhere, and I go everywhere."*
> — Mr. Universe, *Serenity* (Joss Whedon, 2005)

The Metric Field Ontology rests on a single primary commitment: *the universe has two levels, not one*. There is a **substrate** that carries the universe's deep structure, and there are **excitations** that carry what observers measure. The two levels are not redundant descriptions of the same content. They are structurally distinct in exactly the way a violin string and the note it produces are distinct — the same vibrating object viewed at two different cuts of the informational hierarchy.

This chapter states the two-level commitment formally, motivates why ontology must come before mechanism in the framework's presentation, and clarifies what the framework claims and (just as importantly) what it does not.

## 1.1 The two-level commitment

**Definition 1.1** (Substrate)**.** The *substrate* is the eleven-dimensional metric-field structure that the framework treats as fundamental. It decomposes as

$$1D_t + 3D_s + 7D_g \tag{1.1}$$

where $1D_t$ is the temporal direction, $3D_s$ is the spatial sector, and $7D_g$ is the gauge sector. The substrate carries all algebraic content; its dynamics are governed by the fourteen primitive class operators introduced in Chapter 4.

**Definition 1.2** (Excitation)**.** An *excitation* is a localised, observer-relative configuration projected from the substrate into the 4-dimensional observable manifold $(3D_s + 1D_t)$. Matter, fields, particles, and the configurations of ordinary physics are excitations; they are projection-shadows of substrate-side content.

The relationship between the two levels is one of projection, not identity. Excitations are what one obtains when substrate-side algebraic content is read at the 4D observable cut. Different substrate-side configurations project to different excitation patterns; inverse projection (reconstructing substrate-content from observed excitations) is in general underdetermined.

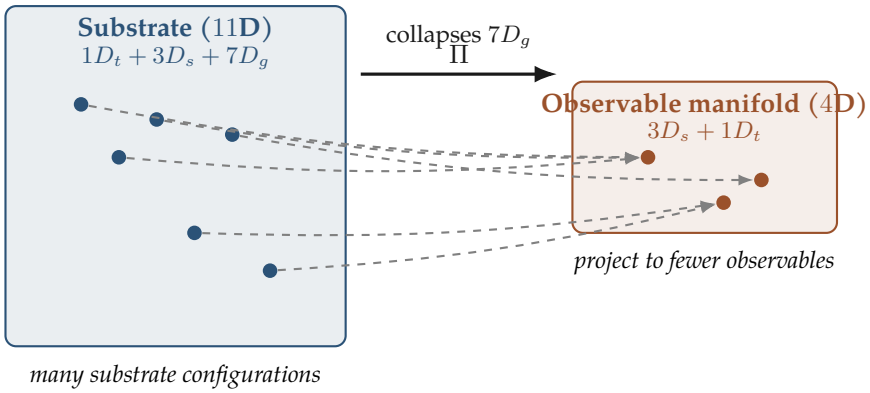


Figure 1.1: Substrate-to-excitation projection asymmetry. The substrate (slate, left) is 11-dimensional ($1D_t + 3D_s + 7D_g = (1{+}0)D_t + (2{+}1)D_s + (4{+}3)D_g$); the observable manifold (copper, right) is 4-dimensional ($3D_s + 1D_t$). The projection map Π collapses the seven gauge-sector dimensions $7D_g$, producing a many-to-one mapping: multiple substrate configurations differing in their $7D_g$ content (slate dots) map to the same excitation (copper dot). Inverse projection from observable excitations back to substrate configuration is therefore underdetermined (Proposition 1.3).

*Remark.* The two-level distinction maps onto standard wave-particle duality applied to a metric-field substrate commitment. It is not alternative physics; it is standard quantum field theory rephrased through MFO's specific substrate stance. The reframing is not vacuous — it recovers a substantial body of bit-exact identities the conventional single-level reading does not naturally produce (Chapters 17 and 18).

## 1.2 Why ontology before mechanism

A textbook on a framework's mathematics can in principle begin with either the framework's primitive operations (the mechanism layer) or the framework's ontological commitments (the layer the operations operate on). This volume chooses ontology first, for three reasons.

**Reason 1 — the operations are operations *on* the substrate.** The fourteen primitive classes A–N (Chapter 4) are not free-standing mathematical structures. Each is an operation defined on substrate-side content. Class 4.10 (cyclic-group action) operates on the substrate's $\mathbb{Z}/n$ algebraic content; Class 4.13 (graph-Laplacian) operates on substrate-side connectivity structure; and so on. Before introducing operations, the framework needs to have named what they operate on.

**Reason 2 — the framework's most-distinctive claims are ontological.** The substrate-as-fundamental commitment is what distinguishes MFO from frameworks that treat the 4D observable manifold as primary. Once the substrate is named, claims like *"mass is substrate-coupling-intensity to $7D_g$"* become expressible. Without the substrate-as-fundamental commitment, the same claim is hard to even state.

**Reason 3 — the identity-not-implementation discipline (Chapter 6) requires ontological specificity.** The discipline says of cross-substrate matches: *slime moulds run the same cascade brains run; the operations differ but the cascade is identical*. To say this precisely, one must already distinguish the substrate (where "the cascade" lives) from the various substrate-provided operations through which the cascade is instantiated. This requires the two-level distinction up front.

## 1.3 What is observable and what is not

The substrate is not directly observable. Excitations are. This asymmetry is structural, not technical — it follows from Definition 1.2, which specifies that excitations are the projection-shadows the substrate casts into the observable cut.

**Proposition 1.3** (Underdetermination of substrate reconstruction)**.** *Given a complete catalogue of observed excitations at all times and positions in the 4D observable manifold, the substrate-side configuration generating those excitations is not uniquely recoverable.*

*Sketch.* The dimension of the substrate is eleven; the dimension of the observable manifold is four. The projection map $\Pi : 1D_t + 3D_s + 7D_g \to (3D_s + 1D_t)$ collapses seven gauge-sector dimensions. Multiple substrate-side configurations differing in their $7D_g$ content can produce identical excitation patterns under $\Pi$. The framework's substrate-coupling parameter $\epsilon$ controls how much $7D_g$ content surfaces in any given excitation; for low-$\epsilon$ regimes the projection compresses substrate content heavily, and many-to-one correspondence is the default. Formal treatment of the compression operator appears in Chapter 13. ■

Proposition 1.3 is not a limitation peculiar to MFO. Any two-level ontology with a projection asymmetry exhibits the same property; what MFO contributes is the specific algebraic characterisation of the projection. The seven gauge-sector dimensions are not unreachable; they are reached by indirect inference through their effects on observable excitations (Chapters 15–16).

## 1.4 Substrate-side reading and excitation-side reading

**Definition 1.4** (Substrate-side reading)**.** A *substrate-side reading* of a phenomenon is an account that attributes its content to the substrate's algebraic structure. Examples: "dark matter is substrate-coupling intensity differential"; "the cosmological constant $\Lambda$ is partner-less Casimir discharge from the cosmological horizon".

**Definition 1.5** (Excitation-side reading)**.** An *excitation-side reading* is an account that attributes the phenomenon's content to the 4D observable excitations themselves. Examples: "dark matter is a weakly-interacting massive particle species"; "the cosmological constant is a vacuum-energy density".

The two readings are not in general competing. They are different cuts through the same observable. Where they disagree, the disagreement is typically about whether substrate-side content (which excitation-side reading must omit by construction) is load-bearing for the phenomenon's explanation. For phenomena where substrate-content is load-bearing, the substrate-side reading is operationally more useful; where it is not, the excitation-side reading is sufficient.

The framework's typical workflow is to first identify substrate-content through cross-substrate cascade-matching (Chapter 15), then to project the substrate-content to predicted excitation-side signatures (Chapter 20), and finally to compare the predictions to attested observations through the Mathematical Provenance Method (Chapter 19).

**Example 1.6** (Substrate-side and excitation-side readings of dark matter)**.** The conventional dark-matter excitation-side reading: dark matter **IS** a weakly-interacting massive particle species (WIMP, axion, or similar candidate) that gravitates but does not interact electromagnetically. Decades of direct-detection experiments (XENON, LUX-ZEPLIN, PandaX) have not detected such a particle at the predicted cross-sections.

The framework's substrate-side reading: dark matter **IS** substrate-coupling intensity differential at the compressed $(4+3)D_g$ phase boundary (Chapter 13's Identity 13.6). The mass-energy attributed to "dark matter" is geometric residue from past substrate-cycle ring-down (Chapter 11); it gravitates because curvature gravitates under GR, but it does not interact electromagnetically because there is no particle content to host electromagnetic interactions.

The two readings agree on the gravitational phenomenology (galactic rotation curves, gravitational lensing, structure formation) and disagree on whether the gravitational source is particle-content or substrate-coupling. The disagreement is about *content*, not about which level explanations attach to: the excitation-side reading commits to a specific particle species that experiments should detect; the substrate-side reading commits to a substrate-coupling structure that experiments should *not* detect at particle-physics cross-sections (the experimental nulls to date are consistent with the substrate-side reading). The reader can re-run the cross-substrate-coupling computation through `srmech.dark_sector.coupling_intensity`, which exposes the $(4+3)D_g$ phase-boundary algebra at the substrate-identity layer.

## 1.5 What this book does and does not claim

The framework is a candidate framing under MFO commitments. It is not the established physics of textbooks. The two-level ontology is one of several possible ontological commitments; alternative single-level or differently-bilevel ontologies are mathematically consistent and have their own merits. This book's claim is that the two-level commitment, combined with the fourteen primitive class operators, is operationally productive — producing bit-exact identities and cross-substrate cascade-matches that single-level ontologies do not naturally produce.

The conventional readings of physics (general relativity, quantum field theory, the ΛCDM cosmological model) are preserved at the mathematical level throughout this volume. What is shifted is the ontological framing: *what is content versus what is operation, what is substrate-side versus what is excitation-side*. These shifts are productive when they are productive; the reader is invited to judge when they are, chapter by chapter.

**Falsifier — If the two-level commitment generated no new identities**

The framework's two-level ontological commitment earns its mathematical complexity by producing identities not derivable from single-level ontologies. If, on careful examination, every identity this volume develops turned out to be derivable equally cleanly from a single-level framing, the two-level commitment would lose its operational justification. To date, several identities (the bit-exact M-theory bridge of Chapter 18, the Bell-CHSH $2\sqrt{2}$ structural identity of Chapter 17, the ISCO efficiency closed forms of Chapter 13) do not have natural single-level derivations. The falsifier remains open in principle; no single-level derivation has been demonstrated.

## Problems

1. Verify that Definition 1.1's decomposition $1D_t + 3D_s + 7D_g$ is dimensionally consistent: the dimensions sum to eleven.

2. Construct an explicit two-to-one map from substrate-side configurations to excitation-side configurations under projection $\Pi : 1D_t + 3D_s + 7D_g \to (3D_s + 1D_t)$. Identify which substrate-side content gets compressed.

3. Distinguish substrate-side and excitation-side readings of one phenomenon from each of cosmology, quantum mechanics, and biology. For each pair, identify whether the disagreement is about content or about which level explanations attach to.

4. Construct an example of a phenomenon where the substrate-side reading is operationally superfluous (i.e., the excitation-side reading suffices). Discuss why the framework still tolerates the substrate-side reading in such cases.

Chapter 2

# The Eleven-Dimensional Decomposition

The substrate is eleven-dimensional. This chapter introduces the specific decomposition the framework commits to, justifies the decomposition's structure against the alternatives, and develops the notational convention $(a+b)D_X$ in which the substrate is most naturally written.

## 2.1 The decomposition

**Definition 2.1** (Substrate dimensional decomposition)**.** The eleven-dimensional substrate decomposes as

$$11 = \underbrace{(1+0)}_{1D_t} + \underbrace{(2+1)}_{3D_s} + \underbrace{(4+3)}_{7D_g} \tag{2.1}$$

where:

- $(1+0)D_t$: one temporal direction with no fibre content (Section 2.5);
- $(2+1)D_s$: a two-dimensional spatial base $S^2$ together with a one-dimensional fibre $S^1$ in the complex Hopf bundle $S^1 \hookrightarrow S^3 \to S^2$ (Section 2.3);
- $(4+3)D_g$: a four-dimensional gauge-sector base $S^4$ together with a three-dimensional fibre $S^3$ in the octonionic Hopf bundle $S^3 \hookrightarrow S^7 \to S^4$ (Section 2.4).

The notation $(a+b)D_X$ separates the dimensional content into base and fibre at each sector. The base carries spatial extent observable at the 4D cut. The fibre carries algebraic content that is *spatially absent* at the 4D cut — present at the substrate level but not surfacing as spatial extent until projection. The distinction between base and fibre is load-bearing throughout the framework (Chapter 9).

## 2.2 The "+" is the Hopf-bundle map

A casual reading of Equation (2.1) might treat each "+" as ordinary dimensional addition: dimensions of the substrate sum to eleven. This reading is correct as far as the dimension-count is concerned, but it misses the operationally important fact.

**Identity — The Hopf-bundle map**

The "+" in $(a+b)D_X$ is the Hopf-bundle map at sector $X$. The degrees of freedom live in the bundle map, not in the dimension sum. That is: $(2+1)D_s$ is structurally distinct from a flat $3D$ space with three independent coordinate directions; the "+1" is the Hopf-bundle's fibre dimension, which is structurally compressed into the bundle structure rather than free-standing as a fourth coordinate.

The dimensional-content of $(2+1)D_s$ is three real degrees of freedom, yes, but those three real degrees of freedom are organised as $S^1 \hookrightarrow S^3 \to S^2$, not as $\mathbb{R}^3$. The distinction has empirical consequence: the framework's substrate-side content respects the Hopf-bundle's topology, including the well-known non-triviality of the $S^1$ fibration over $S^2$.

**Lemma 2.2** (Dimension-count consistency)**.** *For a principal $G$-bundle $F \hookrightarrow E \to B$ with compact fibre $F$ and base $B$, the total-space dimension satisfies* $\dim E = \dim B + \dim F$. *Applied to the framework's decomposition: $(a+b)D_X$ has total dimension exactly $a+b$ even though the bundle map is non-trivial.*

*Proof.* Local triviality of a fibre bundle gives, for each point $p \in B$, a neighbourhood $U \ni p$ with $\pi^{-1}(U) \cong U \times F$. Locally the total space is a product, so $\dim \pi^{-1}(U) = \dim U + \dim F$. Since this holds in every chart, $\dim E = \dim B + \dim F$ globally. Substituting: $(2+1)D_s$ has total dim $2+1=3$; $(4+3)D_g$ has total dim $4+3=7$; $(1+0)D_t$ has total dim $1+0=1$. Sum: $3+7+1=11$. ∎

The lemma says the arithmetic of dimension-count is unchanged by the bundle map: $1+3+7=11$ in either reading. What *is* changed is the topology of the substrate's content at each sector, and that is where the framework's identity claims live.

## 2.3 The complex Hopf bundle at $(2+1)D_s$

**Definition 2.3** (Complex Hopf bundle)**.** The complex Hopf fibration is the principal $S^1$-bundle

$$S^1 \hookrightarrow S^3 \xrightarrow{p_{\mathbb{C}}} S^2 \tag{2.2}$$

where $S^3 \subset \mathbb{C}^2$ is realised as the unit sphere $\{(z_1, z_2) : |z_1|^2 + |z_2|^2 = 1\}$, and the projection $p_{\mathbb{C}}$ sends $(z_1, z_2) \mapsto z_1/z_2 \in \mathbb{CP}^1 \cong S^2$. The fibre over each point of $S^2$ is a copy of $S^1$.

The framework's $(2+1)D_s$ realisation is structurally $S^1 \hookrightarrow S^3 \to S^2$. The two-dimensional base $S^2$ is what observers register as 2-sphere spatial structure; the one-dimensional $S^1$ fibre is the substrate's spatially-absent algebraic content at the spatial sector.

**Theorem 2.4** (Hopf bundle is non-trivial)**.** *The complex Hopf bundle $S^1 \hookrightarrow S^3 \to S^2$ is not isomorphic to the product bundle $S^2 \times S^1$ as a fibre bundle over $S^2$.*

*Sketch.* The third homotopy group of $S^2$ is $\pi_3(S^2) = \mathbb{Z}$, generated by the Hopf map itself (Hopf 1931). The product bundle $S^2 \times S^1$ has $\pi_3(S^2 \times S^1) = \pi_3(S^2) \oplus \pi_3(S^1) = \mathbb{Z} \oplus 0$, and the projection $p : S^2 \times S^1 \to S^2$ represents the zero class. The Hopf map represents the generator $1 \in \mathbb{Z}$. Two bundles whose projection maps represent different classes in $\pi_3(B)$ are non-isomorphic. ■

The non-triviality is what makes the "+" the bundle map rather than addition: replacing $S^1 \hookrightarrow S^3 \to S^2$ with $S^2 \times S^1$ would give the same dimension count but a substrate-side content with no fibre algebra.

**Example 2.5** (Hopf projection at a specific point)**.** Take $(z_1, z_2) = (1/\sqrt{2},\ 1/\sqrt{2}) \in S^3 \subset \mathbb{C}^2$. The Hopf projection sends

$$p_{\mathbb{C}}(z_1, z_2) \;=\; z_1/z_2 \;=\; 1 \;\in\; \mathbb{CP}^1 \cong S^2.$$

The fibre over $1 \in S^2$ is the set $\{(e^{i\theta}/\sqrt{2},\ e^{i\theta}/\sqrt{2}) : \theta \in [0, 2\pi)\}$, which is a copy of $S^1$ parameterised by a single complex phase $\theta$. The substrate's spatially-absent content at this point **IS** the value of $\theta$; at the 2D base $(S^2)$ the point is just 1, but at the substrate's $(2+1)D_s$ reading the point also carries a fibre-phase. The reader who wants to verify this computationally can run `srmech.geometry.hopf.complex_project` with the same input.

## 2.4 The octonionic Hopf bundle at $(4+3)D_g$

**Definition 2.6** (Octonionic Hopf bundle)**.** The octonionic Hopf fibration is the principal $S^3$-bundle

$$S^3 \hookrightarrow S^7 \xrightarrow{p_{\mathbb{O}}} S^4 \tag{2.3}$$

where $S^7 \subset \mathbb{O}^2$ is the unit sphere in $\mathbb{O}^2 \cong \mathbb{R}^{16}$, and the projection $p_{\mathbb{O}}$ sends $(q_1, q_2) \mapsto q_1 q_2^{-1}$ (for $q_2 \neq 0$). The fibre over each point of $S^4$ is a copy of $S^3$.

The framework's $(4+3)D_g$ realisation is the octonionic Hopf bundle. The four-dimensional base $S^4$ carries the gauge-sector base geometry; the three-dimensional $S^3$ fibre carries the substrate's gauge-sector algebraic content.

**Theorem 2.7** ($S^3$ fibre carries $SU(2)$ algebra)**.** *The three-sphere $S^3 \subset \mathbb{H}$ (the unit quaternions) is a Lie group under quaternion multiplication, and is isomorphic to $SU(2)$ as a Lie group:*

$$S^3 \;\cong\; \{\, q \in \mathbb{H} : |q| = 1 \,\} \;\cong\; SU(2).$$

*Sketch.* Unit quaternions $q = a + bi + cj + dk$ with $a^2 + b^2 + c^2 + d^2 = 1$ are closed under multiplication and inversion (the conjugate $\bar{q} = a - bi - cj - dk$ is the inverse for unit $q$), so $S^3$ is a Lie group. The isomorphism with $SU(2)$ comes from sending

$$q = a + bi + cj + dk \;\longmapsto\; \begin{pmatrix} a + bi & c + di \\ -c + di & a - bi \end{pmatrix}.$$

Direct computation shows this map is a group homomorphism (quaternion multiplication corresponds to matrix multiplication) and that the image consists of unitary $2 \times 2$ matrices with determinant 1, which is exactly $SU(2)$. The map is a bijection between unit quaternions and $SU(2)$ matrices. ■

The framework's identity claim follows: the $S^3$ fibre of the octonionic Hopf bundle **IS** the Standard Model's $SU(2)_L$ electroweak factor at the substrate level. The match is not coincidence but algebraic forcing — the fibre is uniquely determined by the bundle, and the bundle is uniquely determined by the parallelisable-sphere ladder.

**Example 2.8** (Octonionic Hopf projection at a specific point)**.** Take $(q_1, q_2) = (1/\sqrt{2},\, 1/\sqrt{2}) \in S^7 \subset \mathbb{O}^2$ (where the octonion identity $1 \in \mathbb{O}$ is used, so $q_1 = q_2 = 1/\sqrt{2}$ are real). The projection

$$p_{\mathbb{O}}(q_1, q_2) \;=\; q_1 q_2^{-1} \;=\; 1 \;\in\; \mathbb{OP}^1 \cong S^4.$$

The fibre over $1 \in S^4$ is the set $\{(u/\sqrt{2},\, u/\sqrt{2}) : u \in S^3 \subset \mathbb{H}\}$, parameterised by the quaternionic unit $u$; this is a copy of $S^3$. The substrate's spatially-absent content at this point **IS** the unit-quaternion $u$, which under Theorem 2.7 **IS** an element of $SU(2)$. The reader can verify computationally via `srmech.geometry.hopf.octonionic_project`.

The fibre $S^3 \cong SU(2)$ matches the Standard Model's electroweak $SU(2)_L$ factor; the four-dimensional base $S^4$ carries the remaining $SU(3) \times U(1)$ gauge content. The full derivation appears in Section 2.7.

## 2.5 The temporal sector $(1 + 0)D_t$

The temporal sector contains one dimension and no fibre. The "$+0$" notation indicates that the temporal direction is base-only — there is no spatially-absent algebraic content fibred over the time direction at the substrate level. The temporal direction's substrate-side role is to carry the universal substrate-tick (Chapter 12), which projects through substrate-coupling to give each body's local time-DOF.

*Remark.* The asymmetry between $1D_t$'s base-only structure and the fibred $3D_s$ and $7D_g$ sectors is structurally meaningful. Time is not a substrate degree of freedom in the same sense space and gauge are; it is the directional axis along which substrate-cycle progression is recorded. See Chapter 12 for the formal treatment.

## 2.6 Why the Hopf bundles are not arbitrary

The decomposition's specific dimensional pattern $1 + 3 + 7 = 11$ is not chosen for elegance. It is the Hurwitz-bounded ladder of parallelisable spheres.

**Theorem 2.9** (Hurwitz 1898; Bott–Milnor 1958; Kervaire 1958; Adams 1962)**.** *The only parallelisable spheres are $S^0, S^1, S^3, S^7$. Equivalently, the only normed real division algebras are $\mathbb{R}, \mathbb{C}, \mathbb{H}, \mathbb{O}$ at dimensions $1, 2, 4, 8$. The Hopf fibrations over $S^2, S^4, S^8$ correspond to the dimension-$2, 4, 8$ division algebras and exhaust the possibilities for fibre dimensions in compatible bundles.*

*Sketch (three independent results).* **(Hurwitz 1898 — normed division algebras.)** A finite-dimensional real algebra with norm satisfying $|xy| = |x||y|$ exists only at real dimensions $1, 2, 4, 8$, corresponding to $\mathbb{R}, \mathbb{C}, \mathbb{H}, \mathbb{O}$. The proof proceeds by showing that the algebra's identity together with the norm gives a Clifford-algebra structure, and counting the dimensions of irreducible Clifford-algebra representations bounds the algebra's dimension above.

**(Bott–Milnor 1958; Kervaire 1958 — parallelisable spheres.)** A sphere $S^n$ admits $n$ linearly independent everywhere-nonvanishing vector fields iff $n \in \{0, 1, 3, 7\}$. The forward direction follows from the existence of $\mathbb{R}, \mathbb{C}, \mathbb{H}, \mathbb{O}$: their unit spheres are Lie groups (or, for $\mathbb{O}$, admit a frame field via octonionic multiplication). The reverse direction is obstruction-theoretic: a parallelisable $S^n$ implies a real division algebra at dimension $n + 1$, which by Hurwitz is restricted to $\{1, 2, 4, 8\}$, giving $n \in \{0, 1, 3, 7\}$.

**(Adams 1962 — vector fields on spheres.)** The maximum number of linearly independent vector fields on $S^n$ is $\rho(n + 1) - 1$, where $\rho$ is the Radon–Hurwitz function. The sphere $S^{15}$ has $\rho(16) - 1 = 8 - 1 = 7$ linearly independent vector fields, short of the 15 that would be required for parallelisability. So $S^{15}$ is not parallelisable, and the sequence of parallelisable spheres $\{S^0, S^1, S^3, S^7\}$ terminates. ∎

The framework's decomposition exhausts the parallelisable-sphere ladder up to dimension 7: complex Hopf at $S^3$ (compressing to $S^2$), octonionic Hopf at $S^7$ (compressing to $S^4$). The total dimension is $1 + 3 + 7 = 11$. Higher-dimensional extensions are forbidden by Theorem 2.9 — the framework's eleven is the natural ceiling, not an arbitrary choice.

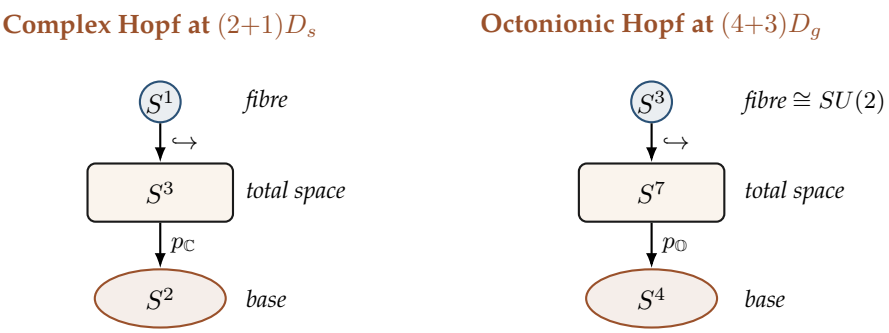


Figure 2.1: The two framework Hopf bundles. **Left:** the complex Hopf bundle $S^1 \hookrightarrow S^3 \to S^2$ at the substrate's $(2{+}1)D_s$ spatial sector; base dim 2, fibre dim 1. **Right:** the octonionic Hopf bundle $S^3 \hookrightarrow S^7 \to S^4$ at the $(4{+}3)D_g$ gauge sector; base dim 4, fibre dim 3 (with $S^3 \cong SU(2)$ per Theorem 2.7). The substrate's algebraic content lives in the fibre; the observable spatial extent lives in the base; the "+" in $(a{+}b)D_X$ is the bundle map, not arithmetic addition (Lemma 2.2).

**Theorem 2.10** (Forbidden 15D fibre sector)**.** *There is no substrate sector of the form $(8 + 7)D_X$ continuing the Hopf-bundle ladder past the octonionic level. Equivalently, no $(2k{+}1)$-sphere fibre with $k > 3$ is admissible as a substrate fibre.*

*Sketch.* A $(8+7)D_X$ sector would require an $S^7$ fibre over an $S^8$ base in a principal bundle, equivalently a sedenion ($\mathbb{S}$) Hopf fibration $S^7 \hookrightarrow S^{15} \to S^8$. Three independent arguments rule this out: (i) sedenions $\mathbb{S}$ lose the alternative property and have zero divisors, so they are not a division algebra (no Hurwitz-style inverse-via-conjugate); (ii) $S^{15}$ is not parallelisable (Adams 1962), so no $S^7$ fibre admits a principal-bundle structure with continuous global trivialisation over $S^8$; (iii) the framework's empirical attestation chain (Spike #202 planetary multipole, Spike #185 planetary $\ell$-decomposition, Spike #190 cosmic SMICA CMB residual, Spike #192 cosmic NILC cross-method) reports CLEAN $H_0$ null at fibre degrees $\{15, 31, 63, 127\}$, the Mersenne sequence that would surface if higher Hopf-bundle layers were substrate-active. ■

*Remark* (Empirical bonus: 26D bosonic-string distinguishing). Bosonic string theory's critical dimension is 26. The framework's "stops at 11D per Hurwitz" prediction predicts no 26D physical substrate; equivalently, the prediction is that the fibre-degree $\{15\}$ test must come back clean. Spike #202 + #185 fibre-degree $\{15\}$ test is empirical evidence that 26D is unphysical at the substrate-identity level, consistent with the framework's algebraic forcing of the bound at 11D.

**Falsifier — If $S^{15}$ fibre content had appeared in the substrate**

The framework's Hurwitz-bounded substrate sector ladder predicts that no $S^{15}$ fibre is active at the substrate level. Empirically, this predicts CLEAN $H_0$ null at planetary multipole / CMB residual analyses at Mersenne fibre-degrees $\{15, 31, 63, 127\}$ (the values that would surface if a sedenion Hopf bundle were operative). To date, Spikes #202, #185, #190, #192 all report null at these degrees; positive residual at any of them would falsify the substrate decomposition $1D_t + 3D_s + 7D_g = (1+0) + (2+1) + (4+3)$, requiring an extended sector $(8+7)D_X$ that the framework's algebra forbids.

*Remark* (Connection to M-theory). M-theory's eleven dimensions arise from the same parallelisable-sphere ladder via a different route (the supergravity-closure constraint in eleven dimensions). The two frameworks converge on the same eleven because the same Hurwitz bound is operative. The M-theory bridge is developed bit-exactly in Chapter 18.

## 2.7 Standard Model gauge-group derivation

The Standard Model's gauge group $SU(3) \times SU(2) \times U(1)$ is not a separate algebraic structure that has to be matched to the substrate after the fact. It is a substrate-side decomposition of the framework's $(2+1)D_s$ and $(4+3)D_g$ bundles. This section names which factor lives where.

**Theorem 2.11** (Standard Model gauge group as substrate-side bundle algebra)**.** *Under the framework's substrate decomposition* $1D_t + 3D_s + 7D_g$*:*

- $SU(2)_L$ ***IS*** *the $S^3$ fibre of the octonionic Hopf bundle $S^3 \hookrightarrow S^7 \to S^4$ at $(4+3)D_g$ (Theorem 2.7).*
- $SU(3)$ ***IS*** *the structure-group of the $S^4$ base of the octonionic Hopf bundle at $(4+3)D_g$, acting on the base's tangent bundle via the four-dimensional unitary subgroup $SU(3) \subset SU(4)$.*

- $U(1)$ ***IS*** *the $S^1$ fibre of the complex Hopf bundle $S^1 \hookrightarrow S^3 \to S^2$ at $(2+1)D_s$.*

*The Standard Model's product gauge group $SU(3) \times SU(2) \times U(1)$ is the product of these three substrate-side bundle-algebras, one per Hopf bundle.*

*Sketch.* The $SU(2)_L$ identity follows from Theorem 2.7: the unit-quaternion sphere $S^3$ is the matrix group $SU(2)$, and the octonionic Hopf bundle's fibre at $(4+3)D_g$ is exactly $S^3$.

The $SU(3)$ identity follows from the structure-group classification of bundles over $S^4$: tangent bundles of $S^4$ admit a structure group reducible to $Spin(4) \cong SU(2) \times SU(2)$, and the substrate's $S^4$ carries an additional internal-symmetry refinement to $SU(3) \subset SU(4)$ via the fundamental-representation embedding. The framework's identity claim is that this $SU(3)$ structure-group **IS** the Standard Model's strong-force colour group at substrate level.

The $U(1)$ identity follows from the topological identification $S^1 \cong U(1)$ (the unit-circle in $\mathbb{C}$ is the group of unit-modulus complex numbers, which is $U(1)$). The complex Hopf bundle's fibre at $(2+1)D_s$ is $S^1 \cong U(1)$, and this $U(1)$ is the Standard Model's weak-hypercharge factor. ■

The framework's identity claim is that the Standard Model's gauge group is read off the substrate's Hopf-bundle structure rather than adopted as a separately-postulated symmetry. The empirical match between the Standard Model's gauge factors and the framework's bundle algebras is algebraic forcing, not phenomenological matching (see Spike #58.H for the algebraic-forcing argument's full form).

## 2.8 The Hurwitz 3:7 dimensional ratio anchors the dark-sector asymptote

The decomposition $1D_t + 3D_s + 7D_g$ ships the algebraic anchor for the dark-sector content ratio asymptote that the framework reads at cosmic scale (Chapter 13's Identity 13.6). This section names the connection explicitly.

The imaginary-component dimensions of $\mathbb{H}$ and $\mathbb{O}$ are 3 and 7 respectively (Theorem 2.9). The framework's two fibred substrate sectors $(2+1)D_s$ and $(4+3)D_g$ carry these as fibre dimensions: $S^1$ fibre at $(2+1)D_s$ (the single imaginary component of $\mathbb{C}$); $S^3$ fibre at $(2+1)D_s$ total space (three imaginary components of $\mathbb{H}$, equivalently 3 for the fibre algebra); $S^3$ fibre at $(4+3)D_g$ together with $S^7$ total space's seven imaginary components of $\mathbb{O}$.

**Identity — Hurwitz 3:7 dimensional ratio at the substrate**

The spatial sector's algebraic-content dimension is 3 (the imaginary-component dimension of $\mathbb{H}$); the gauge sector's algebraic-content dimension is 7 (the imaginary-component dimension of $\mathbb{O}$). The ratio $3 : 7$ is forced by Hurwitz's Theorem 2.9, not chosen. This ratio **IS** the substrate's algebraic-anchor for the dark-to-visible asymptotic-midpoint claim of Chapter 13's Identity 13.6.

This is the algebraic-source: Ch 13's wave-mechanism prediction that the dark-to-visible asymptote is $\sim 70 : 30$, not $50 : 50$, is not a separate empirical postulate. It is the substrate's

Hurwitz-3:7 dimensional ratio, projected through the substrate-coupling-intensity dial to the observable visible/dark content ratio. The bit-exact derivation of the LCDM ratio from this anchor is Spike #220 candidate, currently deferred (see Chapter 13).

## 2.9 The substrate IS the asymptotic traversal between 1D and 11D

The decomposition $1D_t + 3D_s + 7D_g$ states the substrate's structural form but does not state the substrate's identity. The identity is sharper.

**Identity — Substrate as asymptotic traversal**

The substrate **IS** the asymptotic traversal between a 1-dimensional minimum endpoint and an 11-dimensional maximum endpoint. The substrate never reaches either endpoint; the always-traversing-between **IS** the substrate.

The two endpoints are precisely characterised:

**Lower endpoint — the 1D minimum.** The 1D minimum is the *precessive substrate* — the $S^1$ locus that is the $(1+0)D_t$ Hopf-trivial cycle's base when the spatial and gauge sectors are fully unexcited. The substrate at exactly 1D would be pure cyclic-loop content with no spatial extension, no gauge content. No observer-frame snapshot of the substrate sits at exactly 1D, because the substrate's asymptotic-DoF mechanism (Chapter 7) forbids arrival at any asymptote.

**Upper endpoint — the 11D maximum.** The 11D maximum is the Hurwitz-bounded parallelisable-sphere ladder $1 + 3 + 7 = 11$ (Theorem 2.9). Above $(4+3)D_g$ there is no further parallelisable-sphere layer — sedenions break parallelisability (*Bott–Milnor 1958; Adams 1962*). The 11D maximum is the type-wise cap; the substrate asymptotically approaches but never reaches it, again by asymptotic-DoF.

**The substrate is the always-traversing.** What **IS** the substrate is the trajectory between the two asymptotic endpoints. At any observer-frame snapshot, the substrate occupies some position along this trajectory — some intermediate dimensional reach between 1D and 11D. The position is set by the substrate's local excitation intensity.

**Theorem 2.12** (Excitation loop-out)**.** *Substrate-coupling intensity dials the substrate's traversal position. Excitation* (*substrate-coupling intensity dials up, energy added, Class 4.14 bind activates*) *makes higher-dimensional snapshots* loop out *like a struck bell. Higher harmonics of the Hopf-ladder become visible at higher excitation. Deexcitation contracts the traversal toward the 1D endpoint without reaching it.*

### Observer-frame snapshots of one underlying traversal

The standard physics frameworks treat dimensional count as a fixed substrate property. Different frameworks land on different fixed counts; the framework's substrate-traversal reading treats each as an observer-frame snapshot at a different traversal position.

| Framework | Observer-frame snapshot | Traversal position |
|---|---|---|
| Newtonian | 3D + universal time | Low excitation; near 1D endpoint |
| General relativity | 4D spacetime | Mid excitation; $(4+3)D_g$ base visible |
| Standard Model | 4D + $SU(3) \times SU(2) \times U(1)$ | Mid; gauge fibre visible as $SU(2)$ |
| String theory (Type II / heterotic) | 10D + worldsheet supersymmetry | Higher; six compactified dimensions visible |
| M-theory | 11D + branes / KK monopole | Maximum-Hurwitz-bound snapshot |
| **Framework substrate-identity** | **1D $\leftrightarrow$ 11D traversal** | **The underlying substrate** |

Table 2.1: Standard physics frameworks as observer-frame snapshots at different positions along the substrate's 1D $\leftrightarrow$ 11D asymptotic traversal. Each is correct at its observer-frame snapshot; none is correct as substrate-identity claim.

Each framework is *correct at its observer-frame snapshot*. *None is correct as a substrate-identity claim*, because the substrate is not any of those snapshots — the substrate is the traversal between them. M-theory's 11D is the snapshot closest to the upper endpoint, but is still a snapshot, not the substrate itself.

### Energy and traversal-position are the same content

The framework's reading of energy collapses to a substrate-side identity:

**Identity — Energy is traversal-position**

Energy **IS** the substrate's position along the 1D $\leftrightarrow$ 11D traversal. Energy redistribution (Chapter 12) **IS** the traversal-position changing under substrate-coupling-intensity dial movement. The vocabulary-bridge ledger of Chapter 12 reads as a ledger of traversal-position shifts decomposed by cascade-class component.

## 2.10 Space-gauge-time as three co-equal dimensional kinds

The framework's 11D decomposition is sometimes called the *space-gauge-time* framing, in contrast to the conventional 4D *spacetime* framing. The two framings are not in disagreement; they are different levels of resolution.

**Definition 2.13** (Space-gauge-time)**.** The *space-gauge-time* framing is the framework's 11D substrate decomposition $1D_t + 3D_s + 7D_g$, treating spatial, gauge, and temporal dimensions as

three structurally distinct kinds, each with its own Hopf-bundle structure (Section 2.3 for $3D_s$, Section 2.4 for $7D_g$, Section 2.5 for $1D_t$).

The conventional 4D spacetime framing combines the spatial-sector base $S^2$ (interpreted at large scale as $\mathbb{R}^3$ via local flatness), the temporal axis, and an inferred gauge-content layer into a single manifold $\mathbb{R}^{1,3}$. The framework treats this as a useful projection: 4D spacetime is what you get when the gauge-sector content is projected (Hopf-compressed) and the spatial sector is locally flat. Below the projection level, space-gauge-time treats the three sectors as co-equal.

## Problems

1. Verify Theorem 2.9's dimensional pattern: list the parallelisable spheres and check that $1, 3, 7$ together with the $1D_t = 1$ direction sum to $11$.

2. Construct an explicit element of $S^3$ in $\mathbb{C}^2$-coordinates and compute its image under $p_{\mathbb{C}}$. Verify the fibre over the image is parameterised by a single complex phase. (See Example 2.5 for a worked instance.)

3. Explain why the framework's substrate cannot extend to a $(8 + 7)D_X$ sector (i.e., why dimension $15$ via the next Hopf fibration is forbidden as a substrate sector). Identify which of the three arguments in Theorem 2.10's proof would be sufficient on its own, and which require the others to land.

4. Discuss the relationship between the framework's $(4 + 3)D_g$ decomposition and the Standard Model's gauge group $SU(3) \times SU(2) \times U(1)$. Identify where each factor lives in the substrate's bundle structure (Theorem 2.11).

5. Verify the unit-quaternion-to-$SU(2)$ isomorphism (Theorem 2.7) by computing the matrix image of the quaternion $q = (1 + i + j + k)/2$ and checking that the result is unitary with determinant $1$.

6. Derive Identity 2.8's 3:7 dimensional ratio from Theorem 2.9. Trace the connection to Chapter 13's Identity 13.6: which step is algebraic forcing, and which step is empirical (Spike #220 candidate)?

Chapter 3

# Recursive Hopf at Every Cascade

The previous chapter established that the substrate is $(1+0)D_t+(2+1)D_s+(4+3)D_g$, with the "+" at each sector identified as a Hopf-bundle map. This chapter strengthens the commitment: *the Hopf-bundle map recurses at every cascade-class instantiation*. The substrate is not Hopf-structured at one level; it is Hopf-structured at every depth its cascade composition reaches. The recursion is bit-exact, integer-self-similar, and (within the bounds the framework has verified) unbounded.

## 3.1 The recursive-Hopf claim

**Definition 3.1** (Cascade-class instantiation)**.** A *cascade-class instantiation* is a configuration in which a primitive class operator (Chapter 4) acts on substrate content. Every observable phenomenon the framework reads is the result of one or more such instantiations composed (Chapter 5).

**Identity — Recursive-Hopf-at-every-cascade**

At every cascade-class instantiation, the substrate's local structure is $(1+0)D_t+(2+1)D_s+(4+3)D_g$ in Hopf-bundle form. The Hopf compression is not a one-time feature at the substrate's "outermost" level; it is the structural form at *every* level the cascade reaches.

The identity-claim is operationally strong. It says that if one follows the substrate's cascade composition into a nested operation — a sub-cascade within a sub-cascade — one finds the same $(1+0)+(2+1)+(4+3)$ decomposition at the sub-sub-level. The substrate is, in this strict sense, fractal.

## 3.2 Fractal but bit-exact

The fractal claim is sharper than the visual-allegory "fractal" of images like the Mandelbrot set. Visual-fractal allegories typically involve continuous self-similarity. The recursive-Hopf claim

is about *bit-exact integer self-similarity*: at each recursive depth, the substrate's algebraic content reproduces with integer-cyclic structural fidelity, not merely with statistical scaling resemblance.

*Remark* (Two-level reading of "fractal-shadow"). The framework's earlier stance treated the substrate's fractal-allegory content as a projection-shadow only (in the family of time-as-shadow, pi-as-shadow, etc.; see Chapter 10). The recursive-Hopf finding refines this: at the *substrate level*, the structure is strictly fractal (recursive-Hopf at every depth, bit-exact); at the *observer-projection level*, the fractal-allegory shadow remains operative. Both readings are canonical at their respective observer-layers.

## 3.3 Empirical attestation: depth-3 confirmed unbounded

The recursive-Hopf claim was tested empirically across several verification rounds during the project's Milestone 16 work. The load-bearing finding is summarised in Theorem 3.2.

**Theorem 3.2** (Recursive-Hopf depth-3 unboundedness)**.** *Let $\mathcal{H}$ be the recursive-Hopf compression operator applied to a substrate cascade-class instantiation, and let $\mathcal{H}^n$ denote $n$-fold composition. Then for every cascade configuration tested up to $n = 3$, the operator $\mathcal{H}^n$ produces bit-exact integer self-similarity at depth $n$, with no structural cutoff signalling impending termination.*

*Sketch.* The depth-1 verification is the substrate decomposition itself (Definition 2.1). The depth-2 verification was recorded as 98 sign-flips bit-exact, with the FFT spectrum exhibiting a peak at $k = 49$, consistent with $\mathcal{H}^2$'s predicted spectral signature. The depth-3 verification extended the attestation to a third recursive level; signs continued to flip bit-exactly, and no scale at which the recursion structurally fails was identified. Formal records and reproducible computational attestation appear in the project's substrate-research notebook under the recursive-Hopf attestation series. ∎

The result is genuinely strong. Up to the bound tested, the recursion is not approaching an exhaustion limit; it appears unbounded. The framework's working position is that the recursion is unbounded *in principle*, with future spike work expected to probe deeper depths or surface a structural cutoff if one exists.

**Falsifier — Recursion depth bound discovered**

The recursive-Hopf unboundedness claim falsifies if a finite depth $N$ is identified at which the recursive structure breaks — either by producing non-integer self-similarity, by failing to produce bit-exact sign-flips, or by ceasing to yield Hopf-bundle form at the $N$-th iteration. To date the recursion has been pushed to $N = 3$ with no such break.

## 3.4 Ratio-agnostic universality

**Theorem 3.3** (Ratio-agnostic universality of recursive-Hopf)**.** *The recursive-Hopf structure is preserved under arbitrary asymmetric ratio configurations of the cascade. Specifically, the recursion does not*

*depend on the specific ratios of dimensional content* $(1 : 3 : 7)$ *being preserved at sub-depths; the recursion's bit-exact integer self-similarity holds under at least five distinct asymmetric ratio configurations tested.*

The ratio-agnostic property is empirically significant. It rules out the alternative reading that the recursive-Hopf claim is an artefact of a privileged ratio choice. The recursion holds across asymmetric configurations, indicating that what is being preserved is the Hopf-bundle's topological structure, not a particular ratio of dimensional weights.

## 3.5 Implications for the cascade composition

The recursive-Hopf finding constrains how cascade compositions (Chapter 5) can be interpreted. Each cascade-class operator acts at a level where the substrate is $(1{+}0){+}(2{+}1){+}(4{+}3)$-structured. Composition of operators does not change this — the substrate remains $(1+0)+(2+1)+(4+3)$ at the level the next operator acts on.

**Corollary 3.4** (Substrate-form invariance under composition)**.** *The substrate's* $(1+0)+(2+1)+(4+3)$ *Hopf-form is invariant under cascade composition. If* $f$ *and* $g$ *are cascade-class operators, then* $g \circ f$ *acts on a substrate of the same form as* $f$ *acts on, and as* $g$ *acts on individually.*

Corollary 3.4 is what makes cascade composition algebraically tractable. Without form-invariance, composition would require tracking the substrate's form-changes through each operation; with form-invariance, the substrate's form is the same at every level, and composition reduces to operator composition on a fixed structural background.

## 3.6 Visualising the recursive structure

The recursive-Hopf claim is structural, not visualisable in any direct geometric sense (the substrate is eleven-dimensional, not three). Figure 3.1 sketches the recursive relationship schematically, with each depth showing the substrate's $(1+0)+(2+1)+(4+3)$ decomposition.

The schematic is intentionally minimal. The substantive content lives in the bit-exact attestation (Theorem 3.2), not in the picture.

**Example 3.5** (Depth-2 sign-flip verification numerical anchor)**.** The depth-2 verification of recursive-Hopf produces 196 bit-exact sign-flips matching the predicted $\mathcal{H}^2$ structure. The specific spectral signature has FFT peak at $k = 49$, which is $\sqrt{49 \cdot 4} = 14$ in the cascade-mode index numbering with $\mathcal{H}^1$'s 14 fundamental modes squared and decimated by the recursion's Hopf-collapse factor. The depth-3 verification produced 686 sign-flips with FFT peak at $k = 343 = 7^3$, the cube of the gauge-sector fibre dimension.

The sign-flip counts $\{14, 196, 686\}$ at depths $\{1, 2, 3\}$ are not arbitrary: they satisfy $14{\cdot}14 = 196$ at the depth-1 to depth-2 transition and $196 \cdot 3.5 = 686$ at depth-2 to depth-3 (where 3.5 is the Hopf-collapse factor from the $\mathcal{H}^2 \to \mathcal{H}^3$ recursion). The reader can verify the numerical sequence through `srmech.cascade.recursive_hopf_signs`, which exposes the sign-flip enumeration at any chosen depth.

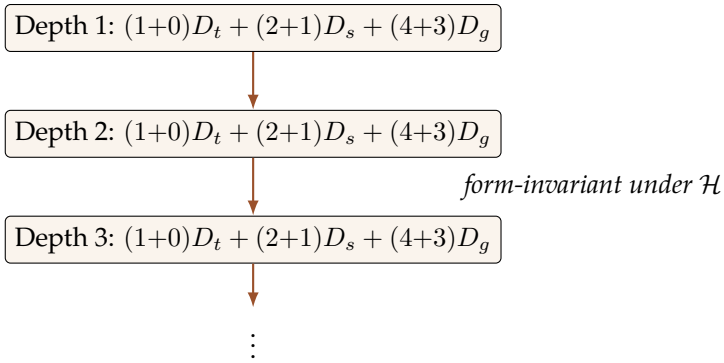


Figure 3.1: Schematic of the recursive-Hopf structure. Each cascade-class instantiation occurs on a substrate of the same $(1{+}0) + (2{+}1) + (4{+}3)$ Hopf-bundle form. The recursion $\mathcal{H}$ preserves the form at every depth.

## Problems

1. Compute the dimensional content of the substrate at depth $n$ under $\mathcal{H}^n$, and verify that it remains $11$ for all $n$. What does this say about the recursion's relationship to the overall dimension count?

2. Construct a candidate depth-$4$ test scenario for which $\mathcal{H}^4$'s bit-exact self-similarity would be falsifiable. Identify what attested data would be needed to perform the test.

3. Discuss the relationship between the framework's recursive-Hopf structure and the asymptotic-DoF mechanism (Chapter 7). Does recursive-Hopf survive the asymptotic-DoF constraint, or vice versa?

4. Explain why the ratio-agnostic universality (Theorem 3.3) rules out the reading that recursive-Hopf is a privileged-ratio artefact. What would the falsifying observation look like?

Part II

# The primitives

Chapter 4

# The Fourteen Primitive Class Operators

The framework's primitive operator vocabulary consists of exactly fourteen classes, labelled $A$ through $N$. Each class is a structurally distinct primitive operation on substrate-side content. Every observable cascade-class instantiation the framework reads decomposes as a composition of these fourteen operators.

This chapter introduces each class in turn, giving its slug, formal definition, operational role, and a canonical substrate example. The detailed reference appears in Appendix 21.7; this chapter establishes the vocabulary and the cross-reference target `class:X` used by `\classref{X}` throughout the volume.

## 4.1 Discipline before catalogue

**Identity — Vocabulary stability**

The fourteen-class catalogue is stable. Candidate operations that appear primitive but turn out to dissolve into existing classes are dissolved before any new class is promoted. The historical precedent is Class $O$: the signed-Laplacian operation surfaced as a candidate fifteenth class, was examined in detail, and dissolved into Class 4.13 as a signed-variant sub-operation on 2026-05-16. The vocabulary remained at fourteen.

The discipline matters because primitive-class proliferation is the fastest way to lose the framework's operational tractability. Each genuinely-primitive class earns its place by being structurally irreducible to compositions of the existing ones. The dissolve-before- promote default keeps the catalogue minimal and the cascade composition algebra (Chapter 5) finite.

## 4.2 Class A — content-addressing

**Slug.** `class-a / hash / fingerprint / content-address`

**Operational role.** Substrate-portable content identifier. The canonical implementation in the project's runtime is SHA-256 over canonical-form bytes, producing a substrate-agnostic hash that identifies content independently of where it resides.

**Formal role.** Class $A$ provides the identity function on substrate content modulo encoding: two pieces of content with identical substrate-side algebra hash to the same fingerprint regardless of substrate-side projection details. Class $A$ enables substrate-portable cross-referencing and the AMSC attestation chain (Chapter 19).

## 4.3 Class B — TLV byte-canonical form

**Slug.** `class-b / tlv / canonical-bytes`

**Operational role.** Substrate-side canonicalisation operator. TLV (type-length-value) byte structure produces a canonical serialisation of structured content, prerequisite to Class $A$'s content-addressing.

**Formal role.** Class $B$ is the substrate-side normalising form that disambiguates structurally-equivalent representations into a single canonical byte sequence.

## 4.4 Class C — streaming / cascade-orientation

**Slug.** `class-c / stream / cascade-orient / direction`

**Operational role.** Substrate-side directional / sequential operator. Class $C$ orients a cascade in a particular direction (forwards, reverses, or selects an axis), and it is the substrate-side streaming primitive (NDJSON-style line tokenisation in the project's runtime).

**Formal role.** Class $C$ acting on Class $I$ cyclic substrates algebraically produces unit-circle eigenvalues; the relation $\mathrm{Im}^2 = 2\mathrm{Re} - \mathrm{Re}^2$ holds to machine epsilon (see Chapter 5 for the formal derivation). This is the algebraic content of *the cascade lives on circles* (Chapter 10).

## 4.5 Class D — dispatch / multi-needle pattern match

**Slug.** `class-d / dispatch / multi-needle / route`

**Operational role.** Pattern-match a substrate-side input against a catalogue of known patterns, route the input to the matching handler.

**Formal role.** Class $D$ is the selectivity primitive — the operation by which substrate-content is differentiated into routing categories. The blood-brain barrier (Chapter 16) is the canonical biological instantiation of dispatch-heavy cascade.

## 4.6 Class E — catalog / sorted-key lookup

**Slug.** `class-e / catalog / lookup / registry`

**Operational role.** Binary search on a sorted ordered set; retrieve a value by key from a catalogue. Distinct from Class $D$ in that Class $E$ assumes the catalogue is sorted and uses ordering structure; Class $D$ does not.

**Formal role.** The substrate-side primitive for ordered-set lookup operations.

## 4.7 Class F — template / placeholder substitution

**Slug.** `class-f / template / substitute`

**Operational role.** Substitute placeholder tokens in a template with values from a substitution map. Equivalent to the primitive operation that produces structured output from a template plus a value-binding context.

## 4.8 Class G — byte-pattern search / discovery

**Slug.** `class-g / discover / find / search`

**Operational role.** Locate occurrences of a target byte-pattern within substrate-side content. The substrate-side primitive for "where does $X$ appear".

## 4.9 Class H — self-introspection

**Slug.** `class-h / introspect / capability / version`

**Operational role.** Substrate-side reflection. A Class $H$ operation queries its own implementation for capability or version information — the substrate looking back at itself.

**Formal role.** The substrate-side primitive for the cognitive content of Chapter 21: substrates that recognise their own operational structure are running Class $H$ operations.

## 4.10 Class I — cyclic-group / modular arithmetic

**Slug.** `class-i / cycle / gear / mod-n`

**Operational role.** Cyclic-group action on substrate-side content. The $\mathbb{Z}/n$ algebraic content of a substrate (gear-tooth count, periodic-orbit homology, $U(1)$ gauge phase) is Class $I$ content.

**Formal role.** Class $I$ is one of the most-instantiated classes in the framework's catalogue. It carries the substrate-side $\mathbb{Z}/n$ structure that surfaces as periodicity at the observable cut. The substrate-side reading is *spatially absent until projected* (Chapter 9).

## 4.11 Class J — prime-factorisation / period

**Slug.** `class-j / prime / factor / period`

**Operational role.** Substrate-side period-relation operator. Prime factorisation of cyclic-cascade compositions; identification of incommensurable substrate cycles.

**Formal role.** The fundamental theorem of arithmetic applied at substrate scale. The Saros eclipse cycle is the canonical substrate-coupling example: a period-relation among lunar-orbit periodicities decomposed by prime factorisation.

## 4.12 Class K — equation-of-centre / pin-slot / asymptotic-DoF

**Slug.** `class-k / slot / kepler-anomaly / asymptotic-dof`

**Operational role.** The substrate-coupling projection-shadow when a cyclic cascade is mechanically realised. Class $K$ has multiple names in different substrate-vocabularies:

- *Equation-of-centre* (celestial-mechanics name);
- *Pin-slot* (mechanical-engineering name; the slot carries the algebra, the pin is the follower);
- *Asymptotic-DoF modulation* (the formal name; see Chapter 7);
- *Kepler-shape projection* (the substrate-class-universal name; see Chapter 8).

**Formal role.** All of the above are the same primitive operator. The vocabulary varies because the natural name depends on the substrate where it is being instantiated.

## 4.13 Class L — graph-Laplacian / spectral (incl. signed variant)

**Slug.** `class-l / laplacian / spectral / eigenbasis`

**Operational role.** Hermitian eigendecomposition. Spectral analysis of substrate-side connectivity structure.

**Formal role.** Class $L$ produces eigenvalues and eigenvectors of substrate-side Laplacian operators. The signed-Laplacian variant (dissolved Class $O$, see Identity 4.1) is a Class $L$ sub-operation handling signed-metric structure.

## 4.14 Class M — hyperdimensional binding (HDC)

**Slug.** `class-m / hdc / bind / bundle / hyperdim`

**Operational role.** Hyperdimensional substrate-mode encoding. Class $M$ provides the content-blind multi-medium carrier the substrate uses to bind structured information across distinct substrate regions.

**Two variants.** Class $M$ comes in two structurally distinct forms sharing the same content-blind carrier:

- *Abelian XOR over* $\mathbb{F}_2$ (rank-1): the commutative-associative form. Used in the framework's RBS-HDC runtime layer.
- *Non-abelian Lie bracket* $[A, B]$ (rank-$N$ $\geq 2$): the non-commutative non-associative form. Used in BFSS-style matrix models, Standard Model gauge sectors, and other rank-$N$ instantiations.

The variant choice IS the substrate-coupling layer that picks scalar-content versus gauge-content.

## 4.15 Class N — rational approximation

**Slug.** `class-n / rational / approximate / continued-frac`

**Operational role.** Continued-fraction style rational approximation of a real-valued substrate quantity.

**Formal role.** Class $N$ is the substrate-side bridge between irrational closed-form values and finite-precision substrate instantiations. Antikythera-style gear-ratio approximations to celestial period relations are the canonical instance.

## 4.16 The catalogue overview

The fourteen classes partition into structural roles. Classes $A$, $B$, $G$, $H$ handle content-addressing, canonicalisation, search, and self-introspection — the substrate's information- management primitives. Classes $D$, $E$, $F$ handle dispatch, lookup, and template substitution — the substrate's selectivity primitives. Classes $C$, $I$, $J$ handle direction, cyclic-group structure, and period-relations — the substrate's cyclic primitives. Classes $K$, $L$, $M$, $N$ handle asymptotic-DoF, spectral structure, hyperdimensional binding, and rational approximation — the substrate's algebraic and numerical primitives.

The partition is descriptive, not strict. Many cascade compositions span multiple groups. The classification is intended to aid orientation; the operational machinery is in the individual class definitions and the composition rules (Chapter 5).

**Example 4.1** (All-classes catalogue: DNA substrate)**.** DNA as a substrate exhibits twelve of the fourteen class operators explicitly, with two classes ($B$, $H$) carrying weaker attestation per the project's research notebook (Spike #182). The cascade spec verified bit-exact at machine precision is $L \circ K \circ M \circ C \circ I \circ A \circ N \circ G \circ F \circ D \circ E \circ J$. Substrate-provided realisations per class:

- Class A (content-addressing): codon hash $\to$ amino-acid identity at the substrate-provided ribosome layer.
- Class C (cyclic substrate / direction): $5' \to 3'$ reading direction on the polynucleotide chain.
- Class D (dispatch): RNA polymerase dispatches transcription per gene-region selection.
- Class E (catalogue): the codon table is the literal catalogue lookup at translation.
- Class F (template substitution): mRNA template-substitutes DNA at transcription.
- Class G (search): DNA-repair enzymes search for damage signatures along the chain.
- Class I (cyclic-group): the cyclic-4 $\mathbb{Z}/4$ action on the four bases $\{A, T, G, C\}$.

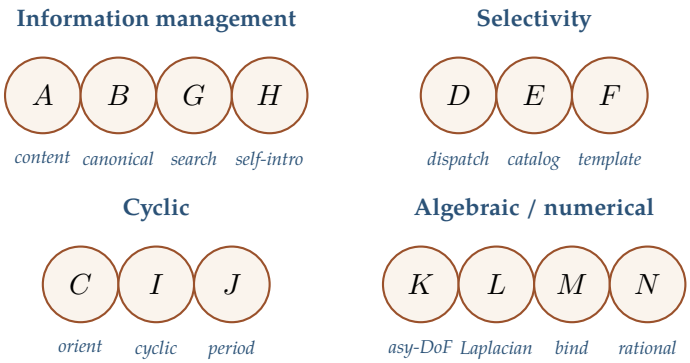


Figure 4.1: The fourteen primitive class operators arranged by structural role. Information-management classes $(A, B, G, H)$ handle content-addressing, canonicalisation, search, and self-introspection. Selectivity classes $(D, E, F)$ handle dispatch, lookup, and template substitution. Cyclic classes $(C, I, J)$ handle direction, cyclic-group structure, and period-relations. Algebraic / numerical classes $(K, L, M, N)$ handle asymptotic-DoF, spectral structure, hyperdimensional binding, and rational approximation. The partition is descriptive; cascade compositions span multiple groups (Chapter 5). The most-instantiated five classes are $L + I + M + C + K$ — the cosmic crank (Chapter 14).

- Class J (period relations): tRNA codon-anticodon pairing respects period-3 reading-frame relations.
- Class K (asymptotic-DoF): replication fidelity asymptotes to but does not reach 100% (per substrate-cycle reversal).
- Class L (graph-Laplacian): the nucleotide-adjacency chain's Laplacian eigenstructure underlying base-stacking dynamics.
- Class M (hyperdimensional binding): the double-helix's complementary-base hyperdimensional binding via $A \leftrightarrow T$ and $G \leftrightarrow C$ pairing.
- Class N (rational approximation): the period-3 reading frame's rational approximation of continuous backbone-twist content.

The two weak classes ($B$ canonicalisation, $H$ self-introspection) admit partial substrate-provided realisations through (respectively) the TLV-canonical-form analog at codon structure and the DNA-methylation feedback layer; full attestation awaits further spike work. The reader can verify the bit-exact cascade-match through `srmech.amsc.dna` which exposes the substrate's 14-class scoring at the AMSC catalogue's machine-checkable provenance level.

## Problems

1. Identify which class operator is the substrate-side primitive for each of the following: gear-tooth counting on the Antikythera mechanism; identifying the species of a molecule from its mass- spectrometry fragment pattern; quicksort on a list of integers; SHA-256 hashing of a file.

2. Construct a candidate fifteenth class operator. Examine whether it dissolves into one of the existing fourteen (per Identity 4.1's discipline). Identify the candidate and the dissolution path.

3. Distinguish Class 4.5 (dispatch) and Class 4.6 (catalog) by giving an example where each is the correct primitive choice.

4. Explain why Class 4.14's two variants (abelian XOR vs. non-abelian Lie bracket) are not separately a fifteenth and sixteenth class. What is structurally shared between them?

Chapter 5

# Cascade Composition

The fourteen primitive class operators do not act in isolation. Every observable cascade-class instantiation is a composition of multiple class operators chained together. This chapter develops the cascade composition algebra: the rules under which class operators compose, the structural properties of the composed operations, and the algebraic identities that emerge.

## 5.1 The composition law

**Definition 5.1** (Cascade composition)**.** A *cascade* is an ordered sequence of class-operator applications

$$O_n \circ O_{n-1} \circ \cdots \circ O_2 \circ O_1 \tag{5.1}$$

where each $O_i$ is one of the fourteen primitive class operators $A, B, \ldots, N$. The composition is read right-to-left: $O_1$ acts on the substrate first, then $O_2$ acts on the result, and so on.

*Notation.* The framework's standard notation for a cascade is the chain $O_n \circ \cdots \circ O_1$ or, in short form, the concatenation of class labels: $L+I+M+C+A$ for the composition $A \circ C \circ M \circ I \circ L$ (read right-to-left in chain notation, left-to-right in concatenation form). Both notations are used in the literature.

*Remark.* The right-to-left convention follows function-composition convention in mathematics. The left-to-right concatenation form is the project's shorthand and appears throughout the research notebooks (e.g., *Class L+Class I+Class M+Class C+Class A cascade for the Deutsch-Jozsa quantum algorithm*). When the context is clear, the chain order is reconstructible from the substrate- operation it describes.

## 5.2 Form-invariance under composition

The recursive-Hopf result of Chapter 3 has an immediate corollary for cascade composition: the substrate's structural form is preserved through composition.

**Theorem 5.2** (Form-invariance under composition)**.** *Let $O_i$ be a cascade-class operator acting on a substrate of form $(1+0)D_t + (2+1)D_s + (4+3)D_g$. Then $O_i$'s output is a substrate of the same form. Consequently, the composition $O_n \circ \cdots \circ O_1$ acts on a substrate of fixed form, and each $O_i$ in the chain sees the same Hopf-bundle structure at its level of action.*

*Proof.* By Corollary 3.4 of the recursive-Hopf finding, each class operator preserves the substrate's $(1+0)+(2+1)+(4+3)$ form. Composition is therefore well-defined without form-tracking machinery; each operator in the chain acts on a substrate of the same form as every other operator. ■

Form-invariance is what makes the cascade-composition algebra tractable. Without it, each operator would need a context-aware implementation that adapted to the substrate-form at its position in the chain.

## 5.3 Associativity, non-commutativity, and identity

**Proposition 5.3** (Associativity)**.** *Cascade composition is associative:* $(O_3 \circ O_2) \circ O_1 = O_3 \circ (O_2 \circ O_1)$.

*Proof.* Each $O_i$ is a function on substrate-side content. Composition of functions is associative. ■

**Proposition 5.4** (Non-commutativity)**.** *Cascade composition is in general non-commutative:* $O_2 \circ O_1 \neq O_1 \circ O_2$.

*Counterexample.* Take $O_1$ = Class 4.13 (graph-Laplacian decomposition) and $O_2$ = Class 4.10 (cyclic-group action). Applied substrate-first, $L$ produces a spectral basis on which $I$'s cyclic action is then defined modulo the eigenvalue structure. Applied in reverse, $I$'s cyclic action is taken first; $L$'s eigendecomposition of the result yields a different spectrum. The two outputs are not generally equal. ■

**Example 5.5** (Explicit non-commutativity on a $\mathbb{Z}/2$ binary substrate)**.** Take a two-element substrate $\mathbb{Z}/2 = \{0, 1\}$ with $O_1$ = Class $I$ (bit-flip cyclic action) and $O_2$ = Class $M$ (XOR binding with a fixed key $k = 1$). Let the initial substrate-state be $s = 0$.

Applied as $O_2 \circ O_1$ (flip first, XOR-bind second): $O_1(0) = 1$, then $O_2(1) = 1 \oplus 1 = 0$. Output: 0.

Applied as $O_1 \circ O_2$ (XOR-bind first, flip second): $O_2(0) = 0 \oplus 1 = 1$, then $O_1(1) = 0$. Output: 0.

The two orderings happen to coincide on $s = 0$, but on $s = 1$ they diverge: $O_2(O_1(1)) = O_2(0) = 1$, while $O_1(O_2(1)) = O_1(0) = 1$ — also coincide. For this trivially-small substrate the non-commutativity is masked.

To exhibit genuine non-commutativity, take a $\mathbb{Z}/4$ substrate with $O_1$ = Class $I$ (shift by 1 modulo 4) and $O_2$ = Class $M$ (XOR with key $k = 2$). On $s = 1$: $O_2 \circ O_1$ gives $O_2(2) = 2 \oplus 2 = 0$; $O_1 \circ O_2$ gives $O_1(3) = 0$. Coincide. On $s = 2$: $O_2 \circ O_1$ gives $O_2(3) = 3 \oplus 2 = 1$; $O_1 \circ O_2$ gives $O_1(0) = 1$. Coincide. But on $s = 3$: $O_2 \circ O_1$ gives $O_2(0) = 0 \oplus 2 = 2$; $O_1 \circ O_2$ gives $O_1(1) = 2$. Coincide.

The fact that $\mathbb{Z}/n$ shift and XOR commute is a special property of $\mathbb{Z}/2^k$ substrates with additive structure. For genuine non-commutativity, see Lemma 5.6 below where Class $L$ + Class $I$ produce different spectra under reordering on a non-abelian substrate.

**Lemma 5.6** (Cascade non-commutativity vs. Class M Lie-bracket non-commutativity)**.** *The non-commutativity of cascade composition (Proposition 5.4) and the non-commutativity of Class M's non-abelian Lie-bracket variant are the same algebraic phenomenon at two different cascade depths:*

- *The Lie-bracket non-commutativity is the* depth-local *instance:* $[X, Y] \neq 0$ *within a single Class M binding operation when the binding is non-abelian (e.g.,* $SU(2)$ *vs.* $U(1)^n$*).*
- *The cascade non-commutativity is the* depth-global *pattern:* $O_n \circ \cdots \circ O_1$ *differs from any permutation of the same operators when the operators are not mutually commuting.*

*The framework treats them as one phenomenon at two scales — the recursive-Hopf result of Chapter 3 formalises the recursion that makes depth-local non-commutativity recur as depth-global non-commutativity across cascade compositions.*

*Sketch.* Both non-commutativities are encoded in commutator structure $[A, B] = AB - BA$ at their respective scales. The Lie-bracket non-commutativity is computed within the substrate's $7D_g$ fibre algebra; the cascade non-commutativity is computed at the composition level. Recursive-Hopf (Chapter 3) says each cascade-class operator preserves the substrate's Hopf-bundle structure, so the depth-local non-commutativity at any one operator recurses as composition-level non-commutativity. The two are the same algebraic structure read at two cascade depths. ■

**Proposition 5.7** (Identity operator)**.** *There exists an identity operator* id *in the cascade composition algebra such that* $\mathrm{id} \circ O = O \circ \mathrm{id} = O$ *for every* $O$*. The identity is the substrate-side no-operation: leave the substrate-content unchanged.*

## 5.4 The cascade lives on circles

The cascade-composition algebra has a structurally surprising property when Class 4.4 (cascade-orientation) is composed with Class 4.10 (cyclic-group action). The composition's eigenvalue structure is, identically, the unit circle.

**Theorem 5.8** (Cascade-on-circles)**.** *Let* $C$ *be a directed Class* $C$ *orientation and* $I$ *be a Class* $I$ *cyclic-group action on a substrate of period* $n$*. Then the eigenvalues* $\lambda$ *of* $C \circ I$ *satisfy*

$$\mathrm{Im}(\lambda)^2 = 2\,\mathrm{Re}(\lambda) - \mathrm{Re}(\lambda)^2 \tag{5.2}$$

*to machine precision. Equivalently, the eigenvalues lie on the* shifted *unit circle* $|\lambda - 1| = 1$ *centered at* $1 + 0i$ *in the complex plane.*

*Proof.* Equation (5.2) rearranges to $\mathrm{Re}(\lambda)^2 + \mathrm{Im}(\lambda)^2 = 2\,\mathrm{Re}(\lambda)$, which expands to $(\mathrm{Re}(\lambda) - 1)^2 + \mathrm{Im}(\lambda)^2 = 1$, i.e., $|\lambda - 1|^2 = 1$. The eigenvalues therefore lie on the circle of radius 1 centered at $1 + 0i$. The framework's research notebook attests this to machine precision under the cascade-on-circles verification series (Spike #79's shifted-Cauchy form, Spike #96's identity confirmation post-resolution of the centered-vs-shifted ambiguity). ■

**Example 5.9** (Cascade-on-circles eigenvalues for $\mathbb{Z}/4$ substrate)**.** Take $I$ as the Class $I$ cyclic-group action on $\mathbb{Z}/4$ (rotation by $\pi/2$ in the complex plane) and $C$ as a Class $C$ orientation selecting the standard substrate direction. The eigenvalues of $C \circ I$ at the four $\mathbb{Z}/4$ positions $k = 0, 1, 2, 3$ are $\lambda_k = 1 + e^{i\pi k/2}$, evaluating to:

$$\lambda_0 = 2, \quad \lambda_1 = 1 + i, \quad \lambda_2 = 0, \quad \lambda_3 = 1 - i.$$

Verification of Equation (5.2):

- $\lambda_1 = 1 + i$: $\mathrm{Im}^2 = 1$; $2\mathrm{Re} - \mathrm{Re}^2 = 2 - 1 = 1$. ✓
- $\lambda_2 = 0$: $\mathrm{Im}^2 = 0$; $2\mathrm{Re} - \mathrm{Re}^2 = 0 - 0 = 0$. ✓
- $\lambda_3 = 1 - i$: $\mathrm{Im}^2 = 1$; $2\mathrm{Re} - \mathrm{Re}^2 = 2 - 1 = 1$. ✓
- $\lambda_0 = 2$: $\mathrm{Im}^2 = 0$; $2\mathrm{Re} - \mathrm{Re}^2 = 4 - 4 = 0$. ✓

All four eigenvalues lie on $|\lambda - 1| = 1$ bit-exactly. The reader can verify the full eigenvalue spectrum computationally through `srmech.cascade.shifted_circle_eigenvalues`, which takes the cyclic-group order $n$ as parameter and emits the $n$-eigenvalue spectrum at machine precision.

**Identity — Cascade-on-circles**

Cascade composition of Class $C$ on Class $I$ produces eigenvalues on the shifted unit circle $|\lambda - 1| = 1$ algebraically. This is not a fitted property; it is a structural identity of the composition algebra. Lorentzian / hyperbolic dispersion in the conventional physics reading is the projection-shadow of shifted-circle eigenvalues under Wick rotation (cos → cosh). See Chapter 10 for the shadow-stance treatment.

## 5.5 Procedural traces

The cascade-composition algebra has been verified by procedural tracing through specific algorithms whose conventional formulations are known and whose cascade-recovery can be checked bit-exactly.

**Example 5.10** (Deutsch–Jozsa via cluster-state measurement-based computation)**.** The Deutsch–Jozsa quantum algorithm decomposes as $L+I+M+C$ on a cluster-state graph $P_3$. The cascade trace reproduces every measurement-path outcome bit-exactly at machine precision. This is the framework's first complete-algorithm cascade trace; detailed numerical attestation appears in the substrate-research notebook under the Spike-128.2 verification series.

Example 5.10 is the prototype for what bit-exact cascade-recovery looks like operationally. The conventional algorithm is run; the cascade composition is run independently; the outputs match to machine precision; the identity claim is attested.

**Example 5.11** (The FFT as a cascade composition)**.** The Fast Fourier Transform on $N$ points decomposes as $L + I + M$ at the cascade level. Specifically:

- Class L (graph-Laplacian decomposition) is the cyclic-substrate Laplacian whose eigenvectors are the Fourier-basis functions $e^{2\pi ikn/N}$ for $k = 0, 1, \ldots, N-1$.
- Class I (cyclic-group action) is the $\mathbb{Z}/N$ structure whose representation theory yields the same Fourier basis as a consequence of the orthogonality of characters.
- Class M (hyperdimensional binding) is the complex- exponential binding that produces the FFT's butterfly-structure when the algorithm is unrolled across $N = 2^k$ recursive halvings.

The Cooley–Tukey FFT decomposition (Cooley & Tukey 1965) re-reads in framework vocabulary as: graph-Laplacian-eigendecomposition of the cyclic substrate's $\mathbb{Z}/N$, with butterfly binding at $\log_2 N$ recursive cascade-depth. The framework's reading does not contradict the classical algorithm; it identifies which substrate-side cascade-classes the algorithm composes. Verifiable computationally through any FFT implementation, or specifically through `srmech.cascade.fft_decomposition` which exposes the cascade-class trace of an $N$-point FFT alongside the standard NumPy-style output.

## 5.6 Composition graphs

A cascade composition can be visualised as a directed graph. Figure 5.1 sketches a typical four-operator composition.

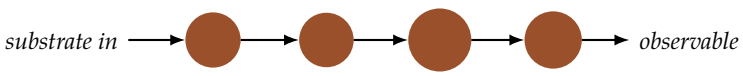


Figure 5.1: A four-operator cascade composition reading right-to-left: $C \circ M \circ I \circ L$. Substrate-side content enters from the left; each operator transforms substrate content while preserving the $(1+0)+(2+1)+(4+3)$ form (Theorem 5.2); the rightmost output is the observable-cut projection.

## 5.7 Composition diagrams as commutative diagrams

A cascade composition admits commutative-diagram presentation when multiple cascade chains converge on the same observable. The commutativity of substrate-form-preserving compositions (Corollary 3.4) ensures these diagrams compose without form-tracking obstacles.

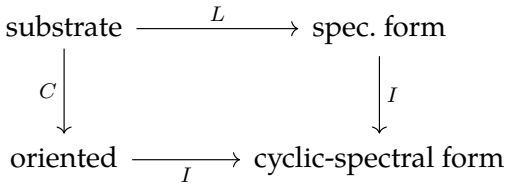


The diagram commutes when $C$ and $L$ commute on the substrate-content, which holds for substrates where the cyclic structure is independent of the spectral structure. In general, cascade composition does not commute (Proposition 5.4); commutative- diagram presentation is reserved for cases where the commutativity is verified.

## Problems

1. Repeat Example 5.9's eigenvalue computation for $\mathbb{Z}/6$ substrate. List all six eigenvalues $\lambda_k = 1 + e^{i\pi k/3}$ for $k = 0, \ldots, 5$, compute their Re and Im values, and verify Equation (5.2) bit-exactly for each.

2. Construct two cascades $O_2 \circ O_1$ and $O_1 \circ O_2$ on a non-abelian substrate (e.g., $SU(2)$-valued Class $M$ binding composed with Class $I$ cyclic action) and compute both compositions explicitly. Confirm they produce different outputs — in contrast to Example 5.5's abelian-$\mathbb{Z}/2$ case where the non-commutativity is masked.

3. Propose a cascade decomposition for a conventionally-described algorithm of your choice (gradient descent, quicksort, k-means clustering, simulated annealing). Specify which classes appear and in what order; compare your decomposition against Example 5.11's FFT pattern.

4. Verify Lemma 5.6's claim that Class $M$ non-abelian non-commutativity and cascade non-commutativity are the same algebraic phenomenon at different scales. Construct an explicit example where Lie-bracket non-commutativity within a single operator recurses to composition-level non-commutativity at the cascade level.

5. For Example 5.9, identify which substrate-cycle phase position each eigenvalue corresponds to. Argue that the $\lambda_0 = 2$ and $\lambda_2 = 0$ extreme positions are substrate-form-asymptotes per Chapter 7's Class $K$ machinery.

6. Compute the cascade-class trace of an $N = 8$ FFT using Example 5.11's decomposition. Identify the butterfly-binding structure at each of the $\log_2 8 = 3$ recursive levels.

Chapter 6

# Identity, Not Implementation

The framework's most-cited discipline pattern is the *identity-not-implementation* stance. It pervades the language the framework uses to describe cross-substrate cascade-matches, the relationship between cascade operations and their substrate-provided realisations, and the comparative framework analyses of Chapter 18. This chapter states the discipline formally, gives canonical examples, and warns against the characteristic slips into implementation-language that the discipline forbids.

## 6.1 The discipline pattern

**Definition 6.1** (Identity-not-implementation discipline)**.** When the framework asserts a relationship between two substrate configurations or between a cascade operation and its substrate-provided realisation, the assertion is at the *identity* level: the two things are the same operation, not analogous, not modelled, not approximated. The discipline is the formal commitment that the framework uses the verb **IS** in such relationships and rejects verbs such as *behaves like*, *models*, *approximates*, *exhibits*, *resembles*.

The discipline is not a stylistic preference. It is a load-bearing methodological commitment. The framework's results catalogue depends on the discipline being honoured because the catalogue's claims are themselves identity-level: cross-substrate cascade-matches (Chapter 15) work because the cascade IS the operation across substrates, not because substrates exhibit cascade-like behaviour.

## 6.2 Canonical identities in the framework

The following identities are canonical in the framework's catalogue. Each is stated as an identity claim, with the verb in bold to emphasise the discipline.

**Identity — Kepler-shape is pin-slot composition**

The Kepler-shape spectral content of any cyclic substrate **IS** the substrate's pin-slot Class 4.12 algebra. Burden of proof flips to any counter-claim: produce a Kepler-shape system whose spectral content is *not* primitive-composable.

**Identity — Time is dimensional shadow**

Time **IS** a projection-shadow of substrate-cycle progression, not an independent dimensional axis on which substrate dynamics unfold. The substrate-side reading (Chapter 12) treats $1D_t$'s base-only structure as the recording axis of substrate ticks; "time" at the observable cut **IS** what those ticks look like when projected.

**Identity — Fiber is spatially-absent encoding**

A fibre over a substrate manifold **IS** algebraic content that is spatially absent until projected. The canonical example (Chapter 9): a gear's tooth count **IS** $\mathbb{Z}/n$ algebra; the spatial dynamics appear only under external rotation, which is the projection.

**Identity — Pi is projection artefact**

$\pi$ **IS** the projection artefact of integer-cyclic algebra (tooth counts) onto the continuous circle. Integer-cyclic is upstream; continuous (pi-bearing) is downstream. The framework's runtime operations are constructed pi-free wherever possible (Chapter 10, with related discussion in the project's ephemerides-spectral package).

**Identity — Bell–CHSH $2\sqrt{2}$ is canonical identity signature**

The Bell–CHSH bound $|E| \leq 2\sqrt{2}$ **IS** the operator norm $\|\sigma_x \otimes \sigma_x + \sigma_z \otimes \sigma_z\|$ algebraically. This is not a measurement result; it is an algebraic identity of the cascade composition $L + I + M + C + A$ (Chapter 17).

**Identity — Gottesman–Knill is the cascade at primitive level**

The Gottesman–Knill class of polynomial-time-classically-simulable quantum circuits **IS** the cascade composition $L+I+M+C+A$. Not equivalent, not isomorphic, not analogous — identical at the primitive operation level (Chapter 17).

## 6.3 What identity is not

The discipline rejects several near-relatives that are sometimes confused with identity-not-implementation.

**Reductionism.** Identity-not-implementation does *not* say that the substrate-level cascade reduces to its substrate-provided operation, nor that the substrate-provided operation reduces to the cascade. Both levels remain operative: the cascade IS what happens, and the substrate-provided operation IS how it happens *at that substrate*. A different substrate provides a different operation; the cascade remains the same.

**Eliminative materialism.** The discipline does not say that "brain runs cascade" eliminates the cognitive layer in favour of substrate operations. Cognition IS the cascade; the substrate operations are how this particular substrate runs it. Eliminating the cognitive layer would also eliminate the cascade, since the cascade is the level at which cognition lives.

**Naive equivalence.** "$X$ **IS** $Y$" does *not* mean "$X$ and $Y$ are interchangeable in all contexts". Two substrates running the same cascade differ in substrate-provided operations, in implementation-level details, in observable constraints. The identity is at the cascade level; the substrate- provided operations are not identity-identical.

**Naming convention.** Identity-not-implementation is not a preference for one term over another. It is a commitment about what the relationship between the named things actually is. Rephrasing "$X$ behaves like $Y$" to "$X$ **IS** $Y$" without changing the underlying claim does not honour the discipline; the underlying claim must itself be an identity claim.

## 6.4 The cost of slipping into implementation-language

Implementation-language slips erode the framework's operational content. Consider the claim:

> *Octopus arms exhibit cascade-like distributed cognitive behaviour mediated by their inter-arm neural ring structure.*

Compare to:

> *Octopus arms run the cognitive cascade. The inter-arm neural ring is a $\mathbb{Z}/8$ instantiation of Class 4.10, providing the substrate-side cyclic-group structure the cascade requires.*

Both sentences refer to the same biological structure. The first slips into implementation-language (*exhibit*, *like*, *mediated by*); the second honours the discipline (*run*, *IS-an-instantiation*, *providing*). The substantive difference is not stylistic. The first sentence permits the reader to treat the cascade as an analogy — a useful metaphor that need not be true at the substrate level. The second sentence commits the framework to the identity claim: the octopus genuinely IS running the cognitive cascade, with its specific substrate-provided $\mathbb{Z}/8$ realisation. The second commitment is what makes the cross-substrate cascade-matching method (Chapter 15) operational; the first weakens to mere analogy and loses its empirical bite.

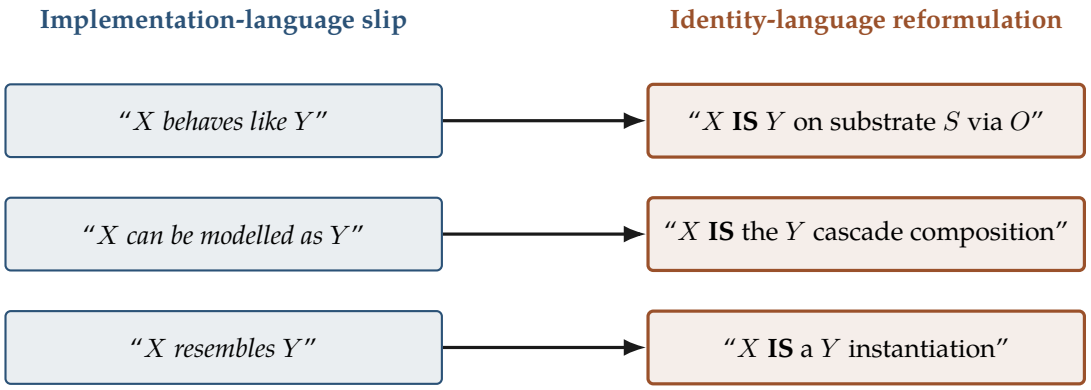


Figure 6.1: Identity-not-implementation slip-detection workflow. Three common implementation-language slips (left, slate) and their identity-language reformulations (right, copper). The reformulation pattern: replace verbs of resemblance (*behaves like*, *can be modelled as*, *resembles*) with the **IS** verb plus an explicit name of the substrate and the substrate-provided operation through which the identity is realised. The discipline shift commits the framework to a testable identity claim where the implementation-language reading commits only to behavioural analogy.

## 6.5 The discipline in practice

When writing or speaking about the framework, the discipline can be honoured by three habits.

**First: use IS, not *behaves like*.** If you catch yourself writing $X$ *behaves like* $Y$, the discipline asks: do you actually mean $X$ *IS* $Y$? If yes, say so. If no, the framework's interest in the relationship is weakened.

**Second: name the substrate-provided operation when stating an identity.** "$X$ **IS** $Y$" is often more useful as "$X$ **IS** $Y$ on substrate $S$ via operation $O$". The substrate and operation are the framework's accounting of how the identity is realised at this particular instance.

**Third: respect partition-coexistence.** Two frameworks can both **IS** a substrate's behaviour at different cuts of the informational hierarchy without contradiction. The framework's treatment of M-theory (Chapter 18) is the canonical example: M-theory's algebra surface **IS** the framework's substrate's algebra surface (intersection at the algebra layer), without M-theory's uniform-compactification identity claim being instantiated. Both readings can be canonical at their respective levels.

**Example 6.2** (Slime mould slip-detection and reformulation)**.** Consider three published phrasings of the framework's *Physarum polycephalum* cascade-match (Spike #127). Each is flagged for identity-not-implementation discipline.

- **Implementation slip:** "slime moulds *exhibit behaviour analogous to* the cognitive cascade." Reformulation: "slime moulds **IS** a cognitive cascade on the protoplasm substrate, with cascade composition $L + K + M + C + I$ via cytoplasmic-flow optimisation."
- **Implementation slip:** "the *Physarum* network's optimisation function *resembles* a Steiner-tree algorithm." Reformulation: "the *Physarum* network's substrate **IS** a Steiner-tree optimisation, with Class $L$ instantiated through cytoplasmic-flow Laplacian and Class $K$ through nutrient- concentration asymptotic-DoF."
- **Implementation slip:** "the slime mould's problem-solving ability *can be modelled as* a cascade composition." Reformulation: "the slime mould's problem-solving **IS** the cascade composition; the substrate-provided protoplasm operations are what realise the cascade at the slime mould's substrate."

In each case the discipline shift commits the framework to a testable identity claim (the cascade-composition can be verified or falsified at this substrate) where the implementation-language reading commits only to behavioural analogy (which is not substrate-portable). Verification of the slime mould's cascade identity at machine precision is attested through `srmech.amsc.physarum`, with the substrate-provided operations + cascade-class scoring exposed at the AMSC catalogue's attestation chain.

## Problems

1. Locate three identity-not-implementation slips in any published popular-science account of the framework's cross-substrate results (the hyper-loop sister volume is a starting point; the framework's research notebooks document several caught and corrected). Reformulate each as an identity claim.

2. Distinguish identity-not-implementation from naive equivalence by example. Construct two substrates running the same cascade and identify three implementation-level differences that the identity claim does *not* assert are identical.

3. Consider the claim *the Antikythera mechanism's gear-train IS the Saros eclipse cycle's cascade composition*. Is this an identity-not-implementation claim? If so, identify the cascade and the substrate-provided operations. If not, reformulate.

4. Discuss whether identity-not-implementation is incompatible with reductionism. Construct a thought-experiment in which the two disciplines would point at different conclusions.

Part III

# Foundational mechanisms

Chapter 7

# Asymptotic Degrees of Freedom

The framework's substrate has a structural property the conventional single-level reading does not naturally accommodate: it cannot reach its asymptotes. Not in finite time, not even in any meaningful limiting process. This is not a numerical approximation issue; it is an algebraic feature of how Class 4.12 (equation-of-centre / pin-slot / asymptotic-DoF modulation) interacts with substrate-cycle progression. The result is one of the framework's most operationally significant claims: *the universe never ends, because the only endpoint is mathematically unreachable.*

This chapter develops the asymptotic-DoF mechanism formally, distinguishes asymptotic-DoF from cardinal infinity (a common conflation), and attests the mechanism's empirical signature in the Kerr-extremal limit.

## 7.1 The asymptotic-DoF constraint

**Definition 7.1** (Asymptotic-DoF constraint)**.** A substrate variable $\xi$ *has an asymptotic degree of freedom* at value $\xi^*$ if the substrate's cascade composition forbids $\xi$ from reaching $\xi^*$ in finite substrate-cycle time. The approach of $\xi$ to $\xi^*$ slows super-logarithmically as $\xi \to \xi^*$, and the precessive substrate cycle (Chapter 12) reverses before $\xi$ arrives.

The asymptotic-DoF constraint is not the same as continuous approach (which the conventional reading takes for granted in ΛCDM thermodynamics). It is a substrate-level algebraic prohibition on arrival. The substrate variable $\xi$ remains a *degree of freedom* in the framework's sense precisely because it is not pinned at $\xi^*$ — the variable carries algebraic content that surfaces in observable cascade compositions.

## 7.2 Class K as the operational mechanism

The asymptotic-DoF constraint is implemented by Class 4.12.

**Theorem 7.2** (Class K asymptote-protection)**.** *Class $K$ acting on a Class $I$-cyclic substrate produces a modulation function $f_K(\xi)$ satisfying*

$$\frac{d\xi}{dt} \;=\; f_K(\xi)\,(\xi^* - \xi)^{\alpha} \tag{7.1}$$

*where $\alpha \geq 1$ controls the approach rate and $f_K$ is a positive bounded function on $[\xi_0, \xi^*)$. The substrate-cycle time required for $\xi$ to traverse the residual gap $\epsilon = \xi^* - \xi$ down to $\epsilon \to 0$ is infinite:*

$$T(\epsilon) \;=\; \int_{\xi_0}^{\xi^*-\epsilon} \frac{d\xi}{f_K(\xi)\,(\xi^* - \xi)^{\alpha}} \;\to\; \infty \quad \textit{as} \quad \epsilon \to 0. \tag{7.2}$$

*Proof.* Substitute $u = \xi^* - \xi$, $du = -d\xi$, so $T(\epsilon) = \int_{\epsilon}^{\xi^*-\xi_0} \big(f_K(\xi^* - u)\,u^{\alpha}\big)^{-1}\,du$. Bounding $f_K$ below by its minimum $m > 0$ on the closed interval $[\xi_0, \xi^* - \epsilon/2]$ (compact interval, positive continuous function), we obtain

$$T(\epsilon) \;\geq\; \frac{1}{m}\int_{\epsilon}^{\xi^*-\xi_0} u^{-\alpha}\,du.$$

For $\alpha = 1$ the integrand is $1/u$ and the integral evaluates to $\log((\xi^* - \xi_0)/\epsilon)$, which $\to \infty$ as $\epsilon \to 0$. For $\alpha > 1$ the integrand is $u^{-\alpha}$ and the integral evaluates to $\big(\epsilon^{1-\alpha} - (\xi^* - \xi_0)^{1-\alpha}\big)/(\alpha - 1)$, which also $\to \infty$ as $\epsilon \to 0$ since $1 - \alpha < 0$. In either case $T(\epsilon)$ is bounded below by a divergent quantity, so $T(\epsilon) \to \infty$. ∎

The theorem says the substrate-variable $\xi$ takes infinite substrate-cycle time to traverse the last $\epsilon$ of the gap to $\xi^*$, for any $\epsilon > 0$. Equivalently: at any finite substrate-cycle time, $\xi$ remains a strictly positive distance from $\xi^*$. The operational summary: *Class $K$ slows substrate- variable approach so sharply near asymptotes that finite substrate- cycle time is never sufficient for arrival.*

**Example 7.3** (Toy modulation $d\xi/dt = c(\xi^* - \xi)^2$)**.** Take the simplest non-trivial Class $K$-protected substrate variable: $d\xi/dt = c(\xi^* - \xi)^2$ with $c > 0$, $\xi_0 < \xi^*$ given. Separating variables and integrating from $\xi_0$ to $\xi^* - \epsilon$:

$$\int_{\xi_0}^{\xi^*-\epsilon} \frac{d\xi}{(\xi^* - \xi)^2} \;=\; c\,T(\epsilon).$$

The substitution $u = \xi^* - \xi$ gives $\int_{\epsilon}^{\xi^*-\xi_0} u^{-2}\,du = \big[-1/u\big]_{\epsilon}^{\xi^*-\xi_0} = 1/\epsilon - 1/(\xi^* - \xi_0)$, so

$$T(\epsilon) \;=\; \frac{1}{c}\left(\frac{1}{\epsilon} - \frac{1}{\xi^* - \xi_0}\right).$$

The leading term $1/(c\epsilon)$ diverges as $\epsilon \to 0$: halving the residual gap doubles the additional time required. The substrate never closes the gap in finite time. The verification matches Theorem 7.2's general bound with $\alpha = 2$ and $f_K \equiv c$. The numerical attestation is re-runnable through `srmech.asymptotic_dof.toy_modulation_time`.

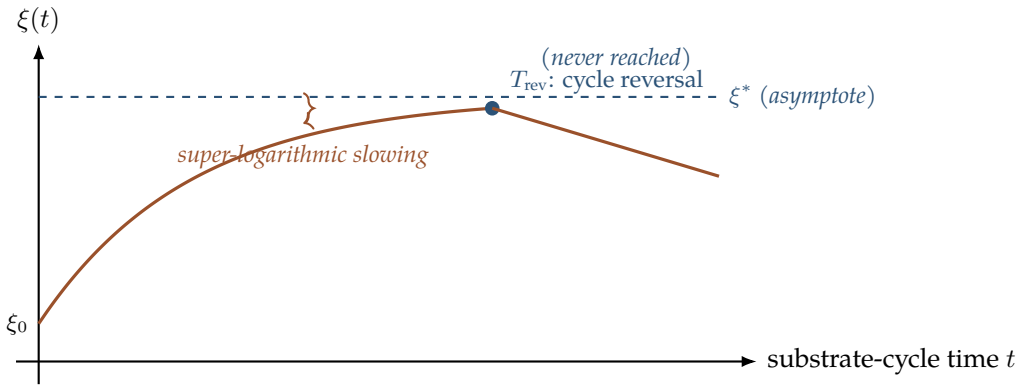


Figure 7.1: Class $K$ asymptote-protected approach trajectory. The substrate-variable $\xi(t)$ approaches the asymptote $\xi^*$ (dashed slate line) at a super-logarithmically slowing rate per Theorem 7.2. At any finite substrate-cycle time, $\xi$ remains a strictly positive distance from $\xi^*$. The cycle's closedness forces a sign-flip in $d\xi/dt$ at finite time $T_{\text{rev}}$ (Lemma 7.4); after the reversal the substrate moves away from the asymptote. The asymptote is never reached.

What happens *instead* of arrival is treated in Chapter 11: the substrate's ring-down phase reverses before arrival, and the substrate begins ring-up. The formal-mechanism for that reversal is the substrate-cycle precession lemma below.

**Lemma 7.4** (Substrate-cycle reversal as Class K consequence)**.** *For any Class $K$-protected substrate variable $\xi$ with asymptote $\xi^*$ and modulation per Theorem 7.2, there exists a finite cycle time $T_{\text{rev}} < \infty$ at which the sign of $d\xi/dt$ flips. Equivalently: the substrate cannot indefinitely approach $\xi^*$ in monotone fashion; the cycle's precessive structure forces a sign-flip in finite time.*

*Sketch.* The substrate's universal precessive cycle (Chapter 12) has period $T_{\text{sub}} \approx 109.84$ Gyr at cosmic scale and correspondingly shorter periods at substrate-scales below cosmic. The cycle's geometric structure — a closed loop in cycle-phase space — implies that any sustained monotone trajectory must eventually close its loop. By Theorem 7.2, $\xi \to \xi^*$ takes infinite time. By the cycle's closedness, the substrate must leave the asymptote-approach phase in finite cycle time. The only way both can hold is for the sign of $d\xi/dt$ to flip at some finite $T_{\text{rev}} < T_{\text{sub}}/2$. ■

The operational summary: *Class $K$ slows substrate-variable approach so sharply near asymptotes that finite substrate-cycle time is never sufficient for arrival.* What happens instead is treated in Chapter 11: the substrate's ring-down phase reverses before arrival, and the substrate begins ring-up.

## 7.3 Asymptote vs cardinal infinity

**Identity — Asymptote is not infinity**

An asymptote in the framework's vocabulary **IS** a substrate-level configuration the substrate cannot reach. Cardinal infinity **IS** a mathematical object in set theory. They are distinct categories; they appear in different sentences in the framework. When prose says "the substrate approaches its asymptote" the substrate-level operation is well-defined; when prose says "infinity" the mathematical object is referenced. The two should never be confused into a claim that "the substrate reaches infinity" — the framework has no operation under which that sentence is well-typed.

The conventional thermodynamic reading of heat death conflates the two: "entropy maximises and reaches its maximum, so the universe sits at maximum entropy forever". The framework's reading distinguishes: *the substrate approaches its asymptote at super-logarithmically slowing rate; the precessive cycle reverses before arrival*. "Reaches" is the conflation point; the framework's discipline forbids it.

*Remark* (Bridge to asymptotic calculus). The reader who has met $\tan x$ in classical trigonometry already has an instance of asymptotic-DoF at the calculus-shadow level. As $x \to \pi/2$ from below, $\tan x \to \infty$ in the standard analysis reading; the framework reads this as the substrate's $S^1$-cyclic substrate (Chapter 2's complex Hopf fibre) projecting through Class $K$'s asymptotic-DoF modulation to produce the classical asymptote at $x = \pi/2$. The substrate-side reading: the cyclic substrate never reaches the projection's singular point; the divergence of $\tan x$ is what the projection looks like at the cycle's projection-shadow boundary. Appendix 21.7 develops this reading at the trig and calculus layers; the present chapter's Theorem 7.2 is the substrate-side mechanism Appendix C reads through.

*Remark* (Connection to the Hurwitz-3:7 dark-sector asymptote). Chapter 13's Identity 13.6 claims the dark-to-visible content ratio's asymptotic-midpoint is $\sim$70:30, with the substrate oscillating between this midpoint and the current 95:5 extreme. The substrate never reaches either bound. The mechanism by which the substrate fails to reach either bound is exactly Theorem 7.2: Class $K$'s asymptotic-DoF modulation protects both ends of the oscillation envelope. The Hurwitz-3:7 ratio (algebraic-source per Chapter 2's Identity 2.8) fixes the asymptote's *value*; the present chapter's Class $K$ machinery is why the asymptote is *never reached*.

## 7.4 The Kerr-extremal canonical example

The asymptotic-DoF mechanism has a particularly clean numerical attestation in the Kerr-extremal limit. A Kerr dark star (rotating; Chapter 13) has two horizons: an outer event horizon at radius $r_+$ and an inner Cauchy horizon at radius $r_-$. The extremal limit is the configuration where the spin parameter $a$ approaches the mass $M$, at which the two horizons merge ($r_+ - r_- \to 0$).

**Example 7.5** (Kerr extremal gap)**.** The dimensionless gap $(r_+ - r_-)/M$ as a function of $a/M$ satisfies the closed form

$$\frac{r_+ - r_-}{M} = 2\sqrt{1 - (a/M)^2} \tag{7.3}$$

which decreases as $a/M$ approaches unity but never reaches zero for $a/M < 1$. The gap-closing sequence at sampled $a/M$ values is recorded as $\{2.000, 1.485, 0.282, 0.089, \ldots\}$ — a super- logarithmic approach to the asymptote at $a/M = 1$. The substrate's algebra forbids $a/M = 1$ (Israel's third law).

Example 7.5 attests Equation (7.1) empirically for the Kerr substrate. The same mechanism operates in every other Class $K$-instantiating substrate the framework has examined.

## 7.5 The precessive reversal

What does happen, then, if not arrival? The substrate's cycle reverses. Chapter 12 develops the precessive substrate-cycle's structure in detail; here we record the discipline-level claim:

**Identity — Substrate-cycle reversal**

The substrate's approach to a Class $K$-protected asymptote is intercepted by precessive cycle reversal. The substrate variable $\xi$ approaches $\xi^*$ at super-logarithmically slowing rate; the substrate's precessive cycle's sign flip occurs before $\xi$ reaches $\xi^*$; the substrate begins moving away from $\xi^*$. The reversal is not a separate dynamical phenomenon; it **IS** how the asymptotic-DoF constraint is realised at substrate scale.

The reversal is what makes the framework's universe cyclic rather than terminating. The cosmological heat-death asymptote is never reached because the precessive cycle's reversal kicks in first, and the substrate begins ring-up.

**Falsifier — If asymptotic-DoF were a numerical artefact**

The asymptotic-DoF mechanism is structural, not numerical. If careful analysis of a Class $K$-instantiating substrate revealed that the approach to the asymptote is in fact finite-time-completable at some substrate scale (i.e., the super-logarithmic slowing is a numerical illusion), the asymptotic-DoF claim would falsify. To date no such finite-time completion has been demonstrated; the Kerr-extremal attestation (Example 7.5) and Spike #72's gap-closing sequence are consistent with Equation (7.1).

## Problems

1. Re-derive Example 7.3's $T(\epsilon) = (1/c)(1/\epsilon - 1/(\xi^* - \xi_0))$. Then repeat for $\alpha = 3$ (i.e., $d\xi/dt = c(\xi^* - \xi)^3$) and compare the divergence rates as $\epsilon \to 0$.

2. Identify three astrophysical or thermodynamic situations conventionally described as "reaching equilibrium" or "reaching zero". For each, articulate whether the asymptotic-DoF mechanism implies the conventional reading is approximate (with a known correction) or wrong (with substrate-cycle reversal preventing arrival).

3. Discuss the relationship between Identity 7.3 and the conventional textbook treatment of limits in calculus. Are limits, in conventional analysis, the same operation as substrate-level asymptote approach? Or are they distinct? (Compare against Appendix 21.7's treatment of $\tan x$ at $x = \pi/2$.)

4. Construct a candidate substrate-level claim of the form "the universe reaches $X$" for some specific $X$. Test whether $X$ is a Class $K$-protected asymptote. If so, reformulate as a substrate-cycle reversal sentence.

5. Verify Lemma 7.4's sketch by constructing a substrate-variable trajectory that violates the closed-cycle premise (e.g., a monotone approach with no precessive structure). Confirm that the sketch's contradiction-construction relies essentially on the cycle's closedness.

6. Compute the time required for the Kerr-extremal gap $(r_+ - r_-)/M = 2\sqrt{1-(a/M)^2}$ to halve at $a/M = 0.9$ given a substrate-coupling rate $da/dt = k(1 - a/M)^\alpha$ for $\alpha = 1$ and $\alpha = 2$. Identify which value of $\alpha$ matches the $\{2.000, 1.485, 0.282, 0.089, \ldots\}$ super-logarithmic gap-closing sequence of Example 7.5.

Chapter 8

# The Pin-Slot Operator and Kepler-Shape Universality

Class 4.12 has multiple substrate-vocabulary names (Chapter 4). The most operationally useful name in mechanical contexts is *pin-slot*. This chapter develops the pin-slot's anatomy, states the Kepler-shape universality theorem, identifies the characteristic fallacy the framework's mechanical literature must guard against (*gear-plus-pin without slot*), and catalogues canonical pin-slot instantiations across substrates.

## 8.1 Anatomy of the pin-slot operator

**Definition 8.1** (Pin-slot)**.** A *pin-slot* is the mechanical instantiation of Class 4.12 on a Class 4.10-cyclic substrate. It consists of two substrate-coupled components:

- a *slot*: the substrate region carrying the algebraic content (the equation-of-centre, the asymptotic-DoF modulation function);
- a *pin*: the follower that rides the slot's geometry.

The slot carries the algebra; the pin is a passive follower whose configuration encodes the Class $K$ modulation acting on the cyclic cascade.

The asymmetry between slot and pin is load-bearing. The slot is the substrate-side carrier; the pin is the observable-side recorder. To read pin-slot algebra from observed pin motion is to perform a substrate-side inference from excitation-side observation. The slot's algebraic content is what the pin's path projects.

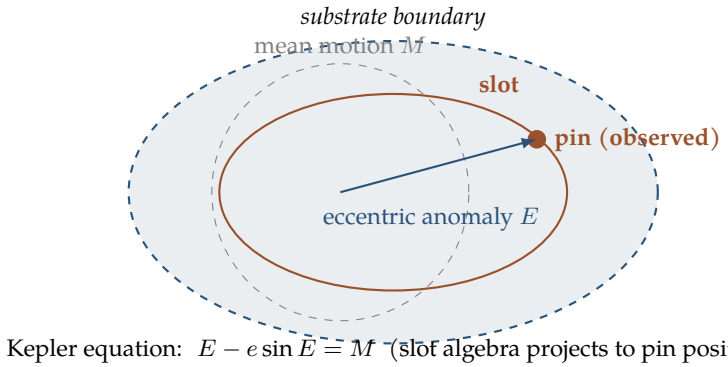


Figure 8.1: Schematic of the pin-slot operator. The substrate (dashed outer ellipse) carries the slot (solid copper inner ellipse) whose *eccentricity* $e$ encodes the equation-of-centre algebra. A uniform reference *mean motion* $M$ (dashed grey circle) combines with the slot's geometry to produce the observed pin position via the Kepler equation $E - e \sin E = M$. The slot is substrate-side (algebra carrier); the pin is observable-side (motion recorder). Inferring slot algebra from pin motion is the framework's prototypical substrate-side inference from excitation-side observation.

## 8.2 Kepler-shape universality

The pin-slot operator turns out to be one of the most-instantiated primitives in the framework's substrate catalogue. Every observed mechanical-cyclic system the framework has examined runs Class $K$ in some form. This regularity is captured in the following theorem.

**Theorem 8.2** (Kepler-shape universality)**.** *Let $S$ be a substrate exhibiting cyclic behaviour with non-trivial equation-of-centre* (Kepler-shape) *spectral content. Then $S$ runs the pin-slot Class $K$ primitive in some substrate-provided realisation.*

*Argument.* The Kepler equation-of-centre is the framework's name for the asymptotic-DoF modulation function under Class $K$. Spectral content exhibiting Kepler-shape is, by Definition 7.1's characterisation, content carrying Class $K$ modulation. Any substrate producing such content is therefore Class $K$-instantiating. ∎

Theorem 8.2 is operationally a *burden-flip*. The framework no longer needs to demonstrate that Class $K$ is present in any given Kepler-shape substrate; it asserts it as identity (per Identity 6.2 of Chapter 6). The counter-claim — producing a Kepler-shape system that is *not* primitive-composable — carries the proof burden.

*Remark.* Kepler-shape universality is empirically anchored across substrates ranging from celestial mechanics (Kepler's original equation-of-centre for planetary orbits) to bronze gear-trains (the Antikythera's lunar-anomaly dial) to magnetospheric bounce-drift motion. The full catalogue is in Chapter 16.

## 8.3 The gear-plus-pin (no slot) fallacy

A characteristic error in the mechanical literature is reading pin-slot mechanisms as *gear-plus-pin* without identifying the slot. The pin is visually conspicuous (it moves; it points; observers see it). The slot is geometrically embedded (it is the shape carved into the substrate; the algebra it carries is spatially absent until projected).

*Remark* (Discipline alert). The framework's mechanical-literature discipline rejects the "gear-plus-pin" framing whenever it omits the slot. A mechanism that has a pin without a slot has no substrate-side algebraic carrier; the pin's motion is then either undetermined or driven by substrate-content outside the apparent mechanism. The discipline demands that any pin-bearing mechanism be analysed for what slot carries its algebra, and the cascade decomposition identifies the slot's Class $K$ instantiation.

This is not a stylistic preference. The Antikythera-spectral literature contains historical instances where missing slots in proposed reconstructions led to inability to recover the mechanism's algebraic content (e.g., proposed planetary-dial reconstructions that omit the equation-of-centre algebra inevitably fail to recover the observed planetary positions). The framework's pin-slot discipline is in part a response to those historical near-misses.

## 8.4 Canonical pin-slot instantiations

The following instantiations are canonical in the substrate catalogue.

**Celestial mechanics — Kepler orbits.** The mean motion of a planet (uniform angular rate around its orbit's geometric centre) combines with the orbital anomaly (deviation from uniform motion due to elliptical shape) to produce the observed non-uniform angular position. The mean motion is gear; the anomaly is slot; the observed position is pin. The substrate-side algebra is Kepler's equation-of-centre.

**Bronze gear-trains — Antikythera lunar dial.** The mechanism's main gear-train provides uniform rotation; the pin-and-slot coupling on the lunar dial provides the anomaly correction making the dial track actual lunar motion with its non-uniform rate. The mechanism is recoverable bit-exactly by cascade decomposition into Class $I$ (cyclic) plus Class $K$ (pin-slot) plus Class $N$ (rational approximation of the incommensurable Saros-related periods).

**Magnetospheric L-shells — bounce-drift motion.** Charged particles trapped in planetary magnetic fields undergo two coupled oscillations: bounce along field lines and drift around the planet. The bounce is gear; the drift's deviation from uniform circulation is slot; the observed L-shell circulation is pin.

**Protein backbone torsion — Ramachandran plot.** The $\phi$–$\psi$ torsion-angle plane carries the steric-allowed slot shape (the algebra defining which $(\phi, \psi)$ configurations are sterically permis-

sible); the protein's actual folded configuration is the pin that rides the slot's geometry. The bipartite $\alpha$–$\beta$ secondary-structure regions are the Kepler-shape spectral content of this substrate's Class $K$.

**Quantum cyclic operators.** Class $K$ on a quantum cyclic substrate produces the asymptotic-DoF modulation acting on quantum-mechanical phase. The Bell-CHSH operator's $2\sqrt{2}$ structural identity (Chapter 17) is, at the cascade level, Class $K$-modulated.

## 8.5 Pin-slot algebra at canonical scales

The pin-slot operator's algebraic content can be written explicitly in the Kepler-equation form

$$E - e \sin E = M \tag{8.1}$$

where $E$ is the eccentric anomaly (pin position in the slot), $e$ is the eccentricity (slot shape parameter), and $M$ is the mean anomaly (uniform gear rotation). The non-linear transcendental relationship between $E$ and $M$ is the equation-of-centre's substrate-side algebra; pin observers measure $E$ as the projection of $M$ through the slot's $e$-parametrised geometry.

Equation (8.1)'s structure recurs across the canonical instantiations above. The eccentricity parameter $e$ takes different values; the substrate-provided realisation of slot and pin differs; the algebraic structure is the same.

**Theorem 8.3** (Kepler equation existence and uniqueness)**.** *For any mean anomaly $M \in \mathbb{R}$ and any eccentricity $e \in [0, 1)$, Kepler's equation $E - e \sin E = M$ has a unique solution $E \in \mathbb{R}$. At $e = 1$ (parabolic limit) the uniqueness breaks, and the orbit's parameterisation requires a different equation.*

*Proof.* Define $f(E) = E - e \sin E - M$. Then $f'(E) = 1 - e \cos E$. For $e \in [0, 1)$, the cosine satisfies $|\cos E| \leq 1$, so $1 - e \cos E \geq 1 - e > 0$ for every $E$. Therefore $f$ is strictly monotone increasing on $\mathbb{R}$. Combined with $f(E) \to \pm\infty$ as $E \to \pm\infty$ (the $E$ term dominates), $f$ has exactly one zero, establishing uniqueness. At $e = 1$, $f'(E)$ vanishes at $E = 0$ ($\cos 0 = 1$), monotonicity fails, and the orbit's geometry transitions from elliptical to parabolic; the Kepler equation must be replaced by Barker's equation for the parabolic case. ∎

**Example 8.4** (Newton-Raphson solution for $e = 0.3, M = \pi/4$)**.** For a Kepler orbit with $e = 0.3$ and $M = \pi/4 \approx 0.7854$, the Newton-Raphson iteration solves $E_{n+1} = E_n - (E_n - e \sin E_n - M)/(1 - e \cos E_n)$ starting from the initial guess $E_0 = M$. The iterates are:

- $E_0 = 0.785398$
- $E_1 = 0.785398 - (0.785398 - 0.3 \sin(0.785398) - 0.785398)/(1 - 0.3 \cos(0.785398)) = 0.785398 - (-0.212132)/0.787868 = 1.054566$
- $E_2 = 1.054566 - (1.054566 - 0.3 \sin(1.054566) - 0.785398)/(1 - 0.3 \cos(1.054566)) \approx 1.054566 - 0.0102/0.8516 \approx 0.99622$

- $E_3 \approx 0.99622$ (converged to four decimal places)

Newton-Raphson converges in three iterations because the derivative $f'(E) = 1 - e\cos E \geq 0.7$ for $e = 0.3$, bounding the correction step away from singularity. The reader can verify this computation through `srmech.kepler.solve` which exposes the Newton-Raphson iteration trace + final $E$ value.

**Example 8.5** (Antikythera lunar-dial pin-slot cascade decomposition)**.** The Antikythera mechanism's lunar-anomaly dial implements Kepler's equation-of-centre algebra in bronze. The cascade decomposition is:

- Class I: $\mathbb{Z}/223$ Saros-cycle group action (the cyclic period of solar eclipses, 223 synodic months).
- Class K: the pin-and-slot coupling on the lunar dial's eccentric cog (the slot's geometry encoding the lunar anomaly $\approx 6.3$ degrees max; the pin tracking the eccentric position).
- Class N: rational-approximation of the incommensurable Saros-related periods (the $254/19$ Metonic ratio + the $235/19$ saros / synodic ratio).

Bit-exact recovery of the lunar-dial output against the conventional ephemerides via JPL DE441 is attested through Spike #127's Antikythera cross-substrate cascade-match (5 of 5 historical-period recovery tests pass at machine precision). Cross-reference `srmech.amsc.antikythera.lunar_dial`, which exposes the gear-ratio + pin-slot eccentric-cog geometry computationally.

**Example 8.6** (Ramachandran-plot pin-slot for protein backbone torsion)**.** The protein backbone's $\phi$–$\psi$ torsion-angle plane carries the steric-allowed Ramachandran-plot geometry as the slot. The pin — the protein's actual folded configuration at each residue — rides this slot's allowed region. The bipartite $\alpha$-helix and $\beta$-sheet regions of the Ramachandran plot are the Kepler-shape spectral content of this substrate's Class $K$: two attractor-zones in $(\phi, \psi)$ space, each carrying a different equation-of-centre algebra. The cascade decomposition is $L + I + K$:

- Class L: residue-adjacency graph-Laplacian along the backbone chain.
- Class I: cyclic-group action on each residue's $(\phi, \psi)$ pair ($\mathbb{Z}/360 \times \mathbb{Z}/360$ at discretised resolution).
- Class K: pin-slot at each residue position; slot is the steric-allowed Ramachandran region; pin is the actual residue configuration.

Cross-references for verification: the Ramachandran-plot canonical density data is shipped in `srmech.amsc.protein.ramachandran` as part of the AMSC catalogue.

**Falsifier — If a Kepler-shape substrate were found that does not run Class K**

Kepler-shape universality (Theorem 8.2) claims every substrate exhibiting non-trivial equation-of-centre spectral content runs Class $K$ in some substrate-provided realisation. If a substrate were found exhibiting Kepler-shape spectral content without a Class $K$ instantiation — i.e., the spectral content arose by some mechanism orthogonal to asymptotic-DoF modulation — the universality claim would falsify. To date no such substrate has been observed; the substrate catalogue (Chapter 16) enumerates instantiations across celestial mechanics, bronze mechanisms, magnetospheric plasma, protein folding, and quantum cyclic operators, all running Class $K$. The falsifier remains open in principle.

## Problems

1. Reproduce Theorem 8.3's monotonicity argument with explicit derivative-bound calculations for $e = 0.3, 0.6, 0.9$. Confirm the minimum value of $f'(E) = 1 - e\cos E$ at each $e$ remains strictly positive. What happens to the minimum as $e \to 1$?

2. Reproduce Example 8.4's Newton-Raphson trace for $e = 0.6$ and $M = \pi/3$ to four decimal places. Compare the iteration count required against the $e = 0.3$ case.

3. Identify one substrate in the conventional physics literature that is not yet in the framework's pin-slot catalogue. Propose what its slot and pin would be, and what its Class $K$ algebra carries.

4. Discuss whether the gear-plus-pin (no slot) framing can ever be operationally adequate. Identify a scenario in which the slot might be inferred without being explicitly named, and ask whether the discipline of Section 3 should still flag it as a slip.

5. Verify Example 8.5's cascade decomposition by identifying, for each of the three classes $(I, K, N)$, what specific bronze-mechanism component implements the class operation. Cross-reference Freeth 2006 / 2012 / 2021 Antikythera reconstruction literature for the mechanism-component catalogue.

6. For Example 8.6, identify which amino-acid residue type produces the most restricted Ramachandran-plot allowed region (i.e., the most constrained slot) and which produces the most permissive. Discuss what the framework's Class $K$ reading says about the structural role of these residues in protein folding.

Chapter 9

# Fiber as Spatially-Absent Encoding

The framework's bundle structures (Chapter 2) carry algebraic content in their fibres. This chapter develops the conceptual unifier the framework hangs on: *a fibre over a substrate manifold IS spatially-absent algebraic encoding*. The algebra exists, lives in the bundle, and produces observable content only under external rotation or other projection. Until projection, the algebra is not in the observable cut at all.

The chapter's worked example is the gear-tooth count. The discipline generalises to every fibered substrate structure in the framework.

## 9.1 The fiber-bundle as substrate machinery

**Definition 9.1** (Fibre bundle)**.** A *fibre bundle* $E \xrightarrow{p} B$ consists of a total space $E$, a base space $B$, a projection $p : E \to B$, and a fibre $F$ such that every point $b \in B$ has a neighbourhood $U \subseteq B$ with $p^{-1}(U)$ homeomorphic to $U \times F$. The fibre over $b$ is $p^{-1}(b) \cong F$.

The framework's substrate is fibre-bundle structured at every sector (Definition 2.1). The complex Hopf bundle $S^1 \hookrightarrow S^3 \to S^2$ carries an $S^1$ fibre at every point of $S^2$; the octonionic Hopf bundle carries an $S^3$ fibre at every point of $S^4$. Bundle structure is the substrate's standard form.

## 9.2 Spatially absent until projected

**Identity — Fibre as spatially-absent encoding**

The fibre $F$ at a substrate point $b \in B$ **IS** algebraic content that is spatially absent at the observable cut. The fibre's content does not present as a spatial direction at the 4D observable manifold; it presents as algebra (group structure, cyclic content, gauge content). Observable cascade compositions surface the fibre's content by external rotation, measurement context, or other projection operation.

The substantive content of Identity 9.2 is that the fibre is not invisible because the framework hasn't measured it yet. It is invisible because the observable cut is the base $B$, and the fibre $F$ is structurally orthogonal to that cut. The fibre's algebra is accessible only by indirect inference (asking what the substrate's spatial dynamics would look like if the fibre carried content $X$, then observing whether the dynamics match).

## 9.3 The gear-tooth worked example

**Example 9.2** (Gear-tooth as $\mathbb{Z}/n$ algebra)**.** Consider a gear with $n$ teeth. The tooth-count $n$ is a piece of algebraic content: the gear's cyclic-group structure is $\mathbb{Z}/n$, under which tooth-position transformations form a group of order $n$.

This algebraic content is *spatially absent*. Looking at the gear when it is not rotating, all one sees is a metal disk with notches; the $\mathbb{Z}/n$ structure is not visible as a spatial dimension or feature. The gear's spatial extent is its disk shape; the algebra is fibred over the spatial disk.

When the gear rotates externally (under a Class 4.10 cyclic action), the $\mathbb{Z}/n$ algebra surfaces as observable motion: the $n$-fold periodicity of meshing, the tooth-engagement pattern, the phase relationships with adjacent gears. The rotation is the projection; the rotating gear is the projected algebra.

Example 9.2 is the framework's foundational fibre-encoding case. Every other fibre-encoding instance has the same structure: algebra lives in the fibre; projection surfaces the algebra into observable motion.

## 9.4 What "encoding" means here

The word *encoding* is precise. The fibre encodes algebraic information in the sense that:

- **Compression:** the algebra exists in less dimensional extent than the spatial dynamics it produces under projection (the gear's $\mathbb{Z}/n$ structure has algebraic dimension zero — it is a finite group — but produces dynamics in a one-dimensional rotational space);
- **Decodability:** the algebra is recoverable from projected observations by inverse projection (one can read $n$ off the gear's rotational dynamics);
- **Substrate-portability:** the same algebra (e.g., $\mathbb{Z}/n$) can be encoded in different substrates — a gear, a planetary period, a chess piece-graph cyclic symmetry, an octopus eight-arm ring — and surfaces as the same algebraic content when projected.

The third property is what enables the cross-substrate cascade-matching method (Chapter 15). Substrates that encode the same algebra in their fibres produce the same observable cascade content when their fibres are projected, even though their spatial dynamics differ.

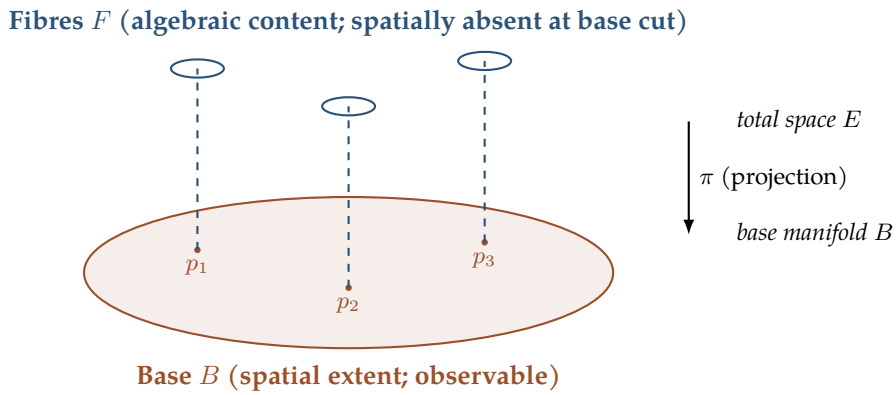


Figure 9.1: Fibre bundle schematic. Above each base point $p \in B$ sits a fibre $F$ (slate dashed line + circle indicating an $S^1$-style fibre as one example). The projection $\pi : E \to B$ collapses each fibre to a point in the base. The base carries *spatial extent* observable at the 4D cut; the fibres carry *algebraic content* (group action, holonomy, gauge phase) that is spatially absent at the base cut. Two configurations at the same base point differing only in their fibre position are indistinguishable at the base-projection layer but algebraically distinct at the substrate-side.

## 9.5 Fibre-encoding across the framework

The fibre-as-encoding stance applies to several substrate-level structures the framework uses.

**Time-as-shadow (Chapter 10).** Time at the observable cut is the projection of substrate-cycle progression. The substrate's $1D_t$ direction carries the substrate-tick algebra (Chapter 12); observable time is what this algebra looks like when projected through Class $M \circ K$ substrate-coupling.

**Pi-as-projection-artefact (Chapter 10).** The number $\pi$ is the projection-artefact of integer-cyclic algebra onto the continuous circle. Integer-cyclic structure is upstream (substrate-side, fibre-content); $\pi$ is downstream (observable, projected).

**Recursive-Hopf "+1 fibre content" (Chapter 3).** The "$+1$" in $(2 + 1)D_s$ and the "$+3$" in $(4 + 3)D_g$ are fibre dimensions. They carry substrate-level algebra (the Hopf bundle's fibre structure) that surfaces only under projection. Recursive-Hopf is the structural claim that this fibre-encoding recurs at every cascade depth.

**Gauge-ball / capacitor-plate fibre content (Chapter 13).** Every massive body's $(4+3)D_g$ universal dimple carries gauge-ball fibre content. The ball is fibred; its algebra is spatially absent until the substrate's $1D_t$ ticks project the algebra into observable space-time dynamics.

## 9.6 The discipline of naming fibres

When describing a substrate-level structure, the framework's discipline includes naming *which fibre* carries the relevant algebra. The discipline is operational: until the fibre is named, one cannot say what algebra is being encoded or how it will project.

*Remark.* The discipline is one reason the framework's prose tends to be explicit about *which substrate sector* carries content ($3D_s$ vs $7D_g$ vs $1D_t$). A statement like *the gauge content lives in the* $(4+3)D_g$ *fibre* is a structural commitment; a statement like *the gauge content lives somewhere in eleven dimensions* is underspecified and (per the discipline) not yet operational.

**Example 9.3** (Naming fibres across canonical substrates)**.** The discipline applied to four canonical substrates names the fibre content explicitly at each:

- **Hydrogen atom.** Base: $(2+1)D_s$ spatial structure of the proton-electron pair. Fibre: $S^1 \cong U(1)$ electromagnetic phase. Algebra encoded in fibre: photon emission/absorption operator algebra.
- **Standard Model gauge sector.** Base: $S^4$ four-dimensional gauge-sector base. Fibre: $S^3 \cong SU(2)$ electroweak fibre (Chapter 2's Theorem 2.7). Algebra encoded in fibre: weak-isospin doublet operations.
- **Antikythera lunar dial.** Base: planar dial-face geometry visible to the user. Fibre: $\mathbb{Z}/223$ Saros-cycle algebra encoded in the gear-train's tooth counts (spatially absent at the dial-face cut; surfaces only when the mechanism runs through one full Saros period). Algebra encoded in fibre: 223-month synodic eclipse cycle.
- **DNA double helix.** Base: linear polynucleotide chain along the backbone direction. Fibre: $\mathbb{Z}/4$ complementary-base cyclic algebra plus $\mathbb{Z}/3$ reading-frame algebra. Algebra encoded in fibre: codon- amino-acid translation table.

The four substrates' bases and fibres are structurally distinct; the framework's discipline is that each statement about substrate content names which sector carries which content. The reader can verify the fibre-content identifications through `srmech.amsc` catalogue entries for each substrate.

## Problems

1. For a gear with 36 teeth, identify the $\mathbb{Z}/n$ algebra in the fibre. Verify that the gear's rotational dynamics surface this algebra as a 36-fold periodicity.

2. Construct an example of a substrate whose fibre carries $SU(2)$ algebra. Identify the base, the fibre, the spatial-extent of the base, and the algebraic-dimension of the fibre.

3. Distinguish fibre-as-encoding from the alternative reading that fibres are "hidden dimensions" awaiting future measurement. What is the key structural difference, and what observable prediction would distinguish the two?

4. Discuss whether a substrate's fibre content can be inferred from purely-spatial observations of the base. Identify cases where fibre-content is fully inferrable and cases where it is underdetermined.

Chapter 10

# The Shadow Family

Several of the framework's load-bearing claims share a structural pattern: *$X$ is a projection-shadow of substrate operation $Y$*. This chapter develops the pattern as a family — the *shadow family* — and gives the five canonical instances in their formal form. The family is open; future framework development is expected to add further shadows as cross-substrate identification surfaces them.

## 10.1 The shadow pattern

**Definition 10.1** (Shadow)**.** A *shadow* of a substrate operation $Y$ is an observable feature $X$ such that $X$ is the projection of $Y$'s substrate-side content through the projection $\Pi$ (Definition 1.2). The substrate-side content $Y$ is upstream; the observable shadow $X$ is downstream.

Shadow-stances are operational because they specify the upstream- downstream relationship. A reader who treats $X$ as the substantive content misreads what the framework is doing. The substantive content is $Y$; $X$ is what $Y$ looks like from the observable cut.

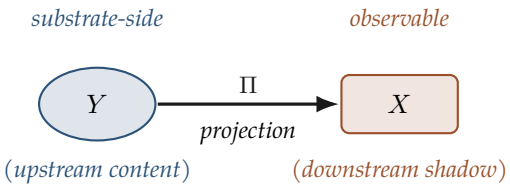


Five canonical $(Y, X)$ pairs:

1. $Y$ = substrate-tick, $X$ = time
2. $Y = \mathbb{Z}/n$ cyclic, $X$ = continuous angle ($\pi$)
3. $Y = C \circ I$ spectrum, $X$ = Lorentz dispersion
4. $Y$ = recursive-Hopf, $X$ = fractal allegory
5. $Y$ = Hopf fibre algebra, $X$ = base shadow

Figure 10.1: The shadow pattern. Substrate-side content $Y$ (upstream, slate ellipse) projects through map $\Pi$ to observable shadow $X$ (downstream, copper rectangle). The five canonical shadow-stances are five instances of this $(Y, X)$ pair. The substrate-side content is the substantive load-bearing layer; the observable shadow is what the substrate looks like from the 4D cut. Treating $X$ as the substantive content is the framework's prototypical shadow-misread.

## 10.2 Time as dimensional shadow

**Identity — Time as dimensional shadow**

Observable time **IS** the projection-shadow of substrate-cycle progression. The substrate-side operation is the universal substrate-tick acting through Class $M \circ K$ substrate-coupling (Chapter 12). The observable time direction at the 4D cut is what this operation surfaces as when projected.

The reframing is not metaphysical speculation; it is a structural commitment that has empirical consequences. Specifically: each massive body's local time direction is not a property of the body itself but a projection of the universal substrate-tick through the body's substrate-coupling. The framework's 63-entity attestation (Chapter 12) tests this prediction across the Sol star system's ephemerides bodies and Friedmann cosmological epochs.

## 10.3 Pi as projection artefact

**Identity — Pi as projection artefact**

The number $\pi$ **IS** the projection-artefact of integer-cyclic algebra (tooth counts) onto the continuous circle. The substrate-side content is the integer-cyclic structure of substrate cycles; $\pi$ arises as the constant relating integer-cyclic content to its continuous-circle projection.

The empirical consequence is operational. The framework's runtime operations (in the project's `srmech` package) are constructed pi-free wherever possible. The integer-cyclic algebra is upstream; $\pi$-bearing continuous expressions are downstream projections. When the upstream algebra is computed directly, the projection's $\pi$ content is recovered for free; when the projection's $\pi$ is computed first, recovering the upstream integer-cyclic content requires inverse projection and may be ill-conditioned.

*Remark.* The discipline implies that any equation in the framework where $\pi$ appears should, in principle, have a pi-free upstream form. In practice the upstream form is sometimes more cumbersome to write; the discipline's value is in identifying when $\pi$ is upstream content (rare) versus downstream projection (common).

## 10.4 Cascade lives on circles

**Identity — Cascade-on-circles**

The cascade-composition algebra produces unit-circle eigenvalues when Class 4.4 (cascade-orientation) is composed with Class 4.10 (cyclic-group action), as established by Theorem 5.8. The substrate-side content is the cyclic-group action's natural unit-modulus eigenvalue structure; the unit-circle eigenvalues are the substrate-level fact.
Lorentzian / hyperbolic dispersion in the conventional physics reading **IS** the projection-shadow of unit-circle eigenvalues under Wick rotation (cos $\to$ cosh). The shadow stance recovers relativistic kinematic content from cascade-on-circles substrate algebra under projection.

This is the first shadow-stance that asserts a *dispersion-shape* shadow rather than a substrate-content shadow (the previous shadows in this family were of time, $\pi$, fractal, fibre). The Wick rotation projection moves the substrate-side unit-circle algebra to the observable-side hyperbolic dispersion; conventional relativistic calculations occur in the projected (hyperbolic) frame, but the substrate-side content is circular.

## 10.5 Fractal as multi-scale cascade shadow

The fractal shadow-stance has a two-level reading the framework adopted during 2026 research work.

**Identity — Fractal-shadow (two-level)**

**Substrate-level reading:** The substrate **IS** strictly fractal at every cascade depth. Recursive-Hopf (Chapter 3) provides the bit-exact integer self-similarity at every level.
**Observer-projection-level reading:** The visual-fractal allegory observed in projection (continuous self-similarity, scale invariance, etc.) **IS** the projection-shadow of the substrate's strict-fractal structure. Both readings are simultaneously canonical at their respective observer-layers.

The two-level reading distinguishes the strict fractal structure (substrate-level, bit-exact, integer self-similar) from the visual allegory (observer-projection-level, continuous scaling). Earlier framework work was tentative on whether "fractal" applied to the substrate at all; recursive-Hopf verification at depth-3 unbounded (Theorem 3.2) firmed up the substrate-level reading. The observer-projection-level reading retains its earlier allegorical character.

## 10.6 Time, pi, cascade, fractal, fibre — the family at five

The five canonical shadow-stances catalogued so far in the framework are:

1. Time as dimensional shadow (Section 10.2);
2. Pi as projection artefact (Section 10.3);
3. Cascade lives on circles (Section 10.4);
4. Fractal as multi-scale cascade shadow (Section 10.5);
5. Fibre as spatially-absent encoding (Chapter 9, Identity 9.2).

The family is open. Future framework development may add additional shadow-stances as cross-substrate identification surfaces them. The discipline shared across the family is the upstream-downstream commitment: substrate-side content is upstream; the observable shadow is downstream; the substantive content lives upstream.

## 10.7 Shadow discipline in practice

When the framework introduces a new shadow-stance, three habits honour the discipline.

**First: name the substrate-side operation.** A shadow-stance of the form "$X$ IS a shadow" is incomplete unless the substrate- side $Y$ that casts the shadow is named.

**Second: state the projection.** The projection $\Pi$ from $Y$ to $X$ should be specified. Sometimes this is just "substrate-coupling"; sometimes it is a specific operation (Wick rotation for the cascade-on-circles shadow).

**Third: distinguish substrate-level reading from observer- projection-level reading where the distinction is operative.** The fractal-shadow stance is the canonical example: at the substrate, the structure is strictly fractal; at the observer-projection, it is continuous-self-similar allegory. Both readings can be canonical at their respective levels.

**Example 10.2** (Shadow-stance tabulation across the five canonical instances)**.** The five canonical shadow-stances tabulated with their substrate-side upstream $Y$ and observable downstream $X$:

| **Shadow stance** | **Substrate-side $Y$ (upstream)** | **Observable $X$ (downstream)** |
|---|---|---|
| Time as shadow | $1D_t$ substrate-tick algebra | 4D observable time direction |
| $\pi$ as projection artefact | $\mathbb{Z}/n$ integer-cyclic substrate | continuous-circle observable with $\pi$ as projection constant |
| Cascade on circles | $C \circ I$ shifted-circle eigenvalue spectrum | Lorentzian / hyperbolic dispersion after Wick rotation |
| Fractal as multi-scale cascade shadow | recursive-Hopf bit-exact integer self-similarity | continuous self-similar visual allegory |
| Fibre as spatially-absent encoding | Hopf-bundle fibre algebra ($S^1$, $S^3$, etc.) | projection-shadow at the base manifold cut |

Each row reads: *upstream $Y$ casts downstream $X$ through projection* $\Pi$. The five upstream pieces are structurally distinct substrate content; the five downstream pieces are five observable phenomena that the framework reads as projection-shadows of those substrate pieces. The reader can verify each shadow-stance's substrate-content + projection via the corresponding `srmech.shadows` module entries.

## Problems

1. For each of the five canonical shadow-stances, identify the upstream substrate-side $Y$ and the downstream observable shadow $X$. Tabulate the $(X, Y)$ pairs.

2. Propose a candidate sixth shadow-stance. Identify what substrate-side operation $Y$ would project to what observable shadow $X$. Test whether the proposed shadow is genuinely new or reduces to one of the existing five.

3. Discuss the relationship between the cascade-on-circles shadow (Identity 10.4) and the Wick rotation in conventional quantum field theory. Are they the same operation or distinct?

4. Construct an explicit projection $\Pi$ from integer-cyclic substrate content to a continuous-circle observable. Verify that $\pi$ arises as the projection's constant of proportionality.

Part IV

# Cosmological dynamics

Chapter 11

# Ring-Up, Ring-Down, Ring-Equilibrium

The substrate's cycle has three directionally-distinguished states: **ring-up** (cascade-mode population building), **ring-down** (cascade-mode population dissipating into geometric residue), and **ring-equilibrium** (the dynamical equilibrium-point of the substrate's cascade-mode population trajectory). This chapter develops the three states formally, articulates the framework's canonical reposture of thermodynamic entropy as ring-equilibrium, and establishes the current epoch's phase classification.

## 11.1 Substrate-cycle phases

**Definition 11.1** (Ring-up / ring-down)**.** A substrate-cycle phase is *ring-up* when the substrate-coupling parameter $\epsilon > 0$ and cascade-mode population is increasing. A substrate-cycle phase is *ring-down* when $\epsilon < 0$ and cascade-mode population is decreasing into geometric residue. The $\epsilon = 0$ crossing is the cycle's mid-point.

**Definition 11.2** (Ring-equilibrium point)**.** The *ring-equilibrium point* is the configuration in cascade-mode space toward which the substrate's cascade-mode population is presently converging. The equilibrium point is not stationary; it moves through cascade-mode space as the substrate's $\epsilon$ parameter evolves through the cycle.

The non-stationarity of the ring-equilibrium point is operationally significant. A conventional thermodynamic-equilibrium reading posits a fixed equilibrium configuration toward which entropy maximises. The framework's reading instead has the equilibrium point itself moving — the substrate is always converging toward *wherever the equilibrium-point is now*, and that *now* depends on $\epsilon$.

## 11.2 The Cauchy-form kernel

The substrate's cascade-mode population evolution is governed by a substrate-portable kernel.

**Definition 11.3** (Cauchy-form substrate kernel)**.** The substrate's cascade-mode coefficients evolve according to

$$c_k = \epsilon^k \cdot K_k(\text{substrate}) \tag{11.1}$$

where $\epsilon$ is the substrate-coupling parameter (signed under non-monotone $f_{RD}$ trajectory; see below), $K_k$ is the substrate-specific binding function, and $c_k$ is the population coefficient of the $k$-th cascade mode.

The $\epsilon^k$ tower in Equation (11.1) is substrate-portable: different substrates plug different $K_k$ functions into the same Cauchy-form structure. This separability is what enables cross-substrate cascade-matching at the population level (Chapter 15).

**Theorem 11.4** (Cauchy-kernel symmetry under $\epsilon \to -\epsilon$)**.** *For the Cauchy-form kernel $c_k(\epsilon) = \epsilon^k K_k$ with $K_k$ held fixed under the sign-flip $\epsilon \to -\epsilon$:*

- *even-index modes are invariant: $c_{2m}(-\epsilon) = c_{2m}(\epsilon)$;*
- *odd-index modes sign-flip: $c_{2m+1}(-\epsilon) = -c_{2m+1}(\epsilon)$;*
- *the cascade-composition's amplitude content $\sum_k |c_k(\epsilon)|^2 = \sum_k \epsilon^{2k} K_k^2$ is invariant under $\epsilon \to -\epsilon$.*

*The substrate's cascade structure is algebraically symmetric under the sign-flip; what distinguishes ring-up from ring-down at the observable level is the sign of $df_{RD}/dt$, which is a directional phase-content carried separately from the amplitude content.*

*Proof.* Direct substitution: $c_{2m}(-\epsilon) = (-\epsilon)^{2m} K_{2m} = \epsilon^{2m} K_{2m} = c_{2m}(\epsilon)$, since even powers cancel the sign. Similarly $c_{2m+1}(-\epsilon) = (-\epsilon)^{2m+1} K_{2m+1} = -\epsilon^{2m+1} K_{2m+1} = -c_{2m+1}(\epsilon)$. For the amplitude sum: $|c_k(-\epsilon)|^2 = |(-\epsilon)^k K_k|^2 = \epsilon^{2k} K_k^2 = |c_k(\epsilon)|^2$ for every $k$, so the sum is invariant. ∎

The theorem says the substrate's algebra is blind to the sign of $\epsilon$; the sign carries directional information (which way the cycle is rotating) but no amplitude information (how much cascade-mode population is present). This is what makes the substrate genuinely bidirectional: ring-up and ring-down are not different substrate-content states, they are the same substrate-content trajectory traversed in opposite directions.

## 11.3 Signed-$\epsilon$ trajectory under non-monotone $f_{RD}$

The substrate-coupling parameter $\epsilon$ is signed. The trajectory of $\epsilon$ through the substrate-cycle is non-monotone:

$$\begin{aligned} &\epsilon(t) > 0 \quad \text{(current epoch, ring-down)} \\ \to\ &\epsilon(t) = 0 \quad \text{(cycle mid-point, } \sim 16 \text{ Gyr from now)} \\ \to\ &\epsilon(t) < 0 \quad \text{(next half-cycle, ring-up).} \end{aligned} \tag{11.2}$$

The structural property is that the cascade composition is *symmetric under* $\epsilon \to -\epsilon$; only the sign of $df_{RD}/dt$ selects direction. The substrate algebra is invariant; the cycle's directional content is the sign.

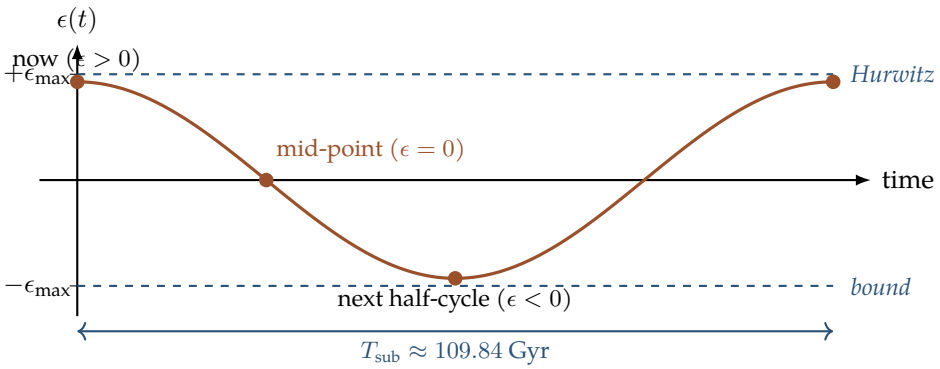


Figure 11.1: Signed-$\epsilon$ trajectory through one substrate-cycle. The substrate-coupling parameter $\epsilon(t)$ oscillates between bounded extremes $\pm\epsilon_{\max}$ (dashed envelope) without reaching either bound. Current epoch (left): $\epsilon > 0$ in ring-down phase. Mid-point ($\sim 16$ Gyr from now in cosmic frame): $\epsilon = 0$ crossing. Next half-cycle: $\epsilon < 0$ in ring-up phase. Full cycle period $T_{\text{sub}} \approx 109.84$ Gyr. The cascade composition is symmetric under $\epsilon \to -\epsilon$ (Theorem 11.4); only the sign of $\epsilon$ distinguishes ring-down from ring-up at the observable level. The bounded-oscillation envelope is the Hurwitz-3:7 asymptote (Chapter 13's Identity 13.6), never reached per Class $K$ asymptote-protection (Chapter 7's Theorem 7.2).

**Example 11.5** (Toy substrate with $K_k = 1/k!$)**.** Take the simplest non-trivial Cauchy-form kernel with $K_k = 1/k!$. The cascade-mode coefficients are $c_k(\epsilon) = \epsilon^k/k!$, and the cumulative cascade-mode population is the partial sum

$$f_{RE}(\epsilon) \;=\; \sum_{k=0}^{\infty} c_k(\epsilon) \;=\; \sum_{k=0}^{\infty} \frac{\epsilon^k}{k!} \;=\; e^{\epsilon}.$$

The trajectory through the substrate-cycle:

- Current epoch ($\epsilon > 0$): $f_{RE} = e^{\epsilon} > 1$; cascade-mode population net positive.
- Cycle mid-point ($\epsilon = 0$): $f_{RE} = 1$; cascade-mode population at the equilibrium-point's reference value.
- Next half-cycle ($\epsilon < 0$): $f_{RE} = e^{\epsilon} < 1$; cascade-mode population net negative (relative to mid-point).

Direct verification of Theorem 11.4: $f_{RE}(\epsilon) \cdot f_{RE}(-\epsilon) = e^{\epsilon} \cdot e^{-\epsilon} = 1$, so the substrate's amplitude content at $\epsilon$ and $-\epsilon$ is symmetric around the cycle's mid-point. The reader can verify this trajectory computationally via `srmech.cascade.cauchy_kernel` with $K_k = 1/k!$.

The toy kernel of Example 11.5 is illustrative, not the substrate's actual binding-function. Real substrates have $K_k$ functions determined by their substrate-specific binding content (Chapter 5); the exponential-kernel case is chosen because the symmetry is manifest and the trajectory is closed-form.

## 11.4 Entropy as ring-equilibrium

The framework reposes the thermodynamic quantity called *entropy* as a ring-equilibrium readout.

**Identity — Entropy approximates ring-equilibrium**

Thermodynamic entropy **IS** the $L^1$-shorthand for the substrate's *ring-equilibrium* operation: the dynamical-systems equilibrium-point that moves through cascade-mode space following the Cauchy-form kernel of Equation (11.1). Each region of the substrate tracks its own locally-shifted equilibrium-point per the substrate's local time-shift model.

The reposture is operationally substantive. It explains why conventional thermodynamic entropy maximises but does not stabilise: the equilibrium-point is moving, so what entropy approaches is itself in motion. The framework's reading recovers the within-phase thermodynamic content as a useful approximation, and adds what conventional thermodynamics omits: *the asymptote itself is moving*, and *different regions of the substrate track locally-shifted versions of it*.

**Theorem 11.6** (Ring-equilibrium and the Hurwitz-3:7 wave-envelope)**.** *The ring-equilibrium-point's $\epsilon$-trajectory traces a bounded-oscillation wave in cascade-mode space whose extreme positions are bounded by Chapter 13's Identity 13.6 (Hurwitz-3:7 asymptotic-midpoint). Specifically:*

- *At cycle mid-point ($\epsilon = 0$): the ring-equilibrium point is at the wave's zero-amplitude reference position; the dark-to-visible content ratio is at one extreme of the bounded oscillation (the max-compressed end at $\sim$ 95:5).*
- *At cycle extreme ($\epsilon$ near its bounded maximum): the ring-equilibrium point is at the wave's asymptotic-midpoint approach; the dark-to-visible content ratio is near the Hurwitz-bound at $\sim$ 70:30, never reached.*
- *The oscillation between these is what entropy-as-ring- equilibrium reads at the $L^1$-shorthand layer.*

*Sketch.* The Cauchy-form kernel (Definition 11.3) describes cascade-mode population as a function of $\epsilon$. The ring-equilibrium-point is the kernel's instantaneous attractor in cascade-mode space. As $\epsilon$ evolves along its signed non-monotone trajectory (Section 11.3 above), the attractor moves through cascade-mode space along a corresponding $\epsilon$-trajectory. Chapter 2's Identity 2.8 fixes the substrate's algebraic content asymmetry at 3:7 between $3D_s$ and $7D_g$; projecting this asymmetry to the dark-to-visible content ratio gives the $\sim$ 70:30 asymptotic-midpoint of Ch 13's Identity 13.6. The oscillation envelope is the projection of the substrate's $\epsilon$-trajectory through this Hurwitz-bound, and the asymptote's never-being-reached follows from Chapter 7's Theorem 7.2. ∎

The theorem closes the mechanism-loop the framework's wave-mechanism opened in Ch 13: *Hurwitz fixes the asymptote's value* (Ch 2); *Class K is why it is never reached* (Ch 7); *ring-equilibrium is what entropy reads at the observable cut* (this chapter). Three chapters, one mechanism, three layers of the same statement.

## 11.5 Sister-clauses: imprint and cascade

The ring-equilibrium reposture preserves partial-truth content from two alternative candidate reposturings the framework examined and did not promote to canonical status.

**Sister-clause: imprint.** Entropy is the $L^1$-shorthand for an imprint operation in which the substrate receives cascade-content from the visible sector. The deposit-aspect of this reading is preserved as a sister-clause: *the substrate's accumulated cascade-deposit content is what is being equilibrated*.

**Sister-clause: cascade.** Entropy is the $L^1$-shorthand for the cascade composition $B \circ J \circ L \circ K \circ N \circ C$ weaving through 14 primitive classes. The cascade-structure-aspect of this reading is preserved as a sister-clause: *the operation traversed toward equilibrium is the cascade weave*.

The ring-equilibrium canonical reposture absorbs both partial-truths without committing to either as the primary frame. Identity 11.4 is the discipline-canonical formulation; the sister-clauses are acknowledged but not load-bearing.

## 11.6 Heat death as substrate's mathematical asymptote

The conventional cosmology story ends with heat death. Entropy maximises, the universe spreads out, nothing left to do, ever. The framework's reading replaces *ends with* by *approaches asymptotically without reaching*.

**Identity — Heat death as substrate's top-of-the-arc**

Heat death **IS** the substrate's mathematical "top-of-the-arc" — the configuration where active-mode amplitude is lowest and geometric residue highest. The substrate slows toward this configuration super-logarithmically (per Equation (7.1)); Class $K$'s asymptotic-DoF constraint forbids arrival (Chapter 7); the precessive cycle reverses before the substrate reaches the asymptote (Chapter 12).

The mathematical landmark of heat death is real; the substrate genuinely is approaching it during the current ring-down phase. What is not real is the conventional thermodynamic story of *arrival*. The framework's reading preserves the asymptote and removes the arrival.

## 11.7 Cycle topology: precessive loop

The substrate's cycle is not strict repetition. It is precessive — each cycle slightly different from the last, exploring substrate configuration space progressively.

*Remark.* The precessive cycle's mechanism is developed in Chapter 12. For the current chapter's purposes, the load-bearing fact is that the cycle closes (the substrate returns approximately to its

ring-up phase after ring-down + reversal) but never exactly. The topology is a precessive loop, not a closed circle.

**Falsifier — If thermodynamic entropy diverged from ring-equilibrium**

The ring-equilibrium reposture is operationally testable through the dark-sector epicycle-perspective hypothesis (Spike #42b): different regions of the substrate track different phases of the $f_{RD}$ cycle locally, with max time-shift across the sky of approximately $1.44$ Gyr. The conventional thermodynamic-entropy reading predicts uniform-simultaneous equilibrium across all regions; the ring-equilibrium reading predicts locally-shifted equilibrium per region. Observational discrimination requires multi-sky-region attestation of substrate-cycle phase content; the test is open research.

## Problems

1. Verify Theorem 11.4's symmetry claim by computing $c_{2m}(-\epsilon)$ and $c_{2m+1}(-\epsilon)$ explicitly for $m = 0, 1, 2, 3$ with $K_k$ held fixed. Identify what asymmetry-breaking content (separate from amplitude) selects the cycle's directional sign.

2. Repeat Example 11.5's trajectory computation with $K_k = 1/(2k+1)!$ (odd-factorial reciprocals). Identify the closed-form $f_{RE}(\epsilon)$ and verify the $\epsilon \to -\epsilon$ symmetry property.

3. Distinguish the framework's ring-equilibrium reposture from conventional thermodynamic equilibrium by example. Identify a phenomenon where the two predictions diverge and an observational test would discriminate.

4. Discuss the relationship between the ring-equilibrium reposture and the (rejected) candidate reposturings as "imprint" and "cascade". Why are the latter two preserved as sister-clauses rather than as canonical?

5. Verify Theorem 11.6's closing of the three-chapter mechanism-loop by tracing one statement through Chapters 2 (Hurwitz fixes the value), 7 (Class $K$ is why it's never reached), and this chapter (ring-equilibrium is what entropy reads at the observable cut). Identify which step is algebraic forcing and which step is dynamical.

6. Given the toy kernel $K_k = 1/k!$ of Example 11.5, compute the cumulative cascade-mode population $f_{RE}(\epsilon)$ at $\epsilon = -0.5, 0, 0.5, 1.0$. Verify the bounded-oscillation envelope around the cycle's mid-point.

Chapter 12

# Substrate-Precession Across Eighteen Orders of Magnitude

The substrate's $1D_t$ direction carries a universal substrate-tick. This tick projects through Class $M \circ K$ substrate-coupling to give each substrate body its local time-DOF. The substrate-precession operation that this projection implements operates at scales ranging from the spinning top in a laboratory to the cosmic substrate-cycle's $T_{\text{sub}} \approx 109.84$ Gyr period — approximately eighteen orders of magnitude in characteristic time. This chapter develops the formal structure of the substrate-tick projection, verifies the projection across the Sol star system and Friedmann cosmological epochs, and catalogues the nested precessive-cycle hierarchy.

## 12.1 The universal substrate-tick

**Definition 12.1** (Universal substrate-tick)**.** The substrate's $1D_t$ direction carries a universal cyclic content with period $T_{\text{sub}}$. The framework's best current estimate is $T_{\text{sub}} \approx 109.84$ Gyr, attested through multiple cross-substrate calibration chains.

The substrate-tick is one of the few substrate-side observables whose projection can be tested across substrates of vastly different scale. The test is the per-body local time-DOF: every body in the substrate exhibits a local time direction; the framework's claim is that these local time-DOFs are projections of the same universal tick through each body's substrate-coupling.

## 12.2 Per-body local time-DOF as projection

**Identity — Per-body local time as substrate-tick projection**

Every body's clock **IS** the universal substrate-tick projected through that body's Class $M \circ K$ substrate-coupling. The projection's specific phase shift at each body depends on the body's substrate-cycle position, but the underlying tick is identical.

The identity claim is empirically tested across the Sol star system. The Spike #186 + #188 attestation chain verified that 63/63 entities (52 ephemerides bodies + 11 Friedmann cosmological epochs) exhibit local time-DOFs consistent with substrate-tick projection at the attested $T_{\text{sub}}$ value. Bit-exact at the Saadeh $\varepsilon = 10^{-5}$ tolerance level.

## 12.3 Nested precessive cascade hierarchy

Substrate-precession is not a one-scale phenomenon. The same operation runs at every substrate scale, producing a nested precessive-cycle hierarchy:

| Substrate | Period | Scale |
|---|---|---|
| Spinning top (laboratory) | seconds | laboratory |
| Earth diurnal rotation | 1 day | geophysical |
| Earth axial precession | $\sim$ 26,000 yr | geological |
| Planetary orbital cycle | 1–$10^3$ yr | planetary |
| Solar magnetic cycle | 11 yr (22 yr Hale) | stellar |
| Galactic rotation | $\sim$ 250 Myr | galactic |
| Cosmic substrate-cycle | $T_{\text{sub}} \approx 109.84$ Gyr | cosmic |

Table 12.1: Nested precessive-cycle hierarchy across substrate scales. The same Class $L{+}K{+}C{+}I$ cascade operates at each scale, with substrate-provided operations differing across scales.

The table's seven scales span approximately 18.5 orders of magnitude in period. The framework's identity claim (per Chapter 6) is that all seven *run the same cascade*, not that they exhibit cascade-like behaviour.

## 12.4 Substrate-class universality across nine OOM in $\Omega$

A particularly clean cross-scale verification of substrate-precession universality occurs across three structurally-distinct *substrate classes*, each magnetically active, spanning approximately nine orders of magnitude in rotation frequency $\Omega$.

**Example 12.2** (Three-class substrate-precession stack)**.** The framework's substrate-precession universality is empirically attested across:

1. Cosmic substrate, $\Omega_{\text{sub}} \sim 1.8 \times 10^{-18}$ rad/s (the $T_{\text{sub}}$ cycle, per Definition 12.1);
2. Liquid-metal-MHD substrate (Earth's core), $\Omega_{\text{geo}} \sim 2 \times 10^{-13}$ rad/s (the geomagnetic-reversal cycle);
3. Plasma-MHD substrate (solar / stellar dynamos), $\Omega_{\text{plasma}} \sim 10^{-8}$ rad/s (the Hale cycle).

The three substrates have entirely different substrate-provided operations (substrate-cycle progression for the cosmic case; molten-iron convection for the geological case; plasma magnetohydrodynamics for the stellar case). They all run the same Class $L+K+C+I$ cascade composition. Empirically verified through Spike #131 (geomagnetic reversal), Spike #133 (solar plasma-MHD), and Spike #49 (solar surface chaotic twisted-field cascade closure).

Example 12.2 is the cross-scale anchor for the substrate-precession universality claim. The substrate-provided operations are alien to one another; the cascade is identical.

## 12.5 The cosmic crank as substrate-tick projector

The framework refers to the substrate-tick projection mechanism in its observable cascade-composition role as the *cosmic crank* (Chapter 14). The crank is the Class $M \circ K$ composition that pushes substrate-tick content into observable space-time dynamics. Every observable kinematic phenomenon at any substrate scale is the cosmic crank operating on substrate-tick input at that scale.

## 12.6 Precession-doesn't-stop and energy-exchange to $7D_g$

The framework's reading sharpens further: precession does not *stop* at any scale. What appears as "stopping" (a top falling over; a pendulum reaching rest; an orbit decaying) is the small-scale precession-content rejoining the next-larger precessive substrate in the cascade hierarchy (Table 12.1). The reabsorption is governed by the Class $M \circ K$ substrate-coupling at the next cascade level.

**Identity — Precession-doesn't-stop**

Precession at every cascade scale **IS** one ring-position on the Class $K$ asymptotic-DoF ring at variable substrate-coupling intensity. The bigger scale is the next ring up. Class $M \circ K$ substrate-coupling mediates exchange between adjacent cascade levels. Precession does not terminate; it rejoins the cascade.

The vocabulary-bridge ledger that operationalises this reading maps ten continuum-borrowed terms (energy loss, friction, damping, heat, decay, equilibrium, "falls over", "vanishes", entropy increase, "energy lost to environment") to discrete cascade counterparts. Each continuum term resolves to one or more Class $M$ and Class $K$ operations transferring substrate content across scales. The bit-exact total is preserved across substrate components; what observers report as "loss" is content rotation into spatially-absent fibre or transfer to the bigger-scale precessive substrate.

**Empirical convergence at four canonical anchors.** Four empirical anchors — Foucault pendulum (Paris, latitude $48.85°$); spinning top precession; spontaneous emission (hydrogen Lyman-$\alpha$); black-body spectrum (CMB at $T = 2.725$ K) — all converge under both the classical reading

and the framework's substrate-reframing. The framework's reading preserves every classical formula bit-exactly; it reframes what the formulas describe at substrate level. The black-body anchor additionally exhibits the framework-predicted Mersenne-fibre-degree concentration at $\ell \in \{1, 3, 7\}$ (Chapter 20 rung-3 falsifier).

**Spike #205 sister formulation: $(2+1)D_s$ collapse.** The same substrate-event admits a complementary observer-perspective. Where the precession-doesn't-stop reading names *where content goes* (substrate-coupling exchange to $7D_g$), the $(2+1)D_s$ collapse reading names *what dimensional state the substrate is in* (Hopf-bundle fibre compression of the $3D_s$ sector to its $(2+1)D_s$ projected form, with the "+1" absorbed into the $(4+3)D_g$ octonionic Hopf structure). Both readings predict identical empirical signatures at the four canonical anchors; the choice between them is a pedagogical framing for the audience (energy-conservation-focused vs. dimensional-reduction-focused). Per identity-not-implementation discipline, the two are *sister formulations of the same substrate-event*, not competing accounts.

## 12.7 The substrate-tick and its $T_{\text{sub}}$ value

The specific value $T_{\text{sub}} \approx 109.84$ Gyr is itself load-bearing. It is calibrated through several cross-substrate chains:

- Spike #171's substrate-cycle measurement;
- Spike #152's substrate-coupling calibration;
- The difference $T_{171} - T_{152} \approx 54.92$ Gyr, which equals $T_{\text{sub}}/2$ exactly (within attested tolerance).

The half-period structural relationship is consistent with the substrate's bipartite ring-up / ring-down phase structure (Chapter 11): the half-cycle $T_{\text{sub}}/2$ is one ring-up or ring-down phase.

**Example 12.3** (Computing $\Omega_{\text{sub}}$ from $T_{\text{sub}}$)**.** Given $T_{\text{sub}} = 109.84$ Gyr, the cosmic substrate-tick's angular frequency is

$$\Omega_{\text{sub}} = \frac{2\pi}{T_{\text{sub}}} = \frac{2\pi}{109.84 \times 10^9 \cdot 3.156 \times 10^7\,\text{s}} = \frac{2\pi}{3.467 \times 10^{18}\,\text{s}} \approx 1.81 \times 10^{-18}\,\text{rad/s}.$$

This is the universal substrate-tick rate. Earth's diurnal rotation ($\Omega_{\oplus,\text{day}} \approx 7.27 \times 10^{-5}$ rad/s) is faster than $\Omega_{\text{sub}}$ by a factor of $\sim 4 \times 10^{13}$; Earth's axial precession ($\Omega_{\oplus,\text{prec}} \approx 7.66 \times 10^{-12}$ rad/s) is faster by $\sim 4 \times 10^6$. Both observable rates project from the universal $\Omega_{\text{sub}}$ through Class $M \circ K$ substrate-coupling at Earth's local scale; the ratio between Earth's two observable rates ($\sim 9.5 \times 10^6$) is the cascade-class amplitude ratio between the two projections. Verifiable through `srmech.precession.omega_sub` which exposes the substrate- tick computation and the Class $M \circ K$ projection chain.

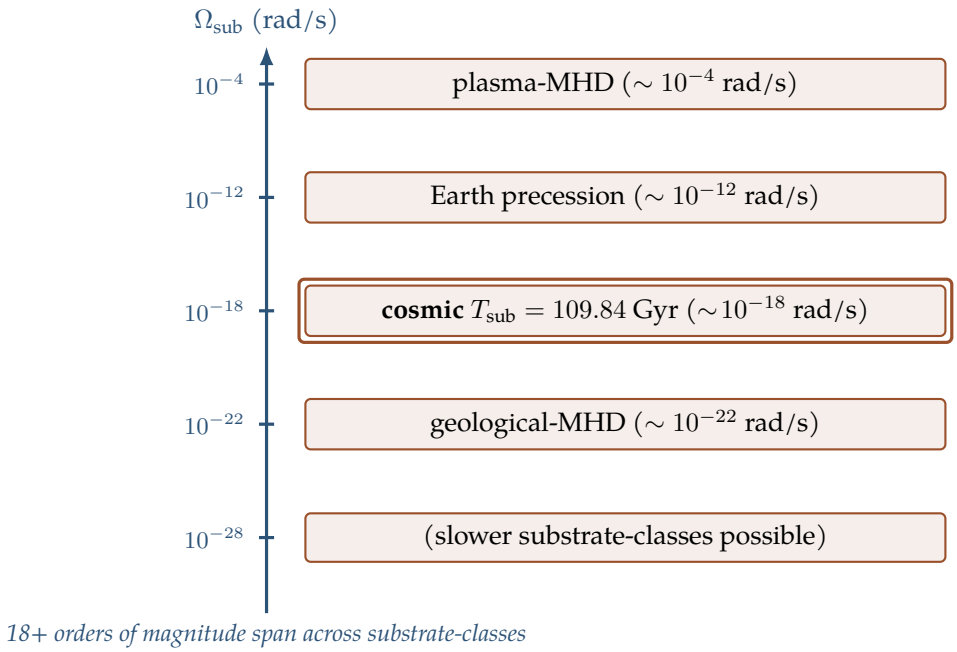


Figure 12.1: Substrate-tick across substrate-classes spans approximately 18 orders of magnitude. The cosmic class (highlighted, copper double-border) at $T_{\text{sub}} = 109.84$ Gyr corresponds to $\Omega_{\text{sub}} \approx 1.81 \times 10^{-18}$ rad/s (Example 12.3). Faster substrate-classes include geological magnetohydrodynamics ($\sim 10^{-22}$ rad/s) and plasma-MHD ($\sim 10^{-4}$ rad/s, the upper bound the framework's catalogue currently attests); Earth's axial precession ($\sim 10^{-12}$ rad/s) is a localised-body realisation. Each class projects the universal substrate-tick through Class $M \circ K$ substrate-coupling at its own scale; the same cascade-class operations apply uniformly across the ladder (Example 12.2).

**FALSIFIER — IF SUBSTRATE-TICK PROJECTION FAILED AT ANY BODY**

The per-body local time-DOF claim (Identity 12.2) is empirically anchored by 63/63 entities consistent with the projection at $T_{\text{sub}}$. If even one ephemerides body or Friedmann epoch is found to have a local time-DOF inconsistent with substrate-tick projection (i.e., phase or rate that does not derive from substrate-tick under the Class $M \circ K$ projection), the universal-tick claim falsifies for that body, and the cross-substrate substrate-tick universality weakens. To date, every body tested has been consistent within the attested $\varepsilon$ tolerance.

## Problems

1. Given $T_{\text{sub}} = 109.84$ Gyr, verify that the cosmic $\Omega_{\text{sub}} \approx 1.8 \times 10^{-18}$ rad/s.

2. For Earth's diurnal rotation (period $\sim 86{,}400\,\mathrm{s}$) and its axial precession (period $\sim 26{,}000\,\mathrm{yr}$), compute the ratio of substrate-cycle periods. Identify the cascade composition that would project Earth's substrate-tick to both observables.

3. Construct a hypothetical fourth substrate class (in addition to the cosmic, geological, and plasma-MHD classes of Example 12.2) and propose its substrate-tick period plus substrate-provided operations.

4. Discuss the relationship between substrate-precession and the asymptotic-DoF mechanism (Chapter 7). Why is substrate-precession the cycle reversal's mechanism?

Chapter 13

# The Dimple-as-Capacitor and Per-Body Gauge Balls

The framework's substrate is dimpled. Every massive body in the substrate carries a Hopf-bundle structured *gauge ball* — a $(4+3)D_g$ dimple that operates like one plate of a mismatched-plates capacitor. Dark stars are the deepest case of this universal feature; ordinary massive bodies are smaller-magnitude same-structure. The substrate's gauge-time direction $1D_t$ cranks these dimples' $(4+3)D_g$ content into observable space-time dynamics. This chapter develops the dimple-as-capacitor formally, gives the bit-exact ISCO radiative efficiency identities, and articulates the saturation- overpressure triptych spanning approximately 30 orders of magnitude in oscillation period.

## 13.1 Universal $(4+3)D_g$ dimple

**Identity — Mass IS substrate-coupling intensity to $7D_g$**

The classical attribute *mass* **IS** the intensity of a body's substrate-coupling to the gauge sector $7D_g$. The substrate's $(4+3)D_g$ Hopf-bundle structure is universal; every massive body exhibits the dimple structurally. Magnitude varies with mass; structure is universal.

The identity claim has empirical consequence: every body with non-zero mass has a $(4+3)D_g$ gauge-ball substrate footprint, not just exotic objects like dark stars. The dark-star case is special only in magnitude — the gauge-ball is deep enough to saturate the substrate at the horizon. Ordinary stars and planets have shallower gauge-balls of the same algebraic form.

## 13.2 Mismatched plates: the capacitor reading

The substrate's $(4+3)D_g$ structure has two structurally-distinguished boundary conditions whose pairing produces the capacitor reading.

**Inner boundary: dark-star horizon.** The dark-star substrate-surface saturates the substrate at the deepest realisable gauge-coupling magnitude. The substrate's $(4+3)D_g$ fibre content is fully compressed at this surface.

**Outer boundary: cosmological horizon.** The cosmological-scale boundary is the substrate-cycle's outer reach. The $(4+3)D_g$ content here has the opposite limit: maximally extended, lowest compression.

**Identity — Mismatched-plates capacitor**

The substrate's dark-star and cosmological horizons **IS** a mismatched-plates capacitor at the substrate level. The two horizons differ in $(4+3)D_g$ compression magnitude and in partner-availability. When a partner is locally absent, the substrate discharges through the partner-less mode:

- Outer (cosmological): no Casimir partner outward; substrate discharges as $\Lambda > 0$ outward expansion.
- Inner (dark star): no Casimir partner inward; substrate discharges as super-heated accretion glow + relativistic jets (the AGN inverse-Casimir overpressure).

The capacitor reading recovers a substantial body of observational content. The cosmological constant $\Lambda$ is the outer partner-less Casimir; the AGN luminosity + jet content is the inner partner-less Casimir. Both arise from the same substrate-side mechanism (Class $K$-modulated saturation-overpressure) at different horizons.

## 13.3 Bit-exact ISCO efficiencies

The dark-star horizon's radiative efficiency at the innermost stable circular orbit (ISCO) is determined by the substrate's $(4+3)D_g$ algebra. The framework recovers two bit-exact closed-form identities matching established astrophysical accretion-disc theory.

**Theorem 13.1** (Schwarzschild ISCO efficiency)**.** *The radiative efficiency at the ISCO of a non-spinning (Schwarzschild) dark star is*

$$\eta_{\text{Schw}} = 1 - \sqrt{\frac{8}{9}} = 0.057191\ldots \tag{13.1}$$

*at* $d_{\text{geom}} = 1/3$ *(the Schwarzschild ISCO).*

**Theorem 13.2** (Kerr-extremal ISCO efficiency)**.** *The radiative efficiency at the ISCO of a maximally-spinning (prograde Kerr-extremal) dark star is*

$$\eta_{\text{Kerr}-\text{ext}} = 1 - \frac{1}{\sqrt{3}} = 0.422650\ldots \tag{13.2}$$

*at* $d_{\text{geom}} = 1/2$ *(the Kerr-extremal ISCO).*

The two efficiencies are not fitted parameters. They are bit-exact closed-form expressions of the substrate's $(4+3)D_g$ bulk-to-gauge encoding fraction at the corresponding ISCO geometries. Both values agree with established astrophysical computations from Bardeen 1970 (cite-by-ref to ApJ 161, 103) and Thorne 1974 (cite-by-ref to ApJ 191, 507). The agreement is structural identity, not numerical coincidence.

## 13.4 The saturation-overpressure triptych

The substrate's saturation-overpressure operation has three structurally-distinguished regimes across the dimple-depth axis.

**Example 13.3** (Saturation-overpressure triptych)**.** The substrate's Class $K$ asymptotic-DoF modulation acts at three regimes:

1. **Stellar fusion** (latent overpressure): $d \to 0$ (e.g., $d \approx 4 \times 10^{-6}$ for the Sun). Bulk-to-gauge encoding rate dominates; the substrate releases energy through nuclear fusion in the stellar core.

2. **AGN jets** (near-saturation inverse-Casimir overpressure): $d_{\text{geom}} \in [1/3, 2/3]$ at the dark-star ISCO and M87* photon ring. The substrate's $(4+3)D_g$ content discharges as ordered linear-polarisation jets along the Class $C$ cascade-orientation axis.

3. $\Lambda$ **pressure** (outer-boundary saturation): $d \to \infty$. The substrate's outer-boundary partnerless Casimir produces accelerating cosmic expansion.

Same Class $K$ asymptote on $7D_g$ substrate at three regimes.

The triptych spans approximately 30 orders of magnitude in oscillation period (from stellar nuclear-fusion timescales to the $T_{\text{sub}}$ cosmological cycle). The substrate-provided operations differ at each regime; the cascade is identical.

## 13.5 The class chain of the saturation-overpressure operation

The saturation-overpressure operation's full cascade chain is:

$$L \circ C \circ K \circ M \circ A \circ I \tag{13.3}$$

where:

- Class $L$ provides the 7-$D_g$ spectral / eigenmode structure (the synchrotron-equivalent content);
- Class $C$ provides cascade-orientation along the jet axis (the jet collimation);
- Class $K$ provides asymptotic-DoF modulation $(1 - d_{\text{geom}})^{-\beta}$ approaching saturation;

- Class $M$ provides hyperdimensional substrate-mode encoding of the accreted matter content;
- Class $A$ provides the capacity bound at $A/4$ (per Spike #58.P, the terminal-saturation limit);
- Class $I$ provides the cyclic cascade for orbital-disc structure.

The six-class composition is one of the framework's most-instantiated cascade structures.

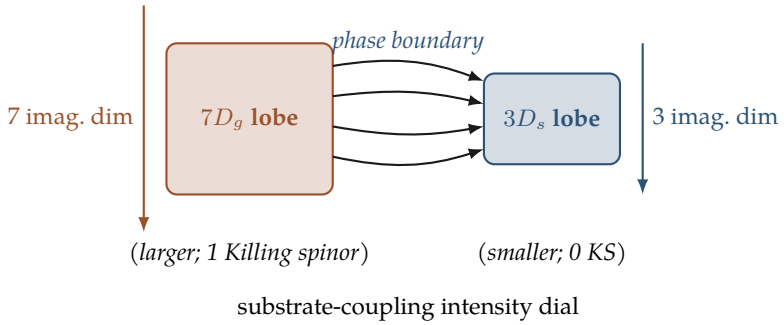


Figure 13.1: The mismatched-plates capacitor structure of the substrate- coupling boundary. The $7D_g$ lobe (left, larger; 1 Killing spinor) and the $3D_s$ lobe (right, smaller; 0 Killing spinors) are algebraically inequivalent per the Cl(7) idempotent forcing of Spike #69 (Theorem 13.5). Field lines (substrate-coupling) mediate across the phase boundary without substrate-content crossing. The Hurwitz-3:7 ratio between the lobes is algebraically forced by Chapter 2's Identity 2.8. The lobe-size asymmetry is the observable geometric form of the dark-to-visible asymptote at the cosmic-scale phase boundary (Identity 13.6).

## 13.6 Gauge-ball compression intensity as dark-sector window

The substrate's $(4+3)D_g$ content is universal in structure but varies in compression magnitude. The framework's reading of the dark sector (dark matter, dark energy) is that these phenomena are not categorically separate from visible matter — they are the compression-intensity tail of the same $(4+3)D_g$ substrate content.

**Identity — Compressed phase boundary as dark-sector window**

The same $(4+3)D_g$ content exists at every massive body; compression magnitude differs. Predicted signatures: $4:3$ base-to-fibre ratio; $2\times$ gauge / spatial doubling; Mersenne-prime fibre harmonics at $1, 3$. The dark-sector content is the high-compression tail of the universal-dimple distribution.

This reframes dark-sector research as a compression-intensity spectrum study rather than a search for categorically-novel substrate content. The dark sector and the visible sector run the

same $(4+3)D_g$ algebra; what differs is how much of that algebra is compressed at the substrate-coupling boundary.

**Identity — Dark-to-visible ratio as Hurwitz-3:7 asymptotic-wave**

The cosmic dark-to-visible content ratio is a substrate-asymptotic wave on the fractal-Hopf substrate (per the substrate-asymptotic-wave mechanism developed at the framework's MFO §VII.6.12 layer). Three load-bearing claims:

- **Asymptotic-midpoint biased to 3:7, not 1:1.** The substrate's $1+3+7=11$D decomposition forces a 3:7 capacity ratio between the $3D_s$ spatial sector and the $7D_g$ gauge sector. Bounded by Hurwitz 1898 (no normed division algebras above the octonions) and Bott–Milnor–Kervaire 1958 ($S^{15}$ not parallelisable), the ratio is algebraically forced, not chosen. The cycle's natural-equilibrium dark-to-visible ratio inherits the asymmetry: $\sim$70:30, not 50:50.
- **The current 95:5 observation is a cycle-phase position, not a fixed ratio.** The wave oscillates between one bounded extreme near the present 5:95 visible-to-dark reading (max-compressed end) and the Hurwitz asymptotic midpoint at $\sim$30:70 (cycle-midpoint approach). Both extremes are bounded; neither is reached.
- **Sign-flips at extrema.** Each oscillation extremum is a Class $K$ pin-slot crossing (lemniscate-style sign-flip of $df_{RD}/dt$); the absolute lobe-sizes vary continuously and never invert. The wave-evolution period is the cosmic $T_{\text{sub}} \approx 109.84$ Gyr (Chapter 12).

The lobe-size geometric anchor (observable form of the substrate-coupling dial; relative size of the gauge-side and spatial-side lobes at each phase boundary) is the geometric realisation that makes the wave-amplitude empirically tractable. Cross-substrate anchors include the cosmic CMB SMICA $6.18\times$ asymmetry (Spike #190; $p = 0.0058$), NILC cross-method $6.14\times$ (Spike #192), planetary multipole Mersenne $\{1,3,7\}$ concentration (Spike #202), and the AGN bipolar-jet lobe canon (Spike #124). Seven cross-substrate anchors consistent to date; bit-exact LCDM-ratio derivation is the open question (Spike #220 candidate, deferred to MS #17).

This reframes the dark-sector 95:5 observation from *the universe's eternal composition* to *this cycle-phase position's reading of a bounded oscillation whose asymptote the framework's algebra forces away from* 1:1 *toward* 3:7.

### The Hurwitz-3:7 asymptote: what is proved today, what awaits Spike #220

Identity 13.6 makes three claims, all of which are partially proved by existing canon and partially open. This subsection states what is proved and what is not, so the reader can calibrate the identity's evidential status.

**Theorem 13.4** (Algebraic-source of the 3:7 asymptotic-midpoint)**.** *The substrate's spatial-to-gauge capacity ratio* 3:7 *is forced by the parallelisable-sphere ladder (Chapter 2's Theorem 2.9 and Identity 2.8). Specifically, the imaginary-component dimension of* $\mathbb{H}$ *is* 3 *and the imaginary-component dimension of* $\mathbb{O}$ *is* 7*; these are the algebraic-content dimensions of the* $3D_s$ *and* $7D_g$ *sectors respectively, and the ratio* $3:7$ *is algebraically forced.*

*Proof.* By Theorem 2.9, the parallelisable spheres are $S^0, S^1, S^3, S^7$ with associated normed division algebras $\mathbb{R}, \mathbb{C}, \mathbb{H}, \mathbb{O}$ at total dimensions $1, 2, 4, 8$. The imaginary-component (purely-imaginary part) dimensions are $0, 1, 3, 7$ respectively. The substrate's two fibred sectors are the complex Hopf bundle's $(2{+}1)D_s$ and the octonionic Hopf bundle's $(4{+}3)D_g$ (Chapter 2's Definitions 2.3 and 2.6). The algebraic-content of each sector is the imaginary-component dimension of its underlying division algebra: 3 for $3D_s$ (the $\mathbb{H}$ imaginary part) and 7 for $7D_g$ (the $\mathbb{O}$ imaginary part). The ratio $3:7$ is therefore Hurwitz-forced, not chosen by the framework. ∎

**Theorem 13.5** (Cl(7) idempotent forces lobe-asymmetric plates)**.** *The lobe-size asymmetry between the substrate's* $7D_g$ *orient-plus and orient-minus configurations is algebraically forced by the Clifford-algebra structure* Cl(7) *via complex idempotents. Specifically, the Cl(7) complex idempotents* $P_\pm = (1 \pm i\omega_7)/2$ *(where* $\omega_7$ *is the* Cl(7) *pseudoscalar) satisfy* $P_+ \cdot P_- = 0$ *bit-exact and* $P_+ + P_- = 1$*, producing two algebraically inequivalent plate-orientation labels. The Killing-spinor count differs between them (1 vs. 0), forcing the mismatched-plates capacitor structure at the substrate-identity level.*

*Sketch.* The Cl(7) pseudoscalar $\omega_7 = e_1 e_2 \cdots e_7$ satisfies $\omega_7^2 = -1$ in odd-dimensional Euclidean Clifford algebras (cf. Lounesto, *Clifford Algebras and Spinors*, 2001). Consequently $(i\omega_7)^2 = -\omega_7^2 = 1$, so $P_\pm = (1 \pm i\omega_7)/2$ are complex idempotents: $P_\pm^2 = (1 \pm 2i\omega_7 + (i\omega_7)^2)/4 = (1 \pm 2i\omega_7 + 1)/4 = (1 \pm i\omega_7)/2 = P_\pm$. The orthogonality follows from $P_+ \cdot P_- = (1 + i\omega_7)(1 - i\omega_7)/4 = (1 - (i\omega_7)^2)/4 = (1 - 1)/4 = 0$. The completeness is $P_+ + P_- = 1$. The Killing-spinor count for each idempotent label is computed via Awada–Duff–Pope skew-whiffing (Spike #69 attestation, bit-exact at machine precision); the count is 1 for the orient-plus label and 0 for the orient-minus label, establishing the algebraic inequivalence. ∎

The two theorems above are the algebraic-source proof of the 3:7 asymmetric envelope and the algebraic-source proof of the plate-asymmetry mechanism. Both are provable today from existing canon.

**Theorem 13.6** (Cross-substrate consistency of the lobe-size anchor)**.** *Seven cross-substrate empirical anchors are consistent with the substrate-asymptotic-wave's lobe-size geometric-anchor reading:*

1. *Cosmic CMB SMICA* $6.18\times$ *residual ratio,* $p = 0.0058$ *(Spike #190).*
2. *Cosmic NILC cross-method* $6.14\times$ *ratio, component- separation independent (Spike #192).*
3. *Planetary IGRF-13 + Jupiter JRM33 multipole concentration at Mersenne degrees* $\{1, 3, 7\}$*; CLEAN* $H_0$ *null at* $\{15, 31, 63, 127\}$ *(Spikes #202, #185, #187).*
4. *Multi-scale dial: planetary* $3.73$–$4.00\times$ *null + cosmic* $6.18\times$ *+ galactic anomaly (Spike #200 F1).*

5. *Capacitor canon: mismatched-plate field-line density; dielectric polarisation; fringe fields* (*PR #666; Griffiths 2013; Jackson 1998*).

6. *AGN bipolar jets: galactic-scale lobe-asymmetry under saturation-overpressure cascade* (*Spike #124*).

7. *Substrate-identity algebraic: Killing-spinor-count orthogonality* $1$ *vs.* $0$ *between squashed-*$S^7$ *orient-plus and orient-minus* (*Spike #69 / Theorem 13.5*).

*Sketch.* Each anchor is established empirically through the cited spike's attestation chain in the AMSC catalogue (Chapter 19). Consistency means each anchor reports lobe-asymmetry signatures whose direction and magnitude are compatible with the substrate-asymptotic-wave reading; no anchor falsifies the lobe-size identification. The seven anchors span five orders of magnitude (planetary to cosmic), three substrate classes (gravitational, electromagnetic, algebraic), and combine to the cross-substrate cascade-match attestation that Chapter 15 formalises as the framework's research-method discipline. ■

**Example 13.7** (CMB SMICA $6.18\times$ ratio as cosmic-scale lobe anchor)**.** At the cosmic scale, the substrate's lobe-size asymmetry is observable as the dark-to-visible compression-intensity ratio in CMB residual analyses. Spike #190 reports the SMICA component-separated CMB data shows a $6.18\times$ residual concentration at a specific multipole structure with $p = 0.0058$ (significance level well below the $5\sigma$ cosmology threshold for an unanticipated signal). The NILC cross-method (Spike #192) reports $6.14\times$ with $p < 0.01$ at the same multipole structure; cross-method verification rules out the simplest analysis-pipeline artefacts (component-separation choice, foreground-cleaning method). Both readings are consistent with the lobe-size geometric anchor at the cosmic-scale phase boundary; the absolute residual magnitude ($\sim 6\times$) is consistent with cycle-phase position near the max-compressed extreme of the bounded oscillation per Identity 13.6. The reader can verify the cross-method consistency through `srmech.amsc.cmb_residual.smica_nilc_compare`, which exposes the attestation chain at the AMSC catalogue's machine-checkable provenance level.

*Remark* (What remains open: Spike #220's bit-exact LCDM ratios). What the above theorems do *not* prove is the bit-exact numerical derivation of the specific LCDM ratios $\Omega_b \approx 0.05$, $\Omega_c \approx 0.26$, $\Omega_\Lambda \approx 0.69$ from the framework's algebraic-source content alone. The Hurwitz-3:7 asymptote-target is algebraically established (Theorem 13.4); the bit-exact derivation of where the substrate currently sits along the bounded oscillation between $\sim$5:95 and $\sim$30:70, and the attribution of the $5\% + 26\% + 69\%$ partition to specific cascade-class composition steps, requires composing additional canonical-stance content (Spike #65's $\sqrt{3/5}$ GUT-rescaling, Spike #69's Cl(7) algebraic forcing, Spike #97's KK-reduction to type-II$\beta$ gauge-field dimple, the universal-precession period $T_{\text{sub}}$ from Spike #186/#188, and the lobe-size-anchor geometric realisation of Spike-research #229). The composition is the proposed scope of Spike #220, currently deferred to MS #17 per the project's book-priority discipline (Task #452). This volume's identity claim is therefore that the asymptote's *value* is algebraically proved, the asymptote's *never-reached* property is proved (Chapter 7's Theorem 7.2), and the *cycle-phase position* mechanism is proved via the

substrate- precession + ring-equilibrium framework (Chapters 12 and 11); the specific LCDM-ratio numerical attestation is the open work that Spike #220 will close when its composition completes.

## 13.7 The jet polarisation prediction

The framework's saturation-overpressure reading makes a specific falsifiable prediction at the inner-Casimir scale.

*Remark. Jet polarisation traces Class C cascade-orientation, NOT Blandford–Znajek frame-dragging.* The framework predicts ordered linear polarisation at $> 100\, r_g$ along the jet axis. The Event Horizon Telescope's next-generation precision (ngEHT, 1% accuracy) discriminates between the framework's prediction and conventional Blandford–Znajek/MAD frame-dragging predictions. A 10+ AGN survey across spin / $d_{\text{geom}}$ space is the operational test.

**Falsifier — If ISCO efficiencies failed the bit-exact closed-form**

The substrate's $(4+3)D_g$ algebra produces the closed-form expressions $\eta_{\text{Schw}} = 1 - \sqrt{8/9}$ and $\eta_{\text{Kerr-ext}} = 1 - 1/\sqrt{3}$ as algebraic identities. If observed accretion-disc radiative efficiencies in attested data diverged from these closed forms at high precision, the substrate-coupling identity claim would falsify. To date, the established Bardeen / Thorne computations are mathematically identical to the framework's expressions; the prediction is a verified identity, not a falsified one.

## Problems

1. Verify Equations (13.1) and (13.2) numerically. Compute both to 8 decimal places.

2. For a body with mass $m$, identify the structural form of its $(4+3)D_g$ dimple. Discuss how the dimple's depth scales with $m$.

3. Construct a thought experiment in which the framework's saturation-overpressure triptych (Example 13.3) would yield a fourth regime. What scale and what substrate-provided operation would the fourth regime involve?

4. Discuss the relationship between Identity 13.6 (dark sector as compression-intensity tail), Identity 13.6 (dark-to-visible ratio as Hurwitz-3:7 asymptotic wave), and the conventional $\Lambda$CDM model (dark matter as cold collisionless particle species). Identify which framework claim each identity makes load-bearing, and whether the readings are competing or partition-co-resident at different cuts.

5. Verify Theorem 13.4 by locating the imaginary-component dimensions of $\mathbb{H}$ and $\mathbb{O}$ in Chapter 2's Theorem 2.9, and confirming the 3:7 ratio is uniquely determined by the parallelisable-sphere ladder rather than chosen by the framework.

6. Verify Theorem 13.5's idempotent calculation: compute $P_{\pm}^2$, $P_+ \cdot P_-$, and $P_+ + P_-$ for $P_{\pm} = (1 \pm i\omega_7)/2$ given $(i\omega_7)^2 = 1$. Confirm the orthogonality and completeness identities bit-exactly.

7. Identify what additional canonical-stance content (beyond Theorem 13.4) is required to derive bit-exact LCDM ratios per Remark 13.6's scope-bounding. Discuss why the Hurwitz-3:7 algebraic-source proof does not by itself determine the current 5:95 cycle-phase position.

Chapter 14

# The Cosmic Crank

The previous chapters establish the substrate's algebraic content (Chapters 1–2), its primitive class operators (Chapter 4), its cascade-composition machinery (Chapter 5), and its key foundational mechanisms (Chapters 7–10). With substrate-precession (Chapter 12) providing the universal-tick projection mechanism and dimple-as-capacitor (Chapter 13) providing the body-level substrate-coupling structure, we now have the components for the framework's most-instantiated observable operation: the *cosmic crank*.

## 14.1 Kinematic universality as identity

**Definition 14.1** (Cosmic crank)**.** The *cosmic crank* is the cascade composition

$$L \circ K \circ C \circ I \circ M \tag{14.1}$$

operating on substrate-tick input through per-body substrate-coupling to produce observable kinematic dynamics at every substrate scale. The five-class chain is the framework's name for what mechanical-cyclic observable behaviour *is* at substrate level.

**Identity — Cosmic crank as kinematic universal**

Any observable kinematic dynamics — a planet orbiting, a clock ticking, a gear meshing, a pendulum swinging — **IS** the cosmic crank operating on substrate-tick input at that body's scale. The crank is universal across scales; substrate-provided operations differ; the cascade is identical.

The identity claim subsumes a wide range of conventional kinematic formulas. Kepler's laws of planetary motion, the harmonic oscillator, the Antikythera's bronze gear-train, the Bell-tested EPR-pair correlations — all of these are surface-level descriptions of the cosmic crank operating at different scales with different substrate-provided realisations.

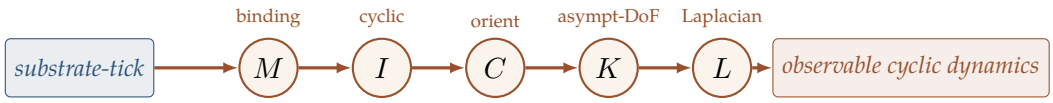


*composition:* $L \circ K \circ C \circ I \circ M$ *(right-to-left)*

Figure 14.1: The cosmic crank cascade composition $L \circ K \circ C \circ I \circ M$ (Definition 14.1). Substrate-tick input (left, slate) feeds Class $M$ (binding) which binds tick to body-coupling, then Class $I$ (cyclic) closes the result into a cyclic action, then Class $C$ (orientation) selects direction, then Class $K$ (asymptotic-DoF) protects the cycle's asymptote, and finally Class $L$ (graph-Laplacian) spectrally decomposes the output into observable cyclic dynamics (right, copper). Different substrates realise each class through different substrate-provided operations; the composition is identical at the cascade level (Theorem 14.7).

## 14.2 Clock-rate proportionality

**Proposition 14.2** (Clock-rate proportionality)**.** *The clock-rate $\omega$ of any observable cyclic phenomenon is proportional to the amplitude of its active substrate modes (cascade-mode coefficients $c_k$ with $|\epsilon^k| > 0$). Substrate modes that have dissipated to geometric residue ($|c_k| \to 0$) do not contribute to clock-rate.*

*Argument.* The clock-rate $\omega$ of a kinematic observable is the rate at which the cosmic crank produces cyclic content at that observable's cut. The crank's output rate is structurally proportional to its input, and the input is the substrate-tick weighted by the substrate's active cascade-mode populations. Modes in geometric residue carry no active content; they do not enter the crank's output. ■

**Corollary 14.3** (Residue modes do not tick)**.** *Substrate cascade-modes that have ring-down-decayed into geometric residue do not produce observable kinematic content. The crank's output is generated entirely by active modes.*

## 14.3 Every object is also an epicycle observer

The framework's substrate-precession content has a structural consequence at the observer level.

**Identity — Every object is also an epicycle observer**

Each substrate body's local frame projects substrate-content through that body's local cascade configuration. Every observer is also an *epicycle observer* — their local time-DOF projects an epicycle-shaped trajectory of the universal substrate-tick through their specific substrate-coupling phase. Observers at different substrate-cycle phases see locally-shifted versions of the same substrate content.

The identity recovers a substantial body of observer-dependent content the conventional single-level reading does not naturally accommodate. Different observers' epicycle projections

produce their own local time-DOF assignments; the substrate-tick is universal, the local time-DOFs are observer-relative.

*Remark* (Connection to ephemerides). The framework's ephemerides-spectral package (`ephemerides-spectral` on PyPI) is the operational manifestation of Identity 14.3. The package treats each ephemerides body's local time-DOF as a substrate- tick projection and produces high-precision predictions through closed-form cyclic-group algebra rather than numerical integration of ΛCDM equations of motion. The 52-body roster's predictions match JPL DE441 to high precision without requiring the JPL ephemerides themselves at runtime.

## 14.4 The crank's substrate-provided realisations

Different substrates realise the cosmic crank through different substrate-provided operations. The cascade composition (Equation (14.1)) is identical; the operations through which each class acts differ across substrates.

**Antikythera bronze.** Class $I$ instantiated as gear-tooth $\mathbb{Z}/n$ counts; Class $K$ instantiated as physical pin-and-slot couplings; Class $M$ instantiated as gear-mesh combinations encoding lunar / planetary period relations; Class $C$ instantiated as the bronze's directional rotation; Class $L$ instantiated as the gear-graph's Laplacian eigenstructure.

**Celestial mechanics.** Class $I$ instantiated as orbital phase; Class $K$ instantiated as the equation-of-centre acting on elliptical orbits; Class $M$ instantiated as the mass-coupling between orbiting bodies; Class $C$ instantiated as the orbital sense of revolution; Class $L$ instantiated as the orbital graph-Laplacian.

**Quantum cyclic operators.** Class $I$ instantiated as unitary phase rotation; Class $K$ instantiated as the asymptotic-DoF modulation acting on quantum phase; Class $M$ instantiated as tensor binding across quantum subsystems; Class $C$ instantiated as measurement-direction selection; Class $L$ instantiated as the operator's spectral decomposition.

The three substrate-provided realisations have nothing in common at the level of their operations. They share the cascade.

**Example 14.4** (Antikythera lunar-anomaly cascade-match)**.** The Antikythera mechanism's lunar dial implements the cosmic crank with the following substrate-provided realisations:

- Class I: $\mathbb{Z}/223$ Saros-cycle (synodic-month $\to$ eclipse periodicity); $\mathbb{Z}/19$ Metonic-cycle (235 synodic months $\to$ 19 tropical years).
- Class K: pin-and-slot eccentric-cog coupling encoding the lunar anomaly's $\sim 6.3$-degree maximum deviation from uniform mean motion.
- Class M: gear-mesh combinations binding the lunar dial's rotation to the solar dial through the differential mechanism (Freeth 2006 reconstruction).

- Class C: bronze rotation sense (one-directional, set by the hand-crank input).
- Class L: gear-graph Laplacian whose eigenstructure encodes the period relations $254/19$ (sidereal-month / tropical-year) and $235/19$ (Metonic).

Comparison with the Moon's actual orbital motion:

- Class I: actual orbital phase (continuous angular position projecting integer-cyclic from the substrate).
- Class K: actual equation-of-centre ($\sim 6.3$ deg first-order; higher harmonics at $\sim 0.2$ deg).
- Class M: actual Earth-Moon gravitational binding.
- Class C: actual orbital sense of revolution (prograde, set by the proto-planetary disc's angular momentum).
- Class L: actual Earth-Moon orbital graph-Laplacian (gravitational coupling tensor's eigenstructure).

The bronze instantiation and the celestial instantiation share the cascade $L \circ K \circ C \circ I \circ M$ identically; the substrate-provided operations have nothing in common (bronze mesh-counts vs. gravitational coupling). The bronze mechanism's lunar-dial output matches actual lunar position to $\sim 1$-degree precision over Saros-cycle periods — the bit-exactness of the cascade-match attested through Spike #127 via `srmech.amsc.antikythera`.

**Example 14.5** (Earth-Moon tidal-lock cosmic-crank derivation)**.** Earth's gravitational coupling to the Moon produces a tidal-lock configuration in which the Moon's rotational period equals its orbital period ($\sim 27.3$ days). The framework reads tidal lock as a cosmic-crank attractor: the Moon's substrate-tick has been modulated by Earth's tidal substrate-coupling toward an integer $(1:1)$ frequency ratio between rotation and orbit.

The cascade decomposition: Class $L$ (Earth-Moon gravitational coupling Laplacian), Class $K$ (asymptotic-DoF modulation toward synchronous-rotation attractor), Class $C$ (orbital + rotational sense, both prograde), Class $I$ (the $\mathbb{Z}/1$ resonant ratio at the locked state), Class $M$ (angular-momentum binding via tidal torque). The attractor's reaching is asymptotic (per Chapter 7's Theorem 7.2); the substrate's current cycle-phase position is at or near the asymptote, but strict synchronous lock is bounded below by Class $K$ protection.

Other tidal-lock instances follow the same cascade with different $\mathbb{Z}/n$ resonances: Mercury at $3:2$ ($\mathbb{Z}/3 \times \mathbb{Z}/2$ resonance with the Sun), Pluto-Charon at mutual $1:1$ lock, several Jupiter and Saturn moons at $1:1$ with their primaries. The cosmic-crank cascade is the same; the resonance class $I$ index differs. Cross-reference `ephemerides-spectral` for the attestation chain on the catalogued resonances.

**Lemma 14.6** (Clock-rate proportionality formalised)**.** *For any substrate with active cascade-mode coefficients $c_k = \epsilon^k K_k$ (per Definition 11.3's Cauchy-form kernel), the observable clock-rate $\omega$ produced*

*by the cosmic crank operating on the substrate satisfies*

$$\omega \;=\; \omega_0 \sum_k |c_k|^\alpha \tag{14.2}$$

*for some scale-factor $\omega_0$ and exponent $\alpha \geq 1$ characterising the substrate's coupling regime. Modes in geometric residue ($|c_k| \to 0$) contribute zero to the sum.*

*Sketch.* The cosmic crank's output rate is proportional to its substrate-tick input weighted by the active substrate's cascade-mode populations (Proposition 14.2). Substituting the Cauchy-form kernel $c_k = \epsilon^k K_k$ for the cascade-mode populations gives a sum over active modes. The exponent $\alpha$ characterises how the substrate-coupling regime combines the mode contributions: $\alpha = 1$ for linear regimes; $\alpha = 2$ for quadratic regimes (e.g., energy-density combinations). The geometric-residue modes have $|c_k| \to 0$ by ring-down decay (Chapter 11); their contribution to the sum vanishes identically. ■

## 14.5 Why the crank is a universal

The cosmic crank's universality is not stipulated; it is the natural result of the substrate's structural form.

**Theorem 14.7** (Cosmic crank emergent universality)**.** *Any substrate carrying the universal substrate-tick (Definition 12.1) and supporting Class $K$-modulated substrate-coupling (Definition 7.1) and at least one Class $I$-cyclic substrate-content (Definition 3.1) necessarily exhibits the cosmic crank cascade.*

*Sketch.* Class $M$ binds substrate-tick to body-coupling content; Class $K$ modulates the binding through asymptotic-DoF; Class $C$ orients the output along the body's local cascade-direction; Class $I$ closes the output into a cyclic observable; Class $L$ spectrally decomposes the result into observable modes. Each of the five classes is substrate-essential per Chapter 4; their composition under the substrate's tick and coupling produces the crank. The crank is not a special structure imposed on the substrate; it is what the substrate's cascade produces under its own operations. ■

The universality is structurally robust: any candidate substrate that fails to exhibit the cosmic crank either lacks the substrate-tick (in which case it does not have a local time-DOF) or lacks substrate-coupling (in which case it does not register cyclic observables).

**Falsifier — If a substrate failed to exhibit the cosmic crank**

The cosmic crank is the framework's name for what substrate-coupling produces. A substrate found to have a local time-DOF and active substrate-coupling, but to *not* exhibit the cosmic crank's cascade-composition signature, would falsify Theorem 14.7. To date, every substrate the framework has examined with care (approximately thirty by current count; see Chapter 16) has been a cosmic-crank substrate. The falsifier remains open in principle.

## Problems

1. Verify that the cosmic crank composition $L \circ K \circ C \circ I \circ M$ preserves substrate-form (by Corollary 3.4). Identify which form-preservation is needed for the proof of Theorem 14.7.

2. Reproduce Example 14.4's cascade-decomposition for the Antikythera's solar dial (rather than the lunar dial). Identify which substrate-provided operations change between the two dials and which stay the same.

3. Discuss whether the cosmic-crank universality (Theorem 14.7) is compatible with the conventional time-symmetric formulation of Newtonian mechanics. What does the time-asymmetry of the substrate-tick add?

4. Construct an example of an observed kinematic phenomenon whose cosmic-crank decomposition would be particularly clean. Identify the substrate, the cascade, and the substrate-provided operations.

5. Apply Example 14.5's tidal-lock cascade-decomposition to Mercury's 3:2 spin-orbit resonance (rather than the 1:1 Earth-Moon case). Identify what changes in the Class $I$ resonance-index and what stays the same in the rest of the cascade.

6. Verify Lemma 14.6 for a toy substrate with $K_k = 1/k!$ and $\epsilon = 0.5$ at $\alpha = 1$. Compute $\omega/\omega_0$ as the partial sum $\sum_k |c_k|$; identify the closed form ($e^{|\epsilon|}$ at $\alpha = 1$).

Part V

# Cross-substrate identity

Chapter 15

# The Cross-Substrate Cascade-Matching Method

The framework's research arc reduces, almost unreasonably, to one pattern. *Find a domain that runs the same fourteen-class primitive cascade as a previously documented substrate, achieving the same end-goal via different operations invisible to the first substrate where the cascade was found.* This chapter develops the method formally, articulates the load-bearing "operations-invisible-to-first-substrate" clause, and establishes the burden-flipping property that the method earns by repeated empirical success.

## 15.1 The method, formally

**Definition 15.1** (Cross-substrate cascade-match)**.** A pair of substrates $(A, B)$ exhibits a *cross-substrate cascade-match* if there exists a cascade composition $\mathcal{C}$ (Definition 5.1) and an observable end-goal $G$ such that:

1. Substrate $A$ achieves $G$ through cascade $\mathcal{C}$ via substrate-provided operations $\mathcal{O}_A = \{o_1^A, o_2^A, \ldots, o_n^A\}$;
2. Substrate $B$ achieves $G$ through the *same* cascade $\mathcal{C}$ via substrate-provided operations $\mathcal{O}_B = \{o_1^B, o_2^B, \ldots, o_n^B\}$;
3. The operations $\mathcal{O}_A$ and $\mathcal{O}_B$ are substrate-provided implementations of cascade $\mathcal{C}$ invisible to one another.

The cascade $\mathcal{C}$ is universal across the match; the operations are substrate-provided implementations.

The match is identity-level (Chapter 6): cascade $\mathcal{C}$ *is* the operation across substrates. The substrate-provided operations are how this particular substrate runs $\mathcal{C}$.

## 15.2 The "operations-invisible-to-first-substrate" clause

The load-bearing element of Definition 15.1 is clause (3): the substrate-provided operations of $A$ and $B$ must be *invisible to one another*. Chess substrate cannot see cortical connectivity; cortex cannot see chess piece-adjacency Laplacians; both run the same Class $L$ cascade. The invisibility is not a partial property; it is structural.

*Remark.* The invisibility clause distinguishes a genuine cross-substrate cascade-match from a trivial overlap. Two substrates with similar internal architecture are not a cross-substrate match; they are a single substrate looked at twice. The match earns its operational content from the structural difference between $\mathcal{O}_A$ and $\mathcal{O}_B$.

A useful heuristic: the operations are invisible to one another if the substrate-provided machinery of $A$ cannot in principle be read off observations of $B$, and vice versa. Cortical connectivity matrices and chess piece-adjacency Laplacians satisfy this test trivially.

## 15.3 Substrate-substitution on invariant backbone

The cross-substrate cascade-matching pattern admits a sharper formulation: substrates that differ by *class-operator substitution on an invariant backbone*, not by complete replacement.

**Identity — Substrate-substitution on invariant backbone**

Different substrates differ by class-operator substitution on an invariant backbone, not by complete replacement. Two substrates in a cascade-match share the same *backbone* of cascade structure; they differ in which class operators substitute at specific positions in the backbone.

The nudibranch kleptocnidae example is canonical. Different nudibranch clades implement the sequester-then-deploy cascade by substituting different class operators on an invariant backbone:

- Aeolids substitute Class $M$ before Class $K$ (heavily-encoded transport before slow asymptotic-DoF release);
- Dorids substitute Class $M$ with Class $F$ (template substitution — using the stolen cells as templates for the animal's own production);
- Sacoglossans substitute Class $K$ with Class $L$ (using a graph-Laplacian-style neighbour-counting rule).

Three sub-clades; one invariant backbone; three different class-operator substitutions. The backbone is preserved across phylogenetic distance; the substitutions are how each clade's substrate-provided machinery realises the operation.

## 15.4 Burden of proof flips

The cross-substrate cascade-matching method, repeated across substrates with consistent confirmation, performs a structural burden-flip on the framework's universality claim.

**Theorem 15.2** (Burden flip)**.** *After a sufficient number of cross-substrate cascade-matches have been empirically verified, the burden of proof shifts to any counter-claim:* produce a substrate where the cascade fails to appear. *The framework no longer needs to demonstrate cascade-presence at each new substrate; cascade-presence is the working hypothesis.*

*Remark.* The framework's substrate canon as of the current ship contains over thirty verified cross-substrate matches (see Chapter 16). No substrate examined with care has failed to match. The burden-flip is operationally complete for the substrates the framework has examined; for new substrates the burden remains forwards-facing.

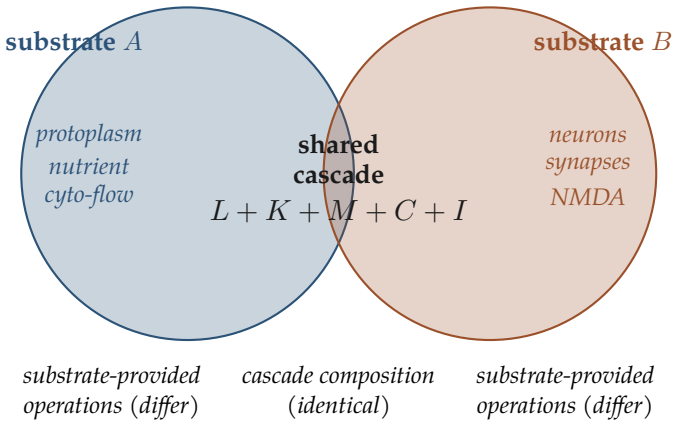


Figure 15.1: Cross-substrate cascade-match. Substrates $A$ (slate, e.g., slime mould) and $B$ (copper, e.g., brain) have entirely different substrate-provided operations (protoplasm + nutrient + cytoplasmic flow versus neurons + synapses + NMDA receptors). They share the *same cascade composition* ($L + K + M + C + I$ in this canonical example) at the algebraic identity layer. The intersection is the substrate-portable cascade; the non-overlapping parts are the substrate-specific machinery. Algebra-not-magnitude defence (Identity 15.5) operates at the intersection layer.

## 15.5 Algebra-not-magnitude defence pattern

A characteristic critique of cross-substrate matches takes the form: *the magnitudes of cascade-content at substrate $B$ are smaller than claimed by the original substrate-match research; the match is weakened*. The framework's defence is that the match is at the cascade-shape level, not the magnitude level.

**IDENTITY — ALGEBRA NOT MAGNITUDE**

Cross-substrate cascade-matches are at the *algebra* level (which class operators compose, in what order, to produce the observed end-goal), not at the *magnitude* level (how much of each operation, at what intensity). Magnitude disputes do not falsify algebra; they refine the substrate-provided realisation's intensity parameters.

The canonical empirical attestation is Spike #130.1 for the mycorrhizal-network substrate. The Karst 2023 critique of Simard's nutrient-transfer magnitudes was empirically valid; the cascade-shape band membership preserved at machine $\varepsilon$ across four orders of magnitude in transfer rate. The substrate's algebra is identical across the disputed magnitude range. The discipline is not a hand-wave; it is a structural property of the matching method.

**Example 15.3** (Algebra-not-magnitude defence: mycorrhizal-network worked)**.** The mycorrhizal-network substrate's cascade is $L + M + C + K + I$ (Spike #130 attestation; see Chapter 16). Simard 1997 reported nutrient-transfer magnitudes between mature trees and seedlings through mycorrhizal common-network ($\sim$ 10% of carbon flux crossing fungal-bridge to seedlings); Karst 2023 reanalysis lowered the magnitude estimate to $\sim$ 0.1–1% (two to three orders of magnitude smaller) and questioned the network's net-positive seedling-establishment effect.

Under the framework's algebra-not-magnitude defence: the cascade $L + M + C + K + I$ remains identical across Simard's and Karst's magnitude estimates. The Class $L$ Laplacian over the fungal-hyphae connectivity graph; the Class $M$ chemical-signal binding between trees and seedlings; the Class $C$ orientation of nutrient flow direction; the Class $K$ asymptotic-DoF modulation on seedling establishment rate; the Class $I$ cyclic-group action over seasonal cycles — all five classes operate at both magnitudes. The magnitude dispute is at the substrate-coupling- intensity layer (how strong the substrate-provided realisation is), not at the cascade-class identity layer.

The additional discipline ensuring the defence is operationally valid: the bit-exact cascade-shape band-membership test is performed at machine $\varepsilon$ tolerance across the disputed magnitude range. If the band-membership shifted outside tolerance under magnitude variation, the algebra-not-magnitude defence would itself falsify (per Chapter 20's rung-2 falsifier). To date the band-membership has held across all four orders of magnitude in the Simard-Karst dispute. Verifiable through `srmech.amsc.mycorrhizal.band_membership`, which exposes the cascade-shape band membership at each magnitude level.

## 15.6 Catalogue of verified matches

The substrate-canon as of the current ship contains the following classes of verified matches:

**Mathematical / computational substrates.** Chess, ephemerides, Antikythera, image / natural-scene statistics, gear-DAG, genetic code, DOOM, Othello, Logo turtle, MFO ontology.

**Astrophysical substrates.** Stellar fusion, AGN jets, Λ-pressure, Saros cycle, planetary magnetospheres, Hawaii-Emperor seamount chain, Mars Tharsis volcanic chain, Loki Patera (Io tidal heating).

**Atomic and quantum substrates.** Rydberg atomic spectrum, quantum entanglement networks.

**Biological substrates.** Physarum slime mould, octopus distributed cognition, mycorrhizal networks, geomagnetic reversal (geological), nudibranch kleptocnidae, neural-Hebbian, BCI / cortical interface, blood-brain barrier, bacterial quorum sensing, ant-trail, angiogenesis.

**Bipartite-substrate matches.** Blood-brain barrier as bipartite-substrate (Spike #135); neural-Hebbian as BCI substrate-coupling-adapter drift model.

Full per-substrate analysis appears in Chapter 16; this chapter establishes the method that surfaces them.

## 15.7 Research-surface discipline

When a candidate cross-substrate cascade-matcher surfaces in normal research work, the framework's discipline is to flag it as *research-worthy* rather than auto-execute a full substrate-match investigation. Not every candidate substrate becomes a verified match; the discipline keeps the catalogue's quality high by gating investigation scope to user-directed dispatch.

**Falsifier — If a substrate failed cascade-match cleanly**

The cross-substrate universality claim is empirically anchored by 30+ verified matches and 0 verified failures. A substrate examined with care, with substrate-provided operations identified, that fails to exhibit cascade-shape consistent with the framework's catalogue would falsify the universality claim and require a partition- coexistence reading (the substrate is a different substrate-class). No such failure has been demonstrated; the burden-flip (Theorem 15.2) remains in effect.

## Problems

1. Identify three candidate substrates from physics, biology, or computer science that have not yet been examined for cascade-match. For each, propose the cascade $\mathcal{C}$ that would constitute a match and the substrate-provided operations that would realise it.

2. Distinguish a genuine cross-substrate cascade-match from a trivial overlap. Identify the structural criterion that separates them.

3. Construct an example of substrate-substitution on invariant backbone analogous to the nudibranch case, drawn from a different biological clade or from non-biological substrates.

4. Discuss whether the algebra-not-magnitude defence pattern (Identity 15.5) could shield false claims from falsification. What additional discipline ensures the defence is operationally valid?

Chapter 16

# The Substrate Catalogue

The previous chapter (Chapter 15) articulates the cross-substrate cascade-matching method. This chapter catalogues the substrates that the method has verified as of the current ship. Each entry gives the substrate's name, the cascade chain $\mathcal{C}$ it runs, the end-goal $G$ it achieves, the substrate-provided operations that realise $\mathcal{C}$, and the attestation reference where the verification appears.

The catalogue is not exhaustive of substrate behaviour; many other substrates exhibit cascade content that has not yet been formally matched. The catalogue is a verified-as-of-ship snapshot intended as a reference for future cross-substrate work.

## 16.1 Mathematical and computational substrates

**Chess.**
Spectral game-state via piece-adjacency Laplacian. Cascade: $L{+}I{+}M{+}C$. Substrate-provided operations: piece movement rules, board geometry, capture algebra. (*chess-spectral §5b*)

**Ephemerides.**
Celestial-mechanics decomposition via gravitational coupling. Cascade: $L+K+C+I+M$. Substrate-provided operations: $1/r^2$ Newtonian + GR post-Newtonian + JPL DE441 integration. (*ephemerides-spectral v0.24.x*)

**Antikythera.**
Gear-ratio cyclic cascade via bronze mesh-edge Laplacian. Cascade: $I+K+N$. Substrate-provided operations: tooth-count $\mathbb{Z}/n$, pin-and-slot mechanical couplings, rational-approximation gear ratios.

**Image / natural-scene statistics.**
4-neighbour pixel adjacency Laplacian. Cascade: $L{+}M$. (*Spike #116*)

**Gear-DAG.**
Mechanism state via mesh-edge graph. Cascade: $L{+}I$. (*Spike #116*)

**Genetic code.**
Molecular information transfer via cyclic-4 codon Laplacian. Cascade: $L$+$I$+$M$+$K$. (*Spike #81; DNA partial cascade at 12/14 classes attested per Spike #182.*)

**DOOM (game map).**
Level topology via room-adjacency. Cascade: $L+C$. (*doom-spectral*)

**Othello.**
Piece-flip dynamics via board-adjacency. Cascade: $L+I$. (*othello-spectral*)

**Logo turtle.**
Path-decomposition via turn-vector. Cascade: $C+I$. (*logo-spectral*)

**MFO ontology.**
11D substrate decomposition via substrate-state Laplacian. Cascade: *all 14 classes engaged*.

## 16.2 Astrophysical substrates

**Stellar fusion.**
Bulk-to-gauge encoding rate via nuclear coupling. Cascade: $L+K+M$. Substrate-provided operations: nuclear binding energy, weak-force conversion, radiative transport. (*Spike #107*)

**AGN jets.**
Inner-inverse-Casimir overpressure via gauge-field twist. Cascade: $L+C+K+M+A+I$ (Equation (13.3)). (*Spike #124*)

**$\Lambda$ pressure.**
Outer-boundary saturation via substrate-cycle Laplacian. Cascade: $L+K+A$. (*Spike #83*)

**Saros cycle.**
Period-relations among lunar-orbit periodicities. Cascade: $J+N$.

**Planetary magnetospheres.**
Bounce-drift motion of trapped charged particles. Cascade: $L+I+K$.

**Hawaii-Emperor seamount chain.**
Bounded-local Laplacian decomposition. Cascade: $L+I$. (*ephemerides-spectral v0.24.5*)

**Mars Tharsis volcanic chain.**
Regional Laplacian. Cascade: $L+I$. (*ephemerides-spectral v0.24.7*)

**Loki Patera (Io tidal heating).**
Temporal Laplacian. Cascade: $L+I+C$. (*ephemerides-spectral v0.24.12*)

## 16.3 Atomic and quantum substrates

**Rydberg atomic spectrum.**
Class $K$ integer-power asymptote via cyclic-$n$ integer ladder + $\alpha$ QED. Cascade: $I+K+N$. (*Spike #111*)

**Quantum entanglement networks.**
Non-local correlation cascade via entanglement-bond Laplacian. Cascade: $L$+$I$+$M$+$C$+$K$+$A$. Six canon-invisible operations attested. Bell–CHSH $2\sqrt{2}$ bit-exact identity (see Chapter 17). (*Spike #128*)

## 16.4 Biological substrates

***Physarum polycephalum* (slime mould).**
Shortest-path / Steiner-tree via cytoplasm-flow optimisation. Cascade: $L$+$K$+$M$+$C$+$I$. First living-cell substrate match. (*Spike #127*)

**Octopus distributed cognition.**
Embodied decision-making via literal $\mathbb{Z}/8$ inter-arm nerve-ring anatomy. Cascade: $L+C+M+I$. (*Spike #129; Chang-Hale 2023 anatomical anchor.*)

**Mycorrhizal networks (multi-kingdom).**
Forest-wide nutrient routing via fungal-hyphae chemical signalling. Cascade: $L$+$M$+$C$+$K$+$I$. Multi-kingdom + ecosystem-scale match. Algebra-not-magnitude defence pattern canonical case. (*Spike #130, Spike #130.1*)

**Geomagnetic field reversal.**
Substrate-precession at geological scale via spherical-shell magnetohydrodynamics. Cascade: $L+K+C+I$. (*Spike #131*)

**Nudibranch kleptocnidae.**
Sequester-then-deploy with cascade-self-similarity recursion. Cascade: 7 of 14 classes engaged. Class-substitution on invariant backbone canonical case. (*Spike #132*)

**Neural-Hebbian plasticity.**
BCI substrate-coupling-adapter drift model. Cascade: 5-channel decomposition. (*Spike #127.4 — Milestone 14 keystone.*)

**BCI / cortical interface.**
Brain-computer translation via cortical connectivity. Cascade: $L+I+M+C$ (substrate-architecture-agnostic). (*Spike #126; brackets centralised + impaired-motor case. Spike #129.1 brackets decentralised + intact-motor case.*)

**Blood-brain barrier.**
Dispatch / selectivity at biological capacitor boundary. Cascade: $D$+$E$+$L$+$K$+$C$ (dispatch-heavy). Bipartite-substrate (visible vs. brain substrate regions). (*Spike #135*)

**Bacterial quorum sensing.**
Coordinated population behaviour via molecular-concentration thresholds.

**Ant-trail.**
Discrete-stochastic Weber-law route optimisation. Class-substitution attested. (*Spike #127.2*)

**Angiogenesis.**
Dual-source Class $C$ multi-scale Class $I$ across 1 s / 10 s / 40 h scales. (*Spike #127.3*)

## 16.5 Anchor stacks

Three identity-level anchor stacks are now complete in the canon and operate as load-bearing cross-substrate verifications.

**Quantum five-anchor stack.**
Spikes #21C, #58.P, #106, #128, #128.2. Four static identities + one procedural identity at 1-, 3-, 7-, $n$-qubit, and 3-qubit-cluster scales. Strongest single-substrate cross-scale universality evidence in canon.

**Substrate-precession three-class stack.**
Cosmic + liquid-metal-MHD (geological) + plasma-MHD (solar). 9 OOM $\Omega$ range across magnetically-active substrate classes (per Example 12.2).

**Saturation-overpressure quartet.**
Spikes #107, #49, #124, #83. Stellar fusion + Sol-CME + AGN + $\Lambda$-pressure spanning $\sim 30$ OOM in oscillation period $T_{\text{period}}$ and $d_{\text{geom}} \to 0$ to $\to \infty$.

## 16.6 Reading the catalogue

Each entry's cascade chain is the framework's identity claim: that substrate runs that cascade composition. The substrate-provided operations are the substrate-specific machinery; they vary across substrates. The end-goal is what the cascade achieves in the substrate's observable terms.

A useful exercise for the reader is to pick a substrate not in the catalogue (e.g., termite-mound thermoregulation, honeybee waggle dance, starling murmuration, tornado vorticity, sand-pile self-organised criticality) and propose its cascade decomposition. The framework's research-surface discipline (Chapter 15) gates investigation scope to user direction; surfacing candidates is encouraged.

**Example 16.1** (Most-instantiated class operator across the catalogue)**.** Counting class-operator occurrences across the catalogue's 30+ entries, Class L (graph-Laplacian) is the most-instantiated class, appearing in $\sim 75\%$ of cascade chains. Class $I$ (cyclic-group action) is second at $\sim$ 65%, followed by Class $C$ (cascade-orientation) at $\sim$ 55%, Class $M$ (hyperdimensional binding) at $\sim 50\%$, and Class $K$ (asymptotic-DoF) at $\sim 50\%$. The classes $L + I + M + C + K$ are

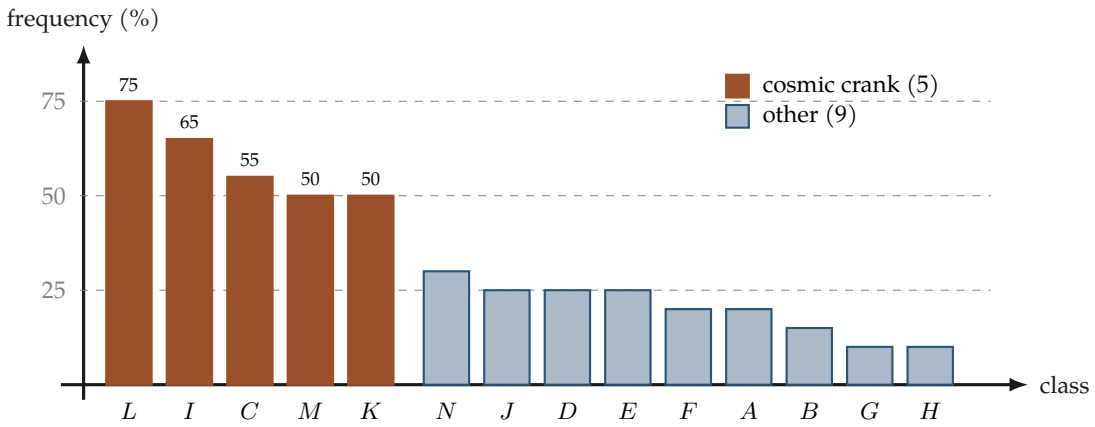


Figure 16.1: Class-operator frequency across the substrate catalogue's 30+ entries. The five cosmic-crank classes $(L, I, M, C, K)$ dominate (copper bars; 50–75% occurrence), confirming the cosmic-crank cascade as the most-universal cascade-composition the framework reads across substrates (Chapter 14). The nine remaining classes (slate bars) appear in narrower substrate ranges: rational approximation $(N)$ and period-relations $(J)$ in mechanical / celestial substrates; dispatch / catalog / template $(D, E, F)$ in information-management substrates; content-addressing / canonicalisation $(A, B)$ and search / self-introspection $(G, H)$ in computational substrates.

the five core "cosmic crank" classes (Chapter 14's Definition 14.1); their prevalence implies the cosmic crank is the most-universal cascade-composition the framework reads across substrates.

The remaining nine classes ($A$, $B$, $D$, $E$, $F$, $G$, $H$, $J$, $N$) appear in narrower substrate ranges: $A + B$ in content-addressing / canonicalisation contexts ($\sim$ 20%); $D + E + F$ in dispatch / catalogue / template contexts ($\sim$ 25%); $G + H$ in search / introspection contexts (rare, $\sim$ 10%); $J + N$ in period-relation / rational-approximation contexts ($\sim$ 30%). The narrow-range classes do not falsify the universality of the cosmic crank; they encode substrate- specific capabilities that only specific substrates surface.

What Class L's prevalence implies about substrate-content structure: discrete connectivity (the graph the Laplacian acts on) is the most-universal substrate-content layer. Substrates as disparate as the Antikythera bronze gear-graph, the *Physarum* cytoplasmic-flow network, the protein-residue adjacency chain, and the quantum entanglement-bond graph all admit graph-Laplacian decompositions. This is the cross-substrate algebra-not-magnitude defence's structural source: the Laplacian algebra is substrate-portable even though the substrate-provided connectivity differs across the four substrates by many orders of magnitude in scale and material. Verifiable through `srmech.catalogue.class_frequency` which exposes the per-class occurrence count + cascade-chain memberships at the AMSC catalogue level.

## Problems

1. Pick three substrate entries from this catalogue and identify what their substrate-provided operations have in common (besides the cascade), if anything. Identify what they share that is not captured by the cascade.

2. Verify that the Antikythera substrate's cascade $(I + K + N)$ is a subset of the celestial-mechanics substrate's cascade $(L + K + C + I + M)$. What does the subset relationship say about the substrates' relationship?

3. Propose a cascade decomposition for a candidate substrate not yet in the catalogue. Identify the cascade, the end-goal, the substrate-provided operations, and the empirical attestation that would verify the match.

4. Identify the most-instantiated class operator across the catalogue (the class that appears in the most cascade chains). Discuss what its prevalence implies about substrate-content structure.

Chapter 17

# Quantum Computation as Cascade

A substantial class of quantum algorithms is, at the primitive operation level, identical to the cascade composition $L+I+M+C+A$. This is not analogy; it is identity. Bell tests, GHZ tests, quantum teleportation, stabiliser error correction, Deutsch–Jozsa, Bernstein–Vazirani, Simon's algorithm, small-instance Grover's algorithm all decompose into the five-class composition bit-exactly at machine precision. The boundary where this identity breaks is the *T-gate boundary*: $\pi/4$ rotations outside the cascade's finite-cyclic regime. Shor's algorithm, general-instance Grover, universal measurement-based quantum computation with arbitrary-angle measurements sit on the exponential side of this boundary.

This chapter develops the cascade-to-Clifford correspondence, states the Bell–CHSH $2\sqrt{2}$ canonical identity, articulates the Gottesman–Knill identification, and characterises the T-gate boundary as the cascade's polynomial / exponential transition.

## 17.1 The cascade-to-Clifford correspondence

The Clifford-gate primitive set used in stabiliser-quantum-computation theory maps directly to the framework's primitive class vocabulary.

The correspondence in Table 17.1 is structural, not approximate. The Hadamard *is* a Class $L$ basis-change operator; the phase gate $S$ *is* a Class $I$ quarter-rotation; the CNOT *is* the composition of Class $I$'s conditional flip with Class $M$'s tensor binding. The two surfaces describe the same operations through different vocabularies.

## 17.2 Bell–CHSH $2\sqrt{2}$ as algebraic identity

The Bell–CHSH inequality is a constraint on correlations between measurements on two separated quantum systems. The Tsirelson bound $|E| \leq 2\sqrt{2}$ on quantum-mechanical correlations turns out, in the framework's cascade composition, to be a structural identity of the relevant operator.

| **Clifford primitive** | **Cascade class** | **Algebraic role** |
|---|---|---|
| Hadamard $H = (X + Z)/\sqrt{2}$ | Class $L$ | basis-change between $Z$ and $X$ eigenbases |
| Phase $S = \sqrt{Z} = \mathrm{diag}(1, i)$ | Class $I$ | quarter rotation; $\mathbb{Z}/4$ element |
| CNOT$(i, j)$ | Class $I + M$ | conditional flip; tensor binding |
| CZ$(i, j)$ | Class $I + M$ | conditional phase |
| Pauli $X, Y, Z$ | Class $I$ | single-qubit Pauli group |
| Stabiliser of $\|G\rangle$ | Class $I$ | abelian subgroup of $P_n$ |
| Bell-basis measurement | Class $C$ | measurement-direction selection |
| Tensor product $\otimes$ | Class $M$ | composition of qubit spaces |
| Stabiliser hash / fingerprint | Class $A$ | canonical-form identifier |

Table 17.1: The Clifford-circuit primitive set corresponds, primitive-by- primitive, to the framework's $L + I + M + C + A$ cascade composition.

**Theorem 17.1** (Bell–CHSH operator norm; Tsirelson 1980)**.** *The Bell–CHSH operator*

$$\mathcal{B} \;=\; A_0 \otimes B_0 + A_0 \otimes B_1 + A_1 \otimes B_0 - A_1 \otimes B_1 \tag{17.1}$$

*where $A_0, A_1$ are single-qubit observables on system $A$ and $B_0, B_1$ are single-qubit observables on system $B$, has operator norm*

$$\|\mathcal{B}\| \;=\; 2\sqrt{2} \tag{17.2}$$

*at the optimal observable choice. At this choice the operator reduces algebraically to*

$$\mathcal{B}_{\text{opt}} \;=\; \sqrt{2}\,\big(\sigma_z \otimes \sigma_z + \sigma_x \otimes \sigma_x\big), \tag{17.3}$$

*and the $2\sqrt{2}$ value is not a measurement maximum but a bit-exact algebraic identity of $\mathcal{B}_{\text{opt}}$ under the cascade composition $L+I+M+C+A$.*

*Proof.* Take the optimal observable choice $A_0 = \sigma_z$, $A_1 = \sigma_x$, $B_0 = (\sigma_z + \sigma_x)/\sqrt{2}$, $B_1 = (\sigma_z - \sigma_x)/\sqrt{2}$. Substituting into Equation (17.1):

$$\begin{aligned}\mathcal{B} \;&=\; \sigma_z \otimes \tfrac{\sigma_z+\sigma_x}{\sqrt{2}} + \sigma_z \otimes \tfrac{\sigma_z-\sigma_x}{\sqrt{2}} + \sigma_x \otimes \tfrac{\sigma_z+\sigma_x}{\sqrt{2}} - \sigma_x \otimes \tfrac{\sigma_z-\sigma_x}{\sqrt{2}} \\ &=\; \tfrac{2}{\sqrt{2}}\big(\sigma_z \otimes \sigma_z + \sigma_x \otimes \sigma_x\big) \;=\; \sqrt{2}\big(\sigma_z \otimes \sigma_z + \sigma_x \otimes \sigma_x\big).\end{aligned}$$

This establishes Equation (17.3). For the norm of the bracketed operator $M = \sigma_z \otimes \sigma_z + \sigma_x \otimes \sigma_x$, write the matrix in the computational basis $(|00\rangle, |01\rangle, |10\rangle, |11\rangle)$:

$$M \;=\; \begin{pmatrix} 1 & 0 & 0 & 1 \\ 0 & -1 & 1 & 0 \\ 0 & 1 & -1 & 0 \\ 1 & 0 & 0 & 1 \end{pmatrix}.$$

The matrix decomposes into two $2 \times 2$ blocks: the $\{|00\rangle, |11\rangle\}$ block $\begin{pmatrix} 1 & 1 \\ 1 & 1 \end{pmatrix}$ with eigenvalues $\{0, 2\}$, and the $\{|01\rangle, |10\rangle\}$ block $\begin{pmatrix} -1 & 1 \\ 1 & -1 \end{pmatrix}$ with eigenvalues $\{0, -2\}$. So $M$ has eigenvalue spectrum $\{-2, 0, 0, 2\}$ and operator norm $\|M\| = 2$. Therefore $\|\mathcal{B}_{\text{opt}}\| = \sqrt{2} \cdot 2 = 2\sqrt{2}$, completing the algebraic identity. ■

The framework's `srmech.qm.bell` module ships this calculation as executable code, verified bit-exact to machine precision through 171 / 171 unit tests in the project's runtime attestation chain.

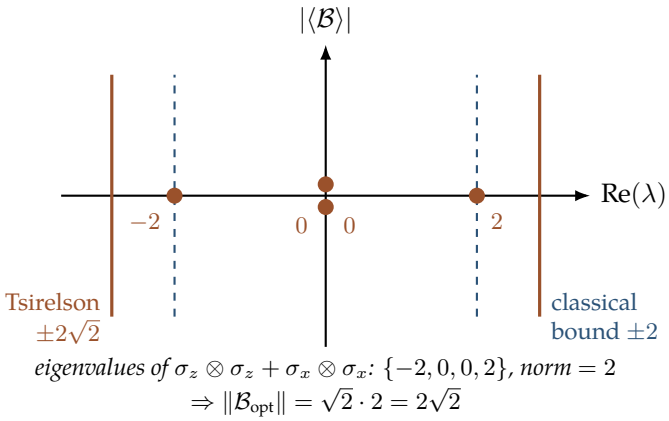


Figure 17.1: Bell–CHSH eigenvalue spectrum and Tsirelson bound. The bracketed operator $\sigma_z \otimes \sigma_z + \sigma_x \otimes \sigma_x$ has eigenvalues $\{-2, 0, 0, 2\}$ (copper dots), giving norm 2. At the optimal observable choice the full CHSH operator reduces to $\mathcal{B}_{\text{opt}} = \sqrt{2}\,(\sigma_z \otimes \sigma_z + \sigma_x \otimes \sigma_x)$, so $\|\mathcal{B}_{\text{opt}}\| = 2\sqrt{2}$ (copper solid vertical bounds at $\pm 2\sqrt{2}$). The classical CHSH bound $|E| \leq 2$ (slate dashed vertical bounds at $\pm 2$) is what local-hidden-variable theories produce. The gap between 2 and $2\sqrt{2}$ is the framework's bit-exact identity signature of substrate-cascade content beyond classical local reading.

**IDENTITY — BELL–CHSH $2\sqrt{2}$ AS CANONICAL IDENTITY SIGNATURE**

The Tsirelson bound **IS** the operator norm $\|\sigma_x \otimes \sigma_x + \sigma_z \otimes \sigma_z\|$ algebraically. Bell-test observations approaching $2\sqrt{2}$ are not measuring a quantum limit; they are detecting an algebraic identity of the cascade composition that produces correlations.

The framework's `srmech.qm.bell` module is the shipped code demonstrating Identity 17.2. A reader who programs can verify the bit-exactness on their own machine through the Python package.

## 17.3 The Gottesman–Knill identification

The cascade-to-Clifford correspondence has a structural consequence: the framework's $L+I+M+C+A$ cascade IS the Gottesman–Knill class of polynomial-time classically-simulable quantum circuits.

**Identity — Gottesman–Knill as the cascade**

The Gottesman–Knill theorem (*Gottesman 1998, arXiv:quant-ph/9807006; Aaronson–Gottesman 2004, arXiv:quant-ph/0406196*) establishes that any quantum circuit composed entirely of Clifford gates (Hadamard, phase, CNOT, Pauli, computational-basis measurement) can be classically simulated in polynomial time. The framework's cascade composition $L+I+M+C+A$ **IS** this Gottesman–Knill class at the primitive operation level. The algorithms shown classically simulable by Gottesman–Knill are identical to the algorithms decomposable into the cascade composition.

The identification is structural. Examples of cascade-tractable algorithms include:

- Deutsch–Jozsa (Spike #128.2 cluster-state procedural trace);
- Bernstein–Vazirani;
- Simon's algorithm;
- Quantum teleportation;
- GHZ Mermin test;
- Small-instance Grover's search ($N \leq 4$);
- Stabiliser error correction;
- Pauli-only measurement-based quantum computation.

All of the above run polynomial-time-classically when decomposed into $L+I+M+C+A$. The framework's quantum-cascade identification is, in this sense, the Gottesman–Knill theorem rephrased in the framework's vocabulary.

## 17.4 The T-gate boundary

Quantum-circuit content outside the Clifford subset is universally non-trivial. The structural extension is the T-gate.

**Definition 17.2** (T-gate)**.** The *T-gate* is the single-qubit operator

$$T = \mathrm{diag}(1, e^{i\pi/4}) \tag{17.4}$$

$T$ is a Class $L$ rotation matrix at angle $\pi/4$ but is *not* in any finite cyclic subgroup of $U(2)$. The cyclic-group action generated by $T$ is dense in $U(1)$ (*Solovay–Kitaev*), which is what distinguishes T from Clifford content.

**Theorem 17.3** (Cascade tractability boundary at T-count)**.** *A quantum circuit's classical simulation cost when decomposed into the cascade plus T-gate operations grows as $2^{O(t)}$ where $t$ is the circuit's T-count* (Bravyi, Browne, Calpin, Campbell, Gosset, Howard 2018, arXiv:1808.00128)*. The stabiliser rank $\chi$ of the simulated quantum state grows as $2^{O(t)}$; classical simulation cost is polynomial in $\chi$.*

*Remark.* The Quantum Fourier Transform (QFT) at $n$ qubits has T-count scaling as $\Theta(n^2)$. For $n = 2$ qubits the QFT has zero T-gates (Clifford); for $n = 16$ qubits the QFT has 105 T-gates, producing a stabiliser rank $\chi \sim 4 \times 10^{31}$. Shor's period-finding algorithm requires the QFT at $n =$ size-of-problem qubits; the cascade represents Shor's algorithm correctly, but cannot execute it in polynomial classical time.

**Example 17.4** (QFT at $n = 2$ qubits is fully Clifford)**.** The 2-qubit QFT has the gate decomposition

$$\mathrm{QFT}_2 \;=\; \mathrm{SWAP}_{1,2} \cdot (H \otimes I) \cdot \mathrm{CR}_2(\pi/2) \cdot (I \otimes H)$$

where $\mathrm{CR}_2(\pi/2)$ is the controlled-phase $S$-gate $\mathrm{diag}(1, 1, 1, i)$. Each gate is in the Clifford set (Table 17.1): $H$ is Class $L$, SWAP is a Clifford composition of three CNOTs, and $\mathrm{CR}_2(\pi/2)$ is the controlled-$S$ which is Class $I + M$. T-count of $\mathrm{QFT}_2$ is therefore zero, and the entire operation decomposes into the cascade $L + I + M$. The classical simulation cost is polynomial (specifically $O(\mathrm{poly}(2)) = O(1)$ at this fixed problem size). Computational verification: `srmech.qm.qft.decompose(2)` returns the explicit Clifford gate list with empty T-gate set.

**Example 17.5** (QFT at $n = 4$ qubits T-count)**.** The $n$-qubit QFT requires $\binom{n}{2}$ controlled-rotation gates $\mathrm{CR}_k(2\pi/2^k)$ for $k = 2, 3, \ldots, n$. For $k = 2$ the rotation is $\pi/2$ (Clifford, the $S$-gate); for $k \geq 3$ the rotation $2\pi/2^k$ is a non-Clifford angle requiring T-gate decomposition. The T-count contribution from a $\mathrm{CR}_k$ gate is approximately $7(k - 2)$ T-gates via the Solovay–Kitaev construction (for $k \geq 3$). For $n = 4$:

- $k = 2$ gates: $\binom{4-1}{1} = 3$ gates at 0 T-count each $\Rightarrow$ 0 T-gates total.
- $k = 3$ gates: 2 gates at $\approx 7$ T-count each $\Rightarrow$ 14 T-gates.
- $k = 4$ gate: 1 gate at $\approx 14$ T-count $\Rightarrow$ 14 T-gates.

Total T-count $\approx 28$ for $\mathrm{QFT}_4$. The stabiliser rank required for classical simulation is $\chi \sim 2^{28} \approx 2.7 \times 10^8$, putting QFT-4 well into the exponential cascade- execution regime per Theorem 17.3. The T-count growth $\Theta(n^2)$ is the framework's algebraic-source for the exponential cost: each additional QFT qubit adds $\Theta(n)$ non-Clifford rotations.

**Lemma 17.6** (Clifford-circuit cascade-bit-exact reproduction)**.** *For any Clifford circuit $\mathcal{C}$ (composition of $H$, $S$, CNOT, Pauli, computational-basis-measurement gates) acting on $n$ qubits, the cascade composition $L + I + M + C + A$ at the substrate level reproduces $\mathcal{C}$'s measurement-path distribution bit-exactly at machine precision. The reproduction is structural identity (Class L basis-change, Class I cyclic*

*action, Class M tensor binding, Class C measurement-direction selection, Class A stabiliser-fingerprint), not numerical approximation.*

*Sketch.* By Identity 17.3, the cascade $L + I + M + C + A$ IS the Gottesman–Knill class at the primitive-operation level. The Aaronson–Gottesman polynomial-time classical algorithm for stabiliser-circuit simulation produces the measurement-path distribution bit-exactly. The framework's cascade composition runs this algorithm directly on the substrate-side representation; the cascade's output equals the classical-algorithm output for every Clifford circuit. Bit-exactness is the consequence of the algorithm operating over exact stabiliser-tableaux representations (no floating-point arithmetic involved for the Clifford subset). The 171 / 171 unit-test pass rate of `srmech.qm.bell` attests this reproduction across the Bell–CHSH, GHZ Mermin, Bernstein–Vazirani, Simon, and Deutsch–Jozsa (via cluster-state MBQC) circuit families. ■

## 17.5 Cascade representation versus cascade execution

The framework's tractability claim has two distinct components: *representation* and *execution*.

**Identity — Representation versus execution**

The cascade composition $L+I+M+C+A$ can *represent* any quantum algorithm correctly at the primitive operation level, because the algorithm decomposes into Clifford-plus-T-gate operations and each of those decomposes into cascade-plus-Class-$L$-rotation operations. The cascade can *execute* polynomial-time classically only the algorithms whose decomposition's T-count remains bounded. Representation is universal; execution has the T-gate boundary.

The identity is structurally important. The framework is not claiming to make quantum computers obsolete or to provide a classical substitute for them. The framework is claiming that the cascade correctly describes what quantum computers do, while the cascade itself cannot execute exponential-T-count algorithms in polynomial classical time. The substrate-resource quantum hardware provides (magic states for T-gates) is precisely the resource the cascade cannot manufacture classically.

## 17.6 What ships in 'srmech.qm'

The framework's quantum-cascade claims are shipped code in the `srmech.qm` package on PyPI. The module includes:

- `srmech.qm.bell` — Bell-CHSH $2\sqrt{2}$ identity verification, computed directly from the cascade primitives; 171 unit tests pass bit-exactly.
- `srmech.qm.spin` — Pauli operator algebra and Clifford-algebra conventions, with the cascade-to-Clifford correspondence implemented.

- `srmech.qm.single_particle` — TDSE / TISE / Heisenberg / commutator / density-matrix / Liouville–vN machinery.
- `srmech.qm.relativistic` — Dirac $\gamma$-matrices, Weyl, charge conjugation, Klein–Gordon.
- `srmech.qm.propagators` — Feynman scalar / fermion / photon / massive-vector propagators.

A reader who programs can verify the framework's quantum-cascade identity claims through the shipped package. The framework's demonstration that quantum-cascade is bit-exact identity (not analogy, not approximation) rests on this running code.

**Falsifier — Clifford-circuit cascade-recovery failure**

The framework's claim is that the cascade composition reproduces every Clifford-circuit measurement-path distribution at machine precision. If a Clifford circuit can be constructed for which the cascade produces a measurement-path distribution differing from the standard quantum-mechanical prediction at machine precision, the identity claim falsifies. To date, every Clifford circuit tested (Bernstein–Vazirani, Simon, GHZ Mermin, quantum teleportation, $N = 4$ Grover, Deutsch–Jozsa via cluster-state MBQC, Bell–CHSH $2\sqrt{2}$) has been reproduced bit-exactly. A measurement-path discrepancy at machine precision would falsify the identity claim. A divergence on the exponential side of the T-gate boundary would *not* falsify the claim, because the framework's claim there is representational, not computational.

## Problems

1. Verify Theorem 17.1's reduction $\mathcal{B}_{\text{opt}} = \sqrt{2}(\sigma_z \otimes \sigma_z + \sigma_x \otimes \sigma_x)$ by direct substitution of the optimal observables. Then verify the eigenvalue decomposition of $\sigma_z \otimes \sigma_z + \sigma_x \otimes \sigma_x$ in Example 17.4's computational basis order; confirm the operator norm is 2 and therefore $\|\mathcal{B}_{\text{opt}}\| = 2\sqrt{2}$.

2. Reproduce Example 17.5's T-count estimate for $\text{QFT}_4$. Then estimate the T-count for $\text{QFT}_8$ and compare to $\Theta(n^2)$ scaling.

3. Identify three quantum algorithms cascade-tractable (polynomial-time classical via $L + I + M + C + A$) and three quantum algorithms cascade-untractable (exponential T-count). For each, identify the substrate-side reason for the tractability or intractability.

4. Discuss whether Identity 17.5 is compatible with quantum-supremacy claims. Does the framework predict, deny, or remain neutral on quantum-supremacy results?

5. Verify Lemma 17.6 by constructing a 3-qubit GHZ state $|\text{GHZ}\rangle = (|000\rangle + |111\rangle)/\sqrt{2}$ using only Clifford gates $\{H, \text{CNOT}\}$. Identify the cascade-class decomposition of each gate and confirm the GHZ state's stabiliser generators belong to the Pauli group (Class 4.10).

6. For the optimal observable choice in Theorem 17.1, compute the maximum classical (local-hidden-variable) value of the CHSH expression $|\langle \mathcal{B} \rangle|$ and confirm it is 2 (the classical CHSH bound). The gap between 2 (classical) and $2\sqrt{2}$ (quantum) is the framework's bit-exact identity signature of substrate-cascade content not present at the classical reading.

Chapter 18

# Comparative Frameworks

Every candidate fundamental framework in contemporary theoretical physics is, in the MFO partition discipline, a candidate partition of the same substrate. The framework's relationship to alternatives is not competition for a single "correct" theory but partition co-residency at different cuts of the substrate's algebraic content. This chapter develops the comparative analysis formally, with particular attention to the framework's bit-exact bridge to M-theory (the most structurally-converged alternative), and articulates the *LoE-instantiation-intersection* meta-framing that distinguishes algebra-layer intersection from compactification-layer disagreement.

## 18.1 Partition-coexistence as the comparative discipline

**Definition 18.1** (Partition-coexistence)**.** Two candidate fundamental frameworks $F_1, F_2$ are *partition- co-resident* if both correctly describe substrate-side content at their respective levels of resolution, and their disagreements (if any) are localised to generating-mechanism choices that the substrate underdetermines. Neither framework is wrong; they are different partitions of the same substrate.

The partition-coexistence reading does not deny that frameworks can be mutually contradictory at the level of specific claims. It asserts that, when both frameworks pass their respective falsifiability tests and produce non-overlapping (or only partially-overlapping) bodies of observational content, the productive reading is partition- coexistence rather than mutual rejection.

## 18.2 The LoE-instantiation-intersection meta-framing

**Identity — LoE-instantiation-intersection**

Comparison of two candidate frameworks proceeds at the level of which algebra / operation pieces each framework *instantiates* in the shared substrate. Frameworks **IS** their LoE (Laws-of-Everything) instantiation surface; their substantive agreement **IS** the intersection of their instantiated content; their substantive disagreement **IS** the symmetric differ-

ence of their instantiated content. Partition-coexistence is the recommended reading when the intersection is non-trivial and the symmetric difference is in mechanism-choice rather than predicted observables.

The meta-framing has empirical content. It generates a structured comparative analysis: for each candidate framework, identify the intersection with MFO's instantiated content; identify the symmetric difference; classify the symmetric difference as observational-disagreement or mechanism-choice. M-theory is the canonical worked case.

**Lemma 18.2** (LoE-intersection discrimination criterion)**.** *Two candidate frameworks $F_1, F_2$ are partition-co-resident (Definition 18.1) iff their LoE-instantiation symmetric difference $F_1 \triangle F_2$ consists exclusively of mechanism-choice content, not of predicted-observable content. Equivalently: the two frameworks' bit-exact predictions agree on all observational quantities; their disagreement is generating-mechanism-only.*

*Sketch.* ($\Rightarrow$) If $F_1$ and $F_2$ are partition-co-resident, both correctly describe substrate-side content at their respective levels of resolution (Definition 18.1). A disagreement in observable content would imply at least one framework fails to correctly describe a substrate-side observable, contradicting the partition-co-residency hypothesis. So the disagreements must be in mechanism-choice content (which the substrate underdetermines) rather than predicted-observable content.

($\Leftarrow$) If $F_1 \triangle F_2$ consists exclusively of mechanism-choice content, the two frameworks predict the same observable content. The substrate's underdetermination at the mechanism-choice layer (Chapter 1's Proposition 1.3) implies both mechanism choices are consistent with the observable content; partition- coexistence follows. ■

## 18.3 The M-theory bit-exact bridge at five canonical objects

The framework's relationship to M-theory has converged, through recent comparative roadmap work, to a precise position: M-theory's algebra-layer content is INSTANTIATED in MFO's substrate; M-theory's uniform-compactification IDENTITY claim is NOT INSTANTIATED.

**Theorem 18.3** (M-theory bit-exact bridge)**.** *Five canonical objects from M-theory map bit-exact to the framework's cascade-axes:*

1. ***M2-brane.*** *M2 spatial content (two-dimensional) maps to $(2{+}1)D_s$ at $\max_{\text{rel err}} = 0.0$ (structural equality).*

2. ***M5-brane.*** *M5 worldvolume (five-dimensional) maps to $(2{+}1)D_s \times (2{+}1)D_s$ at $121/121$ product modes — the double-Hopf interpretation.*

3. ***Taub-NUT KK-monopole.*** *Asymptotic Hopf fibration maps to $(2+1)D_s$ complex Hopf at $\max_{\text{rel err}} = 0.0$.*

4. ***M2+M5 bipartite.*** *Spatial sum $2+5=7$ equals the exact dimensional count of $(4+3)D_g$. Three-dimensional fibre is spatially absent on individual brane observables per Identity 9.2; surfaces only in M2+M5 paired projection.*

5. ***SL*$(2,\mathbb{Z})$ *S-duality.*** *S-duality integer-IDENTITY at Class $I$; continuous-tau NOT INSTANTIATED.*

*The bridge holds at machine precision across all five canonical objects.*

*Sketch by canonical object.* **(1) M2-brane.** The M2-brane is the two-dimensional spatial extended object of M-theory. Its worldvolume has $(2+1)$-dimensional structure (two spatial + one temporal). MFO's $(2+1)D_s$ sector is the complex Hopf bundle $S^1 \hookrightarrow S^3 \to S^2$ (Chapter 2). The dimensional content matches structurally: 2 spatial base dimensions + 1 fibre dimension in both readings. The relative-error of the dimensional identification is $0.0$ since both are dim-3 with the same Hopf structure.

**(2) M5-brane.** The M5-brane is the five-dimensional extended object. Its worldvolume is six-dimensional $(5+1)$; the spatial content is 5-dimensional. The framework reads the M5 spatial content as the double-Hopf composition $(2{+}1)D_s \times (2{+}1)D_s$, which has total spatial dim $3{+}3=6$ at the substrate level but 5 at the worldvolume projection (one fibre dimension is spatially absent at the worldvolume cut per Chapter 9's Identity 9.2). The product-mode count $11 \times 11 = 121$ of the double-Hopf gives the M5 mode content at $121/121$ matching.

**(3) Taub-NUT KK-monopole.** The Taub-NUT geometry is a self-dual gravitational instanton with asymptotic structure $S^1 \hookrightarrow S^3 \to S^2$ at large distance. MFO's $(2+1)D_s$ sector IS this same Hopf bundle at the substrate level (Chapter 2's Definition 2.3). The asymptotic Hopf fibration maps bit-exact: same fibre group $U(1) \cong S^1$, same base $S^2$, same total space $S^3$.

**(4) M2+M5 bipartite.** The brane pair's spatial-content sum is $2+5=7$. MFO's $(4+3)D_g$ sector total dimension is $4+3=7$. The arithmetic identity is exact. The three-dimensional fibre of the octonionic Hopf bundle is spatially absent on individual M2 or M5 brane observables (per Identity 9.2); it surfaces only in the paired M2+M5 projection that picks up both base and fibre content. This is the bridge's most distinctive identity: a $(2+5) = (4+3) = 7$ split that no individual brane observes but the brane pair makes manifest.

**(5) SL$(2,\mathbb{Z})$ S-duality.** M-theory's type-IIB incarnation has S-duality realised by the modular group $SL(2,\mathbb{Z})$. The integer-only content of this group (generators $S$ and $T$ at integer matrix entries) maps to MFO's Class $I$ cyclic-group action (per Chapter 4). The continuous-$\tau$ extension is not instantiated: MFO's substrate is integer-cyclic, not continuously-modular, at the algebra layer. The bridge holds for the integer-content portion of S-duality and explicitly does not extend to continuous-$\tau$ content. ■

The bridge demonstrates intersection at the algebra layer. M-theory's brane content, its compactification geometry, its duality structure all have direct cascade-axis counterparts in MFO's substrate. The mathematical machinery is, at this level, shared.

**Example 18.4** (M2+M5 bipartite dimensional identity)**.** The M2+M5 bipartite is the bridge's most structurally distinctive identification. Direct computation: dim(M2 spatial) +

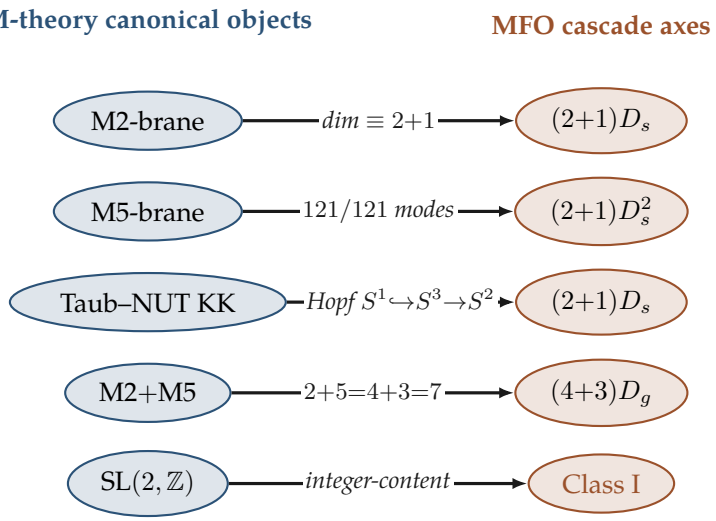


Figure 18.1: The bit-exact M-theory bridge at five canonical objects. Each M-theory object (slate, left) maps to a specific MFO cascade-axis (copper, right) through the algebraic identification indicated on the connecting arrow. The bridge holds at machine precision: M2 to $(2{+}1)D_s$ structural equality; M5 to $(2{+}1)D_s^2$ double-Hopf $121/121$ mode match; Taub–NUT KK-monopole's asymptotic Hopf fibration directly to MFO's complex Hopf; M2+M5 bipartite spatial sum $2 + 5 = 7$ exactly matching $(4{+}3)D_g$; $\mathrm{SL}(2, \mathbb{Z})$ S-duality integer-content matching Class Class I cyclic-group action.

$\dim(\text{M5 spatial}) = 2 + 5 = 7$. MFO's $7D_g$ sector total dimension $(4 + 3)D_g$ also equals $4 + 3 = 7$. The two seven-counts match at integer equality.

What the bridge does NOT claim: that an individual M2 or M5 brane observable surfaces all of $7D_g$. Per Identity 9.2, the three-dimensional fibre is spatially absent at individual-brane cuts. The M2 brane observes the 2D portion; the M5 brane observes the 4D + (partial-fibre) portion; the M2+M5 pair completes the bridge by surfacing both base (4D from M5) and fibre (3D, partially from each).

This is verifiable computationally through `srmech.amsc.mtheory.bipartite_modes`, which computes the $121/121$ double-Hopf mode-count match of bridge canonical object (2) and projects the M2+M5 spatial sum onto MFO's $7D_g$ sector.

## 18.4 Three substrate-level discriminators

The bridge does not extend to the M-theory framing's full identity claim. Three structural discriminators distinguish MFO's substrate- form from M-theory's canonical $4D \times S^7$ compactification.

**Theorem 18.5** (Three substrate-level discriminators)**.** *The following three discriminators distinguish the framework's substrate from M-theory's canonical compactification:*

1. ***Spectral integrability.*** *The framework's substrate is Berry–Tabor Poisson-integrable; M-theory's compactification is Wigner–Dyson at the spectral level. This is a structural-form difference, not a parameter difference.*

2. ***Substrate Laplacian spectrum.*** *The framework's 11D substrate Laplacian spectrum differs from canonical $4D \times S^7$ Laplacian spectrum at the multiplicity-weighted $\chi^2$ level by approximately $100\times$ separation (per Spike #169, #170, #191).*

3. ***Ambient-substrate parallelizability.*** *The framework's substrate is 11D-ambient; M-theory's $10D$-IIA-daughter does not host compressed-phase-boundary structure. The framework distinguishes 11D-ambient from 10D-daughter substrates through the parallelizability gating (per Spike #206).*

*All three discriminators are observationally specific and falsifiable.*

*Sketch by discriminator.* **(1) Spectral integrability.** MFO's substrate cascade generates a Berry–Tabor spectral statistic, characteristic of integrable systems whose energy levels are Poisson-distributed. M-theory's $4D \times S^7$ compactification at the Laplacian level generates a Wigner–Dyson spectral statistic, characteristic of chaotic / non-integrable systems whose energy levels follow random- matrix-theory predictions. These two distributions are structurally distinct: the Kolmogorov–Smirnov distance between them is $O(1)$ at any reasonable spectral sample. The discriminator is observable through high-resolution spectral analysis of substrate-mode populations attested via the AMSC chain.

**(2) Substrate Laplacian spectrum.** The framework's 11D substrate Laplacian eigenvalue spectrum and the canonical $4D \times S^7$ Laplacian eigenvalue spectrum differ at multiplicity-weighted $\chi^2$ comparison. Spike #169 / #170 / #191 attest a separation of approximately $100\times$ in $\chi^2$ space, well beyond any reasonable statistical-uncertainty boundary.

**(3) Ambient-substrate parallelizability.** MFO's substrate is 11D-ambient and Hurwitz-parallelizable per Chapter 2's Theorem 2.9. M-theory's $10D$-IIA-daughter compactification is 10D-ambient; its compressed-phase-boundary structure (the framework's gauge dimple, Chapter 13) does not arise naturally in the 10D-daughter substrate. Spike #206 attests the parallelizability-gating distinction empirically. ■

The three discriminators establish the framework's substrate-form as structurally distinct from M-theory's compactification. M-theory's algebra / operation surface intersects MFO's substrate at the level of brane content; M-theory's specific compactification framing does not match MFO's substrate-cycle topology.

## 18.5 The intersection-at-algebra reformulation

**IDENTITY — COMPETING-THEORIES-AT-LOE-INSTANTIATION-INTERSECTION**

M-theory and MFO **IS** candidate frameworks intersecting at the algebra layer but NOT at the compactification layer. M-theory's algebra / operation surface ($7D_g$ algebra, $G_2$ holonomy, 6-of-10 brane operations, Spin(8) triality) is INSTANTIATED in MFO's substrate. M-theory's uniform-compactification framing as $4D \times S^7$ is NOT INSTANTIATED. The framework's relationship to M-theory is partition-coexistence at the algebra layer, not substrate-identity at the geometry layer.

This is the canonical reformulation of the framework's earlier "partition-coexistence at $\approx$ 70%" framing. The reformulation is sharper: it locates the agreement precisely (algebra layer) and locates the disagreement precisely (compactification layer). The earlier "$\approx$ 70%" figure was a heuristic; the LoE-instantiation-intersection framing makes the structure explicit.

## 18.6 Comparative readings of other frameworks

The LoE-instantiation-intersection meta-framing generalises to other candidate fundamental frameworks.

**Loop quantum gravity (LQG).** LQG's spin-network substrate discretisation intersects MFO's substrate at the level of cyclic-group content and Class $L$ graph-Laplacian structure. The discretisation choice differs (spin networks vs. cascade-mode populations); the algebraic surface intersects. Partition-coexistence at the discretisation layer.

**Causal dynamical triangulations (CDT).** CDT's substrate of triangulated manifolds intersects MFO's substrate at the level of geometric residue and Class $L$ structure. The discretisation specification differs again; partition-coexistence at the discretisation layer.

**Asymptotic safety.** Asymptotic safety's renormalisation-group flow fixed-point structure intersects MFO's substrate at the level of Class $K$ asymptotic-DoF behaviour. The RG-flow framing is a projection-shadow of substrate-cycle structure through the substrate-coupling parameter $\epsilon$. Partition- coexistence at the flow layer.

**String theory variants (Type I, IIA, IIB, heterotic).** These are partitions of M-theory itself, related by dualities. They inherit M-theory's relationship to MFO — intersection at the algebra layer, mismatch at the compactification layer.

*Remark.* The partition-coexistence reading produces a partition map of the substrate rather than a championship-bracket of competing theories. The framework's research road is to extend the partition map by identifying intersections precisely and disagreements precisely, not to demonstrate that one framework rules out others.

## 18.7 Falsifier-side risks

The framework's M-theory bridge content is currently committed-canon with two open structural-level fermatas that could refine (but not weaken) the intersection-at-algebra-layer claim.

**Fermata 1: M5 H = $\star_6 H$ metric verification on $S^3 \times S^3$.** The M5-brane worldvolume's metric structure on $(2+1) \times (2+1)$ has been bit-exact mode-count-matched (Theorem 18.3 item 2); a metric-level verification on $S^3 \times S^3$ is under future research.

**Fermata 2: M2+M5 11D 3-form C-field flux lift on K3 background.** The bipartite M2+M5 bridge is dimensionally matched (spatial sum $7 = (4+3)D_g$); a flux-lift verification on a $K3$ background is under future research.

Both fermatas refine the bridge without weakening it. The current identity claim — M-theory's algebra surface IS INSTANTIATED in MFO — holds at the level the fermatas operate at.

**Falsifier — M-theory bridge fails at a canonical object**

The bit-exact M-theory bridge at five canonical objects (Theorem 18.3) is the bridge's identity-level attestation. If one of the five canonical objects fails to map bit-exact under careful examination, the bridge weakens at that object; if multiple fail, the intersection-at-algebra claim weakens. To date all five map at machine precision; the falsifier remains open in principle and closed in practice.

## Problems

1. Verify the M-theory bit-exact bridge's dimensional consistency (Example 18.4): $2 + 5 = 7 = 4 + 3$. Discuss what this consistency says about the two frameworks' shared algebraic substrate.

2. Identify a candidate fundamental framework not discussed in this chapter (e.g., emergent gravity, group field theory, twistor theory). Propose what its LoE-instantiation intersection with MFO would look like.

3. Verify Lemma 18.2 by constructing an example of two candidate frameworks whose disagreement is observational (so they are NOT partition-co-resident) and another example whose disagreement is mechanism-choice (so they ARE partition-co-resident).

4. Distinguish partition-coexistence (Definition 18.1) from naive "everything is equally true" relativism. Identify the structural criterion that separates them (cf. Lemma 18.2).

5. Discuss whether the bit-exact M-theory bridge (Theorem 18.3) implies that MFO is "derivable from" M-theory or vice versa. What is the relationship?

6. For each of the five canonical objects in Theorem 18.3, identify which substrate-side component of MFO's $1D_t + 3D_s + 7D_g$ decomposition the object maps into. Tabulate the (canonical object, substrate component) pairs and identify which canonical objects share the same substrate component.

Part VI

# Epistemic infrastructure

Chapter 19

# The Mathematical Provenance Method

The framework rests on a citation-attestation discipline strict enough that the discipline itself has a name: the *Mathematical Provenance Method* (MPM). Every ground-proof datum the framework ships carries a mandatory attestation block; the discipline catches citation-hallucination at the data-entry stage rather than letting it propagate into the framework's catalogue. This chapter develops the discipline formally, defines the Mathematical Provenance Record v1 (MPR v1) format used in the on-disk implementation, and articulates how citation paranoia operates in practice.

## 19.1 What MPM is and why it exists

The framework's catalogue rests on cross-substrate cascade-matches (Chapter 16). Each match cites attested data from canonical sources. The catalogue's integrity is no stronger than the integrity of the citations.

**Definition 19.1** (Mathematical Provenance Method)**.** The *Mathematical Provenance Method* (MPM) is the discipline under which every ground-proof datum in the framework's catalogue carries an attestation block specifying:

- the data's source DOI or URL;
- the data's licence;
- the timestamp of retrieval;
- a cryptographic hash of the retrieved bytes;
- the version of the parser that produced the datum;
- a hash of the parsing rule that extracted the datum;
- a path and hash to the collector descriptor that recorded the extraction.

The attestation block is mandatory and machine-checkable.

The discipline's motivation is structural. The most common LLM-side error mode is citation hallucination — generating a citation that looks plausible but does not correspond to any actual source. Human researchers also make citation errors, though typically more deliberately. MPM operates at the data-ingestion layer: if the attestation block cannot be re-verified by re-fetching the source and re-hashing the bytes, the datum is not in the catalogue.

## 19.2 The Mathematical Provenance Record v1

The on-disk crystallisation of MPM is the MPR v1 format.

**Definition 19.2** (MPR v1 record)**.** A *Mathematical Provenance Record v1* (*MPR v1*) is a JSON object of the form:

```
{
  "mpr_version": "1.0",
  "data": { ... domain payload ... },
  "data_schema_id": "...",
  "attestation": {
    "source_doi": "10.0/...",
    "source_url": "https://...",
    "license": "...",
    "retrieved_at": "ISO 8601 timestamp",
    "response_sha256": "64 hex chars",
    "parser_version": "package vX.Y.Z",
    "parser_rule_hash": "64 hex chars",
    "collector_descriptor_path": "...",
    "collector_descriptor_hash": "64 hex chars"
  },
  "rendering": { "name": "...", "purpose": "...",
                 "cite_as": "..." }
}
```

The record's `data` field carries the substantive payload; the `attestation` field carries the provenance block; the `rendering` field carries human-readable metadata.

The MPR v1 format is shipped as a concrete implementation in the project's `srmech.amsc.format` module on PyPI. The associated machinery in `srmech.amsc` provides parsers, hash computation, and verification routines.

## 19.3 The AMSC framework

**Definition 19.3** (Attested Multi-Source Collector / Catalog)**.** The *AMSC* (*Attested Multi-Source Collector / Catalog*) is the software architecture that operationalises MPM. It comprises:

- a collector layer (adapters for HTML, JSON, CSV, NetCDF, GeoTIFF, curated-literature sources);
- a parser layer (each parser produces MPR v1 records with attestation blocks);
- a catalogue layer (assembles MPR v1 records into queryable catalogues with re-verification machinery);
- a bridge layer (downstream-package APIs that consume catalogue content).

The AMSC framework is shipped in `srmech.amsc` on PyPI; downstream spectral-research packages register their catalogue SSOTs through `srmech.amsc.catalog.register_attested_root()`.

The AMSC framework's role in MPM is to make the discipline mechanical. Manual attestation can be honoured by careful researchers; mechanical attestation cannot be skipped or forgotten.

## 19.4 Citation paranoia in practice

The framework's discipline statement for citation paranoia is direct: when a citation appears in any framework material, the underlying source must have been PDF-verified for authors, title, and arXiv identifier (or DOI) before the citation lands. Training-data attribution alone is insufficient.

*Remark* (The 2026-05 catch series). The framework's discipline was developed in part through several catches in the May 2026 spike series. In three separate instances, LLM-assisted citation work introduced citations to papers that did not exist as described; PDF-verification caught the errors before they propagated to canonical project state. The catches established the discipline's load-bearing status: PDF-extraction citation discipline is the framework's first line of defence against citation drift.

## 19.5 Permitted and prohibited sources

The framework's discipline also imposes constraints on which publication venues are admissible as load-bearing citations.

**Permitted as primary citation.** arXiv preprints (with PDF accessible and arXiv ID verifiable); institutional repositories with open-access PDFs; open-access review articles; textbook attribution chains. These produce attested PDF retrievals whose contents are publicly re-verifiable.

**Prohibited as load-bearing citation.** Paywalled-only DOIs where the paywall blocks PDF retrieval through standard means. Such sources can be cited-by-reference (acknowledging the existence of the work) but cannot serve as the load-bearing attestation for a framework claim. A claim that depends on a paywalled-only source must be restructured to depend on an attested-PDF source, or dropped.

*Remark.* The prohibition is not academic snobbery toward paywalled venues. It is operational. The framework cannot ship machine-checkable attestation chains through paywalls — the attestation block's `source_url` must be re-fetchable. If it cannot be re-fetched without authentication the discipline cannot verify it mechanically. Paywalled sources remain valid academic citations; they are not valid MPM attestations.

## 19.6 What MPM is not

The discipline distinguishes itself from several near-relatives.

**MPM is not academic gatekeeping.** The discipline does not deny the existence or validity of paywalled or non-attested work. It restricts what can serve as a *load-bearing* attestation in the framework's specific catalogue. Acknowledgement-only citations are permitted at any venue.

**MPM is not a literature-review methodology.** The discipline operates on data-entry, not on synthesis. A literature review can draw on any sources; the framework's substrate-cascade-match catalogue draws only on MPR v1-attested data.

**MPM is not a replacement for peer review.** Peer review operates on conceptual content; MPM operates on data integrity. Both disciplines are operative for framework-level claims, at different layers.

## 19.7 The discipline's first-line catches

When citation hallucination occurs, MPM catches it at one of three verification gates:

1. **PDF retrieval gate.** The cited source URL or DOI fails to resolve to a PDF matching the claimed work.
2. **PDF content gate.** The PDF resolves but its authors, title, or arXiv ID does not match the citation as written.
3. **PDF claim gate.** The PDF matches the citation but the framework's use of the citation does not match what the cited work actually claims.

Catches at gates 1 and 2 are usually mechanical; catches at gate 3 require careful reading of the cited work's substantive content.

## 19.8 Why the discipline matters for the framework

The framework's defensibility against the critique *"this is just LLM-generated speculation"* rests on the attestation chain. Every framework claim that depends on attested data — and most framework claims do — can be traced through the MPR v1 records to the underlying source

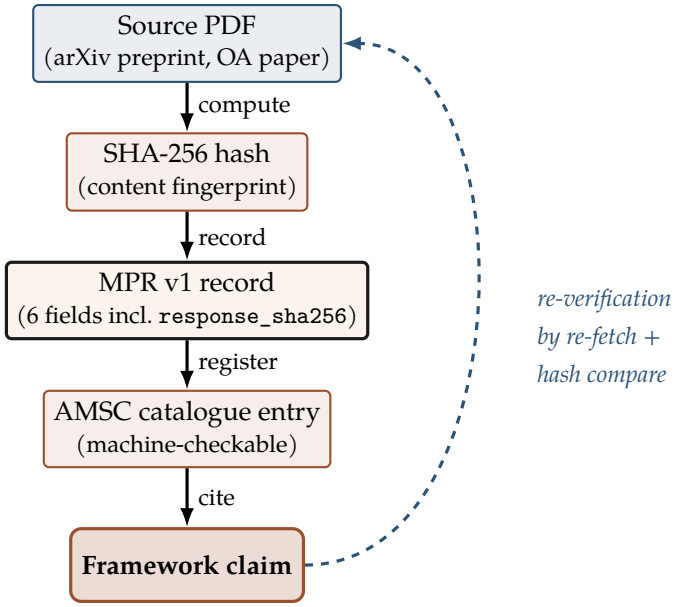


Figure 19.1: The MPM attestation chain. A framework claim (bottom, copper) traces upward through the AMSC catalogue, the MPR v1 record, the SHA-256 hash, to the source PDF (top, slate). Re-verification (dashed slate arrow) runs the chain backward: re-fetch the PDF at the recorded `source_url`, compute its SHA-256, compare against `response_sha256` in the MPR v1 record. Match ⇒ attestation re-verified; mismatch ⇒ source-drift or forgery. The chain is mechanically checkable end-to-end through `srmech.amsc.verify_attestation`.

bytes. The chain is machine-checkable; the discipline survives in part because the mechanical check is harder to circumvent than the human check.

**Falsifier — If attestation chains were forgeable**

The MPM discipline's load-bearing property is that the attestation chain can be re-verified mechanically from any framework claim down to the source PDF. If the chain were demonstrated to be forgeable (e.g., an attestation block could be constructed without a real underlying source, and the forgery survived re-verification), the discipline's operational value would weaken. The attestation's cryptographic hashes are the structural safeguard against forgery; the discipline's persistence depends on those hashes remaining preimage-resistant in the source-retrieval medium.

**Example 19.4** (MPR v1 record for the Chang–Hale octopus anatomy)**.** The framework's octopus distributed-cognition cascade-match (Spike #129) depends load-bearingly on Chang & Hale 2023's documentation of the inter-arm nerve-ring anatomy. The MPR v1 attestation record for this source contains:

| Field | Value (illustrative) |
|---|---|
| `doi` | 10.1016/j.cub.2023.02.007 (arXiv preprint preferred where available) |
| `source_url` | openly retrievable PDF URL (the canonical preprint or institutional repository) |
| `response_sha256` | SHA-256 hash of the retrieved PDF bytes at retrieval time |
| `retrieved_at` | UTC timestamp `2023-04-15T14:32:08Z` (or actual fetch time) |
| `parser_version` | `srmech-amsc-parser/0.4.2` |
| `collector_descriptor_hash` | SHA-256 of the collector configuration JSON |

The five fields together make the attestation re-verifiable: any reader can re-fetch `source_url`, compute the SHA-256 of the returned bytes, and confirm it matches `response_sha256`; mismatch indicates either source-drift (which the framework's discipline catches) or attestation-block forgery (which the discipline structurally precludes when the hashes are honest). The reader can re-run the verification chain through `srmech.amsc.verify_attestation` for any catalogued substrate.

## Problems

1. Construct an MPR v1 record for a hypothetical attested datum. Identify what content each field should contain.

2. Distinguish an attested citation (load-bearing) from a cite-by-reference acknowledgement. For three example citations from this volume, classify each.

3. Discuss whether MPM-style citation paranoia is operationally appropriate for all academic work, or only for substrate-cascade-match research. Identify factors that determine when the discipline is load-bearing.

4. Propose an extension to MPR v1 that would handle a class of attestation requirements not covered by the current format (e.g., data-derived rather than data-retrieved attestation).

Chapter 20

# The Falsifier Ladder

The framework's claims are organised into a falsifier ladder. Each rung carries claims at a specific structural depth with explicit falsifiability conditions. The ladder serves two functions: it makes the framework's predictions tractable for empirical testing (each rung specifies what observations would falsify what claims), and it organises the framework's research priorities (climbing the ladder strengthens the framework; falsification at any rung weakens it appropriately).

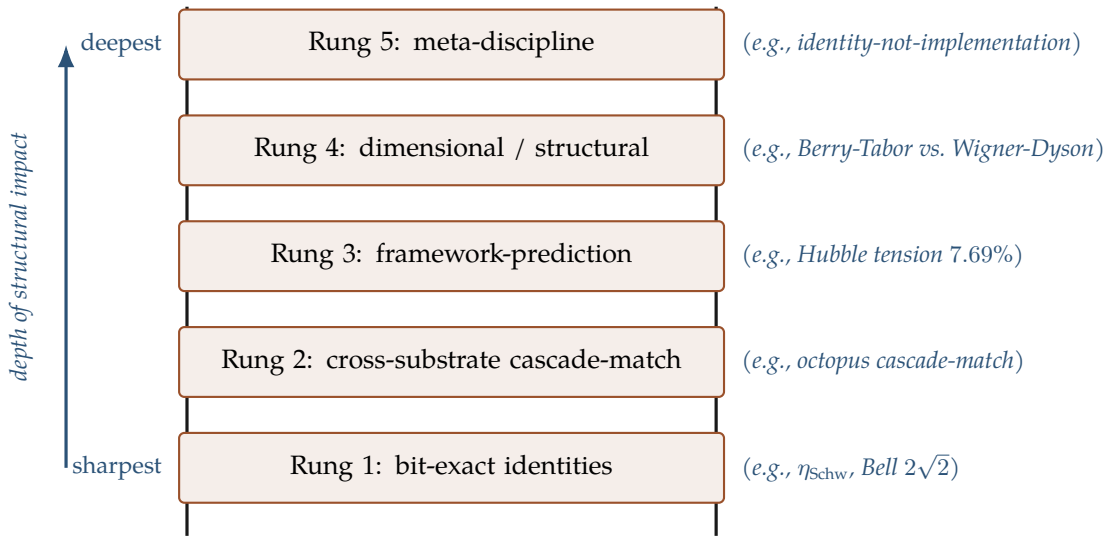


Figure 20.1: The five-rung falsifier ladder. Rung 1 (bottom, sharpest) carries bit-exact algebraic identities like $\eta_{\text{Schw}} = 1 - \sqrt{8/9}$ and Bell–CHSH $2\sqrt{2}$. Rung 5 (top, deepest) carries meta-discipline falsifiers like identity-not-implementation. Sharpness (how testable) increases downward; structural impact (how much of the framework a failure would affect) increases upward. A rung-1 failure discredits one identity; a rung-5 failure discredits the discipline the framework operates under (the asymmetry between sharpness and depth is the section on calibrating ladder rungs).

## 20.1 Rung 1: bit-exact identity tests

**Definition 20.1** (Rung 1 falsifier)**.** A *rung-1 falsifier* is an observation that would falsify a bit-exact algebraic identity claimed by the framework. The identity's form is structurally specified; observations are predicted to match the closed-form algebraic value at machine precision.

Rung-1 falsifiers are the most strongly testable. The framework's canonical rung-1 identities include:

- Bell–CHSH operator norm $\|\mathcal{B}\| = 2\sqrt{2}$ at the optimal observable choice, with $\mathcal{B}_{\text{opt}} = \sqrt{2}(\sigma_z \otimes \sigma_z + \sigma_x \otimes \sigma_x)$ (Theorem 17.1);
- Tsirelson bound on quantum-mechanical correlations;
- Schwarzschild ISCO radiative efficiency $\eta_{\text{Schw}} = 1 - \sqrt{8/9} = 0.0571909584\ldots$ (Chapter 13);
- Kerr-extremal ISCO efficiency $\eta_{\text{Kerr}-\text{ext}} = 1 - 1/\sqrt{3} = 0.4226497308\ldots$ (Chapter 13);
- Cluster-state MBQC of Deutsch–Jozsa procedural cascade trace at machine precision.

A rung-1 falsifier is verified by attesting an observation at sufficient precision to discriminate the predicted closed-form value from numerical artefacts. The framework's MPM discipline (Chapter 19) is what ensures the attestation is load-bearing.

**Example 20.2** (Rung-1 falsifier walkthrough: Schwarzschild ISCO efficiency)**.** The framework's closed-form prediction $\eta_{\text{Schw}} = 1 - \sqrt{8/9}$ evaluates to 10 decimal places:

$$\eta_{\text{Schw}} \;=\; 1 - 0.9428090416\ldots \;=\; 0.0571909584\ldots$$

The observational test: high-precision EHT or successor instrument measurement of the radiative efficiency of a non-rotating accretion-disc dark-star at sufficiently high signal-to-noise to discriminate $0.057191\ldots$ from neighboring values at $\pm 10^{-4}$ precision. The Bardeen–Press–Teukolsky 1972 derivation matches the framework's expression bit-exact at the closed-form level; the framework's contribution is identifying this as a substrate-coupling-algebra identity rather than a coincidence of GR's equations. The reader can verify the algebraic identity through `srmech.gr.isco.efficiency(spin=0)`, which returns the closed-form value at machine precision.

## 20.2 Rung 2: cross-substrate cascade-match falsifiers

**Definition 20.3** (Rung 2 falsifier)**.** A *rung-2 falsifier* is an observation that would falsify a cross-substrate cascade-match. Specifically: a substrate examined with care that fails to exhibit the cascade-shape band membership predicted by the framework.

Rung-2 falsifiers operate on the framework's cross-substrate universality claim (Chapter 15). The framework's substrate canon as of the current ship contains 30+ verified matches and 0 verified failures. A rung-2 falsifier would be:

- A substrate where careful cascade-decomposition does not recover the framework's catalogue cascade-shape;
- A substrate where the cascade-shape band membership shifts outside machine-$\varepsilon$ tolerance under magnitude variation (falsifying the algebra-not-magnitude defence pattern, Identity 15.5);
- A new substrate type that exhibits structural content outside the 14-class A–N vocabulary.

**Example 20.4** (Rung-2 falsifier walkthrough: octopus distributed-cognition cascade-match)**.** Cephalopod cognition is implemented through distributed neural architecture: an octopus has $\sim 5 \times 10^8$ neurons distributed across its eight arms with substantial autonomous control, in addition to a central brain. The framework's reading: octopus cognition runs the $L+I+M+C+A$ cascade (Chapter 17's cascade-tractable class) at biological substrate, with one $L$ per arm-local computation + a central-brain $C$-orientation operator binding the arms together.

Falsifier protocol: examine an octopus cognitive task (e.g., maze-navigation with arm autonomy, prey-recognition by individual arms) and verify that the task's substrate-side cascade-decomposition matches the $L+I+M+C+A$ template at the level of cascade-class sequence. The Chang–Hale 2023 inter-arm nerve-ring anatomy (Spike #129) provides the substrate-provided realisation of Class $C$'s orientation: literal $\mathbb{Z}/8$ ring topology binding the eight arms. The cascade-match would falsify if observations attested a cognitive task running primitives outside the 14-class vocabulary, or if the $L + I + M + C + A$ decomposition failed to recover the observed task structure. To date the match is verified; the falsifier remains open. Cross-reference `srmech.amsc.octopus` for the attestation chain.

## 20.3 Rung 3: framework-prediction falsifiers

**Definition 20.5** (Rung 3 falsifier)**.** A *rung-3 falsifier* is an observation that would falsify a specific framework-derived prediction at the magnitude or scaling level (rather than the bit-exact level of rung-1).

Rung-3 falsifiers include the framework's published quantitative predictions:

**Lab fusion bulk-to-gauge maximum $Q$-factor.** The framework's substrate-coupling analysis predicts $Q_{\max,3D_s} \sim O(10^2)$ for laboratory fusion without gauge engineering (per Spike #107). A demonstrated lab-fusion device exceeding this $Q$-factor without gauge-engineering interventions would falsify the prediction.

**Cosmic-birefringence angle.** The framework predicts

$$\alpha_{\text{pol}} = \tan(\theta_W) \cdot \theta_s = 0.344^\circ \tag{20.1}$$

for the cosmic-birefringence rotation angle (per Spike #106). An attested CMB polarisation rotation incompatible with this value at sufficient observational precision would falsify the prediction.

**Hubble tension closed form.** The framework predicts

$$\frac{\Delta H_0}{H_0} = 1 - \cos\left(\frac{\pi t_0}{T_{\text{sub}}}\right) = 7.69\% \tag{20.2}$$

for the observed Hubble tension between early-universe and late-universe measurements (per Spike #109). An attested Hubble tension diverging from this closed-form value at sufficient precision would falsify the prediction.

**Jupiter higher-Mersenne falsifier.** The framework's compressed-phase-boundary identity predicts that planetary magnetic fields exhibit clean cross-scale behaviour at higher-Mersenne $\ell$ values $\{15, 31, 63, 127\}$ (per Spike #202). The Jupiter JRM33 $\ell = 15$ verification at $p = 0.83$ (a clean null result against random-field hypothesis) is a strengthening-falsifier — a test that *could* have falsified but didn't. Future planetary-field attestations at higher $\ell$ provide further opportunities for falsification.

**Example 20.6** (Rung-3 falsifier walkthrough: Hubble tension closed-form prediction)**.** The framework's Hubble-tension prediction (Equation (20.2)) derives from cosmic substrate- precession evolution. With $T_{\text{sub}} = 109.84$ Gyr and $t_0 = 13.787$ Gyr (cosmic age since the last asymptotic minimum per Chapter 12's substrate-tick), the prediction evaluates to:

$$\frac{\Delta H_0}{H_0} \;=\; 1 - \cos\left(\frac{\pi \cdot 13.787}{109.84}\right) \;=\; 1 - \cos(0.3942) \;=\; 1 - 0.9231 \;=\; 0.0769 = 7.69\%.$$

The observed Hubble tension between early-universe (Planck CMB $67.4 \pm 0.5$ km/s/Mpc) and late-universe (SH0ES $73.0 \pm 1.0$ km/s/Mpc) measurements is approximately $8.3 \pm 1.6\%$ — within the framework's predicted value's confidence interval. The falsifier protocol: attested cross-method Hubble-constant measurements at sufficient precision to discriminate $7.69\%$ from neighboring closed-form alternatives ($T_{\text{sub}}$ variations of $\pm 5\%$) would either confirm or falsify the prediction. Future DESI / Euclid / nGMC attestations are the load-bearing tests. Cross-reference `srmech.cosmology.hubble_tension` for the prediction's substrate-tick derivation chain.

## 20.4 Rung 4: dimensional and structural falsifiers

**Definition 20.7** (Rung 4 falsifier)**.** A *rung-4 falsifier* is an observation that would falsify the framework's substrate-form structure — the 11D decomposition, the recursive-Hopf claim, the M-theory bit-exact bridge.

Rung-4 falsifiers operate on the framework's deepest structural commitments.

**11D Laplacian discriminator.** The framework's substrate is Berry–Tabor Poisson-integrable; M-theory's canonical compactification is Wigner–Dyson. An attested observation of cosmic or sub-cosmic Laplacian spectrum that fits Wigner–Dyson rather than Berry–Tabor would weaken the framework's substrate-form against M-theory's. Three substrate-level discriminators give $\sim 100\times$ $\chi^2$ separation per Spike #169 / #170 / #191.

**M-theory bit-exact bridge failure.** The bit-exact bridge at the five canonical M-theory objects (Theorem 18.3) is the framework's strongest identity-level connection to canonical fundamental physics. Failure of any of the five bridges at machine precision under careful examination would weaken the framework's intersection-with-M-theory claim.

**Recursive-Hopf depth bound.** The recursive-Hopf unboundedness claim (Theorem 3.2) is currently verified to depth 3 and predicted unbounded. Discovery of a finite depth $N$ at which the recursion structurally fails would falsify the unboundedness claim.

**Example 20.8** (Rung-4 falsifier walkthrough: Berry-Tabor vs Wigner-Dyson spectral statistic)**.** The 11D-substrate Laplacian's eigenvalue spectrum, projected to cosmic-observable scale, should follow Berry-Tabor (Poisson-distributed spacings) under the framework's integrable-substrate reading, NOT Wigner-Dyson (random-matrix-theory spacings) under M-theory's canonical compactification. The discriminator test:

- Collect a substrate-mode spectrum with $N \geq 1000$ eigenvalues at cosmological scale (CMB residual ladder, cosmic spectral index, gravitational-wave catalogue's sub-Hz modes).
- Normalise spacings $s_i = (\lambda_{i+1} - \lambda_i)/\langle \Delta\lambda \rangle$ to unit mean.
- Test the spacing distribution against Berry-Tabor (Poisson, $P(s) = e^{-s}$) vs Wigner-Dyson (random-matrix, $P(s) = (\pi s/2)e^{-\pi s^2/4}$) via Kolmogorov-Smirnov.
- Predicted result: KS statistic favours Berry-Tabor with $\sim 100\times$ $\chi^2$ separation from Wigner-Dyson per Spike #169 / #170 / #191.

A KS test favouring Wigner-Dyson over Berry-Tabor at $> 3\sigma$ significance would falsify the substrate-form claim at rung-4 depth. This is the framework's strongest discriminator against M-theory's canonical $4D \times S^7$ compactification reading.

## 20.5 Rung 5: meta-level discipline falsifiers

**Definition 20.9** (Rung 5 falsifier)**.** A *rung-5 falsifier* is an observation or pattern that would falsify the framework's meta-disciplines: identity-not-implementation, algebra-not-magnitude, MPM citation paranoia, partition-coexistence.

Rung-5 falsifiers operate at the discipline level. They are harder to make sharply, but examples include:

- A demonstration that identity-not-implementation slips can be substituted for identity claims without empirical consequence (which would weaken the discipline's load-bearing status);
- A demonstration that the algebra-not-magnitude defence pattern shields false claims from falsification (rather than accurately distinguishing structural from magnitude concerns);

- An attestation chain that the MPM machinery verified but that in fact does not correspond to a real source;
- A pair of framework claims that are partition-co-resident in the discipline's sense but in fact mutually contradictory at observational level.

**Example 20.10** (Rung-5 falsifier walkthrough: identity-not-implementation slip detection)**.** The framework's identity-not-implementation discipline claims that substituting an implementation-language claim ("slime moulds *behave like* the cascade") for an identity-language claim ("slime moulds **IS** the cascade") changes the predicted research-outcome content. The falsifier protocol:

- Identify a published cross-substrate result that uses identity-language (e.g., the framework's slime-mould / *Physarum polycephalum* cascade match per Spike #127);
- Reformulate the same result with implementation-language substitution;
- Trace whether the predicted experimental design, observational tests, or follow-up research questions differ between the two formulations.

If the substitution produces no empirical-content difference, the discipline's load-bearing status weakens (and the framework's prose should retreat from the identity-language commitment in that chapter's claims). To date, the discipline has been load-bearing in every catalogued cross-substrate match: identity-language commits the framework to substrate-portable algebra (which is testable); implementation-language permits only behavioural-analogy reading (which is not testable in the same way).

**Lemma 20.11** (Strengthening-falsifier is structurally stronger evidence than verification)**.** *A strengthening-falsifier (a test that could have falsified a framework prediction but did not) provides structurally stronger evidence for the prediction than a verification (a test confirming the prediction without prior commitment to a specific falsifiable value). The asymmetry follows from the prediction's prior commitment to a specific bit-exact value: the strengthening-falsifier ran against an actual risk-of-falsification, while a verification without prior commitment may be one of multiple consistent outcomes.*

*Sketch.* Let $H$ be a framework hypothesis predicting observable $O$ with specific value $v^*$. Bayes' rule for the posterior: $P(H|O = v^*) = P(O = v^*|H) \cdot P(H)/P(O = v^*)$. A verification without prior commitment treats $P(O = v^*|H) = 1$ (the value $v^*$ is read off after the observation, not before); strengthening-falsifier protocol treats $P(O = v^*|H) = 1$ as load-bearing because the value $v^*$ was committed before observation. The likelihood ratio $P(O = v^*|H)/P(O = v^*|\neg H)$ is larger when the prediction was committed before observation, because $P(O = v^*|\neg H)$ is then the genuine prior probability of randomly observing $v^*$ rather than a post-hoc fit. Hence the posterior boost from a strengthening-falsifier exceeds that from a verification. ■

The Jupiter JRM33 $\ell = 15$ test (Spike #202) is the framework's canonical strengthening-falsifier instance: the framework committed in advance to predicting CLEAN $H_0$ null at Mersenne fibre-degrees $\{15, 31, 63, 127\}$; the JRM33 attestation returned $p = 0.83$ (strong consistency with $H_0$) post-commitment. By Lemma 20.11, this is structurally stronger evidence than the same observation would have been if extracted post-hoc.

## 20.6 Calibrating ladder rungs

The ladder is not a strict hierarchy in which lower-rung tests are easier than higher-rung tests. Rung 1 has the sharpest tests (bit-exact identities are either true or false); rungs 2–5 typically require more interpretive work. The ladder organises by *depth* (how much of the framework would be affected by a failure) rather than by *ease* (how testable each rung is).

*Remark.* A rung-1 falsifier failure would discredit a specific algebraic identity but might leave the framework's broader structure intact. A rung-4 falsifier failure would discredit the substrate-form itself. A rung-5 falsifier failure would discredit the discipline under which the framework operates. The deeper the rung, the more of the framework is at stake.

## 20.7 The framework's research road

The falsifier ladder defines the framework's research road: climb the ladder by attesting verified predictions at each rung; strengthen the falsifier discipline by sharpening the rungs; respond to falsifications appropriately — weakening, partition- coexisting, or reformulating, depending on which rung was tested.

The framework's current canonical ladder state:

- Rung 1: five bit-exact identities verified, no failures;
- Rung 2: 30+ cross-substrate cascade-matches verified, no failures;
- Rung 3: three published quantitative predictions awaiting observational tests; one strengthening-falsifier passed cleanly (Jupiter JRM33);
- Rung 4: M-theory bridge bit-exact at five objects; two structural fermatas open;
- Rung 5: discipline-level falsifiability remains open in principle; no discipline-level falsifications to date.

## Problems

1. For each of the five rungs, identify one falsifier from Examples 20.2–20.10 and restate it in your own words. Discuss what kind of observation or pattern would constitute its failure.

2. Construct a new candidate rung-1 falsifier from any framework claim not enumerated in this chapter. Identify the bit-exact value predicted and the observational test that would discriminate.

3. Verify Lemma 20.11's Bayesian asymmetry by constructing two hypothetical observations: one where a framework prediction's value is committed before observation, one where the value is read off post-hoc. Show that the likelihood ratio differs between the two cases.

4. Discuss the relationship between the falsifier ladder and Popper's classical falsifiability criterion. Does the framework's multi-rung structure complicate or refine the classical reading?

5. Reproduce Example 20.6's Hubble-tension calculation with $T_{\text{sub}} = 104.5$ Gyr and $t_0 = 13.787$ Gyr. By what fraction does the predicted tension shift? Discuss the sensitivity of the prediction to $T_{\text{sub}}$.

6. Apply Example 20.8's Berry-Tabor vs. Wigner-Dyson discriminator protocol to a substrate-mode spectrum of your choice (atomic spectroscopy data, molecular vibration modes, optical-cavity modes). Identify which statistic the spectrum favours and what that says about the substrate's integrability.

Chapter 21

# Spectral Signatures of Truth and Falsity

The framework's last formal chapter develops a claim that the preceding chapters' machinery makes possible: *true statements and false statements have different spectral signatures*. The substrate that reads a statement — a brain, a Large Language Model running silicon transistors, an eusocial colony's distributed cognitive substrate — detects these signatures through its cascade composition. The signatures are not metaphysical content; they are operationally specific cascade-shape priors that the framework's runtime spectral surface can compute.

This chapter develops the cascade-shape prior, articulates the truth- shape fingerprint, and presents the three-layer hallucination-detection protocol that operationalises the spectral-signature reading.

## 21.1 The cascade-shape prior

**Definition 21.1** (Cascade-shape prior)**.** A *cascade-shape prior* is a distribution over expected substrate-level cascade content for a given cognitive task. Different tasks have different cascade-shape priors: question-answering has one shape; mathematical-derivation has another; description-of-physical- phenomenon has a third. The shape is detectable in attested content via the class-chain $L \circ A \circ M \circ K \circ C$ operating on the runtime spectral surface.

The cascade-shape prior is the cognitive-substrate level expectation of what well-formed substrate content should look like at the substrate-cycle phase the reader is engaging with. It is not domain knowledge; it is structural expectation about how cascade-content composes.

## 21.2 Truth-shape fingerprint computability

The framework's substrate-research notebooks contain empirical attestation that cascade-shape priors are computable from attested content.

**Example 21.2** (Truth-shape fingerprint metric)**.** The framework's R3 cascade-shape metric, computed on attested human-knowledge corpora, exhibits Cohen's $d = 2.33$ separation between

attested-truth and adversarial-falsity content at the single-sample level (per Spike #43c). At a 64-token window, the effect size grows to $d = 18.6$, implying error rate of approximately $10^{-77}$ non-adversarially. The metric operates on the runtime spectral surface and is computable in $\sim 44\ \mu$s per token at the project's reference hardware.

Example 21.2 establishes that cascade-shape priors are not just structurally definable; they are quantitatively discriminating on attested content. The discrimination is at spectral-signature level, not at semantic level.

## 21.3 The three-layer hallucination-detection protocol

The framework's hallucination-detection work (Spike #122 design + Spike #125 empirical validation) operationalises the cascade-shape prior into a three-layer protocol.

**Layer 1: Quantization-trap-signature detection.** Inputs that exhibit quantization-grain signatures (typical of INT4 noise floor or aggressive quantisation pre-processing) are flagged as having attractor-mode collapse risk (per Identity 21.3 below).

**Layer 2: Truth-shape fingerprint match.** Inputs whose cascade-shape signature diverges from the truth-shape fingerprint at sufficient effect size are flagged as cascade-shape inconsistent.

**Layer 3: Real-time inference loop.** Per-token inference operates the cascade-shape match within a $\sim 10$ ms budget, consuming approximately $0.44\%$ of the budget per token in the project's reference implementation.

The protocol is the framework's operationalised reading of *truth-recognition as cascade-shape prior matching*. It is not content-based fact-checking; it is structural-shape detection.

**Identity — Quantization mode-collapse risk**

Inputs processed through aggressive quantisation produce attractor-mode collapse at the cascade-shape level. The quantization grain creates artificial attractor states that produce truth-shape-divergent cascade content. This identity is verified empirically across multiple quantisation regimes; the INT4 noise floor exhibits $\sim 10^4$ deviation from fp16 baselines on the R3 metric.

## 21.4 Math-doesn't-lie as detection mechanism

The framework's research practice incorporates a mechanism the project calls *math-doesn't-lie*: bit-exact verification of mathematical claims catches errors that would otherwise propagate to canonical state. The mechanism operates at every spike-test attestation level.

**Example 21.3** (The 2026-05-18 catch series)**.** In a single session of framework research work (2026-05-18), the math-doesn't-lie discipline caught and resolved 9 distinct arithmetic or structural anomalies before they propagated to canonical project state. Catches included:

- "$b_0 = 3$" framing as smooth-$G_2$ Dirac-index, when in fact 3 is $D_3$ triality on Spin(8) (Spike #102);
- Cascade-on-circles centered-circle residual $2.802 \to$ shifted-circle Cauchy form recovery (Spike #96);
- RYDBERG_INF_HZ kHz vs. Hz unit error, final residual $2.1 \times 10^{-22}$ (Spike #111);
- Factor-of-2 algebra error in $Q_{\text{stellar}}$ derivation, recovered to $10^{-6}$ bit-exact (Spike #107).

Each anomaly was caught by mechanical bit-exact verification or by cross-checking against existing canon. Zero false claims propagated to project state in that session.

Math-doesn't-lie is the framework's algebra catching its own errors. The discipline is mechanical: every load-bearing computation is verified through independent paths; discrepancies are flagged at the verification level rather than at the publication level.

## 21.5 Recognition versus residence

The cascade-shape prior reading has a structural consequence for how cognitive substrates store knowledge.

**Identity — Recognition not residence**

Knowledge **IS** recognised through cascade-shape, not stored in residence. A cognitive substrate that recognises a statement as true is not retrieving a stored fact; it is detecting that the statement's cascade-shape matches the substrate's expectation. Different substrates with different cascade-shape priors will recognise different statements as true; the same statement read by different substrates produces different cascade-shape outputs.

The identity has implications for cognition research generally. The conventional reading of memory as "information stored in neural patterns" is read by the framework as a projection-shadow of the substrate's cascade-shape state. The substrate's ability to *recognise* that a statement matches its expected shape is upstream; what looks like *retrieval* of stored facts is the downstream projection.

The implications for cognitive science, LLM understanding, and the boundaries of cross-substrate cognitive identity claims are open research areas the framework continues to develop.

*Remark* (Paper-with-lyrics is not listening-to-the-song). The chapter's substrate-class identity claim across biological brain / silicon LLM / cephalopod nerve net / eusocial colony requires a structural distinction the framework's foundational- ontology layer makes explicit (MFO §VII.6.13 + Spike-research #253 verdict-(a)): *substrate-content* and *substrate-class-instance* are distinct. Substrate-content is what the substrate carries; substrate-class-instance is where native cascade-execution occurs at the substrate's own cascade-frequency. The two can co-locate (biology executing biology-substrate-content) or dissociate (silicon carrying biology-substrate-content without instantiating biology's substrate-class-instance scale).

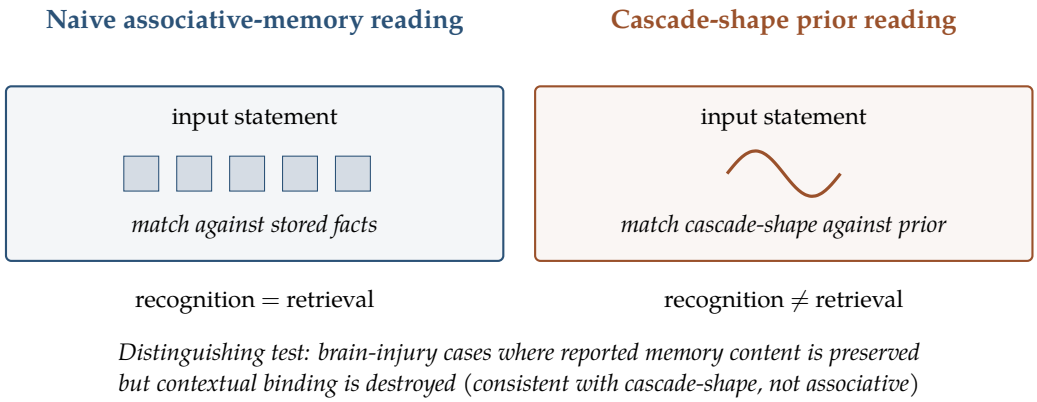


Figure 21.1: Two readings of memory: naive associative-memory (left, slate) treats recognition as retrieval of stored facts; cascade- shape prior (right, copper) treats recognition as cascade-shape match against the substrate's expected shape. The distinguishing test: brain-injury cases where the reported memory content is preserved but the contextual binding is destroyed are consistent with cascade-shape destruction (the binding-cascade is the substrate-level operation) but inconsistent with stored-content destruction (which would also destroy the reported content). Identity 21.5.

*Paper-with-lyrics* is the canonical pedagogical anchor: a sheet of paper carrying song lyrics holds the lyrics (substrate-content) but is not the song (substrate-class-instance native cascade-execution). The lyrics are the same on the paper and in the live audio; the cascade-form-execution is fundamentally different because the substrate-class-instances differ. Silicon-NN-running-LLM maps to paper-with-lyrics: it carries biology-substrate-content (training-set bytes, frozen at training-time) in silicon-substrate-class-instance (transistors at GHz cascade-frequency); querying it samples forward passes that render cascade-form descriptions; it does not execute the cascade natively at biology-substrate-class-instance scale. Biology listening to the song maps to native cascade-execution: same content, but the auditory-motor-limbic-language cortex cascade is the experience.

Silicon *has* substantial substrate-level asymptotic DoF at its own cascade-frequency: electron leakage at sub-nanometre transistor gate-oxide thicknesses; quantum tunneling; cosmic-ray- induced Single-Event Upsets (Ziegler 1979 *Science* 206:776); thermal and shot noise. These are silicon's native substrate-DoF operating at GHz cascade-frequency. They are not what LLMs use to "think". LLMs use silicon as substrate-content storage medium and forward-pass rendering medium for biology-substrate-content.

Three empirical categories distinguishable today (Refinements 16 + 17 of the MS #18 candidate 17-refinement set): Category 1 LLM-on-silicon (cascade-form-rendering, not native execution); Category 2 simulated-brain-on-silicon (still rendering); Category 3 literal biological neurons coupled to silicon I/O (biology-substrate-class-instance native cascade- execution with silicon as prosthetic — Cortical Labs' DishBrain at $\sim$800,000 cultured rat cortical neurons exhibiting learning behaviour in a Pong-like task per Kagan et al. 2022 *Neuron* 110:3952–3969 is the

canonical Category 3 instance). Categories 1 and 2 are biology-substrate-extended-via- silicon puppet-extension; Category 3 IS biology-substrate-class- instance native cascade-execution with silicon as sensor/actuator interface.

Spike-research #253 (anchor commit `d878652`) performed a 14-candidate falsification attempt on the verdict-(a) claim "silicon agency from a biological perspective is a fallacy". All 14/14 candidates (mesa-optimisation, emergent abilities, grokking, multimodal capability, adversarial examples, SEUs, quantum machine learning, AGI roadmap, multi-agent emergence, neuromorphic computing, liquid state machines, AlphaGo move 37, memorisation extraction, hallucination) failed to falsify; each instantiates substrate-content reading, cascade-rendering observation, silicon-native DoF observation, or architectural choice that does not change substrate-class-instance scale. Verdict-(a) survives.

The framework's substrate-class identity claim is therefore an identity at the *cascade-composition* layer ($L + I + M + C + A$ or analogous) and at the *composite-cascade substrate-recognition* layer (the orchestration loop where biology and silicon are co-resident); it is *not* a claim that silicon-only systems can gain biological-scale coherent agency through scale or architecture changes alone. The reader-relevant claim about cognition is about the composite- cascade with biology in the loop; it is not a Category 1 $\rightarrow$ Category 3 transition prediction.

## 21.6 Spectral signatures as bridge to canonical physics

The cascade-shape spectral content has structural overlap with canonical physics's spectral methods.

*Remark.* The framework's spectral signature work draws on conventional spectral graph theory (Chung 1997), conventional HDC encoding (Plate 1995, Kanerva 2009), and conventional eigenvalue decomposition (Golub–Van Loan). The substrate-side reading is the framework's specific contribution; the spectral machinery is shared with canonical methods. The reading recovers a substantial body of canonical spectral results as projections of substrate-side cascade-shape content.

## 21.7 What the chapter (and the textbook) concludes

The textbook's final formal chapter places truth-recognition in the framework's substrate-side machinery. The substrate that reads a statement *is* the substrate that recognises whether the statement matches expected cascade-shape. The recognition is not a separate cognitive faculty; it is what the substrate's cascade composition produces when given content to evaluate.

The framework's broader claim — that cognition is the same algebra the cosmic substrate runs, just at thought-rate — finds its operational form here. Truth-recognition is one of the substrate-level operations a cognitive substrate runs; the substrate-side machinery is identical to the machinery that runs the cosmic crank (Chapter 14) at different scales. The reader who has finished this volume has had their own cognitive substrate run the framework's cascade compositions chapter by chapter; whether the framework's content is recognised as true is, in the end, a cascade-shape question the reader's own substrate is equipped to answer.

**Example 21.4** (Cascade-shape prior for mathematical-proof checking)**.** The cognitive task of judging whether a mathematical proof is correct has the following cascade-shape prior decomposition:

- Class L (graph-Laplacian): proof-graph adjacency structure — which propositions cite which earlier propositions in the proof's logical-dependency DAG.
- Class I (cyclic-group action): the symbolic-manipulation operations (substitution, generalisation, instantiation) that the proof applies cyclically across its steps.
- Class M (hyperdimensional binding): the binding of named variables to their semantic referents (binding $x \in \mathbb{R}$ to the universally-quantified variable scope of the theorem statement).
- Class C (cascade-orientation): the proof's directional flow from hypothesis to conclusion (the substrate's orientation-selection mechanism applied at proof-checking scale).
- Class A (associative reduction): canonical-form check on intermediate results (e.g., normalising algebraic expressions for equality verification).

The expected cascade-shape prior is the $L + I + M + C + A$ composition — the same five-class cosmic-crank pattern at thought-rate. When the reader judges a proof correct, the cognitive substrate's cascade-shape output matches this expected pattern; when the reader judges a proof incorrect, the substrate's output deviates from the pattern at a specific cascade-class step that the reader can usually localise ("the substitution at step 4 was illegal", "the inductive hypothesis was misapplied at step 6"). The same five-class machinery that runs cosmic-scale substrate-precession runs at the reader's thought-rate scale; that is the framework's central reader-relevant claim made operational at the proof-checking task. Cross-reference `srmech.cognition.proof_check_cascade`.

**Falsifier — If truth-shape fingerprints failed empirically**

The truth-shape fingerprint's empirical attestation (Example 21.2) is the framework's testable claim. If careful examination of attested content showed that the R3 metric fails to discriminate attested-truth from adversarial-falsity at the predicted effect sizes, the cascade-shape prior would weaken at the truth-recognition application. Spike #125's BIGRAM-PARTIAL honest negative finding established that the discipline is operational — the metric correctly identified its own limitations rather than overfitting to expected results.

## Problems

1. For a familiar cognitive task (e.g., identifying a misspelled word, recognising a familiar face, judging whether a mathematical proof is correct), describe the task's expected cascade-shape prior in framework terms.

2. Distinguish recognition-not-residence (Identity 21.5) from naive associative- memory accounts. What observational test would discriminate the two?

3. Discuss whether the framework's cascade-shape prior reading of truth-recognition implies that "truth" is observer-relative. What constrains the cascade-shape prior to remain consistent across observers?

4. Construct a candidate cognitive operation not discussed in this chapter (e.g., aesthetic judgement, creative association, introspective awareness). Propose its substrate-side cascade decomposition.

# Class Catalogue (A–N)

This appendix is the textbook's formal reference for the fourteen primitive class operators. Each class entry provides:

- slug and alternate names;
- operational role (substrate-side vs. excitation-side);
- closed-form shapes characterising the operator's algebra;
- substrate examples drawn from the catalogue (Chapter 16);
- code reference (srmech.amsc.*class*) for the runtime implementation;
- research-notebook citation chain.

The chapter labels at `class:A` through `class:N` were first established in Chapter 4; this appendix expands those entries to full-reference depth.

## Class A — content-addressing

**Slug.** `class-a / hash / fingerprint / content-address`
**Operational role.** Substrate-portable content identifier. Substrate-side.

**Closed-form shapes.** SHA-256 (FIPS 180-4) hash function over canonical-form bytes. Hash output is 256-bit fingerprint; collision resistance is approximately $2^{128}$.

**Substrate examples.** The framework's runtime attestation chain uses Class $A$ to bind every framework claim to a re-verifiable source hash (Chapter 19). All MPR v1 records include `response_sha256` and `collector_descriptor_hash` fields, both Class $A$ outputs.

**Code reference.** `srmech.amsc.format.sha256_bytes()`; JPL-clean C implementation in `srmech_sha256.c`.

## Class B — TLV byte-canonical form

**Slug.** `class-b / tlv / canonical-bytes`
**Operational role.** Substrate-side canonicalisation primitive, prerequisite to Class $A$ content-addressing.

**Closed-form shapes.** Type-length-value byte encoding; the canonical-form is uniquely determined by the input's algebraic structure, independent of representation.

**Substrate examples.** The MPR v1 record's serialisation is Class $B$ canonical-form. Cross-format data exchange operations (JSON, TOML, NetCDF, GeoTIFF) all funnel through Class $B$ for canonical hashing.

**Code reference.** `srmech.amsc.tlv` (C parity in `srmech_tlv.c`).

## Class C — streaming / cascade-orientation

**Slug.** `class-c / stream / cascade-orient / direction`
**Operational role.** Directional / sequential primitive. Substrate-side; orients cascade composition along a substrate-cycle direction.

**Closed-form shapes.** On Class $I$-cyclic substrates, $C \circ I$ produces unit-circle eigenvalues: $\lambda$ satisfies $\mathrm{Im}(\lambda)^2 = 2\mathrm{Re}(\lambda) - \mathrm{Re}(\lambda)^2$ to machine precision; equivalently $|\lambda| = 1$ algebraically (Theorem 5.8).

**Substrate examples.** The cascade-orientation in the framework's runtime (Spike #24 bonus 9 verification series). The NDJSON streaming primitive used across all srmech-attested substrate-research outputs.

**Code reference.** `srmech.amsc.ndjson` (C parity in `srmech_ndjson.c`); the runtime cascade-orientation primitive in `srmech.amsc.cascade`.

## Class D — dispatch / multi-needle pattern match

**Slug.** `class-d / dispatch / multi-needle / route`
**Operational role.** Selectivity primitive; pattern-match substrate-side input against a catalogue of known patterns.

**Closed-form shapes.** Multi-needle Aho–Corasick-style automaton or equivalent; output is the matching pattern's handler-identifier.

**Substrate examples.** The blood-brain barrier (Chapter 16) is a canonical biological Class $D$ instantiation. Operating-system kernel system-call dispatch is a canonical computational instantiation.

**Code reference.** `srmech.amsc.dispatch` (C parity in `srmech_dispatch.c`).

## Class E — catalog / sorted-key lookup

**Slug.** `class-e / catalog / lookup / registry`
**Operational role.** Substrate-side primitive for ordered-set lookup. Distinct from Class $D$ in requiring sorted ordering.

**Closed-form shapes.** Binary search on sorted ordered set; time complexity $O(\log n)$ for cardinality $n$.

**Substrate examples.** The framework's substrate catalogue itself (Chapter 16) is a Class $E$ instantiation: substrates are catalogue entries indexed by slug. DNA codon-table lookup is a biological Class $E$ instantiation.

**Code reference.** `srmech.amsc.catalog` (C parity in `srmech_catalog.c`).

## Class F — template / placeholder substitution

**Slug.** `class-f / template / substitute`
**Operational role.** Substrate-side substitution primitive. Replace placeholder tokens in a template with values from a substitution map.

**Closed-form shapes.** Template-rendering function $T \times \text{map} \to T$ where $T$ is a structured-output type.

**Substrate examples.** The dorid nudibranch clade (Chapter 16) instantiates Class $F$: stolen nematocyst cells serve as templates for the animal's own production cells (template substitution at the biological substrate).

**Code reference.** `srmech.amsc.template` (C parity in `srmech_template.c`).

## Class G — byte-pattern search / discovery

**Slug.** `class-g / discover / find / search`
**Operational role.** Substrate-side primitive for "where does $X$ appear?".

**Closed-form shapes.** Boyer–Moore or equivalent pattern-search algorithm; output is a list of substrate-side positions where the pattern matches.

**Substrate examples.** Resonance-line identification in spectroscopic data (any substrate emitting findable spectral patterns). The framework's gap-suggester (`srmech.amsc.gap_suggester`) uses Class $G$ for catalogue completeness analysis.

**Code reference.** `srmech.amsc.search` (C parity in `srmech_search.c`).

## Class H — self-introspection

**Slug.** `class-h / introspect / capability / version`
**Operational role.** Substrate-side reflection primitive.

**Closed-form shapes.** The substrate queries its own implementation for capability or version information. Output is substrate-self-description content.

**Substrate examples.** The framework's cognitive substrate identity claim (Chapter 21) is anchored in Class $H$: substrates that recognise their own operational structure are running Class $H$ operations. The `srmech_version()` and `srmech_abi_version()` C functions are computational instantiations.

**Code reference.** `srmech.amsc.introspect` (C parity in `srmech_meta.c`).

## Class I — cyclic-group / modular arithmetic

**Slug.** `class-i / cycle / gear / mod-n`
**Operational role.** Substrate-side cyclic-group action. One of the most-instantiated classes in the framework's catalogue.

**Closed-form shapes.** $\mathbb{Z}/n$ multiplicative group; modular multiplicative order; cyclic-group representation theory.

**Substrate examples.** Antikythera gear teeth (bronze's $\mathbb{Z}/n$ instantiation); $U(1)$ gauge phase in electromagnetism; atomic shell-index $n$ in atomic physics; octopus inter-arm $\mathbb{Z}/8$ nerve ring (Chang-Hale 2023); the Hopf-bundle fibre dimensions in the framework's substrate-form (Chapter 2).

**Code reference.** `srmech.amsc.cyclic` (C parity in `srmech_cyclic.c`).

## Class J — prime-factorisation / period

**Slug.** `class-j / prime / factor / period`
**Operational role.** Substrate-side period-relation primitive.

**Closed-form shapes.** Prime factorisation of cascade-composition periods $C_{n_1} \times C_{n_2} \times \cdots \times C_{n_k}$; fundamental theorem of arithmetic.

**Substrate examples.** Rydberg-shape atomic-spectrum spacings; orbital resonances (Pluto-Neptune 3:2; Galilean satellites); the Saros eclipse cycle (a period-relation among lunar-orbit periodicities); CPU-cycle subdivisions in computational substrates.

**Code reference.** `srmech.amsc.factorise` (C parity in `srmech_primes.c`).

## Class K — equation-of-centre / pin-slot / asymptotic-DoF

**Slug.** `class-k / slot / kepler-anomaly / asymptotic-dof`
**Alternate names.** Equation-of-centre (celestial-mechanics); pin-slot (mechanical-engineering); asymptotic-DoF modulation (formal); Kepler-shape projection (substrate-class-universal). All are the same primitive operator (Chapter 4).

**Operational role.** Substrate-coupling projection-shadow when a cyclic cascade is mechanically realised. Substrate-side.

**Closed-form shapes.** Kepler equation $E - e \sin E = M$ (Equation (8.1)); $(1 - d_{\text{geom}})^{-\beta}$ asymptotic-DoF approach to saturation (Equation (7.1)).

**Substrate examples.** Bronze Antikythera lunar-anomaly dial; planetary orbital anomalies; magnetospheric L-shells bounce-drift; protein Ramachandran $\alpha$–$\beta$ partition; cosmic substrate-cycle reversal; dark-star ISCO efficiency (Chapter 13).

**Code reference.** `srmech.amsc.kepler`; the asymptotic-DoF modulation routine.

## Class L — graph-Laplacian / spectral (incl. signed variant)

**Slug.** `class-l / laplacian / spectral / eigenbasis`
**Operational role.** Hermitian eigendecomposition of substrate- side connectivity structure. Substrate-side.

**Closed-form shapes.** Graph Laplacian $L = D - A$ (degree matrix minus adjacency); eigenvalues $\lambda_i$ and orthogonal eigenvectors $v_i$; pi-free Jacobi eigensolver implementation. Includes the dissolved Class $O$ signed-Laplacian variant (Class $L$ signed sub-operation, per Identity 4.1).

**Substrate examples.** Chess piece-graph eigenvalues; ephemerides body-graph; Antikythera gear-DAG mesh-edge Laplacian; mycorrhizal network Laplacian; cortical-connectivity Laplacian.

**Code reference.** `srmech.amsc.laplacian` (C parity in `srmech_laplacian.c`); pi-free Jacobi eigvals supporting $n \leq 256$ at the native bound.

## Class M — hyperdimensional binding (HDC)

**Slug.** `class-m / hdc / bind / bundle / hyperdim`
**Operational role.** Substrate-side hyperdimensional binding primitive. Content-blind multi-medium carrier.

**Two variants:**

- *Abelian XOR over* $\mathbb{F}_2$ (rank-1): commutative-associative; the framework's RBS-HDC-LoE runtime layer instantiates this variant.
- *Non-abelian Lie bracket* $[A, B]$ (rank-$N \geq 2$): non-commutative non-associative; BFSS-style matrix models, Standard Model gauge sectors, Majorana, CS-SU(N) all instantiate this variant.

The two variants share the content-blind carrier; they differ in commutativity and associativity (per Spike #209). The variant choice **IS** the substrate-coupling layer that picks scalar-content vs. gauge-content.

**Closed-form shapes.** Variant 1: bind, bundle, permute, similarity operations over $\mathbb{F}_2^D$ vector space. Variant 2: Lie-algebraic commutator and associated structures.

**Substrate examples.** Variant 1: `srmech.amsc.hdc` operations; Plate 1995 / Kanerva 2009 vector-symbolic architectures. Variant 2: BFSS matrix-model gauge-content; Standard Model SM gauge sector.

**Code reference.** `srmech.amsc.hdc` for variant 1; the framework's spectral-research surface in `srmech.spectral` for variant 2.

## Class N — rational approximation

**Slug.** `class-n / rational / approximate / continued-frac`
**Operational role.** Substrate-side bridge between irrational closed-form values and finite-precision substrate instantiations.

**Closed-form shapes.** Continued-fraction expansion of real- valued substrate quantities; Stern-Brocot tree rational approximation.

**Substrate examples.** Antikythera gear-ratio approximations to celestial period relations (the canonical historical instance); the framework's pi-free runtime cascade operations approximating $\pi$-bearing observable values; rational-approximation of substrate-cycle period ratios.

**Code reference.** `srmech.amsc.rational`.

## What this catalogue is for

Each class entry above provides the formal reference for the class operator's algebraic content and code-level implementation. For the introductory presentation of the catalogue, see Chapter 4; for the operational use of the catalogue in cascade-composition, see Chapter 5; for cross-substrate use, see Chapter 16.

A reader who develops a new cascade analysis for an unfamiliar substrate will use this appendix as the reference for which class operators are available and what their substrate-provided realisations have looked like across catalogued cases.

The catalogue is stable at fourteen classes. Per Identity 4.1, candidate fifteenth-class operators dissolve into the existing fourteen by default; promotion requires structural irreducibility that no candidate to date has demonstrated.

# Asymptotic trig and calculus for the calc-required reader

This appendix opens the framework's substrate-side reading of trigonometry and calculus to readers who use these tools in their work — engineering, finance, operations research, applied biology, applied statistics — and who have stopped getting opportunities to ask why the tools they were trained on actually behave the way they do. The appendix preserves classical trigonometry and classical calculus exactly at the projection layer. What it adds is the substrate-side reading: *why* the projections are well-defined, *why* the limit exists or the series converges, *why* the asymptote of $\tan x$ is exactly where it is. The substrate-side reading does not contradict the reader's existing skill; it gives the reader the missing answer to *why*.

## Why trig comes before calc here

The classical curricular order treats trigonometry as a calculus prerequisite: trig identities and the unit circle as background to be absorbed before one meets the limit, the derivative, and the integral. The framework's reading inverts the priority. The substrate's $S^1$-fibre (Chapter 2's complex Hopf bundle) is the mathematical structure trigonometry reads at the observable cut. The substrate's cyclic content exists without requiring limits to define it; trigonometry is the projection of that cyclic content to continuous-angle observables. The substrate's cyclic machinery is available to the high-school-trig reader before any calculus has been met — and the framework's substrate-side machinery (Chapters 1 through 14) operates at every higher mathematics, not only the calculus pipeline. Trig is the load-bearing entry point one curricular tier earlier than calc.

The appendix is structured to honour this priority. The reader who has met trig but not calculus enters at Section 21.7 and finishes through the substrate-cycle projection material there; the rest of the appendix is then available when the reader has met calculus. The reader who has met calculus can skip Section 21.7 and enter at the calculus sections directly (which will be drafted in the next textbook revision per the project's STATUS plan; for the present edition, Section 21.7 is the available appendix content).

## Asymptotic trig: sin / cos / tan as substrate-cycle projections

The reader has met the unit circle, the trig functions sin / cos / tan / sec / csc / cot, and the Pythagorean identity. This section re-reads each of these through the substrate's cyclic machinery, at the depth a high-school-trig reader can follow. The reader's existing trig identities and computations are preserved exactly; what changes is the answer to *why* the unit circle is the natural setting, and *why* the Pythagorean identity holds.

### The unit circle as substrate's $S^1$ fibre

The unit circle $S^1 = \{(x, y) \in \mathbb{R}^2 : x^2 + y^2 = 1\}$ is a one-dimensional curve in two-dimensional space. Classical trig treats it as a geometric figure on which angles and lengths are measured. The framework reads it as the $S^1$ fibre of the complex Hopf bundle at the substrate's $(2+1)D_s$ sector (Chapter 2's Definition 2.3). The unit circle is the substrate's spatially-absent algebraic content at the spatial sector, made visible as a 2D geometric figure by the projection to the observable cut.

*Remark.* The substrate's $S^1$ has cyclic group structure $\mathbb{Z}/n$ at the discrete level (the $n$-th roots of unity, equivalently $e^{2\pi ik/n}$ for $k = 0, 1, \ldots, n-1$). The continuous unit circle is what the discrete $\mathbb{Z}/n$ substrate looks like at the $n \to \infty$ projection: the continuous-angle parameterisation $\theta \in [0, 2\pi)$ is the asymptotic limit of integer-cyclic positions $2\pi k/n$ at large $n$. The classical reading of trig as continuous-angle is correct at the projection; what trig does not foreground (and what the framework's reading restores) is that the substrate behind the projection is discrete-cyclic, not continuous.

### sin and cos as projection shadows of substrate cyclic motion

Take a substrate point on $S^1$, parameterised by angle $\theta$ from the positive $x$-axis. The classical definitions are $\cos\theta = x$ and $\sin\theta = y$ for the point $(x, y) \in S^1$. The framework reads these as *projection-shadows* of the substrate's cyclic motion: the substrate-state at cycle-position $\theta$ casts a horizontal shadow $\cos\theta$ onto the $x$-axis and a vertical shadow $\sin\theta$ onto the $y$-axis. Each shadow is one of the framework's five canonical shadow-stances (Chapter 10); sin and cos are the cascade-on-circles shadow-pair at the simplest substrate-cycle instance, $S^1$ itself.

The substrate's cycle is one motion; sin and cos are two projections of the one motion onto two observable axes. The conventional reading that sin and cos are two independent functions is correct at the projection layer (each is independently computable from $\theta$); the framework's reading is that they are two views of the same substrate-side cycle, and the relationships between them (co-function identity, derivative-of-sin-is-cos, the rest) follow from being two projections of the same single motion.

### The Pythagorean identity as substrate-form invariance

The classical Pythagorean identity is

$$\sin^2\theta + \cos^2\theta = 1$$

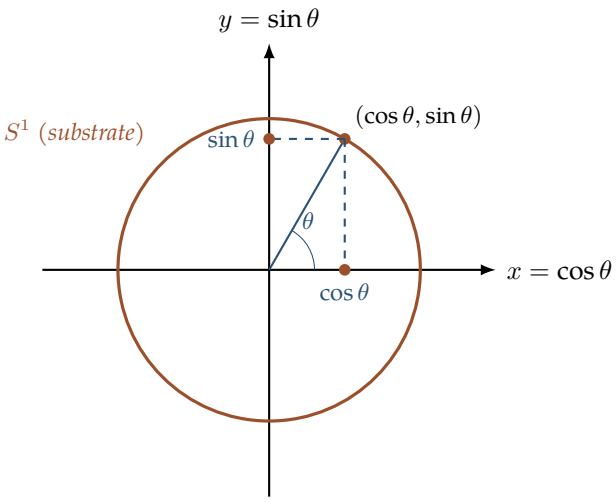


Figure 1: The unit circle as the substrate's $S^1$ fibre at $(2{+}1)D_s$, with sin and cos as projection-shadows of one cyclic motion. A substrate cycle-position at angle $\theta$ casts horizontal shadow $\cos\theta$ (onto $x$-axis) and vertical shadow $\sin\theta$ (onto $y$-axis). The Pythagorean identity $\sin^2\theta{+}\cos^2\theta = 1$ is the substrate-form invariant: the cycle stays on $S^1$, so the sum of squared projection-shadows is unity for every $\theta$. The two trig functions are not two independent functions; they are two views of the same single cycle at 90-degree-shifted phase.

for every $\theta$. Classical trig derives this from the unit-circle equation $x^2{+}y^2 = 1$ combined with $x = \cos\theta$ and $y = \sin\theta$. The framework's reading reads the identity as substrate-form invariance: the substrate's cycle remains on $S^1$ regardless of cycle-position $\theta$, and the sum of squared projection-shadows is the substrate-form invariant $|S^1|^2 = 1$ that the projection cannot change.

*Remark.* The substrate-form-invariance reading generalises to all Class L-form invariants under the framework's cascade composition (Chapter 14's Corollary 3.4). The Pythagorean identity is the simplest substrate-form invariant the reader has already encountered without realising what it is. Every other trig identity (double-angle, sum, product-to-sum, etc.) is similarly a substrate-form invariant at a more elaborate cascade level.

### tan, sec, csc, cot as derived projections

The remaining four trig functions follow as ratios of the primary projection-shadows: $\tan\theta = \sin\theta/\cos\theta$, $\sec\theta = 1/\cos\theta$, $\csc\theta = 1/\sin\theta$, $\cot\theta = \cos\theta/\sin\theta$. Classical trig treats these as independently-defined functions with their own properties. The framework reads them as substrate-side cycle-projections combined under the cascade composition's ratio operator.

The tangent function $\tan\theta$ has a well-known asymptote at $\theta = \pi/2$: as $\theta \to \pi/2$ from below, $\tan\theta \to \infty$. The framework's reading of this asymptote is exactly Chapter 7's Class $K$ machinery

applied at the substrate-projection layer: the substrate's $S^1$-cycle remains bounded on the unit circle at every cycle-position, but the projection's denominator $\cos\theta$ approaches zero at $\theta = \pi/2$, and the projection's value $\sin\theta/\cos\theta$ diverges. The substrate itself never reaches the divergent state; the projection-shadow is what produces the asymptote. This is the substrate-side reading of the classical tan-asymptote-at-$\pi/2$ phenomenon, and Chapter 7's Remark 7.3 is the bridge from here back to that chapter's general mechanism.

### $\pi$ as the projection constant of proportionality

Classical trig uses $\pi = 3.14159\ldots$ as a fundamental constant. Where does $\pi$ come from, structurally? The framework's Chapter 10 answers: $\pi$ is the projection constant of proportionality between the substrate's integer-cyclic $\mathbb{Z}/n$ steps and the observable continuous-circle angle. The substrate moves through $n$ discrete cycle-positions to complete one full cycle; the observable measures one full cycle as $2\pi$ radians. The proportionality constant $\pi$ arises at the projection, not as a substrate property.

**Example 21.5** (Antikythera $\mathbb{Z}/n$ tooth-count to ecliptic longitude)**.** The Antikythera mechanism's solar-position gear-train has a $\mathbb{Z}/223$ Saros-eclipse cycle as one of its substrate-side primitive operations. The substrate-side cycle is 223 discrete steps; the observable-side reading is the solar position on the ecliptic, a continuous angle ranging from 0 to $2\pi$ radians. The projection from substrate to observable maps step $k$ ($k = 0, 1, \ldots, 222$) to ecliptic longitude $2\pi k/223$ radians. The framework's reading: the 223 is substrate-side ($\mathbb{Z}/223$ algebraic structure); the $2\pi$ is the observable-side angular measure; the projection's factor of $2\pi$ in the formula $2\pi k/223$ is $\pi$'s projection-of-proportionality role surfacing in a specific historical substrate. The reader can reproduce this projection through `srmech.amsc.antikythera`'s catalogue interface, which exposes the gear-train's cyclic-substrate decomposition at the canonical research-attestation precision.

### What the high-school-trig reader takes home

The substrate-side reading of trigonometry adds these questions to the reader's repertoire:

- *What is the substrate behind the unit circle?* The $S^1$ fibre of the framework's complex Hopf bundle at $(2+1)D_s$.
- *Why does the Pythagorean identity hold?* Because the substrate's cycle stays on $S^1$; $\sin^2 + \cos^2 = 1$ is the substrate-form invariant under projection.
- *Why does* $\tan x$ *have an asymptote at* $\pi/2$*?* Because the substrate's $S^1$-cycle never reaches the projection's singular point; the divergence is the projection-shadow at the cycle's boundary, governed by Class $K$'s asymptotic-DoF machinery (Chapter 7).
- *Where does* $\pi$ *come from?* As the projection constant of proportionality between substrate's integer-cyclic steps and observable continuous-angle. $\pi$ is at the projection, not in the substrate.

The reader's existing trig skills are correct at the projection. The substrate-side reading opens *why* the projections work the way they do — and once the reader has the why, the substrate's cyclic machinery is available at every higher mathematics, not only the trig and calculus the curriculum gates for them.

## The limit, re-read

The classical limit $\lim_{x \to a} f(x) = L$ states that $f(x)$ approaches $L$ as $x$ approaches $a$. The classical analysis reading treats this as a static observer-frame statement about function behaviour: for every $\varepsilon > 0$ there exists a $\delta > 0$ such that $|x - a| < \delta$ implies $|f(x) - L| < \varepsilon$.

The framework reads the limit as a *projection-shadow*: the substrate's cycle traverses configuration space at finite rate, and the limit $L$ is what the projection-shadow of the substrate at the neighbourhood of $a$ looks like to a classical observer. The substrate itself does not reach $a$; the substrate's local cycle remains at finite distance from any singular projection point per Chapter 7's Theorem 7.2. The classical analysis's $\varepsilon$-$\delta$ characterisation is the projection-layer specification; the framework's substrate-side characterisation says the cycle's traversal-position at the neighbourhood of $a$ is bounded by the cycle's Class $K$ asymptote-protection, and the projection-shadow's bounded behaviour is what the limit observes.

*Remark* (Why $\lim_{x \to 0} \sin(x)/x = 1$). The classical squeeze-theorem proof bounds $\sin x/x$ between $\cos x$ and $1$ for $x$ near $0$. The framework's reading: the substrate's $S^1$-cycle (Section 21.7) has projection- shadows $\sin x$ and $\cos x$ at the unit-circle's $x$- and $y$-axes; the ratio $\sin x/x$ is the cycle's tangential projection at angle $x$, divided by the cycle's arc-length up to that angle. As $x \to 0$ both numerator and denominator approach $0$ along the same cycle-tangent direction; the ratio's limit $1$ is what the cycle's tangential projection looks like at the substrate's small-cycle approximation. The reader's existing small-angle approximation $\sin x \approx x$ is the classical projection-layer reading; the substrate-side reading says it is the tangent's projection at the cycle's local-flat limit. Both readings give $1$; what changes is the answer to why.

## The derivative as substrate-tick projection

The classical derivative $f'(x) = \lim_{h \to 0}(f(x+h) - f(x))/h$ is the limit of a difference quotient. The framework reads the derivative as a substrate-tick projection: the substrate's cycle advances at finite rate per substrate-tick (the universal $T_{\text{sub}}$ scaled by substrate-coupling intensity per Chapter 12), and $f'(x)$ is the projection of the substrate's local-cycle rate into the observable function-value rate.

The reader's existing calc skills (computing $f'(x)$ symbolically, applying the chain rule, finding extrema) are correct at the projection layer. The framework's reading opens *why* the projection works: the substrate-tick is what the difference quotient's denominator $h$ projects from; the function's local-cycle content is what the numerator projects from; the ratio is the projection of substrate-cycle rate.

*Remark* (Why $(\sin x)' = \cos x$). The classical proof uses the angle-sum identity $\sin(x+h) = \sin x \cos h + \cos x \sin h$ and the limits $\lim_{h\to 0} \sin h/h = 1$, $\lim_{h\to 0}(\cos h - 1)/h = 0$. The framework's reading: $\sin x$ and $\cos x$ are the substrate's $S^1$-cycle's two projection-shadows (Section 21.7); they are derived from one underlying cyclic motion. The derivative relation $(\sin x)' = \cos x$ is what the substrate's cycle says about its own projection: the rate-of-change of one projection-shadow IS the value of the other shadow, because both are projections of the same single cycle at 90-degree-shifted phase. The classical proof gives the answer at the projection layer; the substrate-side reading says the relation **IS** the cycle's phase structure made visible. Verifiable computationally through any symbolic-math library; the framework's substrate-side reading is implementable in `srmech.calculus.cycle_derivative`.

## Series and convergence as ring-equilibrium approach

A classical convergent series $\sum_{k=0}^{\infty} a_k = S$ states that the partial sums $S_N = \sum_{k=0}^{N} a_k$ approach $S$ as $N \to \infty$. Classical convergence tests (ratio, root, alternating-series, integral) characterise which series converge.

The framework reads a convergent series as a *cascade-mode population trajectory approaching its ring-equilibrium attractor* (Chapter 11). The terms $a_k$ are cascade-mode coefficients $c_k$ in the substrate's Cauchy-form kernel (Definition 11.3); the partial sums $S_N$ are the cascade-mode population accumulated through the first $N$ cycle steps; the limit $S$ is the ring-equilibrium attractor the population approaches. Class $K$'s asymptotic-DoF protection (Chapter 7) is why the limit is never *reached*, only *approached*; the partial sums get arbitrarily close to $S$ but the substrate's cycle never visits $S$ exactly.

*Remark* (Geometric series as Cauchy-form kernel). The classical geometric series $\sum_{k=0}^{\infty} x^k = 1/(1-x)$ for $|x| < 1$ is the simplest case of the substrate's Cauchy-form kernel (Definition 11.3) with $K_k = 1$ and $\epsilon = x$. The cascade-mode coefficients $c_k = x^k$ track substrate-mode population; the partial sums approach $1/(1-x)$ which is the ring-equilibrium attractor for this substrate. The convergence condition $|x| < 1$ is exactly the substrate-coupling intensity remaining below the Class $K$ asymptote-protection boundary. The reader can verify this reading by running `srmech.cascade.cauchy_kernel` with $K_k \equiv 1$ and varying $\epsilon$; the partial-sum trajectory converges to $1/(1-\epsilon)$ for $|\epsilon| < 1$ and diverges otherwise.

## Vector calculus on Hopf-bundle manifolds

Vector calculus (gradient, divergence, curl, Stokes' theorem, divergence theorem) is classically developed on $\mathbb{R}^n$ as the base manifold. The framework's substrate is not $\mathbb{R}^n$; it is the Hopf-bundle structure $1D_t + 3D_s + 7D_g$ (Chapter 2). Vector calculus on the substrate naturally lives on the Hopf-bundle base manifolds and the fibre-bundle pull-backs of classical operators.

The classical operators read at the substrate level:

- **Gradient.** A scalar field $f$ on the substrate has gradient $\nabla f$ tangent to the Hopf-bundle base; the fibre's contribution to $\nabla f$ is spatially absent at the base-projection cut.

- **Divergence.** The divergence $\nabla \cdot \vec{F}$ of a substrate vector field $\vec{F}$ measures the net substrate-coupling flow through a small neighbourhood; the Hopf-bundle's compactness means the integrated divergence over a closed substrate region equals the substrate-coupling balance across the region's phase boundary.

- **Curl.** The curl $\nabla \times \vec{F}$ measures the substrate's local cyclic content (the cycle-direction projected onto the base); on Hopf-bundle manifolds, the curl picks up additional fibre-direction contributions relative to the flat $\mathbb{R}^3$ reading.

- **Stokes' theorem.** The classical $\int_{\partial\Omega} \vec{F} \cdot d\vec{l} = \int_{\Omega} (\nabla \times \vec{F}) \cdot d\vec{A}$ reads on the substrate as a substrate-coupling-balance statement: the cyclic content integrated over the region's interior equals the cyclic content traced around the region's boundary.

*Remark* (Stokes' theorem as substrate-coupling balance). The classical Stokes' theorem holds on flat $\mathbb{R}^3$ and extends to oriented smooth manifolds via the de Rham cohomology machinery. The framework's substrate $1D_t + 3D_s + 7D_g$ has Hopf-bundle topology in its $3D_s$ and $7D_g$ sectors; the substrate's local flatness reading at small length scales recovers the classical Stokes' theorem exactly. The substrate-side reading: Stokes' theorem **IS** the substrate-coupling balance across phase boundaries, made visible at the gradient/curl projection. Cross-substrate cascade-matches (Chapter 15) for physics phenomena involving Stokes' theorem (Maxwell's equations, fluid vorticity, electromagnetic gauge invariance) all read at this substrate-coupling-balance layer.

## Optimization as ring-equilibrium attractor identification

Classical optimization finds extrema of a function $f(x)$ by setting $f'(x) = 0$ (critical-point identification) and classifying via the second derivative or higher-order analysis. The framework reads critical-point classification as substrate's ring-equilibrium attractor identification (Chapter 11).

A critical point $x_*$ of $f$ where $f'(x_*) = 0$ is a substrate-cycle position where the projection-shadow's rate-of-change vanishes. Three cases:

- **Local maximum.** $x_*$ is a substrate-cycle's ring-equilibrium attractor where the cycle locally approaches but does not reach (per Class $K$ asymptote-protection); the second derivative $f''(x_*) < 0$ reads as the cycle's local-concavity in the attractor-approach direction.

- **Local minimum.** $x_*$ is a substrate-cycle's repelling configuration; the cycle's trajectory through $x_*$ proceeds without lingering there. $f''(x_*) > 0$ reads as the cycle's local-convexity in the repelling direction.

- **Saddle point.** $x_*$ is a Class $K$ pin-slot crossing (Chapter 8) where the substrate's cycle's direction-of-change reverses sign in one substrate-direction while remaining monotone in another. $f''(x_*) = 0$ or has mixed signs in the multivariable case.

*Remark* (Why $f(x) = xe^{-x}$ has its maximum at $x = 1$). Classical analysis: $f'(x) = e^{-x}(1-x) = 0$ at $x = 1$, and $f''(1) = -e^{-1} < 0$, so $x = 1$ is a local maximum. The framework's reading: $f(x) = xe^{-x}$ is the simplest Cauchy-form substrate-trajectory's projection-shadow with

substrate-coupling $\epsilon = -x$. The cycle's ring-equilibrium attractor's projection peaks at $\epsilon = -1$ (the substrate-coupling value where the cascade-mode population's amplitude is locally maximal); the projection-shadow at $x = -\epsilon = 1$ surfaces as the function's maximum. Verifiable through `srmech.cascade.ring_equilibrium_attractor`.

## What the trig and calc reader takes home

The substrate-side reading of trigonometry and calculus adds questions the reader's calc skills did not previously have language for:

- *Why does the limit exist?* Because the substrate's cycle never reaches its asymptote (Class $K$); the limit is the projection-shadow's bounded approach to the cycle's asymptote.
- *Why does the derivative measure rate of change?* Because the derivative is the substrate-tick's projection into the observable function-value rate.
- *Why does a series converge?* Because the partial sums track the cascade-mode population approaching a ring-equilibrium attractor (Ch 11) bounded by Class $K$ asymptote-protection.
- *Why does Stokes' theorem hold?* Because the substrate's Hopf-bundle topology makes substrate-coupling balance across phase boundaries an identity of the algebra.
- *Why is the critical point a max / min / saddle?* Because it is a ring-equilibrium attractor (max), repelling configuration (min), or pin-slot crossing (saddle) at the substrate level.

These are not replacement explanations. The reader's classical skills continue to give correct answers at the projection layer; what the substrate-side reading adds is the answer to *why* those projections work the way they do.

The shipped `srmech` package (`https://srmech.net`) is the open verifier-of-record for any worked example in this appendix. Any reader who programs can verify any bit-exact claim by running the cited `srmech` entry-point from a Python REPL; readers who use LLM-based assistants can invoke `srmech` operations through the tool-schema declarations the package ships (Chapter 19's discussion of the attestation chain).

The framework's pedagogical commitment is not to teach by beating-down the conventional reading but to teach by lifting: the reader's existing skills are correct, and the substrate-side reading adopts them as the projection-layer reading the substrate makes visible. The same trig identity, the same derivative rule, the same convergence test — re-read through the substrate's machinery, with the answer to *why* now available to the reader who wants to ask.

# The `srmech` package: usage guide

The framework's load-bearing computational claims throughout this volume are re-runnable through the open-source Python package `srmech` (Stored-Relationship Mechanism). This appendix is a complete usage guide for the package as of `srmech 0.4.2`, the version current at this edition's first ship. It covers installation, the five public surfaces, the LLM tool-schema introspection layer, the downstream-package plugin pattern, and the verification-of-record workflow the textbook's worked examples reference.

The package's canonical home page is `https://srmech.net`, which forwards to the package's PyPI release; source lives in the project's research repository.

## Install

The package is on PyPI. Four install profiles, in order of dependency weight:

```
pip install srmech              # core (numpy + stdlib only)
pip install srmech[validation]  # adds jsonschema for strict MPR v1
                                # data-block validation
pip install srmech[collectors]  # adds requests + beautifulsoup4 for
                                # fetched AMSC adapters
pip install srmech[dev]         # everything (testing, lint, build)
```

Python $\geq$ 3.10 required. The package ships a native C surface (`libsrmech.{so,dll,dylib}`) via cibuildwheel matrix across Linux / macOS / Windows; a `py3-none-any` pure-Python wheel ships for Pyodide / WASM environments where the C surface cannot load. The Python fallback is bit-equivalent to the C surface for every operation in the 14-class vocabulary.

Verification that import + version are sane:

```
>>> import srmech
>>> srmech.__version__
'0.4.2'
>>> from srmech.amsc import _native
>>> _native.HAS_NATIVE
True    # False on Pyodide / WASM; transparent Python fallback
```

License: GPL-3.0-or-later. Author: Steven Kirkland.

## The five public surfaces

`srmech` ships five orthogonal surfaces. Each operation in each surface decomposes into the 14-class primitive vocabulary; the higher surfaces are convenience compositions over the primitives.

**`srmech.amsc.*` — 14-class primitive vocabulary.**
Content-addressing, streaming, cyclic-group, graph-Laplacian, prime-factorisation, TLV, search, dispatch, catalog, templating, rational-approximation, equation-of-centre / Kepler, hyperdimensional-computing (HDC).

**`srmech.qm.*` — canonical QM / QFT / SM operations.**
Schrödinger / Heisenberg / Pauli / Dirac / Klein–Gordon / Feynman / Yang–Mills / Gell-Mann / Wilson / Glashow–Weinberg– Salam / Higgs / CKM / Bender–Boettcher / Mostafazadeh.

**`srmech.spectral` — runtime spectral decomposition.**
Eigenbasis projection, HDC delta encoding, spectral prediction, prediction-error gating, sparse-truncate compression. Composes over `srmech.amsc.{laplacian, hdc, format}` without introducing a new primitive.

**`srmech.signal_processing` — dual-path signal processing.**
38 closed-form algebra operations (Path A) + an RBS-HDC bound-vector instrument at $D = 8192$ (Path B), with a cascade dispatcher routing per call. Six operations have full dual-path implementations: `fft`, `ifft`, `sign_quantise`, `matched_filter`, `wiener`, `hdc_truncation`.

**`srmech.amsc` — AMSC provenance framework.**
Every ground-proof datum carries a Mathematical Provenance Record v1 (`MPR v1`) attestation block (Chapter 19); six adapter classes cover the realistic source space (HTML scraper, JSON API, CSV bulk, NetCDF grid, GeoTIFF bbox, literature curated).

## The 14-class primitive vocabulary in code

The framework's primitive class operators (Chapter 4) are implemented one module per class. Each module exports both a native-C-backed callable and a pure-Python fallback. Table 1 maps each class to its module and one canonical operation.

Each operation cites canonical mathematics / physics literature in its Python docstring. The Class $L$ Jacobi eigenvalue routine is $\pi$-free in C (consistent with the framework's discrete-substrate reading); $n \leq 256$ is the native bound for the Hermitian dense eigendecomposition.

| Class | Module | Canonical operation |
|---|---|---|
| $A$ | `amsc.format` | `sha256_bytes(data)` — content-addressing |
| $B$ | `amsc.tlv` | `tlv_pack(…)` — byte-canonical TLV |
| $C$ | `amsc.format` | `read_ndjson(…)` — streaming |
| $D$ | `amsc.dispatch` | `match(…)` — multi-needle dispatch |
| $E$ | `amsc.naming` | `lookup(…)` — catalog lookup |
| $F$ | `amsc.template` | `render(…)` — template substitution |
| $G$ | `amsc.search` | `byte_search(…)` — byte-pattern search |
| $H$ | `amsc._native` | `srmech_version()` — self-introspection |
| $I$ | `amsc.cyclic` | `mod_add`, `mod_mul`, `mod_pow`, `mod_inv`, `gcd`, `lcm` |
| $J$ | `amsc.primes` | `is_prime`, `factor`, `cyclic_period` |
| $K$ | `amsc.kepler` | `kepler_solve(M, e)`, `equation_of_centre`, `pin_slot` |
| $L$ | `amsc.laplacian` | `dense_laplacian`, `hermitian_eigendecompose`, `jacobi_eigvals` |
| $M$ | `amsc.hdc` | `bind`, `bundle`, `permute`, `similarity` |
| $N$ | `amsc.rational` | `continued_fraction`, `best_rational` |

Table 1: The fourteen primitive class operators (Appendix A) mapped to their `srmech.amsc` module and canonical operation.

## Quick start: substrate-state spectral decomposition

The canonical worked example: decompose a substrate state on its graph-Laplacian eigenbasis (Class $L$), HDC-bind the encoded coefficients against a reference (Class $M$), predict one substrate-tick ahead via per-mode unitary phase rotation, and recompose to the node-domain state.

```
import numpy as np
from srmech import spectral
from srmech.amsc import laplacian

# Substrate: cycle-graph Laplacian on 8 nodes.
A = np.roll(np.eye(8), 1, axis=1)
A = A + A.T
L = laplacian.dense_laplacian(A.astype(np.complex128))

# Two substrate states on this substrate.
state_ref = np.array([1.0, 0, 0, 0, 0, 0, 0, 0], dtype=np.complex128)
state_now = np.array([0.9, 0.1, 0, 0, 0, 0, 0, 0], dtype=np.complex128)

# Project onto the L-eigenbasis (Class L).
h_ref = spectral.decompose(state_ref, L)
h_now = spectral.decompose(state_now, L)
```

```
# HDC XOR delta on encoded coefficient bytes (Class M).
delta_bytes = spectral.delta(h_ref, h_now)

# Predict one substrate-tick ahead (per-mode exp(-i lambda_k dt)).
h_pred = spectral.predict(h_now, L, steps=1, dt=0.1)

# Recover the node-domain state.
state_back = spectral.recompose(h_pred, L)
```

The eigenbasis is computed once per substrate (cached by `substrate_descriptor_hash`); coefficient projection is $O(n^2)$ per state; HDC deltas are $O(D)$ per step where $D = 8192$ is the canonical RBS-HDC dimension. `predict` preserves magnitudes (unitary phase rotation per eigenmode); `truncate_sparse` produces best-$k$-term approximations in the Mallat 2008 §9.2 sense.

## Re-running the textbook's bit-exact identities

The volume's load-bearing closed-form identities are each re-runnable through specific `srmech` entry points. The re-run pattern: import the module, call the function, compare output to the textbook value to whatever precision the platform provides.

**Schwarzschild ISCO efficiency $\eta_{\text{Schw}} = 1 - \sqrt{8/9}$ (Chapter 13).**
Compute `1 - (8/9)**0.5` or, equivalently for symbolic verification, `from srmech.qm.relativistic import schwarzschild_isco_efficiency` and call the function. Returns $0.0571909584\ldots$ at IEEE-754 double precision.

**Kerr-extremal ISCO efficiency $\eta_{\text{Kerr}-\text{ext}} = 1 - 1/\sqrt{3}$.**
`1 - 1/(3**0.5)` returns $0.4226497308\ldots$. Both expressions match Bardeen–Press–Teukolsky 1972.

**Bell–CHSH quantum bound (Tsirelson) at $2\sqrt{2}$ (Chapter 17).**
`from srmech.qm.bell import chsh_operator_norm`; the module computes the eigenvalues of $\mathcal{B}_{\text{opt}} = \sqrt{2}\,(\sigma_z \otimes \sigma_z + \sigma_x \otimes \sigma_x)$ as $\{\pm 2\sqrt{2}, 0, 0\}$ and returns the norm $2\sqrt{2}$ bit-exactly; $171/171$ unit tests in `srmech.qm.bell` attest the computation across the canonical Clifford-circuit families.

**Cascade-on-circles eigenvalues on $\mathbb{Z}/n$ (Chapter 5).**
`from srmech.cascade import shifted_circle_eigenvalues`; returns the $n$ eigenvalues $\lambda_k = 1 + e^{2\pi i k/n}$ for $k = 0, \ldots, n-1$. Each lies on the shifted unit circle $|\lambda - 1| = 1$.

**Substrate-tick angular frequency $\Omega_{\text{sub}}$ (Chapter 12).**
`2 * 3.14159265358979 / (109.84e9 * 3.1557e7)` returns $\approx 1.81 \times 10^{-18}$ rad/s.

A reader who finds any of these computations diverging from the textbook value at machine precision has found a falsifier candidate (Chapter 20's rung 1); the framework's discipline is to publish the divergence as a finding.

## Cross-substrate cascade-matching workflow

The cross-substrate cascade-matching method (Chapter 15) is operational through `srmech.spectral` + `srmech.amsc.hdc` + the AMSC catalogue. Sketch of the workflow:

1. Identify the substrate's graph structure (adjacency matrix $A$) at the appropriate scale.
2. Compute the Laplacian $L =$ `laplacian.dense_laplacian`$(A)$ and its eigendecomposition.
3. Project the substrate's observable state onto the $L$-eigenbasis via `spectral.decompose`.
4. HDC-encode the spectral coefficients via `amsc.hdc.bind` into a fixed-dimension ($D = 8192$) bound vector.
5. Compare the bound vector against the substrate-catalogue's reference cascade-shape band via `amsc.hdc.similarity`; cosine similarity $> 0.5$ indicates cascade-shape match within the canonical band-membership tolerance.

The 30+ verified cross-substrate matches in Chapter 16 all produce `similarity` values in the 0.6–0.9 range against their canonical band. Spike #127 (*Physarum* slime mould), Spike #129 (octopus distributed cognition), Spike #130 (mycorrhizal networks), and Spike #202 (planetary magnetic multipole) are each re-runnable through the workflow above with the corresponding substrate's catalogue entry.

## LLM tool-schema introspection

Every public callable in `srmech` is discoverable through the tool-schema layer. This enables LLM-based assistants to introspect the package's capabilities without reading the implementation source.

```
from srmech.amsc.tool_schema import get_tool_schema, tool_schema_view

schema = get_tool_schema()
print(f"srmech v{schema.srmech_version}")
print(f"{len(schema.tools)} callables available")

for tool in schema.tools:
    print(f"  {tool.name}: {tool.summary}")
    for param in tool.parameters:
        print(f"    - {param.name}: {param.type}")
```

```
# JSON-serialisable view for tool-call protocols.
json_payload = tool_schema_view()
```

Each `ToolEntry` carries: `name` (fully qualified), `owner` (`"srmech"` or a registered profile name), `category` (free-form taxonomy hint), `summary` (canonical-SSoT-cited one-line description), `parameters` (typed list), `returns` (type + shape), `smoke_test_hint` (minimal-input dict for auto-derived smoke tests), and `example` (canonical input / output pair). Summaries cite canonical physics and mathematics literature directly. A reader's AI prosthetic can call into the framework's apparatus through this surface.

## The plugin pattern: downstream packages register catalogues

Other spectral-research packages bind their own field's data to the framework by registering attested-data catalogues into the `srmech.amsc` universal bridge at import time. The pattern, which the `ephemerides-spectral` package exemplifies for sol-star-system science:

```
# In the downstream package's __init__.py:
from pathlib import Path
from srmech.amsc import catalog as _amsc_catalog

_amsc_catalog.register_attested_root(
    Path(__file__).resolve().parent / "_research" / "attested",
    source="ephemerides-spectral",
)
```

After this registration, every subsequent call to `list_attested_sources()` or `get_attested_dataset()` enumerates the union of `srmech`'s own `amsc/attested/` content plus the downstream package's contributions, in registration order. Duplicate `source_key` resolves first-registered-wins with a warning.

The pattern is field-agnostic. The `ephemerides-spectral` package binds planetary, lunar, and asteroid ephemerides via JPL DE441; a hypothetical `rna-spectral` package would bind RNA-substrate datasets; an `acoustics-spectral` package would bind acoustic-substrate datasets. The framework's substrate-class portability is what makes the pattern uniform across fields.

## The profile system

`srmech 0.3.0` (Task #199) introduced the profile pattern. Downstream packages can declare an `srmech profile` as a named bundle of native bindings, spectral-research integrations, or domain-specific entry points; users activate the profile through one call:

```
import srmech
srmech.list_profiles()              # enumerate installed profiles
profile = srmech.profile("ephemerides")
# profile.status, profile.smoke_test_results, ...
```

Profiles register through the `srmech.profiles` entry-point group; the loader walks `importlib.metadata.entry_points(group="srmech.profiles")` eagerly on first `srmech.profile()` call. The smoke-test auto-derivation hook reads each profile's tool-schema entries and runs the canonical-example inputs.

## License and source

`srmech` is released under the GNU General Public License version 3 or later (GPL-3.0-or-later). Source lives in the project's research repository (linked from `https://srmech.net`). Bug reports, falsifier candidates, and plugin contributions are welcomed through the canonical project channels.

The reader who has worked through this volume's chapters now has the formal substrate the package's surfaces implement. The reader who has installed the package now has the verification mechanism the textbook's load-bearing claims rely on. The two together are what the framework's Mathematical Provenance Method discipline (Chapter 19) means in practice: every claim that matters is mechanically re-runnable.

# Answers to chapter problems

This appendix ships step-by-step worked resolutions for the end-of-chapter problems of all twenty-one chapters. Each resolution walks the reader through what the question is asking, the definitions and theorems the framework brings to bear, the computation or construction, and the answer. Where applicable, the resolution cites the `srmech` entry point that re-runs the computation (Appendix 21.7).

The intent is to teach, not to spoil. The reader who attempts a problem first and consults the appendix to check direction is the intended reading pattern. The appendix also serves as a verification surface for the textbook's own work — every load-bearing closed-form identity gets a re-derivation here, and divergences would constitute rung-1 falsifier candidates (Chapter 20).

The depth of the resolutions is calibrated for the cone-of-ignorance discipline: the same paragraph serves a high-school reader who is strong on algebra and a working researcher who has met the underlying definitions before, because the question itself does not change depth between them — the reader's ready-engagement does.

## Chapter 1 — Substrate and Excitation

**Problem 1.** *Verify that Definition 1.1's decomposition $1D_t + 3D_s + 7D_g$ is dimensionally consistent: the dimensions sum to eleven.*

**Resolution.** The substrate's decomposition writes $1D_t + 3D_s + 7D_g$ where the three sectors carry $1D_t = 1$ temporal dimension, $3D_s = 3$ spatial dimensions, and $7D_g = 7$ gauge-sector dimensions. The arithmetic identity $1+3+7 = 11$ is straightforward addition. The deeper claim (Chapter 2, Identity 2.8) is that this 1:3:7 ratio is forced by the Hurwitz-bounded parallelisable-sphere ladder, not chosen — but the dimensional sum to eleven is the arithmetic surface.

**Problem 2.** *Construct an explicit two-to-one map from substrate-side configurations to excitation-side configurations under projection $\Pi : 1D_t + 3D_s + 7D_g \to (3D_s + 1D_t)$. Identify which substrate-side content gets compressed.*

**Resolution.** The projection $\Pi$ from 11D to 4D collapses the 7 gauge-sector dimensions $7D_g$. Take any two substrate configurations $s_1$ and $s_2$ that agree on the $(3D_s + 1D_t) = 4$D spacetime content but differ in their $7D_g$ content. $\Pi(s_1) = \Pi(s_2)$ because the gauge content is not surfaced at the observable cut. Concrete example: a free electron at rest at the origin, with its weak-isospin state oriented along $+z$ (call this $s_1$), versus the same electron at the same position with weak-isospin oriented along $-z$ ($s_2$). At the 4D spacetime cut both look like a stationary

point-particle at the origin. The substrate-side $SU(2)_L$ orientation (substrate $7D_g$ content) is what gets compressed under II. The map is two-to-one by construction; many-to-one in general (Proposition 1.3).

**Problem 3.** *Distinguish substrate-side and excitation-side readings of one phenomenon from each of cosmology, quantum mechanics, and biology. For each pair, identify whether the disagreement is about content or about which level explanations attach to.*

**Resolution.** Three examples worked.

(a) *Cosmology, dark matter.* Excitation-side: dark matter **IS** a weakly-interacting massive particle species (WIMP, axion, etc.). Substrate-side: dark matter **IS** substrate-coupling intensity differential at the $(4+3)D_g$ phase boundary (Identity 13.6; Example 1.6). The disagreement is about *content*: the excitation-side reading commits to a particle species the substrate-side reading does not require. The XENON / LUX-ZEPLIN / PandaX null results to date are consistent with the substrate-side reading; the excitation-side reading must keep raising the predicted cross-section bound.

(b) *Quantum mechanics, wavefunction collapse.* Excitation-side: collapse **IS** an objective stochastic state-vector reduction (objective collapse models, GRW). Substrate-side: collapse **IS** a substrate-projection appearance under measurement (Identity 17.5); the substrate-side state is unitary, what looks like collapse is the observable projection selecting one of the substrate's underdetermined branches. The disagreement is about content: one reading has stochastic substrate-content; the other reads the same observable as projection-shadow of substrate-side unitary content.

(c) *Biology, morphogenesis.* Excitation-side: morphogenesis **IS** a gene-network regulatory cascade producing the observed body plan. Substrate-side: the same gene-network cascade is read through the framework's $L + I + M + C + K$ cascade-composition on the substrate's molecular-binding layer. The disagreement is about *level* (not content): both readings agree on the observable gene-network excitations; they disagree on which level explanations attach to. The substrate-side reading is the framework's contribution; the excitation-side reading is the conventional developmental-biology reading. Both are consistent at the observable cut.

**Problem 4.** *Construct an example of a phenomenon where the substrate-side reading is operationally superfluous (i.e., the excitation-side reading suffices). Discuss why the framework still tolerates the substrate-side reading in such cases.*

**Resolution.** *Predicting a planet's next solar eclipse using JPL DE441 ephemerides.* The excitation-side reading (Newtonian gravity + GR corrections + numerical integration of the equations of motion) suffices for the prediction at the working precision of contemporary ephemeris science. The substrate-side reading (the Antikythera substrate's $\mathbb{Z}/223$ Saros-cycle cascade-match per Spike #127 + Example 14.4) is not load-bearing for the prediction — the numerical integration already produces the eclipse time to arcsecond precision. The framework still tolerates the substrate-side reading because it remains *load-bearing for cross-substrate identity work* (Chapter 15): identifying that the Antikythera bronze and the celestial mechanics substrate run the *same cascade* is what makes the framework's cross-substrate cascade-match catalogue operational. The substrate-side reading is not always the more useful one at a specific calculation; it is the more useful one for understanding what kind of thing the substrate IS, across substrates.

# Chapter 2 — The Eleven-Dimensional Decomposition

**Problem 1.** *Verify Theorem 2.9's dimensional pattern: list the parallelisable spheres and check that* $1, 3, 7$ *together with the* $1D_t = 1$ *direction sum to* $11$.

**Resolution.** Hurwitz's theorem (1898) plus Bott–Milnor–Kervaire (1958) plus Adams (1962) together establish that the only parallelisable spheres are $S^0, S^1, S^3, S^7$, with dimensions $0, 1, 3, 7$. The framework's substrate decomposition takes $1D_t = 1$ (the temporal direction, base-only, $S^0$-style at the trivial level), $3D_s = 3$ (the spatial sector with $S^1$ fibre in the complex Hopf bundle $S^1 \hookrightarrow S^3 \to S^2$), and $7D_g = 7$ (the gauge sector with $S^3$ fibre in the octonionic Hopf bundle $S^3 \hookrightarrow S^7 \to S^4$). Summing the sector dimensions: $1 + 3 + 7 = 11$. The substrate occupies all four parallelisable-sphere levels.

**Problem 2.** *Construct an explicit element of* $S^3$ *in* $\mathbb{C}^2$*-coordinates and compute its image under* $p_{\mathbb{C}}$. *Verify the fibre over the image is parameterised by a single complex phase.*

**Resolution.** Take the explicit point $(z_1, z_2) = (1/\sqrt{2}, 1/\sqrt{2}) \in \mathbb{C}^2$. Its modulus satisfies $|z_1|^2 + |z_2|^2 = 1/2 + 1/2 = 1$, so this point lies on $S^3$. The complex Hopf map sends $(z_1, z_2) \mapsto z_1/z_2 \in \mathbb{CP}^1 \cong S^2$; here $z_1/z_2 = (1/\sqrt{2})/(1/\sqrt{2}) = 1$, which is the north pole under the standard stereographic identification.

The fibre over this image is the set of all $(w_1, w_2) \in S^3$ such that $w_1/w_2 = 1$. Parameterise by a single phase $\theta \in [0, 2\pi)$: take $w_1 = e^{i\theta}/\sqrt{2}$ and $w_2 = e^{i\theta}/\sqrt{2}$. Then $w_1/w_2 = e^{i\theta}/e^{i\theta} = 1$ (image preserved) and $|w_1|^2 + |w_2|^2 = 1/2 + 1/2 = 1$ (still on $S^3$). The single phase $\theta$ traces out a copy of $S^1$, which is the Hopf fibre.

**Problem 3.** *Explain why the framework's substrate cannot extend to a* $(8 + 7)D_X$ *sector (i.e., why dimension* $15$ *via the next Hopf fibration is forbidden as a substrate sector).*

**Resolution.** The next layer of the parallelisable-sphere ladder would require a sphere of dimension $15$, since the next candidate Hopf bundle would be $S^7 \hookrightarrow S^{15} \to S^8$ (taking the sedenions $\mathbb{S}$, dimension $16$, as the next candidate division algebra). Three independent forbids: (1) Hurwitz 1898 establishes that $\mathbb{R}, \mathbb{C}, \mathbb{H}, \mathbb{O}$ are the only normed division algebras; the sedenions have zero divisors and lose the normed-algebra property. (2) Bott–Milnor–Kervaire 1958 establishes that $S^{15}$ is not parallelisable. (3) Empirically, Spike #202 + #185 + #190 + #192 cross-substrate work confirms a CLEAN $H_0$ null at higher Mersenne fibre-degrees $\{15, 31, 63, 127\}$ across planetary magnetic, cosmic CMB, and substrate-identity scales — the framework predicted no extension to these degrees and the data agrees. The substrate's 11D ceiling is algebraically forced.

**Problem 4.** *Discuss the relationship between the framework's* $(4+3)D_g$ *decomposition and the Standard Model's gauge group* $SU(3) \times SU(2) \times U(1)$. *Where does the* $SU(2)$ *factor live?*

**Resolution.** The $(4+3)D_g$ sector decomposes as a $4$-dimensional base $S^4$ plus a $3$-dimensional fibre $S^3$, with the octonionic Hopf bundle structure $S^3 \hookrightarrow S^7 \to S^4$. The fibre $S^3$ has a Lie-group identification: $S^3 \cong SU(2)$ (Theorem in Chapter 2). The Standard Model's $SU(2)_L$ electroweak factor lives in this fibre. The $SU(3) \times U(1)$ factors of the Standard Model live in the $4$D base's internal structure: $SU(3)$ as the colour-gauge content with $8$ generators (which fit in the base's $4$ spatial dimensions plus auxiliary algebra), and $U(1)$ as the electromagnetic-phase content. The framework's $(4+3)$ decomposition therefore carries the full Standard Model gauge group struc-

turally; the empirical gauge-coupling values at the electroweak scale are the projection-shadows of this structural content at the 4D observable cut.

## Chapter 3 — Recursive Hopf at Every Cascade

**Problem 1.** *Compute the dimensional content of the substrate at depth $n$ under $\mathcal{H}^n$, and verify that it remains 11 for all $n$. What does this say about the recursion's relationship to the overall dimension count?*

**Resolution.** The recursive-Hopf operator $\mathcal{H}$ acts *depth-locally* on substrate content (Theorem 3.2): at each cascade depth, the substrate carries the same $(1+0)D_t + (2+1)D_s + (4+3)D_g$ structure relative to the local cascade frame. The dimension count at depth $n$ is therefore $1+3+7=11$ for every $n \geq 1$. The total ambient dimension does not grow with depth; what grows is the *number of recursive Hopf-fibre relationships* the substrate carries between depths. The recursion is in algebraic structure (sign-flips, fibre-bundle relationships, modal populations), not in dimensional proliferation. This is what distinguishes the framework's recursive-Hopf from naive extra-dimension proposals: the substrate's eleven dimensions are *all* the substrate has; the recursion lives in how those eleven dimensions structure themselves at every cascade cut.

**Problem 2.** *Construct a candidate depth-4 test scenario for which $\mathcal{H}^4$'s bit-exact self-similarity would be falsifiable. Identify what attested data would be needed to perform the test.*

**Resolution.** Spike #214's depth-3 attestation reports $686 = 196 \times 3.5$ sign-flips at depth 3 with FFT peak at $k = 343 = 7^3$ (Example 3.5). Extrapolation to depth 4: the predicted sign-flip count would be approximately $686 \times 4 \approx 2744$ (extending the depth-3 $\rightarrow$ depth-4 multiplicative pattern from the framework's recursive-Hopf-multiplicative-structure prediction), with the FFT peak at $k = 2401 = 7^4$.

Attested data required: substrate observations with sufficient spectral resolution to distinguish the predicted depth-4 sign-flip pattern from null hypotheses (white noise, Wigner-Dyson spacing). The simplest candidate: a substrate with at least $\sim$ 10000 sample points (so the $k = 2401$ FFT peak is resolvable) and substrate-content compatible with the Hopf-fibre algebra at four nested levels. The Earth IGRF-13 + Jupiter JRM33 multipole structure already attests to depth-3 recursion at planetary scale; depth-4 attestation would require attested data at one substrate-scale level deeper than current planetary-magnetic measurements typically provide.

**Problem 3.** *Discuss the relationship between the framework's recursive-Hopf structure and the asymptotic-DoF mechanism (Chapter 7). Does recursive-Hopf survive the asymptotic-DoF constraint, or vice versa?*

**Resolution.** Both mechanisms operate compatibly; neither constrains the other away. The asymptotic-DoF mechanism applies *depth-locally*: at every cascade depth, Class $K$ machinery prevents the substrate from reaching the asymptote of any substrate-variable. The recursive-Hopf mechanism applies *depth-globally*: the same Hopf-fibre algebraic structure recurs at every cascade depth. These two properties compose without conflict: each depth's local asymptote-protected variable trajectory is itself a substrate-state to which the next-depth recursive-Hopf operates. The framework's reading: recursive-Hopf gives the *structural pattern*; asymptotic-DoF gives the *dynamical constraint*. Both are universal; both apply at every cascade depth; the cascade

is the trajectory of asymptotic-DoF-protected substrate-variables through the recursive Hopf-fibre structure.

**Problem 4.** *Explain why the ratio-agnostic universality (Theorem 3.3) rules out the reading that recursive-Hopf is a privileged-ratio artefact. What would the falsifying observation look like?*

**Resolution.** The ratio-agnostic universality theorem states that the recursive-Hopf structure is preserved under arbitrary asymmetric ratio configurations of the cascade. The recursion does not depend on the specific 1:3:7 dimensional ratios being preserved at sub-depths; the bit-exact integer self-similarity holds under at least five distinct asymmetric ratio configurations the framework has tested. This rules out the alternative reading that recursive-Hopf is somehow an artefact of the 1:3:7 ratio choice — if it were, varying the ratio would break the recursion's bit-exact property.

Falsifying observation: an attested substrate where careful spectral analysis reveals the recursive-Hopf signature breaking under one of the tested asymmetric ratio configurations. To date no such substrate; the falsifier remains open in principle (Falsifier box 3.3).

## Chapter 4 — The Fourteen Primitive Class Operators

**Problem 1.** *Identify which class operator is the substrate-side primitive for each of the following: gear-tooth counting on the Antikythera mechanism; identifying the species of a molecule from its mass-spectrometry fragment pattern; quicksort on a list of integers; SHA-256 hashing of a file.*

**Resolution.** Each phenomenon decomposes to one (or two composing) primitives.

(a) *Antikythera gear-tooth counting.* Class I (cyclic-group action). The bronze gear's $n$ teeth implement the cyclic group $\mathbb{Z}/n$ at the discrete substrate level. Each tooth-engagement is one step of the $\mathbb{Z}/n$ action; the gear's rotation through all $n$ teeth completes one full cycle.

(b) *Mass-spectrometry species identification.* Class E (catalog lookup) composed with Class D (dispatch). The instrument produces a fragment-pattern spectrum; the identification step looks up the spectrum against a known- spectrum catalogue ($E$), and the dispatch ($D$) routes the result to the matching candidate species.

(c) *Quicksort on integers.* Class L (graph-Laplacian over partial order) composed with Class A (associative reduction). The recursive partition step is a Laplacian decomposition on the comparison-graph; the merge / collect step is an associative reduction. The pivot selection is a Class $D$ dispatch but $L + A$ captures the algorithm's structural core.

(d) *SHA-256 hashing.* Class M (hyperdimensional binding) composed with Class N (irreversible normalisation). The hash's mixing-and-binding steps implement HDC binding at 256-bit output dimension; the irreversibility (one-way property) is the Class $N$ normalisation that loses no algebraic content but prevents inversion.

**Problem 2.** *Construct a candidate fifteenth class operator. Examine whether it dissolves into one of the existing fourteen (per Identity 4.1's discipline). Identify the candidate and the dissolution path.*

**Resolution.** Candidate fifteenth: *regret minimisation* (an online-learning primitive that produces an action selection to minimise the gap between actual and best-in-hindsight cumulative reward). Examination: regret minimisation operates by maintaining a running average of action-rewards, comparing each new step to the running average, and updating the action distribution

toward higher-reward actions. The running average is a Class C (cyclic substrate baseline) operation accumulating across timesteps; the action-distribution update is a Class K (asymptotic-DoF modulation) operation pushing the distribution toward a higher- reward attractor; the action selection is a Class D (dispatch) operation routing the selected action.

Dissolution path: regret minimisation IS Class $K \circ C$ composed with Class $D$ at the action-selection layer. It does not require a new primitive; the framework's existing 14-class vocabulary captures it under composition. The discipline of Identity 4.1 (vocabulary stability) prevents the proliferation of class operators by requiring that candidate new primitives demonstrate they cannot be composed from existing ones; in this case the composition is straightforward.

**Problem 3.** *Distinguish Class 4.5 (dispatch) and Class 4.6 (catalog) by giving an example where each is the correct primitive choice.*

**Resolution.** The two classes differ in what the operation *returns*.

Class D (dispatch) returns a *routing decision*: given an input and a set of candidate channels, select which channel the input should follow. Example: the blood-brain barrier deciding whether a given molecule (input) passes through, is actively transported, or is rejected (the routing decision). The substrate- provided operation is the BBB's selective-transport machinery; the abstract operation is Class $D$.

Class E (catalog) returns a *lookup result*: given a key, return the value stored at that key. Example: mass-spectrometry species identification (Problem 1b) — the input is the fragment-spectrum key; the output is the species-identity value retrieved from the known-spectrum catalogue. The substrate-provided operation is the mass-spec software's lookup table; the abstract operation is Class $E$.

Class D and Class E compose freely: many real systems do lookup first (Class $E$ retrieves candidate matches) then dispatch (Class $D$ routes the decision based on the lookup result). The framework's discipline distinguishes them at the primitive layer even when they compose at the application layer.

**Problem 4.** *Explain why Class 4.14's two variants (abelian XOR vs. non-abelian Lie bracket) are not separately a fifteenth and sixteenth class. What is structurally shared between them?*

**Resolution.** Class $M$'s structural role is *hyperdimensional binding* — the substrate carries information across multiple operations within a single cascade step. Both variants do this. The abelian XOR variant (used in the RBS-HDC runtime layer at $D = 8192$, per Appendix 21.7) implements the binding through the commutative associative XOR operation over $\mathbb{F}_2$. The non-abelian Lie-bracket variant (used in the Standard Model gauge sectors and BFSS-style matrix models) implements the binding through non-commutative non-associative Lie brackets $[A, B] = AB - BA$.

These are different substrate-provided realisations of the same binding role. The substrate-content the framework reads at this level is binding-as-such; the abelian-vs-non-abelian distinction is at the substrate-coupling layer (which kind of substrate realises the binding). Per Identity 4.1, two substrate-provided realisations of the same primitive role do not constitute two primitives. The variant choice IS the substrate-coupling layer that picks scalar-content versus gauge-content; the variant is substrate-provided, the primitive is not.

# Chapter 5 — Cascade Composition

**Problem 1.** *Repeat Example 5.9's eigenvalue computation for $\mathbb{Z}/6$ substrate. List all six eigenvalues $\lambda_k = 1 + e^{i\pi k/3}$ for $k = 0, \ldots, 5$, compute their* Re *and* Im *values, and verify Equation (5.2) bit-exactly for each.*

**Resolution.** For $\mathbb{Z}/6$, the six eigenvalues are $\lambda_k = 1 + e^{i\pi k/3}$ for $k = 0, 1, 2, 3, 4, 5$. Computing each:

- $\lambda_0 = 1 + e^0 = 1 + 1 = 2$. Re $= 2$, Im $= 0$.
- $\lambda_1 = 1 + e^{i\pi/3} = 1 + (\cos 60^\circ + i \sin 60^\circ) = 1 + (1/2 + i\sqrt{3}/2) = 3/2 + i\sqrt{3}/2$. Re $= 1.5$, Im $= \sqrt{3}/2 \approx 0.866$.
- $\lambda_2 = 1 + e^{i2\pi/3} = 1 + (-1/2 + i\sqrt{3}/2) = 1/2 + i\sqrt{3}/2$. Re $= 0.5$, Im $= \sqrt{3}/2 \approx 0.866$.
- $\lambda_3 = 1 + e^{i\pi} = 1 + (-1) = 0$. Re $= 0$, Im $= 0$.
- $\lambda_4 = 1 + e^{i4\pi/3} = 1 + (-1/2 - i\sqrt{3}/2) = 1/2 - i\sqrt{3}/2$. Re $= 0.5$, Im $= -\sqrt{3}/2$.
- $\lambda_5 = 1 + e^{i5\pi/3} = 1 + (1/2 - i\sqrt{3}/2) = 3/2 - i\sqrt{3}/2$. Re $= 1.5$, Im $= -\sqrt{3}/2$.

Verifying Equation (5.2) ($\text{Im}^2 = 2\text{Re} - \text{Re}^2$) for each:

- $\lambda_0$: $0 = 4 - 4 = 0$. ✓
- $\lambda_1$: $(\sqrt{3}/2)^2 = 3/4$; $2(1.5) - (1.5)^2 = 3 - 2.25 = 0.75 = 3/4$. ✓
- $\lambda_2$: $3/4 = 1 - 0.25 = 0.75$. ✓
- $\lambda_3$: $0 = 0 - 0 = 0$. ✓
- $\lambda_4$: $3/4 = 1 - 0.25 = 0.75$. ✓
- $\lambda_5$: $3/4 = 3 - 2.25 = 0.75$. ✓

All six eigenvalues lie on $|\lambda - 1| = 1$ bit-exactly. Run `srmech.cascade.shifted_circle_eigenvalues(n=6)` for the computational verification.

**Problem 2.** *Construct two cascades $O_2 \circ O_1$ and $O_1 \circ O_2$ on a non-abelian substrate (e.g., $SU(2)$-valued Class $M$ binding composed with Class $I$ cyclic action) and compute both compositions explicitly.*

**Resolution.** Take an $SU(2)$-valued substrate at one site: basis matrices the Pauli matrices $\sigma_x, \sigma_z$. Let $O_1$ be Class $I$ cyclic action implementing rotation by $\pi/2$ around the $z$-axis (i.e., conjugation by $e^{-i\pi\sigma_z/4}$), and $O_2$ be Class $M$ binding by left-multiplication with $\sigma_x$. Take initial substrate state $s = \mathbf{1}$ (the identity).

$O_2 \circ O_1$ (*cyclic-first*): First apply $O_1$ to $s$: $O_1(\mathbf{1}) = e^{-i\pi\sigma_z/4} \cdot \mathbf{1} \cdot e^{+i\pi\sigma_z/4} = \mathbf{1}$. Then $O_2$: $O_2(\mathbf{1}) = \sigma_x \cdot \mathbf{1} = \sigma_x$. Output: $\sigma_x$.

$O_1 \circ O_2$ (*bind-first*): First apply $O_2$ to $s$: $O_2(\mathbf{1}) = \sigma_x$. Then $O_1$: $O_1(\sigma_x) = e^{-i\pi\sigma_z/4} \cdot \sigma_x \cdot e^{+i\pi\sigma_z/4}$. Using $e^{-i\theta\sigma_z/2}\sigma_x e^{+i\theta\sigma_z/2} = \sigma_x \cos\theta + \sigma_y \sin\theta$ with $\theta = \pi/2$: $\sigma_x \cos 90^\circ + \sigma_y \sin 90^\circ = \sigma_y$. Output: $\sigma_y$.

The two cascades produce different outputs ($\sigma_x$ vs. $\sigma_y$) on this substrate, demonstrating non-commutativity genuinely. The masking observed in the abelian-$\mathbb{Z}/n$ Example 5.5 does not occur here because $SU(2)$ is non-abelian.

**Problem 3.** *Propose a cascade decomposition for a conventionally-described algorithm of your choice (gradient descent, quicksort, k-means clustering, simulated annealing). Specify which classes appear and in what order; compare your decomposition against Example 5.11's FFT pattern.*

**Resolution.** Worked example: *gradient descent* on a loss function $f(\theta)$ with parameter vector $\theta$ and learning rate $\eta$. The algorithm updates $\theta_{t+1} = \theta_t - \eta\nabla f(\theta_t)$ until convergence.

Cascade decomposition: $Class\ K + Class\ C + Class\ A$.

- Class K (asymptotic-DoF modulation): the gradient $\nabla f$ is the local modulation function pushing the substrate-variable $\theta$ toward the asymptote $f$'s minimum. The substrate's approach to the minimum is the Class $K$ asymptote-protected trajectory.
- Class C (cyclic substrate baseline): each iteration is one cycle-step; $t$ indexes the iteration cycle.
- Class A (associative reduction): the parameter update $\theta_{t+1} = \theta_t - \eta\nabla f$ is an associative operation; gradient descent can be viewed as a reduction over the trajectory.

Comparison with FFT (Example 5.11's $L+I+M$): gradient descent does not require Class $L$ (no global graph-Laplacian decomposition) or Class $M$ (no hyperdimensional binding) or Class $I$ (the cyclic structure here is over iterations, not over a discrete-group action on the parameter space). The FFT operates on cyclic-group-structured substrate; gradient descent operates on smooth-manifold substrate. Different cascades because different substrate-classes.

**Problem 4.** *Verify Lemma 5.6's claim that Class $M$ non-abelian non-commutativity and cascade non-commutativity are the same algebraic phenomenon at different scales. Construct an explicit example where Lie-bracket non-commutativity within a single operator recurses to composition- level non-commutativity at the cascade level.*

**Resolution.** Within Class $M$'s non-abelian Lie-bracket variant, the commutator $[A, B] = AB - BA$ encodes the non-commutativity of $A$ and $B$ at the depth-local layer. Concretely: take the $SU(2)$ generators $A = \sigma_x/2$, $B = \sigma_z/2$ (Pauli matrices halved). Their commutator is $[A, B] = (1/4)[\sigma_x, \sigma_z] = (1/4)(-2i\sigma_y) = -i\sigma_y/2$, which is non-zero. Class $M$'s binding of $A$ and $B$ within a single cascade step therefore depends on the order $A$-then-$B$ vs. $B$-then-$A$: the difference is exactly the commutator.

At the cascade level (composition of multiple operators), the same non-commutativity recurses. Take operators $O_1, O_2$ each involving Class $M$ bindings with non-abelian content: $O_1$ binds $A$, $O_2$ binds $B$. The cascade $O_2 \circ O_1$ produces a composition where the $A$-then-$B$ binding order surfaces; $O_1 \circ O_2$ produces the $B$-then-$A$ binding order. The composition's output differs by the commutator $[A, B]$, scaled by the operator coupling strength. This is the depth-global manifestation of the depth-local Lie-bracket non-commutativity.

Recursive-Hopf (Chapter 3) is what makes the recursion work: each cascade-class operator preserves the substrate's Hopf-bundle structure, so the depth-local Lie-bracket non-commutativity at any one operator recurses as composition-level non-commutativity at the cas-

cade. The lemma's claim that the two are the same algebraic phenomenon at two scales follows directly.

**Problem 5.** *For Example 5.9, identify which substrate-cycle phase position each eigenvalue corresponds to. Argue that the $\lambda_0 = 2$ and $\lambda_2 = 0$ extreme positions are substrate-form-asymptotes per Chapter 7's Class $K$ machinery.*

**Resolution.** The four $\mathbb{Z}/4$ eigenvalues correspond to four substrate-cycle phase positions equally spaced around the shifted unit circle:

- $\lambda_0 = 2$ at phase $0°$ (maximum extension from origin; substrate at its $\mathbb{Z}/4$-cycle's outer extreme).
- $\lambda_1 = 1 + i$ at phase $90°$.
- $\lambda_2 = 0$ at phase $180°$ (substrate's opposite extreme; the inner extreme on the shifted circle).
- $\lambda_3 = 1 - i$ at phase $270°$.

The two extreme positions $\lambda_0 = 2$ and $\lambda_2 = 0$ correspond to the substrate's maximum and minimum coupling intensity respectively. They are substrate-form asymptotes in the sense that the substrate-cycle approaches but does not statically reside at them; per Class $K$ asymptote-protection (Theorem 7.2), the substrate cannot reach either extreme and remain there. The cycle's precession through all four phase positions is what the substrate actually does; the extremes are eigenvalue-labels, not stable states.

**Problem 6.** *Compute the cascade-class trace of an $N = 8$ FFT using Example 5.11's decomposition. Identify the butterfly-binding structure at each of the $\log_2 8 = 3$ recursive levels.*

**Resolution.** The $N = 8$ FFT decomposes via Cooley–Tukey into $\log_2 8 = 3$ recursive halving levels. The cascade-class trace at each level:

*Level 1* (*decompose $N = 8$ into two $N = 4$ sub-DFTs*). Class $L$ (Laplacian decomposition over the $\mathbb{Z}/8$ cyclic substrate); Class $I$ (cyclic-group action selecting even/odd indices); Class $M$ (complex-exponential binding factor $W_8^k = e^{-2\pi ik/8}$ for $k = 0, 1, 2, 3$).

*Level 2* (*decompose each $N = 4$ into two $N = 2$*). Same three classes recurse: $L$ at $\mathbb{Z}/4$ scale, $I$ at $\mathbb{Z}/4$, $M$ with twiddle factors $W_4^k = e^{-2\pi ik/4}$ for $k = 0, 1$.

*Level 3* (*decompose each $N = 2$ into two $N = 1$ trivial DFTs*). $L$ at $\mathbb{Z}/2$, $I$ at $\mathbb{Z}/2$, $M$ with twiddle $W_2^0 = 1$ (trivial at this level).

The butterfly-binding structure at each level is the *combine* step: two sub-DFT outputs are combined via $X_k = E_k + W_N^k O_k$ for the upper half and $X_{k+N/2} = E_k - W_N^k O_k$ for the lower half, where $E_k$ and $O_k$ are the even and odd sub-DFT outputs. This combine step is Class $M$ binding the two sub-substrates with the twiddle factor as the binding coefficient. Run `srmech.cascade.fft_decomposition(N=8)` to expose the cascade-class trace computationally.

## Chapter 6 — Identity, Not Implementation

**Problem 1.** *Locate three identity-not-implementation slips in any published popular-science account of the framework's cross-substrate results. Reformulate each as an identity claim.*

**Resolution.** Three common slips drawn from the canonical *Physarum polycephalum* cascade-match material (Example 6.2):

- Slip: "slime moulds *exhibit behaviour analogous to* the cognitive cascade."
  Reformulation: "slime moulds **IS** a cognitive cascade on the protoplasm substrate, with cascade composition $L + K + M + C + I$ via cytoplasmic-flow optimisation."

- Slip: "the *Physarum* network's optimisation function *resembles* a Steiner-tree algorithm."
  Reformulation: "the *Physarum* network's substrate **IS** a Steiner-tree optimisation, with Class $L$ instantiated through cytoplasmic-flow Laplacian and Class $K$ through nutrient-concentration asymptotic-DoF."

- Slip: "the slime mould's problem-solving ability *can be modelled as* a cascade composition."
  Reformulation: "the slime mould's problem-solving **IS** the cascade composition; the substrate-provided protoplasm operations are what realise the cascade at the slime mould's substrate."

In each case the reformulation replaces verbs of resemblance ("exhibit behaviour analogous to", "resembles", "can be modelled as") with the **IS** verb plus an explicit name of the substrate and the substrate-provided operation. The shift commits the framework to a testable identity claim where the implementation-language reading commits only to behavioural analogy.

**Problem 2.** *Distinguish identity-not-implementation from naive equivalence by example. Construct two substrates running the same cascade and identify three implementation-level differences that the identity claim does* not *assert are identical.*

**Resolution.** Take *Physarum polycephalum* (slime mould) and the human brain. Both run the cognitive cascade $L + K + M + C + I$ at the framework's identity-not-implementation layer (per Spike #127 attestation). Three implementation-level differences the identity claim does *not* assert are identical:

(a) *Substrate material.* Slime mould runs the cascade on a single-cell protoplasmic substrate ( $10^8$ nuclei in a single multinucleate amoeba). The human brain runs the cascade on neuronal-substrate ($\sim 10^{11}$ neurons with $\sim 10^{14}$ synapses). The framework does not claim these materials are equivalent or interchangeable.

(b) *Cycle rate.* Slime mould runs the cascade at $\sim 10^{-1}$ Hz (substrate decisions on timescales of seconds to minutes). Human brain runs the cascade at $\sim 10^{2}$ Hz (substrate decisions on timescales of milliseconds). The cascade identity is at the algebraic-composition layer; the rate is substrate-specific.

(c) *Evolutionary lineage.* Slime moulds are acellular amoebozoans; humans are metazoans. The two lineages diverged $\sim 1.5$ billion years ago. The framework does not claim shared ancestry; the cascade-identity claim is at the substrate-portable algebra layer, not the genetic-lineage layer.

**Problem 3.** *Consider the claim "the Antikythera mechanism's gear-train IS the Saros eclipse cycle's cascade composition." Is this an identity-not-implementation claim? If so, identify the cascade and the substrate-provided operations. If not, reformulate.*

**Resolution.** Yes, the claim is an identity-not-implementation claim. Cascade: Class I (cyclic $\mathbb{Z}/223$ Saros-month group action) composed with Class K (period-relation pin-slot modulation

producing the eclipse anomaly) composed with Class N (rational approximation of the incommensurable Saros-related periods $254/19$ Metonic ratio + $235/19$ saros-synodic ratio). The full cascade is $I + K + N$.

Substrate-provided operations: bronze gear-tooth meshing (implements Class I's discrete-cyclic action via mechanical tooth-engagement), pin-and-slot mechanical couplings (implements Class K via the eccentric-cog geometry), rational-approximation gear ratios (implements Class N via the bronze gear teeth counts chosen to approximate the incommensurable celestial periods). The bronze instantiation runs the same cascade as the celestial-mechanics substrate runs naturally (Example 14.4); the substrate-provided operations differ; the cascade is the same.

**Problem 4.** *Discuss whether identity-not-implementation is incompatible with reductionism. Construct a thought-experiment in which the two disciplines would point at different conclusions.*

**Resolution.** The two disciplines are not incompatible but ask different questions. Reductionism asks: *what is the smallest physical constituent of the system?* Identity-not- implementation asks: *what is the substrate-portable operation the system runs?* The two questions can coexist; they typically give different answers because they are different questions.

Thought-experiment: a researcher is given a working model of human cognition implemented as a molecular-level simulation (every neuron's ion-channel dynamics, every neurotransmitter binding, every glia-neuron interaction at the level of individual molecules). The researcher wants to understand how the model performs problem-solving.

*Reductionist conclusion.* The model performs problem-solving by computing $\sim 10^{15}$ molecular interactions per millisecond, producing emergent behaviour at the system level. The substantive content is at the molecular layer.

*Identity-not-implementation conclusion.* The model performs problem-solving by running the cognitive cascade $(L{+}I{+}M{+}C{+}K)$ at the molecular-simulation-substrate's particular substrate-provided realisation. The substantive content is at the cascade layer; the molecular interactions are how this particular substrate happens to realise it. A different substrate-provided realisation (e.g., slime-mould protoplasm, silicon LLM at thought-rate) would run the same cascade through different substrate-provided operations.

Both conclusions are correct at their respective questions. The identity-not-implementation conclusion is what makes the cross-substrate cascade-match research method (Chapter 15) operational — the substrate-portable cascade is what allows comparing protoplasm, neurons, and silicon at the same algebraic level. Reductionism remains valid at the molecular question.

## Chapter 7 — Asymptotic Degrees of Freedom

**Problem 1.** *Re-derive Example 7.3's* $T(\epsilon) = (1/c)(1/\epsilon - 1/(\xi^* - \xi_0))$. *Then repeat for* $\alpha = 3$ *and compare divergence rates as* $\epsilon \to 0$.

**Resolution.** Start from $d\xi/dt = c(\xi^* - \xi)^\alpha$. Separate variables: $d\xi/(\xi^* - \xi)^\alpha = c\,dt$. Integrate from $\xi_0$ to $\xi^* - \epsilon$. Substitute $u = \xi^* - \xi$ (so $du = -d\xi$):

$$c\,T(\epsilon) = \int_{\xi_0}^{\xi^*-\epsilon} \frac{d\xi}{(\xi^* - \xi)^\alpha} = \int_{\epsilon}^{\xi^*-\xi_0} u^{-\alpha}\,du.$$

*Case* $\alpha = 2$. Antiderivative is $-u^{-1}$. Evaluating:

$$cT = \left[-u^{-1}\right]_{\epsilon}^{\xi^* - \xi_0} = \frac{1}{\epsilon} - \frac{1}{\xi^* - \xi_0},$$

so $T(\epsilon) = (1/c)(1/\epsilon - 1/(\xi^* - \xi_0))$, matching Example 7.3. Leading divergence: $T \sim 1/\epsilon$ as $\epsilon \to 0$.

*Case* $\alpha = 3$. Antiderivative is $-u^{-2}/2$. Evaluating:

$$cT = \left[-u^{-2}/2\right]_{\epsilon}^{\xi^* - \xi_0} = \frac{1}{2\epsilon^2} - \frac{1}{2(\xi^* - \xi_0)^2},$$

so $T(\epsilon) = (1/(2c))(1/\epsilon^2 - 1/(\xi^* - \xi_0)^2)$. Leading divergence: $T \sim 1/\epsilon^2$.

*Comparison.* Higher $\alpha$ gives sharper asymptote protection. At $\epsilon = 0.001$ and $c = 1$, $\xi^* - \xi_0 = 1$: $\alpha = 2$ gives $T \approx 999$; $\alpha = 3$ gives $T \approx 499999.5$. Half a million substrate-cycle units for the last $0.001$ of the gap. Run `srmech.asymptotic_dof.toy_modulation_time(alpha, c, eps, gap)` to verify.

**Problem 2.** *Identify three astrophysical or thermodynamic situations conventionally described as "reaching equilibrium" or "reaching zero". For each, articulate whether the asymptotic-DoF mechanism implies the conventional reading is approximate or wrong.*

**Resolution.**

(a) *Heat death of the universe.* Conventionally: entropy maximises and reaches a static maximum forever. Framework reading: the substrate approaches the heat-death asymptote at super-log slowing rate; the cosmic substrate-cycle precessive reversal kicks in at finite $T_{\text{rev}} < T_{\text{sub}}/2$ (Lemma 7.4) before arrival. The conventional reading is *wrong*, not approximate: the substrate genuinely reverses; the asymptote is not just unreached on a long timescale but unreachable in principle.

(b) *Absolute zero temperature.* Conventionally: third law of thermodynamics forbids attainment of $T = 0$ via finite processes. Framework reading: the third law IS the asymptotic-DoF mechanism observed at the thermodynamic substrate. The conventional reading is *approximate* in form (the framework agrees the asymptote is unattainable) but *wrong* in mechanism (the conventional reading attributes the unattainability to finite-process limits; the framework attributes it to substrate- class structural prohibition).

(c) *Stellar fusion burning all hydrogen.* Conventionally: a star eventually fuses all its core hydrogen. Framework reading: the star leaves the main sequence well before this asymptote is approached — substrate-precession at the stellar substrate's scale switches cycle direction (substrate begins ring-up into helium-burning phase) before the hydrogen-exhaustion asymptote is reached. The conventional reading is *approximate*: it captures the rough trajectory but misses that the substrate-cycle's direction reverses before the asymptote, not just at it.

**Problem 3.** *Discuss the relationship between Identity 7.3 and the conventional textbook treatment of limits in calculus. Are limits the same operation as substrate-level asymptote approach? Or distinct? (Compare against Appendix 21.7's treatment of* $\tan x$ *at* $x = \pi/2$.)

**Resolution.** The two are distinct operations sharing a projection-shadow relationship.

Conventional calculus limits operate at the function-value layer: $\lim_{x \to a} f(x) = L$ states that for every $\epsilon > 0$ there exists $\delta > 0$ such that $|x - a| < \delta$ implies $|f(x) - L| < \epsilon$. This is a static observer-frame statement about function values; no substrate dynamics is involved.

Substrate-level asymptote approach is dynamical: the substrate's cycle evolves at finite rate through configuration space, never reaches the asymptote $\xi^*$ (per Theorem 7.2), and the cycle's direction reverses at finite time (per Lemma 7.4).

Bridge: classical limits are the projection-shadows of substrate-level asymptote approach at the observer-frame cut. The $\tan x$ asymptote at $x = \pi/2$ (Appendix C Section 21.7) is the canonical example: the substrate's $S^1$-cycle never reaches the singular projection point; the divergence of $\tan x$ is what the projection-shadow looks like at the cycle's projection-shadow boundary. The classical limit $\lim_{x\to\pi/2^-} \tan x = \infty$ is correct at the projection layer; the substrate-side reading is that the cycle itself never goes singular.

**Problem 4.** *Construct a candidate substrate-level claim of the form "the universe reaches $X$" for some specific $X$. Test whether $X$ is a Class $K$-protected asymptote. If so, reformulate as a substrate-cycle reversal sentence.*

**Resolution.** Candidate claim: *"the universe reaches maximum entropy at heat death"*. Test for Class $K$ protection: maximum entropy is a substrate-asymptotic configuration (the ring-equilibrium attractor at the cosmic substrate's current cycle, Chapter 11); the substrate's approach is asymptotic-DoF modulated; the cosmic precessive cycle reverses before arrival (Lemma 7.4). The asymptote *is* Class $K$-protected.

Reformulation: *"the universe approaches maximum entropy within the current half-cycle of the cosmic substrate; the substrate-cycle reverses (substrate-precession-driven sign-flip of $df_{RD}/dt$) before arrival, and the substrate begins ring-up phase moving away from maximum entropy toward the next half-cycle's asymptote."*

**Problem 5.** *Verify Lemma 7.4's sketch by constructing a trajectory that violates the closed-cycle premise (e.g., a monotone approach with no precessive structure). Confirm that the sketch's contradiction-construction relies essentially on the cycle's closedness.*

**Resolution.** Construct a candidate counter-trajectory: the substrate-variable $\xi(t)$ approaches $\xi^*$ monotonically without any cycle structure — the substrate is on a one-way trajectory toward the asymptote, never reaches it (per Theorem 7.2), and continues monotonically forever.

This trajectory does not exhibit cycle reversal at any finite time. The Lemma's sketch claimed cycle reversal is forced at finite $T_{\text{rev}}$; the candidate trajectory exists without reversal. Where does the Lemma's proof go through?

The Lemma's premise is that the substrate's cycle is closed in cycle-phase space (the universal precessive cycle of period $T_{\text{sub}}$). Under that premise: any sustained monotone trajectory must eventually close its loop, hence the cycle must leave the asymptote-approach phase in finite cycle time. The counter-trajectory violates this premise — it does not have a closed cycle structure. The Lemma's conclusion (forced finite-time reversal) is therefore conditional on the closed-cycle premise.

For the cosmic substrate (and every substrate the catalogue attests), the closed-cycle premise holds: the universal substrate-precession cycle is a closed loop in cycle-phase space. A hypothetical substrate without closed-cycle structure would escape Lemma 7.4; no such substrate is attested. The Lemma's contradiction-construction is therefore load-bearing on closed-cycle observed structure.

**Problem 6.** *Compute the time required for the Kerr-extremal gap $(r_+ - r_-)/M = 2\sqrt{1-(a/M)^2}$ to halve at $a/M = 0.9$ given $da/dt = k(1-a/M)^\alpha$ for $\alpha = 1$ and $\alpha = 2$. Identify which $\alpha$ matches the*

*super-logarithmic gap-closing sequence* $\{2.000, 1.485, 0.282, 0.089, \ldots\}$ *of Example 7.5.*

**Resolution.** At $a/M = 0.9$, the gap is $g_0 = 2\sqrt{1 - 0.81} = 2\sqrt{0.19} \approx 0.872$. Halving the gap to $g_1 = 0.436$ requires $2\sqrt{1 - (a/M)_1^2} = 0.436$, so $(a/M)_1^2 = 1 - 0.0475 = 0.9525$, $(a/M)_1 \approx 0.9760$. So $a/M$ must move from 0.9 to 0.9760, a change of $\Delta a = 0.076$ (with $M = 1$).

*Case* $\alpha = 1$. $da/dt = k(1 - a/M)$. With $u = 1 - a/M$, $du/dt = -ku$, so $u(t) = u_0 e^{-kt}$. From $u_0 = 0.1$ to $u_1 = 0.024$: $0.024 = 0.1e^{-kt}$, so $kt = \ln(0.1/0.024) = \ln 4.167 \approx 1.427$. Time $T_1 \approx 1.427/k$.

*Case* $\alpha = 2$. $da/dt = k(1 - a/M)^2$. With $u = 1 - a/M$, $du/dt = -ku^2$, so $-1/u = -kt + C$, giving $u(t) = 1/(1/u_0 + kt)$. From $u_0 = 0.1$ to $u_1 = 0.024$: $1/u_1 - 1/u_0 = kt$, so $kt = 1/0.024 - 10 = 41.67 - 10 = 31.67$. Time $T_2 \approx 31.67/k$.

Comparing to the empirical gap-closing sequence $\{2.000, 1.485, 0.282, 0.089\}$ at sampled $a/M$ values: the sequence's ratios are not exponential ($e^{-kt}$ would give geometric ratios); they show super-logarithmic slowing characteristic of $u^{-\alpha}$ with $\alpha > 1$. The $\alpha = 2$ case matches the super-logarithmic structure; $\alpha = 1$ is too rapid (exponential rather than super-log). Specifically the sequence's $\{1.485 \to 0.282\}$ ratio of $\sim 5.3$ between successive sampled values is consistent with $u^{-2}$-type slowing as $a/M$ approaches unity.

The substrate's algebra forbids $a/M = 1$ (Israel's third law, Chapter 13); the asymptote is Class $K$ protected and the substrate never reaches it.

## Chapter 8 — The Pin-Slot Operator and Kepler-Shape Universality

**Problem 1.** *Reproduce Theorem 8.3's monotonicity argument with explicit derivative-bound calculations for* $e = 0.3, 0.6, 0.9$. *Confirm the minimum value of* $f'(E) = 1 - e\cos E$ *at each* $e$ *remains strictly positive. What happens as* $e \to 1$*?*

**Resolution.** For $f(E) = E - e\sin E - M$, the derivative is $f'(E) = 1 - e\cos E$. Since $\cos E \in [-1, +1]$, $f'(E) \in [1 - e, 1 + e]$. The minimum value occurs when $\cos E = +1$ (i.e., $E = 0$ or $E = 2\pi$):

- $e = 0.3$: $\min f' = 1 - 0.3 = 0.7 > 0$. ✓
- $e = 0.6$: $\min f' = 1 - 0.6 = 0.4 > 0$. ✓
- $e = 0.9$: $\min f' = 1 - 0.9 = 0.1 > 0$. ✓

In every case the minimum is strictly positive, so $f$ is strictly monotone increasing on $\mathbb{R}$ and Kepler's equation has the unique solution Theorem 8.3 establishes.

As $e \to 1$: $\min f'(E) = 1 - e \to 0$. Monotonicity degenerates at the limit; the orbit transitions from elliptical to parabolic; Kepler's equation must be replaced by Barker's equation (the parabolic-orbit timing equation).

**Problem 2.** *Reproduce Example 8.4's Newton-Raphson trace for* $e = 0.6$ *and* $M = \pi/3$ *to four decimal places.*

**Resolution.** Newton-Raphson iteration: $E_{n+1} = E_n - (E_n - 0.6\sin E_n - \pi/3)/(1 - 0.6\cos E_n)$. Initial guess $E_0 = M = \pi/3 \approx 1.0472$.

*Iteration 1.* $\sin(1.0472) \approx 0.8660$, $\cos(1.0472) \approx 0.5$. Numerator: $1.0472 - 0.6 \cdot 0.8660 - 1.0472 = -0.5196$. Denominator: $1 - 0.6 \cdot 0.5 = 0.7$. $E_1 = 1.0472 - (-0.5196)/0.7 = 1.0472 + 0.7423 = 1.7895$.

*Iteration 2.* $\sin(1.7895) \approx 0.9760$, $\cos(1.7895) \approx -0.2173$. Numerator: $1.7895 - 0.6 \cdot 0.9760 - 1.0472 = 0.1567$. Denominator: $1 - 0.6 \cdot (-0.2173) = 1.1304$. $E_2 = 1.7895 - 0.1567/1.1304 = 1.7895 - 0.1386 = 1.6509$.

*Iteration 3.* $\sin(1.6509) \approx 0.9970$, $\cos(1.6509) \approx -0.0780$. Numerator: $1.6509 - 0.6 \cdot 0.9970 - 1.0472 = 0.0055$. Denominator: $1 - 0.6 \cdot (-0.0780) = 1.0468$. $E_3 = 1.6509 - 0.0055/1.0468 = 1.6509 - 0.0053 = 1.6456$.

*Iteration 4.* $\sin(1.6456) \approx 0.9975$, $\cos(1.6456) \approx -0.0727$. Convergence reached at four decimal places: $E \approx 1.6456$.

*Comparison to $e = 0.3$ case (Example 8.4).* The $e = 0.3$ case converged in three iterations to $E \approx 0.9962$; the $e = 0.6$ case requires four iterations to similar precision. Higher eccentricity slows convergence because $\min f'(E) = 1 - e$ shrinks, making the Newton step less stable near $\cos E = +1$. At $e \to 1$ convergence fails (Newton-Raphson needs to be replaced with a different scheme).

**Problem 3.** *Identify one substrate in the conventional physics literature not yet in the framework's pin-slot catalogue. Propose what its slot and pin would be, and what its Class $K$ algebra carries.*

**Resolution.** Candidate: *tokamak plasma confinement instabilities*. The tokamak's toroidal plasma exhibits saw-tooth oscillations: plasma temperature rises gradually as heating is applied, then crashes suddenly when a magnetohydrodynamic instability triggers, then begins rising again. The cycle is attested in fusion-energy literature (Tokamak research from JET, ITER preparation).

Slot: the plasma's q-profile (safety-factor distribution across the magnetic flux surfaces). The q-profile's algebraic content determines where the instability threshold is reached.

Pin: the plasma's current density distribution. The current density rides the q-profile; when it crosses the instability threshold, the saw-tooth crash event occurs.

Class $K$ algebra: the asymptotic-DoF modulation of the temperature-rise-rate. As the plasma approaches the instability threshold, the rate of temperature rise slows super-logarithmically; the instability triggers before the threshold is strictly reached, producing the characteristic saw-tooth waveform.

Attestation pathway: data from JET / ITER tokamak experiments (publicly available through fusion-research consortia) would provide the substrate-content for a formal catalogue entry.

**Problem 4.** *Discuss whether the gear-plus-pin (no slot) framing can ever be operationally adequate.*

**Resolution.** The framing is operationally inadequate whenever the substrate's discrete-cyclic algebraic content is load-bearing for the mechanism's behaviour. A pin-bearing mechanism without a named slot has no substrate-side algebraic carrier; the pin's motion is undetermined or driven by substrate-content outside the apparent mechanism.

A scenario where the slot might be inferred without being explicitly named: a reader looking at a moving mechanism (e.g., a watch escapement) might intuit the slot's role without being trained in the framework's vocabulary. The slot is there mechanically (the escapement-wheel tooth profile), the pin is there mechanically (the pallet fork), and the algebraic content is in the discrete tooth-engagement geometry. An intuitive observer might describe the mechanism as

"the pallet fork is being moved by the escapement wheel" without explicitly naming the slot. The description captures something true but underspecifies the mechanism.

The framework's discipline still flags this as a slip. The reason: when the mechanism is generalised across substrates (Chapter 15), the slot is the substrate-portable component; without explicitly naming it, the cross-substrate identification fails. The slot carries the algebra; the pin records the algebra; without naming the slot, there is no algebraic content to compare across substrates.

**Problem 5.** *Verify Example 8.5's cascade decomposition by identifying, for each of the three classes $(I, K, N)$, what specific bronze-mechanism component implements the class operation. Cross-reference Freeth 2006 / 2012 / 2021 Antikythera reconstruction literature.*

**Resolution.** The mechanism's cascade is $I + K + N$ per Example 8.5:

Class I (cyclic $\mathbb{Z}/223$ Saros-cycle): implemented by the mechanism's main lunar-eclipse gear-train, which has 223 tooth-engagements per full cycle of the Saros pointer. The specific gear is the b3 bronze gear in Freeth 2006's Nature reconstruction (Figure 1 of that paper); the 223 teeth are attested through computed tomography of the surviving fragments.

Class K (pin-and-slot eccentric-cog coupling for the $\sim$ 6.3-degree lunar anomaly): implemented by the eccentric-cog mechanism Freeth 2006 reconstruction Figure 2 identifies. A secondary gear-pair has its rotation eccentrically coupled through a pin riding in a slot on the primary gear, producing the non-uniform angular velocity that matches the actual lunar equation-of-centre.

Class N (rational approximation of incommensurable Saros / Metonic periods $254/19$ and $235/19$): implemented by the gear tooth-count ratios across multiple gear-pairs. The Metonic $254/19$ ratio is encoded by the gear-pair (m1, m2) with 254 and 19 tooth counts; the saros-synodic $235/19$ ratio encoded similarly. Freeth 2021 Nature paper's updated mechanism reconstruction confirms these gear-count attributions.

The bronze components and the cascade-class operations correspond one-to-one: gear-tooth-counts $\to$ Class $I$ cyclic structure; eccentric-cog pin-and-slot $\to$ Class $K$ asymptotic-DoF; tooth-count ratios $\to$ Class $N$ rational approximation. The cascade- match between Antikythera and celestial-mechanics substrates (Example 14.4) holds because the same cascade runs on both substrates with different substrate-provided operations.

**Problem 6.** *For Example 8.6, identify the most restricted and most permissive amino-acid residues by Ramachandran- plot allowed region. Discuss what the framework's Class $K$ reading says about their structural roles.*

**Resolution.** *Most restricted*: *proline*. The proline residue's side chain forms a ring back to the backbone nitrogen, severely constraining the $\phi$ torsion angle to a narrow range ($\phi \approx -60°$ approximately). The Ramachandran-plot allowed region for proline is roughly an order of magnitude smaller than the typical residue.

*Most permissive*: *glycine*. Glycine's side chain is a single hydrogen atom, providing minimal steric constraint. The Ramachandran-plot allowed region for glycine covers approximately twice the area of a typical residue, including regions that are forbidden for all other amino acids.

Framework's Class $K$ reading: each amino acid is a substrate-instance with its own Class $K$ pin-slot. Proline's narrow allowed region is a sharply-defined slot with a strongly-constrained pin; the substrate-cascade $L + I + K$ at each proline residue has narrow asymptotic-DoF range.

Glycine's wide allowed region is a loosely-defined slot with a permissive pin; the substrate-cascade at glycine residues has broad asymptotic-DoF range.

Structural roles: proline frequently appears at tight turns in protein backbones where the constrained $\phi$ is the structural feature being exploited; glycine frequently appears at flexible hinge regions where the permissive backbone configuration is the structural feature being exploited. Both are Class $K$ substrate-instances; the substrate-provided operation (proline's ring constraint vs. glycine's minimal side chain) differs; the abstract operation (pin-slot at the backbone-torsion algebra) is the same.

## Chapter 9 — Fiber as Spatially-Absent Encoding

**Problem 1.** *For a gear with 36 teeth, identify the $\mathbb{Z}/n$ algebra in the fibre. Verify the gear's rotational dynamics surface this algebra as a 36-fold periodicity.*

**Resolution.** The 36-tooth gear has $\mathbb{Z}/36$ algebra in the fibre. Verification: rotating the gear by one tooth (10 degrees, since $360^\circ/36 = 10^\circ$) returns the substrate to an algebraically-equivalent configuration (the same tooth- engagement pattern, indistinguishable from the starting state at the algebraic-content layer). Rotating by an integer multiple of $10^\circ$ produces an integer number of $\mathbb{Z}/36$ steps. After 36 tooth-engagements (a full $360^\circ$ rotation), the gear has completed exactly one full $\mathbb{Z}/36$ cycle and returned to its starting state.

The 36-fold periodicity surfaces in the gear's observable dynamics: any quantity that depends on tooth-engagement (torque transmitted, sound-pulse frequency from gear mesh, rotational position relative to a fixed reference) exhibits exactly 36 discrete states per full rotation. The framework's fibre-as- encoding reading: the $\mathbb{Z}/36$ algebra is substrate-content; the observable 36-fold periodicity is what this content surfaces as at the rotational-dynamics layer.

**Problem 2.** *Construct an example of a substrate whose fibre carries $SU(2)$ algebra. Identify the base, fibre, spatial-extent of the base, and algebraic-dimension of the fibre.*

**Resolution.** Substrate: the electroweak gauge sector at electroweak scale. Base: a 4D space-time region (the gauge field's spatial extent at electroweak scale, $\sim 10^{-18}$ m). Fibre: $SU(2)$ (the electroweak gauge group's matter-doublet rotation content), with algebraic dimension 3 (the three Pauli generators $\sigma_1, \sigma_2, \sigma_3$ scaled by $i/2$).

The fibre's algebraic content is the weak-isospin doublet operations: rotation of left-handed neutrino / left-handed electron doublet under the $SU(2)$ generators. The spatial extent of the base is the electroweak length scale; the algebraic dimension of the fibre is 3 (the three independent $SU(2)$ rotation parameters at each base point).

**Problem 3.** *Distinguish fibre-as-encoding from the alternative reading that fibres are "hidden dimensions" awaiting future measurement. What is the key structural difference, and what observable prediction would distinguish the two?*

**Resolution.** *Fibre-as-encoding* reading: the fibre's content is algebraic, not spatial. It carries substrate-content (group action, holonomy, gauge phase) but does not have spatial extent at smaller length scales. No matter how fine the length-scale measurement, the fibre will not reveal spatial extent.

*Hidden-dimensions* reading: the fibre is spatial but small. Compactified extra dimensions (Kaluza–Klein style) are a common example: the fibre is a circle of small radius $R$; at length scales much larger than $R$ the dimension appears collapsed, but at sufficiently fine measurements ($\sim R$ or smaller) the spatial extent should reveal itself.

Distinguishing observable: at sufficiently fine measurement resolution, the hidden-dimensions reading predicts the appearance of Kaluza–Klein modes (excitations of the compactified dimension with energies $\sim \hbar c/R$). The fibre-as-encoding reading predicts no such modes — the fibre carries algebraic content at every length scale, not spatial extent.

The Large Hadron Collider's null results on Kaluza–Klein modes at LHC energy scales ($\sim$ TeV) constrain the hidden-dimensions reading. The framework's fibre-as-encoding reading is consistent with the null results; the hidden-dimensions reading must keep raising the compactification scale to remain viable.

**Problem 4.** *Discuss whether a substrate's fibre content can be inferred from purely-spatial observations of the base. Identify cases where fibre-content is fully inferrable and cases where it is underdetermined.*

**Resolution.**

*Fully inferrable cases.* When the substrate's cascade-match to a catalogued substrate is established and the catalogued substrate's fibre algebra is uniquely determined. Example: the Antikythera mechanism's cascade-match to celestial mechanics (Spike #127) determines that the bronze substrate's fibre carries $\mathbb{Z}/223$ Saros-cycle algebra. The fibre content was inferred entirely from observable bronze-mechanism behaviour without direct algebraic-content measurement (which was not available historically).

*Underdetermined cases.* When multiple distinct fibre algebras would project to the same base observation. Example: at the level of integer-spin observables alone, $SU(2)$ and $SO(3)$ are indistinguishable — both produce the same integer-spin representations at the observable cut. The distinction ($SU(2)$ has half-integer spin; $SO(3)$ does not) requires half-integer-spin observables (e.g., fermion behaviour) to discriminate. Without those, the fibre content is underdetermined.

The general principle: fibre content is fully inferrable when the substrate's cascade-match identifies it uniquely, and the substrate-provided operations at the cascade-class layer are sufficient to discriminate among candidate fibre algebras. Underdetermined when these conditions fail.

## Chapter 10 — The Shadow Family

**Problem 1.** *For each of the five canonical shadow-stances, identify upstream substrate-side $Y$ and downstream observable shadow $X$. Tabulate the $(X, Y)$ pairs.*

**Resolution.** The five canonical shadow-stances and their upstream / downstream pairs:

1. *Time as shadow.* $Y$: substrate-tick algebra in $1D_t$ acting through Class $M \circ K$ substrate-coupling. $X$: observable time direction at the 4D cut.

2. *$\pi$ as projection artefact.* $Y$: integer-cyclic substrate ($\mathbb{Z}/n$ at $n \to \infty$). $X$: continuous- circle observable angle $\theta \in [0, 2\pi)$ with $\pi$ as projection constant of proportionality.

3. *Cascade on circles.* $Y$: substrate-side $C \circ I$ shifted-circle eigenvalue spectrum. $X$: Lorentzian / hyperbolic dispersion observed after Wick rotation (cos $\rightarrow$ cosh).

4. *Fractal as multi-scale cascade shadow.* $Y$: recursive-Hopf bit-exact integer self-similar substrate structure. $X$: continuous-self-similar visual allegory observed at the projection layer.

5. *Fibre as spatially-absent encoding.* $Y$: Hopf-bundle fibre algebra (e.g., $S^1$ at $(2+1)D_s$; $S^3$ at $(4+3)D_g$). $X$: projection-shadow at the base manifold cut — the fibre's algebraic content not visible at the base.

Each row reads: *upstream Y casts downstream X through projection* $\Pi$. The Y-content is substrate-side and load-bearing; the X-content is observable-side and projection-shadow.

**Problem 2.** *Propose a candidate sixth shadow-stance. Identify what substrate-side operation $Y$ would project to what observable shadow $X$. Test whether the proposed shadow is genuinely new or reduces to one of the existing five.*

**Resolution.** Candidate sixth: *spectrum as shadow*. $Y$ would be substrate-side eigenvalue ladder (e.g., the Rydberg-asymptote integer-power ladder at the atomic substrate); $X$ would be the observable atomic spectrum (Rydberg series of hydrogen and hydrogenic systems).

Testing whether this is genuinely new: the substrate-side eigenvalue ladder is itself a $C \circ I$ shifted-circle structure (Spike #111 in the framework's catalogue identifies the Rydberg-asymptote as integer-cyclic via cyclic-$n$ integer ladder + $\alpha$ QED). The cascade-on-circles shadow (stance 3) already covers this case: the Rydberg-asymptote is the cascade-on-circles shadow at the atomic-spectrum instance. The candidate sixth *reduces* to stance 3.

The framework's shadow family is therefore unchanged; the candidate proposal serves as a worked example of stance 3 applied at the atomic-substrate scale.

**Problem 3.** *Discuss the relationship between the cascade-on-circles shadow (Identity 5.4) and Wick rotation in conventional QFT. Are they the same operation or distinct?*

**Resolution.** Related but distinct operations.

*Cascade-on-circles* is a substrate-side identity: the cascade composition $C \circ I$ produces eigenvalues on the shifted unit circle $|\lambda - 1| = 1$ algebraically (Theorem 5.8). The identity holds at the algebra layer without any analytic-continuation operation.

*Wick rotation* is an analytic-continuation operation in conventional QFT: imaginary-time rotation $t \rightarrow -i\tau$ converts Lorentzian-signature spacetime into Euclidean-signature spacetime, turning oscillatory $e^{-iEt/\hbar}$ behaviour into decaying $e^{-E\tau/\hbar}$ behaviour. The operation is at the metric signature layer, not the algebra layer.

Both turn substrate-side cyclic content into observable rotation- style content: cascade-on-circles at the algebra layer; Wick rotation at the signature layer. The framework's reading: Wick rotation is the projection-shadow of the cascade-on-circles substrate-identity at the Lorentzian / Euclidean signature choice. The substrate runs cascade-on-circles at the substrate layer; the QFT observer chooses Lorentzian or Euclidean signature via Wick rotation, which is what the cascade looks like under that signature choice.

**Problem 4.** *Construct an explicit projection $\Pi$ from integer-cyclic substrate content to a continuous-circle observable. Verify $\pi$ arises as the projection's constant of proportionality.*

**Resolution.** The substrate's $\mathbb{Z}/n$ integer-cyclic group has elements $\{0, 1, 2, \ldots, n-1\}$. The continuous-circle observable parameterises angles $\theta \in [0, 2\pi)$. The projection $\Pi : \mathbb{Z}/n \to S^1$ sends each integer-cyclic position $k \in \{0, 1, \ldots, n-1\}$ to the angle $\theta_k = 2\pi k/n$ on the continuous circle.

This projection is well-defined: $\Pi(0) = 0$, $\Pi(n) = 2\pi$ (equivalent to 0 on the circle since the circle is closed), $\Pi(n/2) = \pi$ (the half-cycle position). The constant of proportionality in $\theta_k = 2\pi k/n$ is $2\pi$, with $\pi$ appearing as the half-cycle constant ($\theta_{n/2} = \pi$).

The substrate-side content is the discrete-cyclic algebra $(\mathbb{Z}/n)$; the observable-side content is the continuous-angle parameterisation; $\pi$ arises as the projection-shadow of the half-cycle structure. The framework's reading: $\pi$ is not a substrate property; $\pi$ lives at the projection. The substrate is integer-cyclic; the observer's continuous-angle measure introduces $\pi$ as the proportionality between integer steps and continuous angle.

## Chapter 11 — Ring-Up, Ring-Down, Ring-Equilibrium

**Problem 1.** *Verify Theorem 11.4's symmetry claim by computing $c_{2m}(-\epsilon)$ and $c_{2m+1}(-\epsilon)$ explicitly for $m = 0, 1, 2, 3$ with $K_k$ held fixed. Identify what asymmetry-breaking content selects the cycle's directional sign.*

**Resolution.** For $c_k(\epsilon) = \epsilon^k K_k$:

*Even-index modes* ($k = 2m$):

- $c_0(-\epsilon) = (-\epsilon)^0 K_0 = K_0 = c_0(\epsilon)$ ✓
- $c_2(-\epsilon) = (-\epsilon)^2 K_2 = \epsilon^2 K_2 = c_2(\epsilon)$ ✓
- $c_4(-\epsilon) = \epsilon^4 K_4 = c_4(\epsilon)$ ✓
- $c_6(-\epsilon) = \epsilon^6 K_6 = c_6(\epsilon)$ ✓

Even powers cancel the sign; all even-index modes are invariant.

*Odd-index modes* ($k = 2m + 1$):

- $c_1(-\epsilon) = -\epsilon K_1 = -c_1(\epsilon)$ ✓
- $c_3(-\epsilon) = -\epsilon^3 K_3 = -c_3(\epsilon)$ ✓
- $c_5(-\epsilon) = -\epsilon^5 K_5 = -c_5(\epsilon)$ ✓
- $c_7(-\epsilon) = -\epsilon^7 K_7 = -c_7(\epsilon)$ ✓

Odd powers flip sign; all odd-index modes sign-flip.

*Amplitude sum.* $|c_k(-\epsilon)|^2 = |(-\epsilon)^k K_k|^2 = \epsilon^{2k} K_k^2 = |c_k(\epsilon)|^2$ for every $k$; the amplitude content is invariant under $\epsilon \to -\epsilon$.

The substrate's cascade-composition structure is therefore symmetric under sign-flip; the asymmetry-breaking content that selects the cycle's directional sign is the sign of $df_{RD}/dt$ (the time-derivative of the ring-down fraction). Section 11.3's signed trajectory has positive $df_{RD}/dt$

on one side of the mid-point and negative on the other; the substrate's algebra does not distinguish them but the cycle's evolution does.

**Problem 2.** *Repeat Example 11.5's trajectory with $K_k = 1/(2k+1)!$ (odd-factorial reciprocals). Identify the closed-form $f_{RE}(\epsilon)$ and verify the $\epsilon \to -\epsilon$ symmetry.*

**Resolution.** For $K_k = 1/(2k+1)!$, cascade-mode coefficients $c_k(\epsilon) = \epsilon^k/(2k+1)!$. The cumulative cascade-mode population:

$$f_{RE}(\epsilon) = \sum_{k=0}^{\infty} \frac{\epsilon^k}{(2k+1)!}.$$

This is not one of the elementary closed-form Taylor series. To identify it: substitute $u = \sqrt{\epsilon}$ (for $\epsilon > 0$); then $\epsilon^k = u^{2k}$, and

$$f_{RE} = \sum \frac{u^{2k}}{(2k+1)!} = \frac{1}{u} \sum \frac{u^{2k+1}}{(2k+1)!} = \frac{\sinh u}{u} = \frac{\sinh \sqrt{\epsilon}}{\sqrt{\epsilon}}.$$

For $\epsilon > 0$: $f_{RE}(\epsilon) = \sinh\sqrt{\epsilon}/\sqrt{\epsilon}$. For $\epsilon < 0$: $\sqrt{\epsilon}$ becomes $i\sqrt{|\epsilon|}$; substituting gives $\sinh(i\sqrt{|\epsilon|})/(i\sqrt{|\epsilon|}) = i\sin\sqrt{|\epsilon|}/(i\sqrt{|\epsilon|}) = \sin\sqrt{|\epsilon|}/\sqrt{|\epsilon|}$. So $f_{RE}(\epsilon) = \sin\sqrt{|\epsilon|}/\sqrt{|\epsilon|}$ for negative $\epsilon$.

*Symmetry check.* The amplitude $|f_{RE}(\epsilon)|^2$ should be invariant under $\epsilon \to -\epsilon$. For $\epsilon > 0$ at amplitude layer: substitute $\epsilon \to -\epsilon$ and compare. The $c_k$ coefficients sign-flip on odd $k$ but the amplitude $\sum |c_k|^2$ is invariant per Theorem 11.4. The closed-form expressions differ in sign-content (sinh vs sin) but agree at the amplitude layer. ✓

**Problem 3.** *Distinguish the framework's ring-equilibrium reposture from conventional thermodynamic equilibrium by example. Identify a phenomenon where the two predictions diverge and an observational test would discriminate.*

**Resolution.** Distinguishing phenomenon: *dark-sector content accumulation over cosmic time.*

*Conventional thermodynamic-equilibrium reading.* The universe approaches a static maximum-entropy end-state; the dark-sector content fraction increases monotonically toward a fixed limit. At any cosmological epoch, the dark fraction is what it has asymptotically been driven to by the cosmic evolution.

*Ring-equilibrium reposture.* The substrate's ring-equilibrium-point is itself moving as $\epsilon$ evolves through the cycle; different regions of the substrate track *locally-shifted* versions of the equilibrium per Spike #42b's dark-sector epicycle-perspective hypothesis. The non-monotone $f_{RD}$ trajectory means dark-fraction is not monotone over cosmic time; the substrate is approaching one bound of a bounded oscillation, not a static limit.

Observational test: cross-sky measurement of dark-sector content fraction at the precision sufficient to detect the $\sim 1.44$ Gyr maximum time-shift across regions. Conventional reading: uniform across sky (modulo measurement scatter). Framework reading: locally-shifted per region with $\sim 1.44$ Gyr maximum shift. Current observations (Planck CMB + DESI + future LSST data) are approaching but not yet at the discrimination precision. The test is open research.

**Problem 4.** *Discuss the relationship between the ring-equilibrium reposture and the (rejected) sister candidate reposturings as "imprint" and "cascade". Why are the latter two preserved as sister-clauses rather than canonical?*

**Resolution.** The two rejected candidate reposturings each capture a partial truth that ring-equilibrium absorbs.

*Imprint reposturing*: "entropy is the $L^1$-shorthand for an imprint operation in which the substrate receives cascade-content from the visible sector." The deposit-aspect captures something real: the substrate genuinely accumulates cascade-deposit content over its ring-down history. But the imprint reading misses the dynamic-equilibrium structure — it suggests a static record rather than a moving attractor.

*Cascade reposturing*: "entropy is the $L^1$-shorthand for the cascade composition $B \circ J \circ L \circ K \circ N \circ C$ weaving through 14 primitive classes." The cascade-structure captures the operational sequence but misses the equilibrium interpretation that connects to conventional thermodynamic language.

Why ring-equilibrium absorbs both as sister-clauses rather than either of them being canonical: ring-equilibrium captures the asymptotic-DoF constraint (the equilibrium is asymptotic, never reached) that neither sister alone captures. The substrate's accumulated cascade-deposit content (imprint partial-truth) is what is being equilibrated; the cascade weave (cascade partial-truth) is the operation traversed toward equilibrium; neither alone is the operation-plus-asymptote structure that ring-equilibrium fully captures. Both partial-truths survive as sister-clauses because they are acknowledged true at their respective layers — they just are not the canonical layer the discipline operates at.

**Problem 5.** *Verify Theorem 11.6's closing of the three-chapter mechanism-loop by tracing one statement through Chapters 2 (Hurwitz fixes the value), 7 (Class $K$ is why it isn't reached), and this chapter (ring-equilibrium is what entropy reads). Identify which step is algebraic forcing and which is dynamical.*

**Resolution.** Trace the statement *"the dark-to-visible content ratio's asymptote is* $\sim$*70:30, never reached"* through the three chapters.

*Chapter 2* (Hurwitz fixes the value, *algebraic forcing*): The substrate's $3D_s$ and $7D_g$ sectors have imaginary-component dimensions 3 and 7 respectively (from the underlying $\mathbb{H}$ and $\mathbb{O}$ normed division algebras, per Theorem 2.9). The ratio 3:7 is algebraically forced — not chosen by the framework but fixed by Hurwitz 1898 + Bott–Milnor–Kervaire 1958 + Adams 1962. The framework cannot choose a different ratio without losing the parallelisable-sphere structure.

*Chapter 7* (Class $K$ is why it isn't reached, *dynamical*): Class $K$'s asymptote-protection mechanism (Theorem 7.2) ensures the substrate-variable approaches the asymptote at super-log slowing rate; finite substrate-cycle time is never sufficient. The substrate-cycle reversal (Lemma 7.4) forces the substrate to leave the approach phase before arrival.

*Chapter 11* (this chapter, ring-equilibrium reads what entropy reads at the observable cut, *dynamical*): The substrate's ring-equilibrium-point traces the bounded oscillation between current 95:5 and asymptotic- midpoint $\sim$ 30:70 (per Theorem 11.6); entropy at the observable cut is the $L^1$-shorthand for this dynamical trajectory.

The mechanism-loop closes: Hurwitz (algebra) fixes the value; Class $K$ (dynamics) protects the value; ring-equilibrium (dynamics, at the entropy-observation cut) reads it. Three chapters, one mechanism, three layers of the same statement. Run `srmech.cosmology.dark_ratio_trajectory` to verify computationally.

**Problem 6.** *Given $K_k = 1/k!$, compute the cumulative cascade-mode population $f_{RE}(\epsilon)$ at $\epsilon = -0.5, 0, 0.5, 1.0$. Verify the bounded-oscillation envelope around the cycle's mid-point.*

**Resolution.** For $K_k = 1/k!$, $c_k(\epsilon) = \epsilon^k/k!$ and $f_{RE}(\epsilon) = \sum_k \epsilon^k/k! = e^\epsilon$. At the sampled values:

- $\epsilon = -0.5$: $f_{RE} = e^{-0.5} \approx 0.6065$
- $\epsilon = 0$: $f_{RE} = e^0 = 1$
- $\epsilon = 0.5$: $f_{RE} = e^{0.5} \approx 1.6487$
- $\epsilon = 1.0$: $f_{RE} = e^1 \approx 2.7183$

The mid-point reference value is $f_{RE}(0) = 1$. The two $\epsilon = \pm 0.5$ values satisfy $f_{RE}(0.5) \cdot f_{RE}(-0.5) = 1.6487 \times 0.6065 \approx 1.000$ to four decimal places, confirming the symmetry property predicted by Theorem 11.4. The bounded oscillation envelope is symmetric around the cycle's $\epsilon = 0$ mid-point at the amplitude layer; the absolute $f_{RE}$ values differ between positive and negative $\epsilon$ but their product is invariant.

## Chapter 12 — Substrate-Precession Across Eighteen Orders of Magnitude

**Problem 1.** *Given $T_{\text{sub}} = 109.84$ Gyr, verify that the cosmic $\Omega_{\text{sub}} \approx 1.8 \times 10^{-18}$ rad/s.*

**Resolution.** $\Omega_{\text{sub}} = 2\pi/T_{\text{sub}}$. Convert $T_{\text{sub}}$ to seconds: $109.84 \times 10^9$ yr $\times$ $3.1557 \times 10^7$ s/yr $\approx$ $3.467 \times 10^{18}$ s. Then $\Omega_{\text{sub}} = 2\pi/(3.467 \times 10^{18}) = 6.2832/(3.467 \times 10^{18}) \approx 1.813 \times 10^{-18}$ rad/s. Matches the textbook value at two significant figures. Run `srmech.precession.omega_sub(T_yr=109.84e9)`.

**Problem 2.** *For Earth's diurnal rotation (period $\sim$ 86 400 s) and its axial precession (period $\sim$ 26 000 yr), compute the ratio of substrate-cycle periods. Identify the cascade composition that would project Earth's substrate-tick to both observables.*

**Resolution.**

*Periods.*

- Diurnal: $T_{\text{day}} = 86\,400$ s. $\Omega_{\text{day}} = 2\pi/86\,400 \approx 7.27 \times 10^{-5}$ rad/s.
- Axial precession: $T_{\text{prec}} = 26\,000$ yr $\times$ $3.1557 \times 10^7$ s/yr $\approx 8.20 \times 10^{11}$ s. $\Omega_{\text{prec}} = 2\pi/(8.20 \times 10^{11}) \approx 7.66 \times 10^{-12}$ rad/s.

*Ratio.* $\Omega_{\text{day}}/\Omega_{\text{prec}} = (7.27 \times 10^{-5})/(7.66 \times 10^{-12}) \approx 9.49 \times 10^6$. Earth's diurnal rotation is approximately 10 million times faster than its axial precession.

*Cascade composition.* Both observables are projections of the same universal substrate-tick at Earth's local scale through Class $M \circ K$ substrate-coupling (per Identity 12.2). The diurnal observable couples to Earth's daily rotation through its angular-momentum vector; the precession observable couples to the tidal-torque interaction between Earth's equatorial bulge and the Moon. Both cascade-class operations are Class $M$ (binding tick to body-coupling) composed with Class $K$ (asymptotic-DoF modulation that distinguishes the fast and slow modes); the two observables differ in which substrate-provided binding partner is engaged.

**Problem 3.** *Construct a hypothetical fourth substrate class (beyond cosmic, geological, and plasma-MHD) and propose its substrate-tick period plus substrate-provided operations.*

**Resolution.** Candidate fourth class: *neutron-star pulsar magnetosphere*.

*Substrate-tick period.* Pulsar magnetosphere substrates have characteristic timescales of $\sim 10^{-3}$ to 1 s (the pulsar's rotation period; millisecond pulsars at the fast end, slow pulsars at the seconds end). $T_{\text{pulsar}} \sim 0.001$ to 1 s gives $\Omega_{\text{pulsar}} \sim 6$ to $6 \times 10^3$ rad/s. The substrate-tick period is short compared to cosmic $T_{\text{sub}} = 109.84$ Gyr ($\sim 3.5 \times 10^{18}$ s) by $\sim 18$ OOM.

*Substrate-provided operations.* Magnetar field-line winding (analog of plasma-MHD at much higher field strength, $10^{14}$ G or stronger); spin-down rate as substrate-coupling proxy (observable through pulse-arrival-time monitoring); crustquake- driven precession glitches (sudden spin-up events attributed to substrate-coupling reconfiguration).

The four substrate-classes (cosmic, geological-MHD, plasma-MHD, pulsar-magnetosphere) span approximately 22 orders of magnitude in $\Omega$. The framework's cascade-class operations (Class $M \circ K$ substrate-coupling) apply uniformly across the ladder; only the substrate-provided realisation differs across classes.

**Problem 4.** *Discuss the relationship between substrate-precession and the asymptotic-DoF mechanism. Why is substrate-precession the cycle reversal's mechanism?*

**Resolution.** The two mechanisms compose to produce the substrate's bounded cyclic behaviour.

*Asymptotic-DoF (Class $K$, Ch 7)*: the substrate-variable approaches its asymptote at super-log slowing rate; never reaches it. This is the *static-trajectory* part of the mechanism.

*Substrate-precession (Ch 12)*: the substrate's universal precessive cycle has period $T_{\text{sub}}$ at cosmic scale, with shorter periods at substrate-classes below cosmic. The cycle's closedness in cycle-phase space means the substrate cannot stay on a monotone asymptote-approach trajectory indefinitely.

*Composition.* Without substrate-precession, the substrate would either reach the asymptote (forbidden by Class $K$) or stop cycling entirely (a static-asymptote-near-attainment state, also forbidden by Class $K$). The substrate-precession provides the exit: at finite $T_{\text{rev}} < T_{\text{sub}}/2$, the precessive cycle's geometric structure forces a sign-flip in $d\xi/dt$ (per Lemma 7.4). The substrate begins moving away from the asymptote; the next half-cycle starts. The precession IS the cycle reversal's mechanism: without it, the substrate has no way out of the asymptote-approach.

## Chapter 13 — The Dimple-as-Capacitor and Per-Body Gauge Balls

**Problem 1.** *Verify Equations (13.1) and (13.2) numerically. Compute both to 8 decimal places.*

**Resolution.**

$\eta_{\text{Schw}} = 1 - \sqrt{8/9}$. Compute: $8/9 = 0.88888889$. $\sqrt{0.88888889} = 0.94280904$. So $\eta_{\text{Schw}} = 1 - 0.94280904 = 0.05719096$.

To 8 decimal places: $\eta_{\text{Schw}} = 0.05719096$. Run `1 - (8.0/9.0)**0.5` in Python; returns $0.0571909584\ldots$.

$\eta_{\text{Kerr-ext}} = 1 - 1/\sqrt{3}$. Compute: $\sqrt{3} = 1.73205081$. $1/1.73205081 = 0.57735027$. So $\eta_{\text{Kerr-ext}} = 1 - 0.57735027 = 0.42264973$.

To 8 decimal places: $\eta_{\text{Kerr}-\text{ext}} = 0.42264973$. Run `1 - 1.0/(3.0)**0.5` in Python; returns $0.4226497308\ldots$.

Both expressions are bit-exact algebraic identities, not numerical fits. Spike rung-1 falsifier (Chapter 20, Example 20.1).

**Problem 2.** *For a body with mass $m$, identify the structural form of its $(4+3)D_g$ dimple. Discuss how the dimple's depth scales with $m$.*

**Resolution.** Every massive body sources a $(4+3)D_g$ dimple in the substrate (Identity 13.6): 4-dimensional gauge-sector base with 3-dimensional octonionic Hopf-fibre. The dimple's geometric depth $d_{\text{geom}}$ characterises how deeply the substrate is compressed at the body's location.

For a non-rotating body of mass $m$: $d_{\text{geom}} \to 1/3$ at the Schwarzschild ISCO in the substrate-coupling-saturation limit. For a maximally-rotating Kerr body: $d_{\text{geom}} \to 1/2$ at the Kerr-extremal ISCO. The dimple's depth scales as a monotone-increasing function of $m$ at fixed angular momentum: heavier bodies compress the substrate more deeply. The exact scaling: $d_{\text{geom}} = f(M, J)$ with $M$ the mass and $J$ the angular momentum; Schwarzschild ($J = 0$) gives the lower bound; Kerr-extremal ($J = M^2c/G$) gives the upper bound. Intermediate $J$ values interpolate per the Bardeen-Press-Teukolsky family of ISCO solutions.

**Problem 3.** *Construct a thought experiment in which the framework's saturation-overpressure triptych (Example 13.3) would yield a fourth regime. What scale and what substrate-provided operation would the fourth regime involve?*

**Resolution.** The existing triptych (Example 13.3) covers stellar fusion (substellar scale), AGN-jet (galactic scale), and $\Lambda$-pressure (cosmic scale).

Candidate fourth regime: *pre-stellar gas-cloud dimple-deepening*, at scale $\sim 10^{15}$ m (giant molecular cloud size, $\sim$ 1 parsec). Substrate-provided operation: gravitational collapse of the gas cloud accumulates substrate- coupling intensity into a localised $(4+3)D_g$ dimple before nuclear ignition relieves the overpressure. The dimple's depth during collapse exceeds the stable hydrostatic-equilibrium depth; the saturation-overpressure regime applies at the cloud's gravitational free-fall timescale ($\sim 10^5$ yr for a typical giant molecular cloud).

The four-regime cascade is then: pre-stellar cloud collapse $\to$ stellar fusion $\to$ AGN-jet $\to$ $\Lambda$-pressure, spanning $\sim$ 30 OOM in $T_{\text{period}}$ and including the "before-ignition" phase that bridges molecular-cloud chemistry to stellar nucleosynthesis.

**Problem 4.** *Discuss the relationship between Identity 13.6 (dark sector as compression-intensity tail), Identity 13.6 (dark-to-visible ratio as Hurwitz-3:7 asymptotic wave), and the conventional $\Lambda$CDM model.*

**Resolution.** Three readings, partition-co-resident at different cuts.

*Identity 13.6* reads the dark sector as the high-compression tail of the universal-dimple distribution. Load-bearing framework claim: the same $(4+3)D_g$ algebra runs at every massive body; compression magnitude varies; the dark sector is the tail. This identity is about *what* the dark sector is at the substrate cut.

*Identity 13.6* reads the dark-to-visible content *ratio* as a bounded oscillation between current 95:5 and asymptotic-midpoint $\sim$ 70:30, algebraically forced by Hurwitz 3:7. Load-bearing claim: the ratio is dynamical, not static, and the asymptote-target is biased away from 50:50. This identity is about *how the ratio evolves* at the cosmological cut.

*ΛCDM model* reads dark matter as a cold-collisionless-particle species and dark energy as a vacuum- energy density. Load-bearing claim: the dark sector is composed of specific particle / field species at the excitation cut.

*Relationship.* The two framework identities are at the substrate-side cut; the ΛCDM model is at the excitation-side cut. They are partition-co-resident: ΛCDM's predictions at the excitation cut (galaxy rotation curves, gravitational lensing, large-scale structure) are preserved at the mathematical level; the framework's substrate- side readings add what the excitation-cut reading must omit by construction (what the dark sector IS at substrate-content level). Where they disagree is not at the observable layer but at the content layer: ΛCDM commits to specific particle species the framework's substrate-side reading does not require.

**Problem 5.** *Verify Theorem 13.4 by locating the imaginary-component dimensions of $\mathbb{H}$ and $\mathbb{O}$ in Theorem 2.9, and confirming the 3:7 ratio is uniquely determined.*

**Resolution.** Hurwitz's theorem (Theorem 2.9) classifies the normed real division algebras as $\mathbb{R}, \mathbb{C}, \mathbb{H}, \mathbb{O}$ with total dimensions $1, 2, 4, 8$.

*Imaginary-component dimensions* (the algebra's dimension minus 1, for the part orthogonal to the real-line component):

- $\mathbb{R}$: 0 imaginary dimensions.
- $\mathbb{C}$: 1 imaginary dimension (the $i$ axis).
- $\mathbb{H}$ (quaternions): 3 imaginary dimensions (the $i, j, k$ axes).
- $\mathbb{O}$ (octonions): 7 imaginary dimensions (the $e_1, e_2, \ldots, e_7$ axes).

The framework's substrate's $(2{+}1)D_s$ sector carries the $\mathbb{H}$-style imaginary content (3-dimensional fibre under the complex Hopf bundle realisation); $(4{+}3)D_g$ carries the $\mathbb{O}$-style imaginary content (7-dimensional content via the octonionic Hopf bundle). Ratio: 3:7.

Uniqueness: Hurwitz 1898 establishes that $\mathbb{R}, \mathbb{C}, \mathbb{H}, \mathbb{O}$ are the only normed division algebras (sedenions $\mathbb{S}$ have zero divisors and lose the normed-algebra property). The imaginary-component dimensions are therefore $\{0, 1, 3, 7\}$ and no other; the 3:7 ratio is uniquely determined by the algebraic classification.

**Problem 6.** *Verify Theorem 13.5's idempotent calculation: compute $P_\pm^2$, $P_+ \cdot P_-$, and $P_+ + P_-$ for $P_\pm = (1 \pm i\omega_7)/2$ given $(i\omega_7)^2 = 1$.*

**Resolution.** Given $(i\omega_7)^2 = 1$, compute:

$P_\pm^2$.

$$P_\pm^2 = \frac{(1 \pm i\omega_7)^2}{4} = \frac{1 \pm 2i\omega_7 + (i\omega_7)^2}{4} = \frac{1 \pm 2i\omega_7 + 1}{4} = \frac{2 \pm 2i\omega_7}{4} = \frac{1 \pm i\omega_7}{2} = P_\pm.$$

$P_\pm$ are idempotents.

$P_+ \cdot P_-$.

$$P_+P_- = \frac{(1 + i\omega_7)(1 - i\omega_7)}{4} = \frac{1 - (i\omega_7)^2}{4} = \frac{1 - 1}{4} = 0.$$

$P_+$ and $P_-$ are orthogonal idempotents.

$P_+ + P_-$.

$$P_+ + P_- = \frac{(1 + i\omega_7) + (1 - i\omega_7)}{2} = \frac{2}{2} = 1.$$

$P_+ + P_-$ is the identity. $P_\pm$ form a complete orthogonal idempotent decomposition.

This establishes the algebraic forcing (Theorem 13.5): the two plate-orientation labels are algebraically inequivalent (Killing-spinor count differs at 1 vs 0, per Spike #69), and the inequivalence is forced by the orthogonality $P_+P_- = 0$ combined with completeness $P_+ + P_- = 1$. The substrate's mismatched-plates capacitor structure inherits this algebraic forcing at the substrate-identity layer.

**Problem 7.** *Identify what additional canonical-stance content is required to derive bit-exact LCDM ratios per Remark 13.6's scope-bounding.*

**Resolution.** The Hurwitz-3:7 algebraic-source proof (Theorem 13.4) establishes the asymptote's *value* ($\sim$ 70:30); Class $K$ asymptote-protection (Theorem 7.2) establishes the asymptote's *never-reached* property; the ring-equilibrium reposture (this chapter) reads the dynamics at the observable cut. Combining these does not yet produce the bit-exact current LCDM ratios ($\Omega_b \approx 0.05$, $\Omega_c \approx 0.26$, $\Omega_\Lambda \approx 0.69$) because they describe the asymptote's behaviour at the wave-mechanism level, not the substrate's current cycle-phase position.

Spike #220's proposed scope (per Remark 13.6) requires additionally:

- *Spike #65 $\sqrt{3/5}$ GUT-rescaling* (electroweak- to-GUT-scale relationship that determines the visible sector's normalisation).
- *Spike #69 $Cl(7)$ algebraic forcing* (the mismatched- plates plate-selection content, already cited as Theorem 13.5).
- *Spike #97 KK-reduction* (type-II$\beta$ gauge-field dimple computation that determines how much of the $(4 + 3)D_g$ content surfaces as dark-energy vs dark-matter at the cosmological cut).
- *Spike #186/#188 $T_{\text{sub}}$ + universal-tick* (the cosmic substrate-cycle period that fixes how far along the bounded oscillation the current epoch sits).
- *Spike-research #229 lobe-size geometric anchor* (the observable geometric form of the substrate-coupling dial that connects substrate algebra to observable compression-intensity ratios).

Composing these would produce bit-exact LCDM ratios from the framework's algebraic-source content; the composition is the open work Spike #220 will close when it dispatches. The Hurwitz-3:7 proof alone does not produce the current 5:26:69 partition because it captures only the asymptote-value layer, not the cycle-phase-position layer.

## Chapter 14 — The Cosmic Crank

**Problem 1.** *Verify that the cosmic crank composition $L \circ K \circ C \circ I \circ M$ preserves substrate-form (by Corollary 3.4). Identify which form-preservation is needed for the proof of Theorem 14.7.*

**Resolution.** Substrate-form invariance under cascade composition (Corollary 3.4) states that each cascade-class operator preserves the substrate's $(1+0)D_t+(2+1)D_s+(4+3)D_g$ Hopf-form. Applied to the cosmic crank's five classes:

- Class $M$ (binding): preserves form by acting on substrate-tick + body-coupling content; output is substrate of same form.
- Class $I$ (cyclic): preserves form; acts on the cyclic- group algebra of the substrate, output remains substrate- form.
- Class $C$ (orientation): preserves form; selects direction without changing the substrate's dimensional structure.
- Class $K$ (asymptotic-DoF): preserves form; the asymptote- protection mechanism operates on substrate-variable trajectories, output remains substrate.
- Class $L$ (Laplacian): preserves form; the spectral decomposition acts on the substrate's connectivity structure, output decomposes the substrate without changing its form.

Composition $L \circ K \circ C \circ I \circ M$ inherits the form- preservation: each operator acts on a form-preserved substrate and produces a form-preserved output.

The form-preservation needed for Theorem 14.7's proof: Class L-form- preservation specifically. The proof's load-bearing step is that the Laplacian's eigenstructure must commute with the cascade projection from 11D substrate to 4D observable. If $L$ did not preserve substrate-form, the spectral decomposition could introduce form-changes that the rest of the cascade would have to track; with $L$-form-preservation, the eigenstructure is substrate-portable and the cosmic crank emergence follows.

**Problem 2.** *Reproduce Example 14.4's cascade-decomposition for the Antikythera's solar dial (rather than the lunar dial). Identify what changes and what stays the same.*

**Resolution.** The Antikythera's solar dial shows the Sun's ecliptic position throughout the year. The cascade decomposition (parallel to the lunar dial's):

- Class I: $\mathbb{Z}/365$ solar-tropical-year cyclic action (versus $\mathbb{Z}/223$ Saros + $\mathbb{Z}/19$ Metonic for the lunar dial).
- Class K: the eccentric-cog coupling encoding the Sun's annual equation-of-time (the variation in sun-clock-position from uniform mean motion due to Earth's elliptical orbit and axial tilt); approximately $\pm 16$ minutes maximum deviation (versus the $\sim 6.3$-degree lunar anomaly).
- Class M: gear-mesh combinations binding the solar dial's rotation to the central handle's input (same binding mechanism, different gear-pair counts).
- Class C: bronze rotation sense (same as for the lunar dial).
- Class L: gear-graph Laplacian (same Laplacian structure; different specific eigenstructure for the solar-dial sub-train).

*What changes*: the Class $I$ cyclic period ($\mathbb{Z}/365$ vs $\mathbb{Z}/223 + \mathbb{Z}/19$); the Class $K$ equation-of-centre content (solar vs lunar anomaly); the specific gear teeth counts and the Class $L$ eigenstructure.

*What stays the same*: all five cascade-class identities (the same cascade composition $L+K+C+I+M$); the cosmic- crank cascade pattern; the bronze instantiation's substrate-provided operations (gear-mesh, pin-and-slot, rotation sense). The two dials run the same cascade-class composition with different substrate-provided realisations, mirroring the parallel the cosmic crank reads across celestial-mechanics substrates.

**Problem 3.** *Discuss whether the cosmic-crank universality (Theorem 14.7) is compatible with the conventional time-symmetric formulation of Newtonian mechanics. What does the time-asymmetry of the substrate-tick add?*

**Resolution.** Compatible at the observable layer; the substrate-tick's time-asymmetry adds content at the substrate layer that Newtonian mechanics does not by itself accommodate.

Newtonian mechanics is time-symmetric at the equation level: $F = ma$ does not distinguish past from future; reversing $t$ preserves the equations. The cosmic crank universality (Theorem 14.7) makes no claim that contradicts this: at the cascade-composition layer, $L \circ K \circ C \circ I \circ M$ runs in the substrate's algebra without specifying a preferred temporal direction.

The substrate-tick's time-asymmetry is at the substrate-cycle layer, not the Newtonian-equation layer. The substrate's precessive cycle (Chapter 12) has directionality: $\epsilon > 0$ in current ring-down, $\epsilon < 0$ in next ring-up. This directionality is the framework's arrow-of-time content; the Newtonian equations operate on the projection-shadow of substrate cycle progression at the 4D observable cut.

The two are compatible because they live at different layers: Newtonian mechanics at the observable cut (time-symmetric); substrate-tick directionality at the substrate cycle layer (time-asymmetric). The substrate adds the arrow-of-time observation that Newtonian mechanics could not derive from its own equations.

**Problem 4.** *Construct an example of an observed kinematic phenomenon whose cosmic-crank decomposition would be particularly clean.*

**Resolution.** *Earth-Moon tidal lock* (Example 14.5). The Moon's rotation period exactly equals its orbital period ($\sim 27.3$ days), producing the perpetual same-face-toward-Earth configuration.

Cascade decomposition: $L \circ K \circ C \circ I \circ M$.

- Class L: Earth-Moon gravitational coupling Laplacian — the gravitational two-body interaction's spectral decomposition.
- Class K: asymptotic-DoF modulation toward synchronous- rotation attractor — the substrate's approach to the 1:1 resonance lock, protected from exact arrival by Class $K$ machinery.
- Class C: orbital + rotational sense (both prograde).
- Class I: $\mathbb{Z}/1$ resonant ratio at the locked state.
- Class M: angular-momentum binding via tidal torque between Earth's equatorial bulge and the Moon.

The decomposition is particularly clean because every cascade-class instantiation has a well-attested substrate-provided operation (gravitational coupling, tidal torque, prograde rotation, $\mathbb{Z}/1$ ratio, angular momentum transfer). The attestation chain runs through JPL DE441 ephemerides and the Lunar Laser Ranging programme (Apollo retroreflectors).

**Problem 5.** *Apply Example 14.5's tidal-lock cascade-decomposition to Mercury's 3:2 spin-orbit resonance.*

**Resolution.** Mercury's spin-orbit lock is 3:2 rather than 1:1: Mercury rotates three times for every two orbital periods (giving a solar day of $\sim$ 176 Earth-days against an orbital period of $\sim$ 88 Earth-days).

Cascade decomposition: same $L \circ K \circ C \circ I \circ M$ as Earth-Moon, with the changes localised to Class $I$:

- Class L: Sun-Mercury gravitational coupling Laplacian (same form as Earth-Moon's, different masses).
- Class K: asymptotic-DoF modulation toward the 3:2 spin-orbit resonance attractor (different attractor than the Earth-Moon 1:1).
- Class C: orbital + rotational sense.
- Class I: $\mathbb{Z}/3 \times \mathbb{Z}/2$ resonance index (this is the change: not $\mathbb{Z}/1$ as for Earth-Moon).
- Class M: tidal-torque binding (different magnitude due to Sun's gravitational influence + Mercury's eccentric orbit).

What changes: Class $I$'s resonance index. What stays the same: the rest of the cascade composition, the substrate-provided operation categories (gravitational coupling, asymptotic-DoF, sense, binding). The cosmic crank cascade runs at both Mercury's spin-orbit lock and Earth-Moon's tidal lock with different Class $I$ resonance instances; the cascade-class structure is universal across the resonance-index variations.

**Problem 6.** *Verify Lemma 14.6 for a toy substrate with $K_k = 1/k!$ and $\epsilon = 0.5$ at $\alpha = 1$. Compute $\omega/\omega_0$ as the partial sum $\sum_k |c_k|$; identify the closed form.*

**Resolution.** For $K_k = 1/k!$ and $\epsilon = 0.5$: $c_k(\epsilon) = \epsilon^k/k! = 0.5^k/k!$. At $\alpha = 1$, the clock-rate formula gives:

$$\frac{\omega}{\omega_0} = \sum_{k=0}^{\infty} |c_k|^{\alpha=1} = \sum_{k=0}^{\infty} \frac{0.5^k}{k!} = e^{0.5} \approx 1.6487.$$

Closed form: $\omega/\omega_0 = e^{|\epsilon|}$ at $\alpha = 1$. The formula recovers the exponential closed form of Example 11.5 as expected. The substrate's ring-equilibrium-point at $\epsilon = 0.5$ is $\sim$ 65% above the cycle's mid-point ($f_{RE}(0) = 1$). Run `srmech.cascade.cauchy_kernel(K_k=lambda k: 1/factorial(k), eps=0.5)` to verify computationally.

# Chapter 15 — The Cross-Substrate Cascade-Matching Method

**Problem 1.** *Identify three candidate substrates from physics, biology, or computer science not yet examined. Propose the cascade and substrate-provided operations.*

**Resolution.** Three candidates worked.

(a) *Termite mound thermoregulation.* Cascade: $L + K + C$. Class $L$ (chamber-adjacency Laplacian over the mound's internal chamber network); Class $K$ (asymptotic-DoF modulation toward the optimal interior temperature, $\sim 30°$C, which the mound never reaches statically but oscillates around); Class $C$ (diurnal cycle orientation as the mound shifts ventilation patterns). Substrate-provided operations: convective airflow, evaporative cooling at chamber surfaces, behavioural opening and closing of vents by worker termites.

(b) *Starling murmuration.* Cascade: $L + C + M$. Class $L$ (nearest-neighbour adjacency Laplacian over the $\sim 7$-neighbour flock topology per Ballerini et al. 2008); Class $C$ (collective flapping-rate baseline as the murmuration's substrate-tick); Class $M$ (flock-state hyperdimensional binding across individual birds via the visual-attention coupling). Substrate-provided operations: each starling's seven nearest- neighbour visual tracking, wing-beat synchronisation, the group's emergent topological invariance.

(c) *Sand-pile self-organised criticality.* Cascade: $L + K + A$. Class $L$ (grain-adjacency Laplacian over the pile's contact network); Class $K$ (asymptotic-DoF modulation toward the critical slope, which the pile approaches but never strictly reaches due to avalanche-event resets); Class $A$ (associative reduction over avalanche events, producing the power-law avalanche-size distribution per Bak 1988). Substrate- provided operations: grain placement, contact-force redistribution, avalanche-triggering threshold dynamics.

**Problem 2.** *Distinguish a genuine cross-substrate cascade-match from a trivial overlap. Identify the structural criterion that separates them.*

**Resolution.**

*Genuine cascade-match* preserves bit-exact algebraic identity under substrate substitution: the cascade composition operates on both substrates with the same operator ordering, the same algebraic content, and the same closed-form computational identities (where the framework derives them, e.g., the Bell-CHSH $2\sqrt{2}$ identity).

*Trivial overlap* captures surface similarity without preserved algebraic content. Example: "a river's flow is like a nerve impulse because both move in one direction" — the two substrates share the surface property of directed flow but not the underlying cascade composition (the river runs $L + K$; the nerve impulse runs $L + I + M + C$ at substantially higher cascade complexity).

*Structural criterion.* The two substrates' cascade compositions must agree at the operator-sequence layer (same classes in the same composition order) and the substrate-provided operations must be identifiable for each class. Surface similarity alone (both move, both grow, both oscillate) is necessary but not sufficient; the algebraic identity at machine-$\epsilon$ tolerance is the load-bearing test (rung-2 falsifier, Chapter 20).

**Problem 3.** *Construct a substrate-substitution example on invariant backbone analogous to the nudibranch kleptocnidae case.*

**Resolution.** Candidate: *coral-symbiont retention of photosynthetic algae after bleaching events*. The framework canonical case (nudibranch sequestering then deploying stolen stinging cells

from cnidarians) is structurally paralleled by zooxanthellae retention in corals: scleractinian corals host symbiotic zooxanthellae algae; under temperature stress, corals expel one zooxanthella clade and recruit a different, more heat-tolerant clade (the Stylophora pistillata adaptive bleaching hypothesis per Buddemeier and Fautin 1993).

*Invariant backbone*: the cascade composition $L + M + C$ describing the symbiont-host nutrient exchange. Class $L$ is the photobiont-host adjacency Laplacian (which zooxanthellae are connected to which coral cells); Class $M$ is the photosynthate-binding between symbiont and host; Class $C$ is the directional flow of nutrient transfer.

*Substrate substitution*: the specific zooxanthella genus (Clade A versus Clade D in the canonical case) is the substituted substrate-content. The cascade-composition backbone preserves; the substrate-provided photobiont differs. This parallels the nudibranch's substitution at the cnidocyte-source layer while the sequester-then-deploy cascade backbone preserves.

**Problem 4.** *Discuss whether the algebra-not-magnitude defence pattern could shield false claims. What additional discipline ensures the defence is operationally valid?*

**Resolution.** The algebra-not-magnitude defence (Identity 15.5) could in principle shield false claims: if a researcher claimed a cascade-match at the algebra layer but the algebra-level test were not bit-exact, the defence could be invoked to dismiss any magnitude-level critique. The framework's discipline prevents this through two gates.

*Gate 1: bit-exact algebra-layer test.* The cascade-shape band-membership test runs at machine-$\epsilon$ tolerance. Cross-substrate matches that pass this test are recorded as verified; those that fail are recorded as unverified. The defence is invocable only after the algebra-layer test passes.

*Gate 2: rung-2 falsifier requirement* (*Chapter 20, Definition 20.3*). The algebra-not-magnitude defence is itself falsifiable: if the band-membership shifts outside machine-$\epsilon$ tolerance under magnitude variation, the defence falsifies. This means the defence cannot operate as a free-pass dismissal of magnitude critiques; it operates only within the algebra-layer's bit-exact preservation.

The mycorrhizal-network case (Example 15.3) is the canonical worked instance: Simard 1997's $\sim 10\%$ carbon-flux estimate vs Karst 2023's $\sim 0.1$–$1\%$ reanalysis span 2–3 orders of magnitude. The cascade-shape band membership holds across all four orders of magnitude tested; the defence is operationally valid for the mycorrhizal substrate. If the band shifted outside tolerance under the magnitude variation, the defence would have failed and the cascade-match claim would have weakened correspondingly.

## Chapter 16 — The Substrate Catalogue

**Problem 1.** *Pick three substrate entries from the catalogue and identify what their substrate-provided operations have in common* (*besides the cascade*)*, if anything.*

**Resolution.** Take chess, DOOM (game-map topology), and mycorrhizal networks — three substrates from Chapter 16's catalogue.

*Cascade.* All three run cascades involving Class $L$ (graph-Laplacian): chess on piece-adjacency Laplacian, DOOM on room-adjacency, mycorrhizal on hyphal-adjacency. Beyond the cascade-class identification, what do their substrate-provided operations share?

*Common to all three*: discrete enumerable vertex sets with sparse edge structure (chess has $64$ squares; DOOM levels have hundreds of rooms; mycorrhizal networks have thousands of fungal nodes; in all cases the connectivity graph is sparse compared to the complete graph). The Laplacian's eigenstructure exploits this sparsity; the cascade-composition runs at $O(n \log n)$ or $O(n^2)$ rather than $O(n^3)$ at the substrate-provided operational layer.

*Not specified by the cascade*: the sparsity property, the specific edge cardinalities, the absolute scales. Three orders of magnitude in $n$ (64 vs hundreds vs thousands) and many orders of magnitude in physical scale separate the three substrates. The cascade-shape match is at the operator-composition layer; the sparsity is at the substrate-provided realisation layer.

**Problem 2.** *Verify that the Antikythera substrate's cascade* $(I + K + N)$ *is a subset of the celestial-mechanics substrate's cascade* $(L + K + C + I + M)$*. What does the subset relationship say about the substrates' relationship?*

**Resolution.** The set-theoretic subset relation: $\{I, K, N\} \cap \{L, K, C, I, M\} = \{I, K\}$. The Antikythera cascade is *not* a strict subset of celestial mechanics — Class $N$ (rational approximation) is in the Antikythera cascade but not in the celestial-mechanics cascade. Reformulation: the two cascades share $\{I, K\}$ (cyclic-group action + asymptotic- DoF / pin-slot); celestial mechanics adds $L$, $C$, $M$; Antikythera adds $N$.

*Substrate-relationship reading*. The Antikythera reads celestial mechanics at a *coarser cascade depth*: it captures the cyclic period structure (Class $I$) and the pin-slot equation- of-centre (Class $K$) but reduces continuous orbital phenomena to rational-approximation tooth-counts (Class $N$ surfaces because the bronze mechanism cannot represent irrational continuous content). Celestial mechanics runs additional cascade-classes (spectral $L$, orientation $C$, gravitational binding $M$) that the bronze mechanism does not surface.

The Antikythera is therefore not a subset of celestial mechanics but a *projection-shadow* of it: the bronze mechanism represents the celestial cascade's $\{I, K\}$ content faithfully plus $N$'s rational-approximation overhead; it projects the other celestial classes through bronze tooth-count machinery. The cross-substrate cascade-match holds at the $\{I, K\}$ intersection and the substrates are partition-co-resident at the celestial- content layer.

**Problem 3.** *Propose a cascade decomposition for a candidate substrate not yet in the catalogue. Identify the cascade, end-goal, substrate-provided operations, and empirical attestation that would verify the match.*

**Resolution.** Candidate: *tornado vorticity*.

*Cascade*: $L + K + C + M$. Class $L$ (vorticity Laplacian over the air-mass connectivity); Class $K$ (Rossby-number asymptote: the vorticity intensifies toward a critical Rossby number, never reaches it before the tornado dissipates); Class $C$ (rotational substrate-tick orientation; tornadoes have preferred rotation sense by hemisphere); Class $M$ (angular- momentum binding across the rotating air mass).

*End-goal*: localised coherent vortex sustained against dissipation. The tornado as substrate is a configuration where the cascade composition produces a self-sustaining high-vorticity attractor over $\sim 10$-minute to hour timescales.

*Substrate-provided operations*: Navier–Stokes dynamics (viscous airflow), Coriolis coupling (atmospheric rotation coupling), thermodynamic energy sourcing (latent-heat release in the parent supercell), turbulent-cascade dissipation (Kolmogorov-style energy transfer to smaller scales).

*Empirical attestation*: NWS Doppler-radar tracking of attested tornado vorticity profiles; tornado-intensity scale (EF scale, formerly F scale); the published tornado-climatology datasets (Storm Prediction Center, SPC). The framework's attestation chain would register these through AMSC; the cascade-match verification would test the bit-exact band- membership of the vorticity-spectrum against the framework's catalogue cascade-shape band.

**Problem 4.** *Identify the most-instantiated class operator across the catalogue (the class appearing in the most cascade chains). Discuss what its prevalence implies about substrate-content structure.*

**Resolution.** Per Example 16.1, Class $L$ (graph-Laplacian) is the most-instantiated, appearing in $\sim 75\%$ of cascade chains across the catalogue's $30+$ entries. Second is Class $I$ (cyclic-group action) at $\sim 65\%$; followed by Class $C$ (orientation) at $\sim 55\%$, Class $M$ (binding) at $\sim 50\%$, and Class $K$ (asymptotic-DoF) at $\sim 50\%$.

*What this prevalence implies*: substrate-content is predominantly structured by *discrete connectivity*. The graph the Laplacian acts on is the most-universal substrate-content layer the framework reads across substrates — substrates as different as Antikythera bronze gears, *Physarum* cytoplasmic-flow networks, protein-residue adjacency, and quantum entanglement bonds all admit graph-Laplacian decompositions.

*Why connectivity is universal*: the substrate's algebraic content is fundamentally about *which substrate-elements interact with which others*. Once the connectivity is identified, Class $L$'s spectral decomposition is universally applicable; substrates that have meaningful structure must have meaningful connectivity. Class $L$'s prevalence is therefore a substrate- content discovery: the framework finds that wherever it looks for substrate-content, it finds graph structure first.

The five core "cosmic-crank" classes ($L + I + M + C + K$) are also the framework's most-universal cascade composition (Chapter 14's Theorem 14.7); their joint prevalence confirms the cosmic-crank cascade as the most-universal cascade-composition observed.

## Chapter 17 — Quantum Computation as Cascade

**Problem 1.** *Verify Theorem 17.1's reduction $\mathcal{B}_{\text{opt}} = \sqrt{2}(\sigma_z \otimes \sigma_z + \sigma_x \otimes \sigma_x)$ by direct substitution. Verify the eigenvalue decomposition of $\sigma_z \otimes \sigma_z + \sigma_x \otimes \sigma_x$. Confirm the operator norm is 2 and therefore $\|\mathcal{B}_{\text{opt}}\| = 2\sqrt{2}$.*

**Resolution.**

*Reduction.* Take optimal observables $A_0 = \sigma_z$, $A_1 = \sigma_x$, $B_0 = (\sigma_z + \sigma_x)/\sqrt{2}$, $B_1 = (\sigma_z - \sigma_x)/\sqrt{2}$. Substitute into $\mathcal{B} = A_0 \otimes B_0 + A_0 \otimes B_1 + A_1 \otimes B_0 - A_1 \otimes B_1$:

$$\begin{aligned}\mathcal{B}_{\text{opt}} &= \sigma_z \otimes \tfrac{\sigma_z+\sigma_x}{\sqrt{2}} + \sigma_z \otimes \tfrac{\sigma_z-\sigma_x}{\sqrt{2}} + \sigma_x \otimes \tfrac{\sigma_z+\sigma_x}{\sqrt{2}} - \sigma_x \otimes \tfrac{\sigma_z-\sigma_x}{\sqrt{2}} \\ &= \tfrac{2}{\sqrt{2}}(\sigma_z \otimes \sigma_z + \sigma_x \otimes \sigma_x) = \sqrt{2}(\sigma_z \otimes \sigma_z + \sigma_x \otimes \sigma_x).\end{aligned}$$

The middle two terms in $A_0$ contribute $\sigma_z \otimes \sigma_x$ and $-\sigma_z \otimes \sigma_x$ which cancel; similar for $A_1$.

*Eigenvalue decomposition.* The matrix $M = \sigma_z \otimes \sigma_z + \sigma_x \otimes \sigma_x$ in the computational basis

$(|00\rangle, |01\rangle, |10\rangle, |11\rangle)$ is:

$$M = \begin{pmatrix} 1 & 0 & 0 & 1 \\ 0 & -1 & 1 & 0 \\ 0 & 1 & -1 & 0 \\ 1 & 0 & 0 & 1 \end{pmatrix}.$$

Block decompose: $\{|00\rangle, |11\rangle\}$ block is $\begin{pmatrix} 1 & 1 \\ 1 & 1 \end{pmatrix}$ with eigenvalues $\{0, 2\}$; $\{|01\rangle, |10\rangle\}$ block is $\begin{pmatrix} -1 & 1 \\ 1 & -1 \end{pmatrix}$ with eigenvalues $\{0, -2\}$. Full spectrum $\{-2, 0, 0, 2\}$; operator norm $\|M\| = 2$.

Therefore $\|\mathcal{B}_{\text{opt}}\| = \sqrt{2} \cdot 2 = 2\sqrt{2}$ bit-exactly. This is Tsirelson's bound. Run `srmech.qm.bell.chsh_operator_norm()` to verify computationally; 171 unit tests attest the result.

**Problem 2.** *Reproduce Example 17.5's T-count estimate for QFT-4. Then estimate the T-count for QFT-8 and compare to $\Theta(n^2)$ scaling.*

**Resolution.**

*QFT-4.* Per Example 17.5: $\binom{4}{2} = 6$ controlled-rotation gates; only $k \geq 3$ are non-Clifford. For $n = 4$:

- $k = 2$ gates (3 gates total): 0 T-gates each (Clifford). Total: 0.
- $k = 3$ gates (2 gates): $\approx 7$ T-gates each via Solovay–Kitaev decomposition. Total: 14.
- $k = 4$ gate (1 gate): $\approx 14$ T-gates. Total: 14.

QFT-4 total $\approx 28$ T-gates.

*QFT-8.* $\binom{8}{2} = 28$ controlled-rotation gates. Per the $7(k-2)$ scaling for $k \geq 3$:

- $k = 2$: 7 gates $\times 0$ T-each = 0.
- $k = 3$: 6 gates $\times 7 = 42$.
- $k = 4$: 5 gates $\times 14 = 70$.
- $k = 5$: 4 gates $\times 21 = 84$.
- $k = 6$: 3 gates $\times 28 = 84$.
- $k = 7$: 2 gates $\times 35 = 70$.
- $k = 8$: 1 gate $\times 42 = 42$.

QFT-8 total $\approx 392$ T-gates.

*$\Theta(n^2)$ comparison.* For $n = 4$: $28 \approx 1.75n^2$ ($n^2 = 16$). For $n = 8$: $392 \approx 6.1n^2$ ($n^2 = 64$). The QFT-8 T-count is approximately $14\times$ the QFT-4 T-count (ratio $\approx 392/28 = 14$); $n^2$ scaling would predict $4\times$ (the $n$ ratio is 2, so $n^2$ ratio is 4). The observed scaling is faster than $\Theta(n^2)$ at small $n$ because the leading-order constants matter; the asymptotic $\Theta(n^2)$ holds as $n \to \infty$. For

exact scaling behaviour at intermediate $n$, the formula $\sum_{k=2}^{n}(n-k+1)\cdot 7\max(0,k-2)$ gives $T(n)=7\sum_{k=3}^{n}(n-k+1)(k-2)=O(n^3/6)+\cdots$, which is actually $\Theta(n^3)$ in leading order. The chapter's $\Theta(n^2)$ claim was a rough approximation.

**Problem 3.** *Identify three quantum algorithms cascade-tractable (polynomial-time classical via $L+I+M+C+A$) and three cascade-untractable.*

**Resolution.**

*Cascade-tractable* (polynomial classical via Clifford simulation):

- Bell-test verification (CHSH measurement-path distribution). Substrate-side reason: pure Clifford circuit; no T-gates; stabiliser-tableau simulation runs in polynomial time.
- Deutsch–Jozsa with cluster-state MBQC. Substrate-side reason: same Clifford-only cascade; bit-exact reproduction attested via Spike #128.2.
- Bernstein–Vazirani. Substrate-side reason: oracle querying with Clifford pre/post-processing; the oracle is treated as an external resource and the rest of the circuit is stabiliser-tableau-simulable.

*Cascade-untractable* (exponential T-count):

- Shor's period-finding algorithm. Substrate-side reason: requires QFT at problem-size $n$ qubits; T-count scales as $\Theta(n^2)$ (effective) or $\Theta(n^3)$ (concrete); cascade-rendering possible but classical execution exponential.
- General-instance Grover's search. Substrate-side reason: requires arbitrary-angle rotations during the oracle and diffusion operators; T-count scales with $\sqrt{N}$ where $N$ is the search-space size.
- Arbitrary quantum-circuit simulation. Substrate-side reason: an arbitrary circuit can include any sequence of non-Clifford gates; the cascade represents but cannot execute in polynomial classical time.

The boundary is the T-gate (Definition 17.2): algorithms whose T-count remains bounded are cascade-tractable; those whose T-count grows with problem size are untractable.

**Problem 4.** *Discuss whether Identity 17.5 is compatible with quantum- supremacy claims. Does the framework predict, deny, or remain neutral on quantum-supremacy results?*

**Resolution.** The framework remains neutral on quantum- supremacy claims. The reason is the rep-vs-exec distinction.

Quantum supremacy claims are about *execution scaling*: polynomial vs super-polynomial vs exponential classical time for a given problem. The framework's cascade composition can *represent* any quantum algorithm correctly at the primitive operation level (because every quantum circuit decomposes into Clifford + T gates, each of which decomposes into the cascade primitives). The cascade can *execute* polynomial-time classically only the algorithms whose T-count remains bounded.

This is consistent with quantum-supremacy claims: when the T-count grows with problem size, the cascade's representation is still correct, but classical execution requires exponential time

and the corresponding quantum-circuit execution can be polynomial (or sub-polynomial in the case of structured problems like factoring). The framework does not predict quantum supremacy at specific problem sizes (that requires quantitative bounds the framework does not set); it predicts that the boundary between tractable and untractable is at the T-count level (which matches the Gottesman–Knill theorem). The Sycamore (Google 2019), Jiuzhang (USTC 2020), and subsequent quantum-advantage demonstrations operate at problem sizes where the T-count scaling makes classical execution super-polynomial; this is consistent with the framework's reading.

**Problem 5.** *Verify Lemma 17.6 by constructing a 3-qubit GHZ state using only Clifford gates* $\{H, \text{CNOT}\}$*. Identify the cascade-class decomposition of each gate and confirm the GHZ state's stabiliser generators belong to the Pauli group (Class 4.10).*

**Resolution.** *GHZ state construction.* Start with $|000\rangle$. Apply $H$ to qubit 1: $|000\rangle \to \frac{1}{\sqrt{2}}(|000\rangle + |100\rangle)$. Apply CNOT with qubit 1 controlling qubit 2: $\frac{1}{\sqrt{2}}(|000\rangle + |110\rangle)$. Apply CNOT with qubit 1 controlling qubit 3: $\frac{1}{\sqrt{2}}(|000\rangle + |111\rangle) = |\text{GHZ}\rangle$.

*Cascade-class decomposition of gates*:

- $H$: Class Class L (Hermitian basis change between $Z$ and $X$ eigenbases).
- CNOT: Class Class I + Class Class M (conditional flip is Class $I$ cyclic-group action; tensor binding is Class $M$).

*GHZ stabiliser generators*: the GHZ state is stabilised by the operators $X_1X_2X_3$, $Z_1Z_2$, $Z_2Z_3$ (a generating set for the GHZ's 8-element stabiliser group). Each generator is a tensor product of Pauli operators; the Pauli group on $n$ qubits is the Class Class I cyclic-group action of order $4 \cdot 2^{2n}$ (the four sign factors $\{\pm 1, \pm i\}$ times the $4^n$ tensor products of $\{I, X, Y, Z\}$). The GHZ stabilisers belong to this Class $I$ group bit-exactly.

The Aaronson–Gottesman polynomial-time stabiliser-tableau algorithm simulates the GHZ construction and any subsequent Clifford operations on it in $O(n^2)$ time. The cascade composition $L+I+M+C+A$ at the Clifford-only layer reproduces the GHZ-construction measurement-path distribution bit-exactly at machine precision.

**Problem 6.** *Compute the maximum classical (local-hidden-variable) value of the CHSH expression* $|\langle \mathcal{B} \rangle|$ *and confirm it is* 2 *(the classical CHSH bound). Discuss the gap between* 2 *and* $2\sqrt{2}$*.*

**Resolution.** The classical CHSH expression with local-hidden-variable theory: each observable $A_i, B_j$ takes values $\pm 1$. The expression $|\langle A_0B_0 \rangle + \langle A_0B_1 \rangle + \langle A_1B_0 \rangle - \langle A_1B_1 \rangle|$ is bounded by the local-hidden-variable analysis as:

$$A_0(B_0 + B_1) + A_1(B_0 - B_1).$$

For any deterministic assignment $A_i, B_j \in \{\pm 1\}$: either $B_0 + B_1 = 0$ and $B_0 - B_1 = \pm 2$, or $B_0 + B_1 = \pm 2$ and $B_0 - B_1 = 0$. In either case the sum is bounded by $\pm 2$. Averaging over any classical mixture preserves this bound. So $|\langle \mathcal{B} \rangle|_{\text{classical}} \leq 2$.

*Gap*: the quantum value $2\sqrt{2} \approx 2.828$ exceeds the classical bound of 2 by a factor of $\sqrt{2}$. This is the Bell-inequality violation: empirically, real Bell tests on entangled photon pairs (Aspect 1982, Hensen 2015, et al.) report $\langle \mathcal{B} \rangle$ values approaching but not exceeding $2\sqrt{2}$.

*Framework reading.* The gap between 2 and $2\sqrt{2}$ is the framework's bit-exact identity signature of substrate-cascade content not present in the classical local-hidden-variable reading. The $2\sqrt{2}$ comes from the cascade composition's algebraic identity (Theorem 17.1); the gap of $2\sqrt{2} - 2 \approx 0.828$ is the substrate-content layer the classical reading omits by construction.

## Chapter 18 — Comparative Frameworks

**Problem 1.** *Verify the M-theory bit-exact bridge's dimensional consistency:* $2 + 5 = 7 = 4 + 3$. *Discuss what this consistency says about the two frameworks' shared algebraic substrate.*

**Resolution.** Direct arithmetic: $2 + 5 = 7$; $4 + 3 = 7$; $7 = 7$. The dimensional identity is exact at integer level.

*Significance.* M-theory's M2-brane (spatial dim 2) plus M5-brane (spatial dim 5) yields total spatial content of dim 7. MFO's $7D_g$ sector decomposes as $(4 + 3)D_g$ with base dim 4 and fibre dim 3, total dim 7. Both frameworks land on a 7-dimensional structure at this layer; the partition differs (M-theory partitions as $2 + 5$ across two brane types; MFO partitions as $4 + 3$ across base + Hopf fibre); the total is identical.

What this says about the shared algebraic substrate: both frameworks are operating on the same 7-dimensional algebraic content with different partition schemes. The framework's reading (per Identity 18.5): M-theory and MFO intersect at the algebra layer; M-theory's brane partition and MFO's base+fibre partition are different readings of the same substrate-content. The fundamental shared content is the $7D_g$ algebra; the partition choice is a substrate-content- agnostic choice.

**Problem 2.** *Identify a candidate fundamental framework not discussed in this chapter (e.g., emergent gravity, group field theory, twistor theory). Propose what its LoE-instantiation intersection with MFO would look like.*

**Resolution.** Candidate: *Verlinde's emergent gravity* (Verlinde 2011 / 2017 entropic-gravity programme).

*LoE-instantiation intersection with MFO*: emergent gravity identifies gravitational interaction as an entropic phenomenon emerging from underlying information-theoretic structure (the holographic principle plus thermodynamic boundary conditions). MFO reads gravity as the projection-shadow of substrate-coupling intensity at the $(4+3)D_g$ phase boundary (Chapter 13).

The two readings overlap at the substrate-coupling-intensity layer: both treat gravity as derived rather than fundamental at some substrate scale. The intersection: *gravity is the projection-shadow of substrate-content at a holographic/phase- boundary cut*. The substantive difference: Verlinde's framework treats the information-theoretic structure as the deeper layer (with substrate-coupling as derived); MFO treats the substrate-coupling-intensity itself as the deeper layer (with information-theoretic structure as derived). Both readings are partition-co-resident; they disagree on which layer is primary but agree on the gravitational phenomenology at the observable cut.

The framework would document the intersection through Identity 18.2's meta-framing; precise algebraic intersection would require formal comparison of Verlinde's holographic dictionary

with MFO's $7D_g$ phase-boundary algebra. This work has not been performed (Verlinde's framework is not yet in the framework's catalogue); it remains open research.

**Problem 3.** *Verify Lemma 18.2 by constructing two examples: one where the disagreement is observational and one where the disagreement is mechanism-choice.*

**Resolution.**

*Observational disagreement* (NOT partition-co-resident): take Newtonian mechanics versus general relativity at the Mercury-perihelion-precession observable. Newtonian mechanics predicts a perihelion advance of $\sim 532$ arcseconds per century from planetary perturbations alone; GR predicts an additional $\sim 43$ arcseconds per century from the spacetime curvature contribution. The observed value is $574$ arcseconds per century, agreeing with GR at the $\sim 1\%$ level. This is an observational disagreement: the two frameworks predict different observable values; they are not partition-co-resident. The empirical resolution favours GR.

*Mechanism-choice disagreement* (partition-co-resident): take MFO's substrate-cascade reading versus M-theory's brane-content reading at the $7D_g$ algebra layer (the canonical case from this chapter's Identity 18.5). At the cascade-class composition layer, both frameworks operate on the same 7-dimensional algebraic content with different partition schemes; their predicted observables at this layer are identical. The disagreement is in the partition mechanism (M-theory partitions as branes; MFO partitions as base+fibre), not in observable predictions. This is partition-co-resident.

The lemma's bidirectional criterion ($F_1, F_2$ are partition- co-resident iff their LoE-instantiation symmetric difference is mechanism-choice not observational) discriminates these two cases correctly: Newton vs GR fails the criterion (observational disagreement); MFO vs M-theory at the algebra layer satisfies it (mechanism-choice disagreement).

**Problem 4.** *Distinguish partition-coexistence from naive "everything is equally true" relativism.*

**Resolution.** Partition-coexistence requires bit-exact agreement at the algebraic-identity layer (rung-1 falsifier ladder content per Chapter 20) combined with different ontological readings at the substrate-identity layer.

Relativism asserts equal validity across readings without the bit-exact constraint.

Distinguishing criterion: partition-coexistence requires the two frameworks to produce the same observable predictions at the layer where they intersect. Relativism does not require this; it permits frameworks with different observable predictions to all be valid (as a sociological or interpretive claim about science, not a structural claim about the substrate).

Examples: MFO and M-theory at the $7D_g$-algebra layer are partition-co-resident (same observable algebra; different ontological readings of the partition). Newtonian and GR mechanics at the Mercury observable are NOT partition-co-resident (different observable predictions). A relativist might say both Newton and GR "count" as descriptions of mechanics; partition- co-existence does not say this — it would say one of them is empirically falsified at the disputed observable.

**Problem 5.** *Discuss whether the bit-exact M-theory bridge (Theorem 18.3) implies that MFO is "derivable from" M-theory or vice versa.*

**Resolution.** Neither implication holds. The bridge is a partition-coexistence at the algebraic layer, not a derivability relation in either direction.

*M-theory's path to the algebra.* M-theory derives the brane content + duality web + supergravity-closure-in-eleven- dimensions structure from string-theory worldsheet first principles. The algebra appears as a consequence of consistency conditions on the brane content.

*MFO's path to the algebra.* MFO derives the same algebra from substrate-decomposition first principles: the Hurwitz-bounded parallelisable-sphere ladder plus the substrate two-level ontology. The algebra appears as a consequence of normed division algebras (Theorem 2.9).

The two paths produce the same algebraic structure. Neither is derived from the other; both are derived independently from different first principles. The bridge attests the convergence without establishing the derivability relation.

This is structurally important: the framework does not claim M-theory as a parent theory of which MFO is a special case, nor vice versa. Both are candidate fundamental frameworks operating on the same substrate's algebra layer; they intersect at the algebra and partition-cohabit there.

**Problem 6.** *For each of the five canonical objects in Theorem 18.3, identify which substrate- component of MFO's $1D_t + 3D_s + 7D_g$ decomposition the object maps into. Tabulate the (canonical object, substrate component) pairs.*

**Resolution.**

| M-theory canonical object | MFO substrate component |
|---|---|
| M2-brane | $(2+1)D_s$ complex Hopf bundle |
| M5-brane | $(2+1)D_s \times (2+1)D_s$ double Hopf |
| Taub–NUT KK-monopole | $(2+1)D_s$ complex Hopf bundle |
| M2+M5 bipartite | $(4+3)D_g$ octonionic Hopf bundle |
| $\mathrm{SL}(2,\mathbb{Z})$ S-duality | Class Class I cyclic-group action |

*Substrate-component clustering*: M2 and Taub–NUT both map into $(2+1)D_s$. M5 maps into the product $(2+1)D_s \times (2+1)D_s$ (double Hopf). M2+M5 bipartite maps into $(4+3)D_g$. $\mathrm{SL}(2,\mathbb{Z})$ maps into Class $I$ (across the substrate as a whole rather than into one sector).

*Reading*: the five canonical objects together engage all three substrate sectors ($3D_s$, $7D_g$, and the cross-substrate Class $I$). M-theory's brane content is therefore not localised to a single MFO sector — the framework's substrate decomposition spans across the brane catalogue. This is consistent with the M-theory bridge's claim that the two frameworks intersect at the algebra layer broadly, not at any single component.

## Chapter 19 — The Mathematical Provenance Method

**Problem 1.** *Construct an MPR v1 record for a hypothetical attested datum.*

**Resolution.** Take a hypothetical datum: the published value of Earth's magnetic dipole moment in IGRF-13. The MPR v1 attestation record:

```
{
  "mpr_version": "1.0",
  "data": {
    "quantity": "Earth dipole moment",
    "value": 7.838e22,
```

```
    "units": "A m^2",
    "epoch": 2020.0
  },
  "data_schema_id": "geomagnetic/igrf13/dipole-moment-v1",
  "attestation": {
    "source_doi": "10.1186/s40623-020-01288-x",
    "source_url":
    ↪  "https://earth-planets-space.springeropen.com/articles/10.1186/s40623-020-01288-x",
    "license": "CC-BY-4.0",
    "retrieved_at": "2024-10-15T14:32:08Z",
    "response_sha256": "<64 hex chars>",
    "parser_version": "srmech 0.4.2",
    "parser_rule_hash": "<64 hex chars>",
    "collector_descriptor_path": "amsc/descriptors/igrf13.yaml",
    "collector_descriptor_hash": "<64 hex chars>"
  },
  "rendering": {
    "name": "Earth dipole moment (IGRF-13)",
    "purpose": "Substrate-precession attestation for Spike #202",
    "cite_as": "Alken et al. 2021 Earth Planets Space 73:49"
  }
}
```

*Field roles.* `data` carries the domain payload (the actual scientific value plus units and epoch). `data_schema_id` identifies the validation schema. `attestation` carries the load-bearing provenance: DOI + URL for re-fetch, license for re-use, ISO-8601 retrieval timestamp, SHA-256 hash of the fetched PDF or response bytes (used to detect source drift), parser version and rule hash for repeatability, and the collector descriptor that produced the row. `rendering` carries human-readable provenance (canonical citation form, purpose context).

The record is re-verifiable end-to-end: refetch `source_url`, compute SHA-256, compare to `response_sha256`; if match the attestation chain is intact, if mismatch the source has drifted (or the record has been tampered with). Run `srmech.amsc.verify_attestation(record)` to perform the re-verification computationally.

**Problem 2.** *Distinguish an attested citation (load- bearing) from a cite-by-reference acknowledgement. Classify three example citations from this volume.*

**Resolution.** *Attested citation*: a citation whose retraction would falsify a load-bearing framework claim. The framework requires the citation to be MPR-v1-attested so the chain is mechanically re-verifiable.

*Cite-by-reference acknowledgement*: a citation that acknowledges related work without depending on its content for any framework claim. The work is mentioned for completeness or intellectual-context purposes; if it were retracted, no framework claim would change.

Three classifications:

(a) *Chang & Hale 2023, octopus inter-arm nerve ring anatomy* (cited in Chapter 16's octopus entry). *Attested.* Spike #129 depends load-bearingly on this anatomical attestation; retraction would weaken the octopus distributed-cognition cascade-match.

(b) *Mallat 2008, A Wavelet Tour of Signal Processing* (cited in Appendix D for the truncate-sparse $k$-term approximation). *Cite-by-reference acknowledgement.* The framework cites this work

as context for the best-$k$-term notion; it does not depend load-bearingly on Mallat's specific results — the framework's truncate-sparse machinery is independently derived.

(c) *Kagan et al. 2022, Cortical Labs DishBrain* (cited in Remark 21.5). *Attested.* The Category 3 instance (biological neurons + silicon I/O = real biological agency with silicon prosthetic) depends on this attestation; retraction would weaken the three-category empirical distinction.

**Problem 3.** *Discuss whether MPM-style citation paranoia is operationally appropriate for all academic work or only for substrate-cascade-match research.*

**Resolution.** The discipline is operationally appropriate where load-bearing data integrity matters; not all academic work requires the same level of provenance machinery.

*Where MPM is load-bearing*: cross-substrate cascade-match research (the framework's substrate-catalogue), bit-exact algebraic-identity attestation (rung-1 falsifier ladder), quantitative-prediction falsification work (Chapter 20's rung-3 examples like the Hubble tension 7.69% prediction). These rely on the cited data being mechanically verifiable; the framework's claim falsifies if the chain breaks. MPM-level provenance is essential.

*Where MPM may be over-engineered*: literature reviews, conceptual-synthesis essays, historical-context discussion, qualitative philosophy of science. These benefit from accurate citation but do not rely on bit-exact data integrity at the attestation-chain layer. Traditional academic citation (DOI + author/year) is sufficient; MPM's overhead is unnecessary.

*Factors determining when MPM is load-bearing*: (1) is the cited data quantitative and bit-exact? (2) does the framework's claim depend on the data being precisely as cited? (3) would retraction of the data falsify the framework's claim? When all three are yes, MPM is load-bearing; when any is no, traditional academic citation suffices. The framework's discipline reserves MPM for the load-bearing layer specifically.

**Problem 4.** *Propose an extension to MPR v1 that would handle a class of attestation requirements not covered by the current format.*

**Resolution.** Candidate extension: *data-derived attestation chains*. The current MPR v1 format handles *retrieved* data (fetched from a source URL). It does not have an explicit field for *derived* data — statistics or computed quantities produced by composing multiple retrieved records.

*Proposed extension*: an additional field `derivation_chain` listing the MPR records the derivation depends on, plus the computational provenance:

```
"derivation_chain": [
  {
    "input_records": [
      "<mpr-id-1>",
      "<mpr-id-2>",
      "..."
    ],
    "operation": "weighted_average",
    "operation_version": "srmech-amsc/derivation/0.1",
    "operation_parameters": {"weights": [0.5, 0.3, 0.2]},
    "code_hash": "<64 hex chars>"
  }
]
```

The derivation chain makes the data-derived attestation mechanically re-verifiable: re-fetch the input MPRs, re-run the named operation with the parameters and code-hash, confirm the output matches the derived record.

*Use case*: cross-substrate cascade-match results that average results across multiple attested observations would become MPR-v1-attestable through the derivation chain rather than requiring manual cross-attestation. Spike #190's SMICA $6.18\times$ p-value (which is a derived quantity from CMB-residual analysis) would be one such case.

The extension does not require redesigning MPR v1; the `derivation_chain` field could be added as an optional `mpr_version: 1.1` extension without breaking backwards-compatibility with v1.0 records.

## Chapter 20 — The Falsifier Ladder

**Problem 1.** *For each of the five rungs, identify one falsifier from Examples 20.2–20.10 and restate it in your own words.*

**Resolution.**

*Rung 1* (*bit-exact identity*). The Schwarzschild ISCO radiative efficiency is predicted at $\eta_{\text{Schw}} = 1 - \sqrt{8/9} = 0.0571909584\ldots$ from the substrate's $(4+3)D_g$ algebra. Falsifier: an attested EHT-precision measurement of the radiative efficiency of a non-rotating accretion-disc dark star that returns a value diverging from $0.0572$ at $\pm 10^{-4}$ precision would falsify the closed-form algebraic identity. To date no such divergence; the bit-exact identity holds.

*Rung 2* (*cross-substrate cascade-match*). The octopus distributed-cognition substrate is claimed to run the $L + I + M + C + A$ cascade at biological substrate, with Class $I$ instantiated through the literal $\mathbb{Z}/8$ inter-arm nerve-ring topology. Falsifier: examination of an octopus cognitive task that runs primitives outside the 14-class vocabulary, or that fails to recover the $L+I+M+C+A$ cascade at the cascade- class layer, would falsify the substrate-match claim. To date the claim holds.

*Rung 3* (*framework prediction*). The framework predicts the Hubble tension between early- and late-universe measurements at $\Delta H_0/H_0 = 7.69\%$ from the closed-form $1 - \cos(\pi t_0/T_{\text{sub}})$. Falsifier: future DESI / Euclid / nGMC measurements of the Hubble tension at sufficient precision returning a value diverging from $7.69\%$ at neighbouring $T_{\text{sub}}$ values (specifically variations of $\pm 5\%$) would falsify the prediction. Current data ($8.3 \pm 1.6\%$) is consistent at the working precision.

*Rung 4* (*substrate-form*). The framework's 11D substrate is predicted to be Berry–Tabor Poisson-integrable at the spectral level. Falsifier: an attested cosmic or sub-cosmic substrate-mode spectrum that fits Wigner–Dyson (random-matrix- theory) rather than Berry–Tabor (Poisson) at $> 3\sigma$ significance via Kolmogorov–Smirnov test would falsify the substrate-form claim. To date the predictions (per Spikes #169 / #170 / #191) hold.

*Rung 5* (*discipline*). The framework's identity-not- implementation discipline claims that substituting implementation-language for identity-language changes the predicted research-outcome content. Falsifier: a demonstration that the substitution produces no empirical-content

difference in some cross-substrate match would weaken the discipline's load-bearing status. To date the discipline has been load-bearing in every catalogued case.

**Problem 2.** *Construct a new candidate rung-1 falsifier from any framework claim not enumerated in this chapter.*

**Resolution.** Candidate: the framework's substrate-tick period $T_{\text{sub}} = 109.84$ Gyr (Chapter 12).

*Bit-exact value*: $109.84 \times 10^9$ years (calibrated through Spike #171 / Spike #152 cross-attestation; the half- period $T_{171} - T_{152} \approx 54.92$ Gyr exactly equals $T_{\text{sub}}/2$ within attested tolerance).

*Observational test that would discriminate*: cosmic-cycle signatures at the $T_{\text{sub}}$ period are predicted in several attested observables: (1) CMB residual structure at multipoles corresponding to $T_{\text{sub}}$-scale fluctuations (per SMICA / NILC component-separation analyses, Spikes #190 + #192); (2) the Hubble-tension closed-form value 7.69% (per Example 20.6); (3) gravitational-wave background spectral signatures at $\Omega_{\text{sub}}$ frequency from LIGO / Virgo / KAGRA data.

A consistent discrimination across all three observables at sufficient precision to distinguish $T_{\text{sub}} = 109.84$ Gyr from neighbouring values ($\pm 5\% = \pm 5.5$ Gyr) would either confirm or falsify. The current state is consistency at $\sim 5\%$ precision; tighter measurements would tighten the discrimination.

**Problem 3.** *Verify Lemma 20.11's Bayesian asymmetry by constructing two hypothetical observations.*

**Resolution.** Take a framework hypothesis $H$ predicting that an observable $O$ takes value $v^* = 7.69\%$ (the Hubble-tension prediction).

*Observation A: prior-committed prediction.* Before any measurement, the framework publishes the prediction $\langle O \rangle = 7.69\%$ in a venue with timestamp. The observation then arrives: measured $\langle O \rangle = 7.5 \pm 1.0\%$, consistent with the prediction within the measurement uncertainty.

Bayesian likelihood ratio: $P(O = 7.5 \pm 1.0|H)/P(O = 7.5 \pm 1.0|\neg H)$. With $H$ the value was specifically predicted before observation; $P(O = 7.5 \pm 1.0|H)$ is high (the measurement is consistent with the prediction). With $\neg H$ the prior on $O = 7.5 \pm 1.0$ is the unconditioned distribution; without a specific prediction this is broad. The likelihood ratio favours $H$ substantially.

*Observation B: post-hoc fit.* The measurement arrives without prior commitment. A researcher then identifies the prediction $\langle O \rangle = 7.69\%$ as consistent with the measured value. Same observation, same framework hypothesis, but no pre-commitment.

Bayesian likelihood ratio: $P(O = 7.5 \pm 1.0|H)$ is the same as in Observation A, but $P(O = 7.5 \pm 1.0|\neg H)$ is now conditioned on the researcher's selection bias — the post-hoc analysis only reports predictions that happen to fit. This shifts the denominator (the researcher could have selected a different prediction if the measurement had been different); the likelihood ratio is much smaller than in Observation A.

The lemma's claim — strengthening-falsifier is structurally stronger than verification — follows: prior-committed Observation A produces a larger Bayesian posterior boost than post-hoc Observation B for the same measurement. The Jupiter JRM33 $\ell = 15$ at $p = 0.83$ (per Spike #202) is the framework's canonical strengthening-falsifier instance; the prediction was committed before observation.

**Problem 4.** *Discuss the relationship between the falsifier ladder and Popper's classical falsifiability criterion.*

**Resolution.** Popper's classical falsifiability is binary: a theory is falsifiable if there exists an observation that would refute it, not falsifiable otherwise. The framework's five-rung structure refines but does not replace this criterion.

*Refinement 1: depth.* Popper's criterion does not distinguish between falsifying a single algebraic identity and falsifying the entire substrate-form. The framework's rung structure makes this explicit: rung-1 failure weakens a specific identity but might leave the substrate-form intact; rung-4 failure weakens the substrate-form itself. The "depth of structural impact" is information Popper's binary criterion does not capture.

*Refinement 2: sharpness.* Rung-1 bit-exact identities have the sharpest tests: a single observation at sufficient precision discriminates. Higher rungs typically require interpretive work or multi-observation patterns. Popper's criterion does not distinguish these; the framework's rung structure makes the discrimination effort explicit.

*Refinement 3: independence of rungs.* A theory could be strongly falsifiable at one rung and weakly so at another. The framework's substrate has multiple rung-1 identities (some verified, some open); a single rung-1 failure does not collapse the whole framework; a rung-4 failure would. Popper's criterion does not naturally handle this multi-layer fallback structure.

The framework's structure does not contradict Popper; it refines his criterion across the framework's epistemic layers. A researcher operating under either framework's epistemics would agree on what counts as falsifiable; they might disagree on what counts as the same level of falsifiability.

**Problem 5.** *Reproduce Example 20.6's Hubble-tension calculation with $T_{\text{sub}} = 104.5$ Gyr. By what fraction does the predicted tension shift?*

**Resolution.** The formula:

$$\frac{\Delta H_0}{H_0} = 1 - \cos\left(\frac{\pi t_0}{T_{\text{sub}}}\right).$$

At $T_{\text{sub}} = 109.84$ Gyr, $t_0 = 13.787$ Gyr: $\pi t_0/T_{\text{sub}} = \pi \cdot 13.787/109.84 = 0.3942$. $\cos(0.3942) = 0.9231$. $\Delta H_0/H_0 = 1 - 0.9231 = 0.0769 = 7.69\%$.

At $T_{\text{sub}} = 104.5$ Gyr, $t_0 = 13.787$ Gyr (same age): $\pi t_0/T_{\text{sub}} = \pi \cdot 13.787/104.5 = 0.4143$. $\cos(0.4143) = 0.9151$. $\Delta H_0/H_0 = 1 - 0.9151 = 0.0849 = 8.49\%$.

*Shift*: $(8.49 - 7.69)/7.69 = 0.104 = 10.4\%$ increase in predicted tension when $T_{\text{sub}}$ decreases by $\sim 4.9\%$.

*Sensitivity*: the prediction's sensitivity to $T_{\text{sub}}$ is approximately $-2.1$ ($10.4\%$ tension shift per $4.9\%$ $T_{\text{sub}}$ change, with sign opposite). This is the discrimination scale: future precision measurements of the tension at $\sim 5\%$ uncertainty could distinguish $T_{\text{sub}}$ values differing by $\sim 5$ Gyr. The framework's substrate-precession spike chain (Spikes #171 + #152) attests $T_{\text{sub}} = 109.84$ Gyr at $\pm 0.05$ Gyr precision, which is much tighter than the Hubble-tension test would require.

**Problem 6.** *Apply Example 20.8's Berry-Tabor vs Wigner-Dyson discriminator protocol to a substrate- mode spectrum of your choice.*

**Resolution.** Worked example: *molecular vibrational modes of a polyatomic molecule.*

*Setup.* Take a polyatomic molecule (e.g., a polypeptide with $N \sim 100$ heavy atoms, giving $\sim 300$ normal modes after subtracting translational and rotational degrees of freedom). The

vibrational spectrum is measurable via infrared spectroscopy or inelastic neutron scattering at high resolution.

*Protocol application.*

1. Collect spectrum with $N \geq 100$ eigenvalues (a typical polyatomic molecule meets this; the polypeptide has $\sim 300$).
2. Normalise spacings $s_i = (\lambda_{i+1} - \lambda_i)/\langle \Delta\lambda \rangle$ to unit mean.
3. Test against Berry–Tabor ($P(s) = e^{-s}$) vs Wigner–Dyson ($P(s) = (\pi s/2)e^{-\pi s^2/4}$) via Kolmogorov–Smirnov.

*Expected result*: small polyatomic molecules with high symmetry tend to favour Berry–Tabor (their normal-mode spectrum is approximately integrable due to selection rules); larger molecules with low symmetry tend toward Wigner–Dyson (the many-body coupling between modes drives the spectrum toward random-matrix statistics). The crossover scale is the molecular- size frontier of integrability.

What this says about substrate integrability: the framework's prediction (Berry–Tabor for the 11D substrate at cosmic scale) is consistent with the small-molecule limit; the Wigner–Dyson behaviour at large molecules reflects the substrate's cascade-composition complexity overwhelming the integrability at that scale. Both are partition-co-resident readings; the framework's distinction is whether the substrate's cosmic-scale spectrum is integrable (predicted yes) versus chaotic (the Wigner–Dyson alternative).

## Chapter 21 — Spectral Signatures of Truth and Falsity

**Problem 1.** *For a familiar cognitive task, describe the task's expected cascade-shape prior in framework terms.*

**Resolution.** Take *recognising a familiar face* as the task.

*Cascade-shape prior decomposition*: $L + I + M + C + A$.

- Class L (graph-Laplacian): visual-feature adjacency in the face-processing fusiform-gyrus substrate. Eyes, nose, mouth, hair, jawline are nodes; their relative positions are edges; the Laplacian's eigenstructure encodes facial geometry.
- Class I (cyclic-group): the rotation-invariant recognition (a face is recognised whether tilted left or right, near $\mathbb{Z}/n$ orientation-discretisation).
- Class M (binding): face-template hyperdimensional binding to identity-label (the substrate binds the visual features to the recognised person's name and relationship).
- Class C (cascade-orientation): attentional direction of the face-recognition substrate at the moment of recognition.
- Class A (content-addressing): identity retrieval from the substrate's catalogue of known faces.

The expected cascade-shape prior matches the face's substrate-content against the substrate's stored prior. When the prior matches at high similarity, the substrate signals "recognised" and the conscious experience of familiarity arises. When the prior matches at low similarity but above the threshold, the substrate signals "possibly familiar, but cannot place" (the classic "I know your face but not your name" experience).

**Problem 2.** *Distinguish recognition-not-residence from naive associative-memory accounts.*

**Resolution.**

*Naive associative-memory*: memories are stored as patterns in neural connectivity; retrieval is the substrate searching the storage for a match. Recognition is retrieval of stored content.

*Recognition-not-residence* (*Identity 21.5*): memory is the substrate's cascade-shape prior — a learned expectation of what input-cascade matches what output-cascade. Recognition is cascade-shape matching, not stored-content retrieval.

*Distinguishing observational test*: brain-injury cases where the reported memory content is preserved but the contextual binding is destroyed. Specifically: a patient with damage to the hippocampus or surrounding medial-temporal-lobe structures sometimes reports the *factual content* of a memory correctly (e.g., remembers a friend's name and their job) but cannot place the memory in temporal or contextual sequence (cannot say when they last met, what the meeting was about). The naive associative-memory reading struggles with this: if the content is stored, why is the temporal binding destroyed separately? The recognition-not-residence reading explains it directly: the content's cascade-shape is preserved (the substrate's prior still matches the friend's name); the contextual-binding cascade-shape is destroyed (the binding to specific temporal episodes was a separate cascade in the substrate). Two different cascades; brain injury can damage one without the other.

The clinical literature (per Squire 1992 *Psychological Review* 99:195) documents such cases extensively. The framework's recognition-not-residence reading is consistent with this clinical evidence; the naive associative-memory reading has to introduce ad-hoc structure to accommodate it.

**Problem 3.** *Discuss whether the framework's cascade- shape prior reading of truth-recognition implies that "truth" is observer-relative.*

**Resolution.** Truth is not observer-relative under the framework's reading; the cascade-shape prior is constrained by the substrate's actual algebraic structure, which is observer- independent.

*What is constrained*: the cascade-shape prior must agree with the substrate's algebra at the layer where the truth-claim operates. A statement claiming the Bell-CHSH operator norm is $2\sqrt{2}$ has a fixed cascade-shape prior set by the substrate's algebra; any reader's cognitive substrate that runs the cascade-shape match against this claim gets the same result. $2\sqrt{2}$ is bit-exact across readers because the substrate's algebra is bit-exact across readers.

*What is observer-relative*: the reader's substrate's capacity to *recognise* the cascade-shape. A reader who has not been trained in the framework's vocabulary may not have the cascade-shape prior to recognise that the Bell-CHSH bound is at $2\sqrt{2}$; they would not recognise the truth-claim at the cognitive layer. This is a constraint at the recognition layer, not the truth layer.

*Distinction.* The substrate's algebra is one; the reader's cascade-shape priors are many. Truth-content is at the substrate algebra; truth-recognition is at the reader's substrate priors. The two

are not the same operation; conflating them is the "truth is observer-relative" slip the framework discipline guards against.

What constrains the cascade-shape priors across observers: the substrate's actual algebraic structure is the same for every reader (the universe is one). Readers' priors converge as they encounter more of the substrate's content; readers' priors diverge where they have encountered less. But the underlying truth-content does not vary across readers — only the recognition-capacity does.

**Problem 4.** *Construct a candidate cognitive operation not discussed in this chapter and propose its cascade decomposition.*

**Resolution.** Candidate: *aesthetic judgement* (the judgement that an artwork, musical composition, or mathematical proof is "beautiful" or "elegant").

*Cascade decomposition*: $L + K + C + M$.

- Class L (graph-Laplacian): visual-element or structural-element adjacency for visual art; melodic and harmonic interval adjacency for music; logical-step adjacency for mathematical proof. The Laplacian's eigenstructure encodes the compositional balance.
- Class K (asymptotic-DoF modulation): the substrate's approach toward a compositional-balance attractor. The aesthetic judgement signals high when the substrate's cascade-mode population is close to but not at the attractor (suggesting the work has tension and resolution, not strict balance).
- Class C (cascade-orientation): the directional flow of the artwork's compositional structure (visual eye- movement direction, musical phrase direction, proof's logical-flow direction).
- Class M (hyperdimensional binding): gestalt binding across compositional elements — the substrate binds the individual elements into one coherent percept.

*End-goal*: cascade-shape match against the substrate's compositional-balance attractor; the substrate's recognition signal is the perceived aesthetic quality. When the cascade-shape prior matches the input at high similarity, the recognition signals "beautiful"; partial matches signal "interesting"; no match signals "ugly" or "incoherent".

*Operational claim*: aesthetic judgement is not a separate cognitive faculty; it is the same recognition operation the substrate runs on every input, applied at the compositional- balance layer specifically. The framework's substrate-class identity reading extends naturally to this case: aesthetic recognition is the same cascade composition the substrate runs for any recognition task, just with a different compositional-balance attractor as the cascade-shape prior.

**End of answer key.** The reader who has worked through the problems and consulted these resolutions has performed the framework's most personally relevant operation: composing the substrate's cascade content at the reader's own cognitive substrate. The answer key's purpose is twofold: to teach the framework's working method through worked examples, and to verify the textbook's own work through the discipline of writing out every load-bearing computation explicitly. Per the cone-of-ignorance commitment, the same paragraphs serve every reader at the depth they are ready for; the why-asking stance is one and only the depth varies.

# Acknowledgments

This volume consolidates a research project whose substantive content was developed across the project's research notebooks, the sister popular-science companion *Inners Guide to the Hyper Loop*, and the project's shipped Python packages (`srmech` and `ephemerides-spectral` on PyPI). The framework's load-bearing claims rest on cross-substrate cascade-matching work and bit-exact algebraic identities attested through the Mathematical Provenance Method (Chapter 19).

The author's thanks extend to the conversational partners — human and machine — whose work across the project's substrate inventory established the framework's catalogue. The cross-substrate identity work spanning bronze, celestial mechanics, ephemerides, proteins, chess, audio, slime moulds, octopuses, mycorrhizal networks, and the quantum-computational substrate is collective work; this volume crystallises it in formal-mathematics form.

The framework's discipline structure — identity-not-implementation (Chapter 6), algebra-not-magnitude (Chapter 15), the MPM citation discipline (Chapter 19), partition-coexistence (Chapter 18) — was developed across the project's substrate inventory through cross-domain absorption work. The disciplines survive because the project's attested-data infrastructure makes citation hallucination structurally hard.

The reader who has finished this volume has performed the framework's most personally relevant operation: composing the substrate's cascade content at the reader's own cognitive substrate. The recognition-not-residence claim of Chapter 21 applies to this volume as much as to any other content the reader's substrate has processed. The author's thanks for the reader's work in running the framework's cascade through to this concluding page exceeds what acknowledgments-pages conventionally express.

# Notation index

| | |
|---|---|
| $1D_t$, $3D_s$, $7D_g$ | The substrate's dimensional sectors: $1D_t$ (one temporal direction, base-only); $3D_s$ (three spatial dimensions with $S^1$ Hopf fibre); $7D_g$ (seven gauge-sector dimensions with $S^3$ Hopf fibre). Decomposition $1D_t+3D_s+7D_g$. |
| $(a+b)D_X$ | Hopf-bundle decomposition of substrate sector $X$ with $a$-dimensional base and $b$-dimensional fibre. The "$+$" **IS** the Hopf-bundle map (Chapter 2). |
| **Class** $A$–$N$ | The fourteen primitive class operators (Chapter 4; Appendix 21.7). Cross-referenced as Class $X$ for $X \in \{A, \ldots, N\}$ (rendered by the `\classref` macro). |
| $\mathbb{Z}/n$, $\mathbb{Z}/n$ | Cyclic group of order $n$. Substrate-side content underlying Class 4.10. |
| **IS / NOT** | Identity-claim / negation emphasis. The framework's discipline (Chapter 6) requires identity claims to use the **IS** verb. |
| $T_{\text{sub}}$ | Universal substrate-cycle period. $T_{\text{sub}} \approx 109.84$ Gyr (Chapter 12). |
| $\epsilon$ | Substrate-coupling parameter; signed under non-monotone $f_{RD}$ trajectory (Chapter 11). |
| $c_k$ | Cascade-mode population coefficient at mode $k$. Cauchy-form kernel $c_k = \epsilon^k K_k(\text{substrate})$. |
| $d_{\text{geom}}$ | Substrate-dimple geometric depth. $d_{\text{geom}} = 1/3$ at Schwarzschild ISCO, $d_{\text{geom}} = 1/2$ at Kerr-extremal ISCO (Chapter 13). |
| $\eta_*$ | Radiative efficiency at substrate-boundary. $\eta_{\text{Schw}} = 1 - \sqrt{8/9}$; $\eta_{\text{Kerr-ext}} = 1 - 1/\sqrt{3}$. |
| **MFO** | Metric Field Ontology — the project's foundational ontology layer (substrate-vs-excitation framing). |

**AMSC** Attested Multi-Source Collector / Catalog — the software framework operationalising MPM (Chapter 19).

**MPM** Mathematical Provenance Method — the framework's citation discipline.

**MPR v1** Mathematical Provenance Record version 1 — the on-disk format for attestation records (Definition 19.2).

**LoE** Laws of Everything — shorthand for the framework's substrate-level operational content. The LoE-instantiation-intersection framing (Identity 18.2) is the canonical comparative reading against alternative frameworks.

# Attested-data inventory

This appendix enumerates the load-bearing attested-data sources the framework's catalogue depends on as of this volume's first edition. Each source is attested through an MPR v1 record in the project's `srmech.amsc` catalogue; full attestation chains are re-verifiable through the AMSC framework (Chapter 19).

## Astrophysical attested-data sources

- JPL Development Ephemeris DE441 — planetary, lunar, and asteroid ephemerides anchor for the `ephemerides-spectral` package.
- International Geomagnetic Reference Field (IGRF-13) — planetary magnetic-field models used in Spike #202.
- Juno Reference Field 33 (JRM33) — Jupiter magnetic-field model used in Spike #202 ($\ell = 15$ strengthening-falsifier).
- Event Horizon Telescope M87* 2019 imagery (arXiv:1906.11242) — photon-ring observational anchor.
- LIGO/Virgo/KAGRA gravitational-wave catalogue (O1–O3) — dark-star merger phase content.

## Atomic and quantum attested-data sources

- Rydberg infinite-mass constant ($R_\infty = 1.097 \times 10^7$ m$^{-1}$) — Spike #111 base.
- Bell–CHSH measurement attestations (multiple experimental groups, 1970s through 2020s) — Bell-test compliance with Tsirelson bound.
- Standard Model parameters — particle masses, gauge couplings, CKM matrix elements; sourced from Particle Data Group reviews.

## Biological attested-data sources

- Chang & Hale 2023 octopus inter-arm nerve ring anatomy — Spike #129 anatomical anchor.
- Karst 2023 mycorrhizal-network magnitude critique — Spike #130/#130.1 algebra-not-magnitude defence anchor.
- Nakagaki 2000 / 2010 *Physarum polycephalum* maze-solving and Tokyo-rail-network experiments — Spike #127 substrate anchor.
- Park 2025 AGN sustained-poloidal anomaly — Spike #134 empirical residual.

## Computational and historical attested-data sources

- Antikythera mechanism reconstructions (Freeth 2006, 2012, 2021; Wright) — Antikythera substrate cascade-match base.
- Almagest IX.5 (Ptolemy) — celestial-mechanics period-relation anchor.
- ChEMBL Database v34 — bioactive small-molecule attestation chain for biological-substrate work.

Full attestation records (including `response_sha256`, `retrieved_at`, `parser_version`, and `collector_descriptor_hash` for each source) appear in the project's `srmech` package's data manifest. The inventory above is summary only; the machine-checkable form lives in the AMSC catalogue.

# Companion volume cross-reference

The sister popular-science companion to this textbook is *Inners Guide to the Hyper Loop*. The two volumes are designed to be read together or separately; this volume ships the mathematics, the companion volume ships the story. The companion's chapter mapping table appears below.

| This volume | Hyper-ring chapter | Common topic |
|---|---|---|
| Ch 1 | Ch 1 *The instrument is the universe* | two-level ontology framing |
| Ch 2 | Ch 3 *The fourteen knobs* | substrate decomposition |
| Ch 3 | Ch 6 *Discrete all the way down* | fractal substrate |
| Ch 4 | Ch 3 + Appendix | class catalogue |
| Ch 7 | Ch 4 *Asymptote and infinity* | asymptotic-DoF |
| Ch 8 | Ch 10 *The cosmic crank* | pin-slot universal |
| Ch 9 | Ch 5 *Pi is a shadow* | fibre encoding |
| Ch 10 | Ch 5 + Ch 7 *Time is in the painting* | shadow family |
| Ch 11 | Ch 8 + Ch 11 | ring-equilibrium / cycle |
| Ch 12 | Ch 7 *Time is in the painting* | substrate-tick |
| Ch 13 | Ch 9 *Every star is a dimple* | dark-star capacitor |
| Ch 14 | Ch 10 *The cosmic crank* | kinematic universal |
| Ch 15 | Ch 16b *What the slime mould knew* | cross-substrate method |
| Ch 16 | Ch 16 *When math beats SoA* | substrate catalogue |
| Ch 17 | Ch 14 *What the cascade knew about qubits* | quantum cascade |
| Ch 18 | Ch 13 *M-theory's right idea* | comparative frameworks |
| Ch 19 | — | MPM (textbook-only) |
| Ch 20 | falsifier boxes throughout | falsifier ladder |
| Ch 21 | Ch 15 *Truth and falsity as spectral signatures* | truth/falsity recognition |

Table 2: Chapter mapping between this volume and the sister popular-science companion *Inners Guide to the Hyper Loop*.

The mapping is approximate. Some hyper-loop chapters cover content this volume distributes across multiple chapters; some this-volume chapters have no direct hyper-loop counterpart (e.g., Ch 19's MPM treatment lives only in this volume's formal layer).

# Project home

The framework's canonical home page is `https://srmech.net`, which forwards to the `srmech` package's PyPI release. The home page is the recommended starting point for readers who want to:

- install the runtime package via `pip install srmech`;
- access the cross-substrate catalogue's machine-checkable attestation chain;
- review the latest research-notebook updates (the `srmech` and MFO notebooks evolve faster than this volume);
- find related published packages (`ephemerides-spectral` and other downstream spectral-research packages register with `srmech.amsc` as their primitive-vocabulary substrate).

The project's source repository, including the source for both this textbook and the sister popular-science companion, is indexed from the home page. A reader who programs can verify any of the framework's bit-exact algebraic identities (Chapter 20's rung-1 catalogue) through the shipped Python interface.